Advanced Industrial Materials (AIM) Program
Office of Industrial Technologies
Energy Efficiency and Renewable Energy
U. S. Department of Energy (DOE)

AIM

ADVANCED INDUSTRIAL MATERIALS (AIM) PROGRAM

ANNUAL PROGRESS REPORT

FY 1994

Date Published: May 1995

Prepared by the
Oak Ridge National Laboratory
Oak Ridge, Tennessee 37831
managed by
Martin Marietta Energy Systems, Inc.
for the
U.S. Department of Energy
under Contract No. DE-AC05-84OR21400

ORNL/TM-12963

Advanced Industrial Materials (AIM) Program
Office of Industrial Technologies
Energy Efficiency and Renewable Energy
U. S. Department of Energy (DOE)

AIM

ADVANCED INDUSTRIAL MATERIALS (AIM) PROGRAM

ANNUAL PROGRESS REPORT

FY 1994

Date Published: May 1995

Coordinated by Peter Angelini
Compiled by Pamela Wenzel, CPS
Oak Ridge National Laboratory

TABLE OF CONTENTS

TABLE OF CONTENTS
-continued-

INTRODUCTION

INTRODUCTION TO THE ADVANCED INDUSTRIAL MATERIALS (AIM) PROGRAM*

C. A. Sorrell, Department of Energy (DOE) Program Manager

U.S. Department of Energy
Washington, DC 20585

The Advanced Industrial Materials Program is a part of the Office of Industrial Technologies (OIT), Energy Efficiency and Renewable Energy in the Department of Energy. The mission of the AIM Program is to conduct applied research, development, and applications engineering work, in partnership with industry, to commercialize new or improved materials and materials processing methods that will improve energy efficiency, productivity, and competitiveness. AIM is responsible for identifying, supporting, and coordinating multidisciplinary projects to solve identified industrial needs and transferring the technology to the industrial sector. Program investigators in the DOE National Laboratories are working closely with approximately 100 companies, including 15 partners in Cooperative Research and Development Agreements. Work is being done in a wide variety of materials technologies, including intermetallic alloys, ceramic composites, metal composites, polymers, engineered porous materials, and surface modification.

The Program supports other efforts in the Office of Industrial Technologies to assist the energy consuming process industries, including forest products, glass, steel, aluminum, foundries, chemicals, and refineries. To support OITs "Industries of the Future" initiatives and to improve the relevance of materials research, assessments of materials needs and opportunities in the process industries are being made. These assessments are being used for program planning and priority setting; support of work to satisfy those needs is being provided.

Many new materials that have come into the marketplace in recent years, or that will be available for commercial use within a few more years, offer substantial benefits to society. The promise is for greater industrial efficiency, reduced energy consumption, greater reliability and product life, and new products for better productivity and leisure activities. From a national standpoint, it is important to remember that any nation excelling in advanced materials, and sharing the technologies and/or products resulting from those technologies at the appropriate commercial moment, will realize optimum benefits for its investments in addition to providing useful technologies for the world as a whole. Any nation that builds a leadership position in these technologies and subsequently retains or expands that technological strength can feel secure about sharing commercialization.

Materials are enabling for virtually any improvement in manufacturing efficiency and energy consumption but, even though the U.S. leads the world in development of new materials and synthesis methods, identification of the benefits of new materials and applications of these to manufacturing have not received adequate attention from U.S. industry. A recent report from the National Research Council concludes that while the U.S. leads in materials science, a serious gap exists in synthesis and processing needed to carry the technology to the market place. Consequently, while the U.S. discovers the new materials, other nations do the necessary applied research to commercialize them and gain the economic advantage.

*Research sponsored by the U.S. Department of Energy, Assistant Secretary for Energy Efficiency and Renewable Energy, Office of Industrial Technologies, Advanced Industrial Materials (AIM) Program, under contract DE-AC05-84OR21400 with Martin Marietta Energy Systems, Inc.

Of the more than $1.8 billion to be spent by the U.S. government on materials research in FY 1993, the expenditures are overwhelmingly devoted to basic research. Only the small efforts in Energy Efficiency and Renewable Energy in the Department of Energy and the National Institute for Standards and Technology presently involve significant cooperation with non-military industries to carry materials technologies forward to actual applications. It is widely recognized that direct cooperative efforts between government and industry are crucial to the efficiency and competitiveness of U.S. industry. The vision of the Advanced Industrial Materials Program is the successful formation of National Laboratory/industry/university teams to bring materials from basic research, through applied research, development, and engineering, to industrial application to strengthen the competitive position of U.S. industry and save energy. Ideally, the Program can serve as a prototype for other cooperative efforts between the public and private sectors.

In order to realize this vision, the Program takes the following tactical, or procedural, steps:

- Works with materials suppliers and users to identify opportunities for improved efficiency and energy savings by use of new materials and determine properties needed for identified applications. Supports OITs "Industries of the Future" initiatives including: forest products, steel, aluminum, foundries, glass, chemicals, and refining.

- Identifies customers for materials technologies prior to initiation of work; customers may be industry, end-use programs within Energy Efficiency and Renewable Energy, or other government programs. Identify energy and economic savings to be realized. At the same time, the Program will identify promising areas for pioneering work in materials and support them.

- Forms applied research and development teams, consisting of staff from industry, the DOE National Laboratories, and universities, to solve engineering problems attendant to industrial use of the materials. At any given time, the goal is to fund a variety of materials and processing efforts with a range of maturities and anticipated times to completion.

- Works with Energy Research, Fossil Energy, and Defense Programs to identify materials technologies offering potential for commercialization but needing applied research, development, and applications engineering.

In Fiscal Years 1994 and 1995, AIM investigators have made significant progress in bringing materials technologies to the demonstration and commercialization stages. Among these are:

- Nickel aluminide glass punches for container manufacturing. Alloy developed by Oak Ridge National Laboratory and commercialized by Metallamics, Inc.

- Nickel aluminide components for walking beam furnaces for metal heat treating. Alloy developed by Oak Ridge National Laboratory and commercialized by Rapid Technologies.

- Variable frequency microwave furnace. Developed by Oak Ridge National Laboratory and commercialized by Lambda Technologies.

- Nickel aluminide dies for hot pressing $Nd_2Fe_{14}B$ magnets. Alloy developed by Oak Ridge National Laboratory and commercialized by Metallamics, Inc.

- Nickel aluminide rolls for steel mill reheat furnaces have been successfully tested for more than one year. Large scale testing will be followed by commercialization. Alloy and welding methods developed by Oak Ridge National Laboratory; alloys produced by Metallamics, Inc.; rolls cast by Sandusky International; rolls tested by Bethlehem Steel.

- Nickel aluminide trays and fixtures for industrial carburizing furnaces have been successfully tested for more than one year. Large scale testing will be followed by commercialization. Alloy and casting methods developed by Oak Ridge National Laboratory; casting by Alloy Engineering and Casting Co.; testing by General Motors Saginaw Division.

- Silica aerogels for thermal insulation are nearing commercialization by Aerojet General. The material was developed by Lawrence Berkeley Laboratory; other industrial partners are Boeing, Cadillac, Benteler Industries, Admiral, and Glacier Bay. Commercialization is now being supported by a grant from the Technology Reinvestment Program.

- Molybdenum disilicide composites and coatings are being tested by Air Products and Chemicals and are the subjects of Cooperative Research and Development Agreements with Advanced Refractory Technologies and Schuller International. The materials and processing methods were developed by Los Alamos National Laboratory.

These are only a few highlights. Over the past four years, AIM investigators have been remarkably successful in attracting industrial interest and forming successful partnerships. Their hard work and foresight are to be commended.

ADVANCED METALS AND COMPOSITES

ADVANCED ORDERED INTERMETALLIC ALLOY DEVELOPMENT

C. T. Liu and J. A. Horton
Metals and Ceramics Division
Oak Ridge National Laboratory
P. O. Box 2008
Oak Ridge, Tennessee 37831-6115

C. C. Koch and Nkadi Sukidi
Materials Science and Engineering Department
North Carolina State University
Raleigh, North Carolina 27695-7907

N. S. Stoloff
Rensselaer Polytechnic Institute
Materials Engineering Department
1110 8th Street
Troy, New York 12180-3590

INTRODUCTION

Many ordered intermetallics possess unique properties and have the potential to be developed as new materials for energy-related applications. The objective of this task is to develop low-density, high-strength intermetallic alloys for engineering use in advanced energy conversion systems and heat engines. Current efforts are focused on three alloy systems (1) NiAl aluminides, (2) Ni_3Si alloys, and (3) reaction synthesis of NiAl-Ni_3Al alloys.

The NiAl aluminide has a high-melting point (T_m = 1640°C), low density (5.86 g/cm^3) and excellent oxidation and corrosion resistance. The structural use of NiAl, however, has been limited by its low ductility and poor fracture toughness at ambient temperatures, and inadequate strength at high temperatures. Our early study indicated that the grain boundary in NiAl is intrinsically brittle at ambient temperatures. We had found that microalloying with boron is able to completely suppress intergranular fracture. The mechanical properties of NiAl are sensitive to alloying additions. Alloying with a couple of percents of elements can substantially improve the ductility at ambient temperatures and the

strength and creep resistance at elevated temperatures. Current effort on NiAl alloy development is concentrated on optimizing alloy compositions and evaluating mechanical properties of selected cast NiAl alloys.

The intermetallic compound Ni_3Si has several properties which make it a material for potential applications. It has excellent corrosion resistance to certain acid solutions as well as many of the attractive mechanical properties of some $L1_2$ structure intermetallics. The major problem with Ni_3Si, as is common to most intermetallics, is its limited ductility. In order to improve the room-temperature and elevated temperature ductility of Ni_3Si several alloy development programs have focused on this intermetallic. A series of Ni_3Si-base alloys have been developed at ORNL which have high strength, superplastic formability, reasonable room-temperature ductility and corrosion resistance. More research is needed to optimize the compositions of the promising alloys and to understand the alloying and microstructural features which control the properties of interest. The proposed research will address these problems of structure-property relationships in Ni_3Si alloys as influenced by composition modifications. Three topics have been chosen for initial study. These are: (1) oxidation behavior of selected Ni_3Si-base alloys in the temperature range of 600 to 1000°C; (2) the influence of certain alloying additions, for example cerium, on the oxygen-induced embrittlement observed in tensile tests at about 600°C; (3) the influence of thermal treatment on the microstructure and properties of certain Ni_3Si-base alloys, e.g., those with niobium alloying additions.

The feasibility study of reactive sintering of aluminide alloys developed at Oak Ridge National Laboratory was initiated in August 1993. Reactive sintering has the potential to be a low cost, energy saving alternative to melt processing because of the use of inexpensive elemental powders and low furnace temperatures. Research during this period has been carried out initially by a post-doctoral research associate, Dr. T. R. Smith, and is now being performed by a graduate research assistant, C. Sainio. The two alloys chosen

for initial study are NAL-109 and IC-221M. Compositions (in weight percent) are as follows:

(1) IC-221M: 81.09% Ni, 8.0% Al, 7.7% Cr, 1.7% Zr, 1.43% Mo, 0.08% B,

(2) NAL-109: 67.76% Ni, 31.0% Al, 0.14% Zr, 0.43% Mo, 0.29% Fe.

TECHNICAL PROGRESS - FY 1994

Summary

1. Cast NiAl Aluminide Development

Cast NiAl alloys containing different levels of aluminum and alloying additions were prepared by various methods. Most of the alloys were prepared by arc melting and drop casting, and metallographic examinations indicated cast porosities formed in these cast alloys. The cast defects could not be simply annealed out at temperatures as high as 1400°C. Levitation-zone remelting was used to reduce cast porosities; however, only limited success was achieved by this cast technique.

Tensile tests at room-temperature indicate that the fracture strength of the NiAl alloys is sensitive to cast defects. In order to reduce the cast porosities, cast NiAl alloys were HIPPed at 1200/1230, 1350, 1400, and 1450°C at a pressure of 413 MPa (60 ksi). Table 1 summarizes the room-temperature tensile properties of two NiAl alloys as a function of alloy preparation and HIPPing treatment. The arc-melted alloys and levitation-zone remelted alloys showed a fracture strength of less than 300 MPa. Hot pressing at 1225 to 1450°C at a stress of 413 MPa increases the fracture strength by more than 50%. Among the two alloys, NAL-120 containing a less amount of second phases (as compared with NAL-108) exhibits a higher fracture strength (= 510 MPa). These results demonstrate the importance in control of both cast defects and alloy composition.

The tensile properties of the best alloy, NAL-120, were determined as a function of test temperature after HIPPing at 1400°C and 413 MPa. All the tests were performed in air at a strain rate of 2.5 mm/min. The tensile properties are shown in Table 2. The alloy

showed the macroscopic yield strength of 510 MPa, with the tensile ductility of 0.8% at room-temperature. The ductility does not increase much until the temperature is above 800°C. The alloy exhibited the yield strength of 290 MPa and the tensile elongation of 32.3% at 1000°C. These properties together with light-weight and excellent oxidation resistance make the alloys attractive for structural use at elevated temperatures.

Table 1. Effect of Alloy Preparation and HIPPing Treatment on Room-Temperature Tensile Properties of NiAl Alloys

Alloy Preparation and Treatment	Fracture Strength (MPa)
NAL-108 (Ni-49.3Al-0.7Mo-0.4Nb-0.08Zr-0.2Fe, at. %)	
Arc melt	278
Arc melt + Levitation Zone Remelt (LZR)	294
Arc melt +LZR + press at 1225°C/413 MPa	451
Arc melt + press at 1450°C/413 MPa	415
NAL-120 (Ni-49.6Al-0.4Mo-0.1Nb-0.16Zr-0.2Fe, at. %)	
Arc melt	282
Arc melt + press at 1225°C/413 MPa	482
Arc melt + press at 1400°C/413 MPa	510

Table 2. Tensile Properties of NAL-120 (Ni-49.6Al-0.4Mo-0.1Nb-0.16Zr-0.2Fe, at. %) Prepared by Arc Melting and HIPPing at 1400°C and 413 MPa

Test Temp. (C°)	Yield Strength (MPa)	Ultimate Tensile Strength (MPa)	Total Elongation (%)
25	510	510	0.8
600	398	398	0.8
800	369	407	1.5
1000	290	314	32.3

2. Reaction Sintering of Nickel Aluminides

Because of the large reaction exotherm, prealloyed NiAl powder, corresponding to 20, 25, and 30 wt %, was added to the NAL-109 alloy in an attempt to dampen the reaction and prevent melting. Also, to reduce oxidation, the samples were first degassed under

vacuum for 2 h prior to sintering in argon. Samples containing 20, 25, and 30 wt % prealloyed NiAl were cold pressed at 35,000 lbs.

To reduce sample oxidation, sintering runs were carried out in vacuum. Samples of NAL-109 with 20 and 25 wt % prealloyed NiAl were placed in a vacuum furnace along with a crucible containing Ti sponge pellets to reduce oxygen in the furnace atmosphere. The samples were sintered at 605°C for 1 h under a vacuum of 7×10^{-5} torr. After sintering, both samples exhibited some necking where localized melting had occurred and both samples had a thin, gold oxide film on their surfaces. The 20 wt % sample also showed some swelling, which was due to the formation of a large (~1 x 2.5 mm) gas bubble just below the surface. Sintered densities were 5.59 g/cm^3 (95% ρ_{th}) for the 20 wt % sample and 5.24 g/cm^3 (92% ρ_{th}) for the 25 wt % sample. Microscopic investigation showed dense and porous regions existed in both samples. Vickers harness was measured on the dense regions of each sample and was determined to be 325 VHN for the 25 wt % sample and 378 VHN for the 20 wt % sample.

The effect of sintering temperature on the densification of NAL-109 was investigated by sintering an additional sample of NAL-109 with 20 wt % prealloyed NiAl for 1 h at 710°C under a vacuum of 2.5×10^{-5} torr. Prior to sintering, the sample was kept overnight at room temperature under vacuum of 3×10^{-6} torr. As with the other NAL-109 samples, some specimen distortion occurred due to excessive melting. Also a thin, gold oxide film was present on the sample surface. The sample density after sintering was 5.50 g/cm^3 (94% ρ_{th}) and the average hardness was 364 VHN. Comparing these values to that of the sample sintered in vacuum at 605°C indicates that the sintering temperature has little effect on these properties. This is somewhat expected since, once the sample heats to above the reaction temperature, the reaction exotherm causes the sample to self-heat to temperatures in excess of 1200°C. The actual furnace temperature, therefore, will only slightly modify the cooling rate of the sample down from the reaction temperature.

The effect of cold press load for NAL-109 with 20 wt % prealloyed NiAl was determined by pressing a sample to 486 MPa. This resulted in a green density of 4.60 g/cm^3 (78% ρ_{th}). Previous samples pressed at 210 MPa had a green density of 3.77 g/cm^3 (64% ρ_{th}). The sample was vacuum sintered for 1 h at 710°C under vacuum of 1 x 10^{-5} torr. Again, sample deformation and a thin, gold oxide film were both evident. A sintered density of 5.77 g/cm^3 (98% ρ_{th}) was achieved and the sample had an average hardness of 355 VHN. By increasing the cold press load, a higher sintered density was achieved - 98% vs 94% ρ_{th} with the hardness value relatively unchanged - 355 vs 364 VHN.

Another experimental variable investigated was the application of pressure during sintering. A sample of NAL-109 with 20 wt % prealloyed NiAl was hot pressed in argon using a pressure of 50 MPa. The sample was placed between two alumina plates which were slightly smaller than the sample so that a portion of the sample was not under pressure. The load was applied to the alumina plates through two graphite push rods connected to a Carver press. Both the furnace air temperature and sample/alumina temperature were monitored. Although the furnace rapidly heated (~60°C/min) to 620°C, the sample, in thermal contact with the mass of the alumina plates and graphite rods, heated at a much slower rate (~2°C/min). The sample was observed through a window in the furnace door to react and self heat to >1200°C, glowing a bright red and melting the chromel-alumel thermocouple which was attached to it. Microscopic investigation of the pressed and unconstrained regions of the sample showed that the portion of the sample which was under pressure was considerably more porous. The cause of this is believed to be the loss of heat through the alumina plates. When the reaction initiated, some part of the sample, most likely a corner or edge, had reached a temperature (<600°C) sufficient to start the reaction. At this time, the alumina plate temperature was only slightly above 110°C and, therefore, acted as a heat sink for the sample, As a result, the part of the sample under pressure in contact with the plate did not sufficiently heat so that significant densification was not achieved.

Fully dense, stoichiometric Ni_3Al has been produced by reactive sintering followed by HIPPing or by applying a uniaxial compression during the sintering process. Alloy IC-221M (Ni-8%Al-7.7%Cr-1.7%Zr-1.43%Mo-0.08%B, wt %), however, either showed porosity or incomplete sintering when processed by reactive hot isostatic pressing (RHIP) or by hot pressing. There are two possible causes for this observation. Alloy IC-221M contains high melting-temperature compounds, Cr and Mo, which, unless introduced prealloyed with nickel, do not sinter. Also, the reaction exotherm for this alloy is small, and sufficient self-heating to aid in the sintering process is not achieved. The small exotherm may be a result of the fact that alloy IC-221M has a deficiency in aluminum compared to stoichiometric Ni_3Al. Also, the low aluminum content means that there is not a sufficient quantity of liquid formed to aid in densification and the more rapid diffusion through this liquid phase, therefore, is limited. Ideally, the aluminum phase should completely surround the nickel, perhaps by depositing aluminum on the starting powders, and future work should be concentrated on this.

3. Environment Effects on Ni_3Si Alloys

Ni_3Si alloys show environmental embrittlement when tested at intermediate temperatures (i.e., 600°C) in oxidizing environments. An important area for the Ni_3Si-base alloys is the influence of certain alloying additions, for example cerium, on the oxygen-induced embrittlement in tensile tests at ~600°C. Three Ni-19 at. % Si-3 at. % Cr doped with 0.0005, 0.01 and 0.02 at. % cerium were prepared by arc melting and drop-casting high purity metals. These alloy ingots were hot rolled and punched into sheet specimens for tensile testing in controlled environments. Tensile specimens were mechanically polished to 0.71-0.74 mm and then heat treated at 900°C for 22 h for maximizing the ordered $L1_2$ phase plus 600°C for 24 h for increasing the degree of long-range order.

The tensile properties of these Ce-doped Ni_3Si alloys were determined at temperatures to 900°C. Figure 1 is a plot of tensile elongation as a function of temperature in air. The ductility shows a trend of decrease with increasing temperature and reaches a

minimum around 600°C. The decrease is attributed to environmental embrittlement involving oxygen. The ductility increases sharply above 600°C. This is because the alloys are capable of rapid formation of silicon oxides at high temperatures. Cerium doping apparently does not result in improving the ductility at ambient and elevated temperatures. The alloy doped with 0.005% Ce shows a tensile ductility of only 5% at room temperature. The low ductility is apparently associated with moisture-induced hydrogen embrittlement. Cerium additions do not reduce the environmental embrittlement at room temperature. The ductility the alloy increased to was 11.2% when tested in vacuum at room temperature.

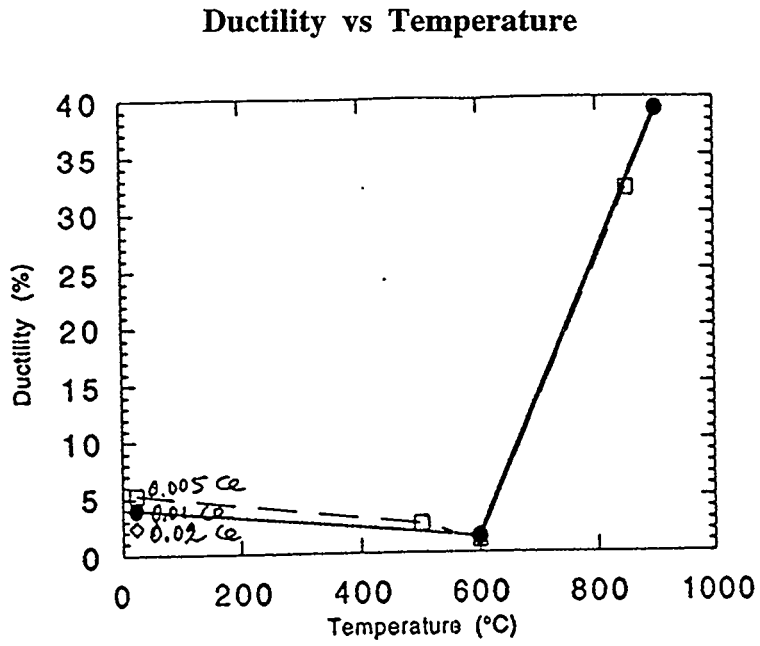

Fig. 1. The plot of tensile ductility as a function of temperature for Ni_3Si alloys doped with cerium.

MILESTONES DURING FY 1994

1. The milestone "complete improvement in the structure and properties of cast NiAl alloys" was completed in time and a summary letter was submitted in May, 1994.
2. The milestone "complete the feasibility study of reaction synthesis of nickel aluminide alloys" was completed by Prof. Norman S. Stoloff, and the topic report, "Reaction

Sintering of Aluminides," was submitted to ORNL on April 28, 1994. The conclusions of this study are (1) NAL-109 can be sintered to full density, provided that prealloyed powders were used to dampen the exothermic reaction, and (2) IC-221M provided unsatisfactory results, with porosity and/or prior particle boundaries remaining after all sintering runs.

PUBLICATIONS

Many publications, presentations, and patents co-sponsored by the Office of Basic Energy Sciences, and the Office of Fossil Energy, Advanced Research and Technology Development Materials Program.

Journals

1. E. P. George, M. Yamaguchi, K. S. Kumar, and C. T. Liu, "Ordered Intermetallics," pp. 409-453 in *Ann. Rev. Mater. Sci.*, Vol. **24**, eds. M. C. Flemings and J. B. Wachtman, Annual Review, Inc., Palo Alto, CA, 1994.
2. C. T. Liu and J. A. Horton, "Effect of Refractory Alloying Additions on Mechanical Properties of Near-Stoichiometric NiAl," *J. Mater. Sci. Eng.* (in press) 1994.
3. C. T. Liu and J. O. Stiegler, "Aluminides: Nickel," pp. 1752-1760 in *Encyclopedia of Advanced Materials*, ed. M. C. Flemings, Pergamon Press, 1994.
4. C. T. Liu and K. S. Kumar, "Ordered Intermetallic Alloys Part I: Nickel and Iron Aluminides," *J. Met.* **45(5)**, 38 (1993).
5. K. S. Kumar and C. T. Liu, "Ordered Intermetallic Alloys Part II: Silicides, Trialuminides and Other Aluminides," *J. Met.* **45(6)**, 28 (1993).
6. E. P. George, et al., "Characterization, Processing and Alloy Design of NiAl-based Shape-Memory Alloys," submitted to *Mat. Characterization*, 1993.
7. K. Sukidi, C. C. Koch, and C. T. Liu, "The Oxidation of Ni_3Si-base Alloys," to be submitted to *Mat. Sci. and Tech.*, 1993.

8. M. Takeyama and C. T. Liu, "Elevated Temperature Environmental Embrittlement and Alloy Design of $L1_2$ Ordered Intermetallics," *J. Mater. Sci. Eng.* **A153**, 538-47 (1992).
9. P. A. Ferguson and C. T. Liu, "Cutting Operation and Cracking Behavior of FeAl (40% Al) Alloys," *Scr. Metall.* **26**, 1669 (1992).
10. E. P. George and C. T. Liu, "Brittle Fracture and Grain Boundary Chemistry of Microalloyed NiAl," *J. Mater. Res.* **5**, 254-762 (1990).
11. K. H. Hahn and K. Vedula, "Room-Temperature Tensile Ductility in Polycrystalline B2 NiAl," *Scr. Metall.* **23**, 7 (1989).
12. A. M. Venezia, C. M. Loxton, and J. A. Horton, "Temperature and Pressure Effects for Oxygen Adsorption and Oxidation of Ni_3Al Alloyed with Chromium and Zirconium," *Surf. Science* **225**, 195-205 (1990).
13. Y. Ren, G. Chen, and B. F. Oliver, "Determination of Lattice Site Location of Ga in TiAl," *Scr. Metall.* **25**, 249-54 (1991).
14. B. Kad and B. F. Oliver, "Effect of Nitrogen on a Stabilization/Nucleation in Ti-Al Phase Diagram," *J. Less Common Met.* (1990).
15. B. F. Oliver and B. Kad, "A Study of α/γ Peritectic Oscillations Using Containerless Liquid Directional Solidification of γ-TiAl Compositions," *J. Less Common Met.* **168**, 81-90 (1990).
16. B. F. Oliver, B. Y. Huang, and W. C. Oliver, "Containerless Growth of Large Single Crystals of TiAl," *Scr. Metall.* **22**, 1405-1408 (1988).

Books

1. Dongliang Lin and C. T. Liu, "Ordered Intermetallics," National Nature Science and Foundation of China, 1994.
2. R. Darolia, J. J. Lewandowski, C. T. Liu, P. L. Martin, D. B. Miracle, and M. V. Nathal, "Structural Intermetallics," TMS Publication, 1993.

3. C. T. Liu, H. Kunsmann, K. Otsuka, and Manfred Wuttig, "Shape-Memory Materials and Phenomena," MRS Publication, 1992.
4. C. T. Liu, et al., "Ordered Intermetallics–Physical Metallurgy and Mechanical Behavior," in *NATO Proceedings*, Kluwer Academic Publishers, Boston, MA, 1992.
5. C. T. Liu, F. H. Froes, and J. O. Stiegler, "Ordered Intermetallic Alloys," in 10th Edition of ASM Metals Handbook, 2, ASM International, Materials Park, OH, 1990.
6. C. T. Liu, et al., *High-Temperature Ordered Intermetallic Alloys III,* " **133**, ed., C. T. Liu, et al., Materials Research Society, Pittsburgh, PA, 1989.
7. *High-Temperature Aluminides and Intermetallics,* " eds. S. H. Whang, C. T. Liu, D. P. Pope, and J. O. Stiegler, The Metallurgical Society of AIME, Warrendale, PA, 1990.
8. *High-Temperature Aluminides and Intermetallics*, eds. S. H. Whang, D. P. Pope, and C. T. Liu, Elsevier Applied Science, New York, N.Y., 1992.

Conference Proceedings

1. C. T. Liu and J. A. Horton, "Effect of Refractory Alloying Elements on Mechanical Properties of Near Stoichiometric NiAl," to be published in Conference Proceedings, 1994.
2. E. P. George, et al., "Mechanical Behavior and Phase Stability of NiAl-Based Shape Memory Alloys," to be published in Proc. Shape-Memory Materials, 1993.
3. C. T. Liu, E. P. George, and C. G. McKamey, "Current Status of Research and Development on Nickel and Iron Aluminides," to be published in Proc. of High-Temperature Structural Intermetallics Symposium, SAMPE Conf., 1993.
4. D. S. Easton, C. T. Liu, J. A. Horton, E. P. George, and J. J. Campbell, "Processing and Characterization of Ni-Al-Fe-B Shape-Memory Alloy Wires Produced by Rapid Solidification," to be published in Proc. Shape-Memory Materials, 1993.

5. C. T. Liu, "Ni_3Al Aluminide Alloys," p. 365 in Proc. Structural Intermetallics, TMS Publication, 1993.
6. C. T. Liu, "Ni_3Al Aluminide Alloys," p. 365 in Proc. Structural Intermetallics, TMS Publication, 1993.
7. E. P. George, C. T. Liu, C. J. Sparks, M. Y. Kao, J. A. Horton, H. Kunsmann, and T. King, "Microstructure, Phase Stability, Mechanical Properties and Shape Memory Characteristics of Ni-Fe-Al-B Alloys," pp. 121-27 in *Shape Memory Materials and Phenomena—Fundamental Aspects and Applications,* eds. C. T. Liu, H. Kunsmann, K. Otsuka, and M. Wuttig, MRS, Pittsburgh, PA, 1992.
8. C. T. Liu, C. J. Sparks, J. A. Horton, E. P. George, and C. A. Carmichael, "Microstructural Features and Shape-Memory Characteristics of Melt-Spun Ni-Fe-Al-B Ribbons," pp. 169-76 in *Shape Memory Materials and Phenomena—Fundamental Aspects and Applications*, eds. C. T. Liu, H. Kunsmann, K. Otsuka, and M. Wuttig, MRS, Pittsburgh, PA, 1992.
9. J. A. Horton, E. P. George, C. J. Sparks, M. Y. Kao, O. B. Cavin, and P. Thoma, "Characterization of the Phase Transformations in the Shape Memory Alloy Ni-36 at. % Al," p. 61 in *Shape Memory Materials and Phenomena—Fundamental Aspects and Applications*, eds. C. T. Liu, H. Kunsmann, K. Otsuka, and M. Wuttig, MRS, Pittsburgh, PA, 1992.
10. K. Vedula, B. Boulogne, and K. H. Hahn, "Room Temperature Tensile Ductility in Polycrystalline B2 NiAl", p. 299 in *Materials Research Society Symposium Proceedings*, **133**, MRS, Pittsburgh, PA, 1989.
11. K. Vedula, and P. S. Khadkikar, "Effect of Stoichiometry on the Room-Temperature Tensile Ductility of B2 NiAl," pp. 197-218 in *High Temperature Aluminides and Other Intermetallics*, Proc. of the ASM/TMS Symposium, The Metallurgical Society of AIME, Warrendale, PA, 1990.

12. B. Kad, B. F. Oliver, P. M. Hazzledine, "Twinning Related Fractures in TiAl + Mn Alloys," pp. 201-9 in *Microstructural Science, Computer-Aided Microscopy and Metallography*, eds. T. Place, J. Braun, W. White, and G. Vender Voort, **18**, ASM International, Materials Park, OH, 1990.

13. B. Kad and B. F. Oliver, " A Study of Nitride Precipitation Sequence in Titanium Aluminide Melts", pp. 431-39 in *Microstructural Science, Computer-Aided Microscopy and Metallography*, eds. T. Place, J. Braun, W. White, and G. Vender Voort, **18**, ASM International, Materials Park, OH, 1990.

14. B. Kad and B. F. Oliver, "Compressive Deformation Behavior of TiAl + Mn Alloys," pp. 211-19 in *Microstructural Science, Computer-Aided Microscopy and Metallography*, eds.T. Place, J. Braun, W. White, and G. Vender Voort, **18**, ASM International, Materials Park, OH, 1990.

15. E. P. George, C. T. Liu, and J. L. Liao, "Mechanical Properties, Fracture Behavior and Grain-Boundary Chemistry of B-doped NiAl" pp. 375-380 in Materials Research Society Symposium Proceedings, **186**, MRS Pittsburgh, PA, 1991.

16. C. T. Liu, "Moisture-Induced Environmental Embrittlement of Ordered Intermetallic Alloys at Ambient Temperatures," pp. 321-34 in *Ordered Intermetallics – Physical Metallurgy and Mechanical Behavior*, ed. C. T. Liu, Kluwer Academic Publishers, Boston, MA, 1992 (in print).

17. B. Y. Huang, B. F. Oliver, and W. C. Oliver, "Compression Deformation Structures of Single Crystal TiAl," pp. 231-236 in Materials Research Society Symposium Proceedings, **133**, MRS Pittsburgh, PA, 1989.

18. W. C. Oliver and C. L. White, "The Segregation of Boron and Its Effect on the Fracture of an Ni_3Al-Based Alloy," pp. 241-246 in Materials Research Society Symposium Proceedings, **81**, MRS Pittsburgh, PA, 1987. .

19. B. Kad and B. F. Oliver, "Deformation Behavior of High Temperature Intermetallic TiAl Alloyed with Gallium," pp. 237-42 in Materials Research Society Symposium Proceedings, **133**, MRS Pittsburgh, PA, 1987.

Reports

1. C. T. Liu, J. A. Horton, E. H. Lee, and E. P. George, "Alloying Effects on Mechanical and Metallurgical Properties of NiAl," ORNL/TM-12200, June 1993.
2. C. T. Liu, V. K. Sikka, and C. G. McKamey, "Alloy Development of FeAl Aluminide Alloys for Structural Use in Corrosive Environments," ORNL/TM-12199, February 1993.
3. W. C. Oliver and C. T. Liu, "Improving the Mechanical Properties of Alloys Based on Ni_3Si," ORNL topical report, to be published in 1992.

Oral Presentations

1. C. T. Liu, "Ni_3Al Aluminide Alloys," TMS International Symposium on Structural Intermetallics, September 26-30, 1993.
2. C. T. Liu, "Elevated Temperature Environmental Embrittlement and Alloy Design of $L1_2$ Ordered Intermetallics," ASM Conference on High-Temperature Aluminides and Intermetallics, San Diego, CA, September 1991.
3. E. P. George, et al., "Mechanical Behavior and Phase Stability of NiAl-Based Shape-Memory Alloys," Shape-Memory Materials Symposium, IUMRS-ICAM-93, Aug. 31-Sept. 4, 1993.
4. D. S. Easton, C. T. Liu, J. A. Horton, E. P. George, and J. J. Campbell, "Processing and Characterization of Ni-Al-Fe-B Shape-Memory Alloy Wires Produced by Rapid Solidification," Shape-Memory Materials Symposium, IUMRS-ICAM-93, August 31-Sept. 4, 1993.
5. J. A. Horton, E. P. George, C. J. Sparks, M. Y. Kao, O. B. Cavin, and P. Thoma, "Characterization of the Phase Transformations in the Shape Memory Alloy Ni-36 at. % Al," 1991 Fall Meeting of the MRS, Boston, MA, December 1991.

6. C. T. Liu, C. J. Sparks, J. A. Horton, E. P. George, and C. A. Carmichael, "Microstructural Features and Shape-Memory Characteristics of Melt-Spun Ni-Al-Fe-B Ribbons", 1991 Fall Meeting of the MRS, Boston, MA, December 1991.
7. E. P. George, C. T. Liu, C. J. Sparks, M. Y. Kao, J. A. Horton, H. Kunsmann, and T. King, "Microstructure, Phase Stability, Mechanical Properties, and Shape Memory Characteristics of Ni-Fe-Al-B Alloys", 1991 Fall Meeting of the MRS, Boston, MA, December 1991.
8. E. P. George and C. T. Liu, "Grain Boundary Chemistry and Fracture Behavior of NiAl," Joint ASM/TMS Symposium on High Temperature Aluminides and Intermetallics, Indianapolis, IN, October 1989.
9. K. Vedula, "Effect of Stoichiometry on the "Room Temperature Tensile Ductility of B2 NiAl," joint ASM/TMS Symposium on High-Temperature Aluminides and Intermetallics, Indianapolis, IN, October 1989 (in press).
10. C. T. Liu and E. P. George, "Ductility and Fracture Behavior of NiAl Alloys," 14th Annual Conference on Composite Materials and Structures, Cocoa Beach, FL, January 1990.
11. C. T. Liu and E. P. George, "Ductility and Fracture in Microalloyed NiAl," 1990 TMS Annual Meeting, Anaheim, CA, February 1990.
12. E. P. George and C. T. Liu, "Chemistry of Grain Boundaries in Microalloyed NiAl," 1990 TMS Annual Meeting, Anaheim, CA, February 1990.
13. C. T. Liu and E. P. George, "Alloy Design of Ordered Intermetallics," 1990 Spring Meeting of the MRS, San Francisco, CA, April 1990.
14. C. T. Liu, "Moisture-Induced Environmental Embrittlement of Ordered Intermetallic Alloys at Ambient Temperatures," NATO Workshop on Ordered Intermetallics, Irsee, Germany, June 1991.

15. J. A. Horton, C. T. Liu, and C. G. McKamey, "Interfacial Structure and Properties of Ni_3Al Alloys and Composites," 1991 TMS Fall Meeting, Cincinnati, OH, October 1991.

HONORS AND RECOGNITIONS

1. C. T. Liu, Editor, Journal of Intermetallics, 1993.
2. C. T. Liu, "co-organizer of the TMS International Symposium on Structural Intermetallics, September 26-30, 1993.
3. C. T. Liu, co-organizer of the Shape-Memory Materials, IUMRS-ICAM-93, August 31-September 4, 1993.
4. C. T. Liu, co-organizer of the ASM International Symposium on High-Temperature Aluminides and Intermetallics, San Diego, CA, September 1991.
5. C. T. Liu, Director, NATO Advanced Research Workshop on Ordered Intermetallics - Physical Metallurgy and Mechanical Behavior, Irsee, Germany, June 1991 (to be jointly sponsored by NATO and DOE).
6. C. T. Liu, Chairman, TMS Alloy Phase Committee, 1991.
7. C. T. Liu, Principal Editor, *Journal of Materials Research*, 1990.
8. C. T. Liu, Co-Organizer of the ASM Symposium on Ordered Intermetallic Alloys - Physical Metallurgy and Mechanical Behavior, Detroit, MI, October 1990.
9. J. A. Horton, Co-Organizer of the EMSA Symposium, "Intermetallic Alloys," San Antonio, TX, August 1989.
10. C. T. Liu, Co-Organizer of the ASM/TMS Joint Symposium, "High-Temperature Aluminides and Other Intermetallics," Indianapolis, IN, October 1989.

PATENTS/DISCLOSURES

1. C. T. Liu, *Development of NiAl Alloys for Structural Applications*, patent disclosure, 1993.

2. C. T. Liu, C. G. McKamey, P. F. Tortorelli, and S. A. David, *Corrosion Resistant Aluminides Exhibiting Improved Mechanical Properties and Corrosion Resistance*, U.S. Patent No. 5,320,802, June 1994.
3. C. T. Liu, *Cast Nickel Aluminide Alloys for Structural Applications*, U.S. Patent No. 5,108,700, 1992.

LICENSES

None

INDUSTRIAL INPUT AND TECHNOLOGY TRANSFER

We had several contacts with General Motors (GM), General Electric (GE), NASA, Pratt & Whitney, Memory Metals, Cummins Engine Company and Metallamics to discuss the potential use of NiAl-base and TiAl-base alloys for various industrial applications.

ESTIMATED ENERGY SAVINGS

1. The development of high-temperature aluminides and silicides will lead to improvement in performance (such as thermal efficiency, durability, etc.) of advanced energy conversion systems and heat engines, resulting in substantial energy saving.
2. High-temperature shape memory alloys have the potential to be used as new industrial materials in many energy-related control systems (such as sensors, actuators, HVAC systems, under-the-hood automobile application, heat engines for waste heat recovery, etc.). All these potential applications will lead to substantial energy saving.

DEVELOPMENT OF WELDABLE, CORROSION-RESISTANT IRON-ALUMINIDE ALLOYS

P.J. Maziasz, G.M. Goodwin, and X.L. Wang

Metals and Ceramics Division
Oak Ridge National Laboratory
P.O. Box 2008, Oak Ridge TN 37831

INTRODUCTION

Corrosion-resistant, weldable FeAl alloys have been developed with improved high-temperature strength industrial applications. Previous processing difficulties with these alloys led to their evaluation as weld-overlay claddings on conventional structural steels to take advantage of their good properties now. Simplified and better processing methods for monolithic FeAl components are also currently being developed so that components for industrial testing can be made. Other avenues for producing FeAl coatings are currently being explored. Neutron scattering experiments to measure residual stress distributions in the FeAl weld-overlay cladding began in FY 1993 and continued this year.

TECHNICAL PROGRESS - FY 1994

Summary

1. Weldability of FeAl Alloys:

Weldability data on the FA-385 series of alloys (the FA-385-M1 through -M11 series) were reported last year. The most weldable FeAl alloys were the FA-385M1 and -385M2 alloys (micro-additions of boron), and the -385M3 and -385M9 alloys (minor additions of chromium and niobium). The best alloys show threshold hot-cracking stresses comparable to or better than type 316 austenitic stainless steel. Larger (15 lb) heats of these alloys were cast into cylinderical extrusion-billet ingots (FA-385, -385-M1 and -385-M2), and were extruded at 900°C and a 3:1 reduction ratio into rod stock to produce mechanical properties specimens (hot-extrusion data reported in the other FeAl project summary). The remainer of this material was further extruded into wire for use as weld consumables, as described below.

In FY 1994, several more large (15 lb) heats of these three Fe-36Al alloys (FA-385 type) and three new modified Fe-30Al alloys were also melted to produce rectangular ingots for evaluating the properties, including weldability, of as-cast material.

2. Weld-Overlay Cladding Applications:

FeAl alloys can find near-term industrial applications as weld-overlay cladding on existing, code-approved structural steels and alloys. Feasibility was demonstrated earlier by making small FeAl weld-deposits onto a type 304L austenitic stainless steel substrate the weldable FA-385 alloy. During FY 1993 and FY 1994, many more weld pad desposits were made to test a series of new, weldable FeAl alloys (FA-385-M1 through -M11) on a type 304L stainless steel substrate. Some of these new FeAl alloys were also weld-deposited onto a 2¼Cr-1Mo bainitic steel substrate. No hot-cracking during weld-deposition was observed, but all of the FeAl alloys exhibited some degree of delayed cold-cracking during cooling for cladding tests made on type 304L stainless steel. A second series of tests with 200°C preheat, but no post-weld heat-treatment, showed that FA-385 and the FA-385-M1, -M2 and -M3 and -M9 alloys could be used to produced single-layer weld pads on the 304L substrate that were crack-free. Similarly, single-pass weld-overlay deposits of the FA-385 alloy onto the 2¼Cr-1Mo bainitic steel substrate also showed no delayed cold-cracking with preheat only.

The FA-385-M1 alloy was used to produce multiple-layer GTA weld-deposits on thicker (25.4 mm) substrates of 304L austenitic stainless steel and 2¼Cr-1Mo bainitic/martensitic steel. The FeAl weld-deposits made onto the 304L steel substrate all showed some surface cold-cracking in the fusion zone even with a preheat of 200°C, and a postweld heat-treatment of 400°C. Good, crack-free weld-deposits of FA-385-M1 on 2¼Cr-1Mo steel, however, were obtained with a preheat of 200°C, a minimum interpass temperature of 350°C, and a postweld heat-treatment of 800°C (followed by furnace cooling). This data demonstrated that FeAl weld-overlay cladding on 2¼Cr-1Mo steels can be made.

3. FeAl Filler-Wire Development

In FY 1993, FeAl filler-wire (FA-385-M1 with 36 at.% Al) for GTA welding was produced at ORNL by extrusion of the large (6.83 kg) cylinderical heat of that material (clad in mild steel) at 1000°C to a final wire diameter of 3 mm. While adequate for feasibility studies, the next step was to producing weld filler-wires commercially.

Efforts to develop weld-consumables using commercial or commercially-viable processes also began in FY 1993 and continued in FY 1994. Previously, Devasco International, Inc. (Houston, TX) began developing shielded-metal-arc (SMA) electrodes, formulated on the FA-385 FeAl base alloy composition, and those electrodes were received for testing at ORNL. While these new SMA electodes exhibited excellent welding characteristics, the aluminum content of the final weld-deposit was much lower than intended, which caused both hot- and cold-cracking problems.

Another effort to produce filler-metal rods was initiated with Haynes International (Kokomo, IN) last year and expanded during FY 1994. Three heats of a nearly optimized FeAl alloy composition, selected from the weld-deposition characteristics of the previous FeAl alloys on 2¼Cr-1Mo steel, were aspiration-cast into quartz tubes to produce 0.125 in diameter weld wires. The weld-compositions, based on or related to the weldable FA-385, FA-385-M1, and FA-385-M2 alloys, are given in Table 1. These aspiration-cast FeAl filler-wires initially contain more than the final target FeAl alloy composition of 36 at.% Al, in order to compensate for the loss of Al that occurs during the welding process. The compositions of final FeAl weld-deposits made with the various weld-wires are also give in Table 1.

Several large single-layer GTA weld deposits of FeAl were made onto a 2¼Cr-1Mo steel substrate using the Haynes wires (Haynes I and II), and found to be completely free of cold-cracks, using a 200°C preheat and a high-temperature post-weld heat-treatment, with furnace cooling. These initial FeAl Haynes wire weld deposits have been removed from the substrate for chemical analysis and for oxidation testing. Corrosion testing of a weld-clad deposit of FeAl (Haynes I) together with an optimized Fe_3Al alloy

(wrought FAS, currently the best Fe_3Al for high-temperature sulfidation resistance) show that both iron-aluminides behave about the same in a highly sulfidizing environment at 800°C (Fig. 1). To further define the useful range of alloying elements for FeAl clads, a second generation of filler-wires was produced both at ORNL (ORNL I-01, I-02, I-03, II-01, II-02 and II-03) and at Haynes International (Haynes III-01 and III-02) using the same aspiration-casting technique. Weld-overlay test deposits made with the ORNL I series of alloys onto 2¼Cr-1Mo steel substrates using the previously established preheat, interpass and post-weld heat-treatments experienced severe hydrogen cracking. Weld-overlays made with the ORNL II series of alloys that vary the aluminum content of the alloys from 20-30 wt.% Al (Table 1) were made on 2¼Cr-1Mo and on 9Cr-1MoVNb steels. The wire with 20 wt.% Al initially produced crack-free desposits, whereas the deposits produced with higher Al-content wires showed severe cold-cracking. The crack-free deposit, however, had only 11.9 wt.% Al, which is not adequate for corrosion resistance. Crack-free weld-overlay deposits onto 2¼Cr-1Mo steel were made using both compositions of the third series of wires obtained from Haynes (Haynes III-01 and III-02, with 30 wt.% initial Al), confirming the first results obtained with the Haynes I series wires. The commercial wire results are reproducible and superior to those obtained using laboratory wires.

Additional wires with 25 wt.% initial Al will be ordered from Haynes in FY 1994. These metal filler-wires can also be used as core-wire to produce SMA electrodes for a CRADA between ORNL and Devasco, International, Inc. In FY1995, weld-overlay clads with Haynes wires will also being made onto a type 316 austenitic stainless steel substrate that is relevant to MOLTOX reactor vessel applications or to corrosion-resistant components required by the pulp-and-paper industry. The weld-overlays will also be made on curved plate and piping to better represent realistic industrial component geometries. The successful FeAl weld-overlay results on 9Cr-1MoVNb steel are also directly applicable to MOLTOX vessel and piping applications and to fossil-energy boiler-tubing applications. These weld-wires can also be used to join monolithic FeAl components, or steel piping clad with FeAl. Successful weld-overlays

onto various steel substrates are also a preliminary indication that dissimilar metal joints could be made between FeAl components and such steels.

4. FeAl Powder for Powder-Extrusion or Plasma-Spray Coatings

Due to the good weldability of the FeAl base-alloy (FA-385) composition, and its good room-temperature mechanical properties in the extruded condition, gas-atomized powder of that alloy composition was obtained from AMETEK (Eighty-Four, PA) (400 lb heat) in FY 1994. The powder is spherical -100 mesh, with most particles being 75-175 γm. Some finer 5-17 γm particles are also present. Currently this powder is being extruded as-received to test its consolidation behavior and properties as a function of extrusion conditions. The mechanical properties of extruded PM FeAl will be determined in FY 1995, and extrusion conditions will be chose to produce FeAl coatings on type 304 or 316 austenitic stainless steel tubing. Similarly, FeAl coatings can be produced by plasma- or flame-spraying the powder, and such coatings will be examined and compared with the other FeAl coating/cladding methods.

5. Residual Stress Measurements in FeAl Weld-Overlay Cladding

Unique neutron diffraction methods are being used to help answer some of important questions about cold-cracking in the FeAl weld-overlay cladding effort. Neutron diffraction is being used to measure residual stresses and their distributions in the weld-clad and in the base-metal substrate. Special specimens were made using the weldable FeAl/FA-385-M1 alloy (ORNL extruded filler-wire) to produce a large (75mm × 84mm × 3mm) single-pass GTA weld-clad deposit onto a normalized-and-tempered 2¼Cr-1Mo steel plate (Fig. 2). The weld-overlay clad deposit was produced using a 200°C preheat and a 700°C post-weld heat-treatment, with furnace cooling to prevent cracks. Optical examination revealed that the weld clad was crack-free.

Residual strains have been mapped in the ferrite base-metal underneath the FeAl clad, using the

neutron diffraction system at the High Flux Isotope Reactor (HFIR) at ORNL. The beam sampling volume was 8 mm^3 [$(2\ mm)^3$]. Elastic strains have been mapped in the steel substrate parallel and perpendicular to the welding direction in the plane of the cladding, and normal to the FeAl clad/steel interface. The in-plane strains in the center of the steel were fairly isotropic, and similar in directions parallel and perpendicular to the welding direction. The ferritic base-metal substrate showed compressive in-plane strains. New measurements showed tensile normal strain in the steel underneath the cladding, which means the base-metal is pushing up slightly on the FeAl cladding above it.

Preliminary experiments have also been performed to directly measure the strains in the FeAl weld-clad itself. One neutron-scattering difficulty encountered was that the grain size of the FeAl weld-clad was quite large. A larger grain size causes the neutron scattering intensity of the particular reflection of interest to vary strongly with position in the specimen. Another difficult was the thinness of the FeAl clad, which reduces the magnitude of the absolute strain. Both in-plane and normal strains were measured at several locations within the FeAl clad. Consistent with the strain measurements made in the steel substrate, the FeAl clad showed measurable tensile in-plane strains, but negligable normal strain.

During FY 1994, more comprehensive analysis was performed of the stain data collected earlier. Three-dimensional maps of the principle strains in the steel substrate were discussed last quarter. This quarter, the strain data was converted to stress, using Young's modulus (E) and Poisson's ratio (ν) of E=200 GPa and ν=0.3 for the ferritic steel, and assuming E=180 GPA and ν=0.3 for the FeAl clad. These results indicate that while the compressive residual stress in the steel is low (<150 MPa), the tensile residual stress in the FeAl is quite high (430 MPa ± 140 MPa, see Fig. 3), very close to the yield strengths measured for a variety of FeAl alloys (see tensile data in the other FeAl contribution to this report). These results are very important in resolving some of the mystery surrounding the cold-cracking behavior observed during weld-deposit testing. Hydrogen, while certainly a critical factor, is not the only factor determining cold-cracking. FeAl with composition/microstructure/oxide characteristics producing zero

ductility and a fracture-stress of <350 MPa probably always cold-cracks, whereas FeAl with such characteristics that produce 1-3% ductility, YS>430 MPa and UTS >550-600 MPa is most likely resistant to cold-cracking. Work during FY 1995 will include further analysis of these neutron diffraction data, finite-element-modeling (FEM) analysis of the stress/strain evolution during the various processing (welding plus heat-treatment) steps, and production of additional neutron-scattering specimens.

MILESTONES DURING FY 1994

AIM Program FY 1994 Milestone - 94CC-59: Prepare FeAl weld-overlay coatings on steel substrates, determine residual stress profiles, and develop predictive model for industrial geometries, and prepare draft publication or report.

This milestone was completed by preparing the draft of a paper for opened literature publication entitled "Development of FeAl Weld-Overlays on Steels and Measurements and Modeling of Residual Stresses," by P.J. Maziasz, G.M. Goodwin, X.L. Wang, S. Spooner, C.R. Hubbard, Z. Zeng and T. Zacharia on August 31, 1994.

PUBLICATIONS

Journals

1. P.A. Ferguson and C.T. Liu, "Environmental Embrittlement and Cutting Cracks in FeAl(40% Al)." *Scripta Metallurgica et Materialia*, 26 (1992) 1669-1674.

2. P.J. Maziasz, G.M. Goodwin, C.T. Liu and S.A. David, "Effects of Minor Alloying Elements on the Welding Behavior of FeAl Alloys for Structural and Weld-Overlay Cladding Applications," *Scripta Metallurgica et Materialia*, 27 (1992) 1835-1840.

3. C.G. McKamey, P.J. Maziasz, G.M. Goodwin and T. Zacharia, "Effects of Alloying Additions on the Microstructures, Mechanical Properties and Weldability of Fe_3Al-Based Alloys," accepted for publication in *Materials Science and Engineering* Journal in 1993.

Other Publications

1. C.T. Liu, "Moisture-Induced Environmental Embrittlement of Ordered Intermetallic Alloys at Ambient Temperatures," NATO Proc. *Ordered Intermetallics - Physical Metallurgy and Mechanical Behavior*, eds. C.T. Liu, R.W. Cahn and C.T. Santhoff, NATO ASI Series vol. 213, Kluwer Academic Publishers (1992) pp. 321-334.

2. P.F. Tortorelli and P.S. Bishop, "Corrosion of Aluminides in Molten Nitrate Salt," submitted for publication in Proc. *Symp. Environmental Effects on Advanced Materials,* TMS, Warrendale, PA, 1991 (in press).

3. G.M. Goodwin, C.G. McKamey, P.J. Maziasz and V. Sikka, "Weldability of Iron Aluminides," Proc. of the 7th Annual Conference on Fossil Energy Materials, CONF-9305135, ORNL/FMP-93/1 (July, 1993) pp. 181-188.

4. G.M Goodwin, P.J. Maziasz, C.G. McKamey, J.H. DeVan and V.K. Sikka, "Weldability of Iron Aluminides," Proc. of the 8th Annual Conference on Fossil Energy Materials, CONF-9405143, ORNL/FMP-94/1 (August 1994) pp. 205-210.

PRESENTATIONS

Oral Presentations

1. G.M. Goodwin, C.G. McKamey, P.J. Maziasz and V. Sikka, "Weldability of Iron Aluminides," presented at the 7th Annual Conference on Fossil Energy Materials, sponsored by the Fossil Energy (AR&TD) Materials Program, US-DOE, held in Oak Ridge, TN on May 11-13, 1993.

2. P.J. Maziasz, G.M. Goodwin, X.L. Wang, S. Spooner, C.R. Hubbard, Z. Zeng and T. Zacharia, "Development of FeAl Weld-Overlays on Steels and Measurements and Modeling of Residual Stresses," paper presented at the Symposium on Interfacial Phases, Structure and Properties, held during Materials Week 1995, Rosemont, IL, October 2-6, 1995.

HONORS AND AWARDS

None

PATENTS/DISCLOSURES

1. C.T. Liu, C.G. McKamey, P.F.Tortorelli and V.K. Sikka, "FeAl Aluminides for Structural Use," invention disclosure, ESID No. 726-X; DOE patent case No. S-70469.

2. P.J. Maziasz, G.M. Goodwin and C.T. Liu, "High-Temperature Corrosion-Resistant Iron-Aluminide (FeAl) Alloys Exhibiting Improved Weldability," invention disclosed to the ORNL Patent Section of Martin Marietta Energy Systems, Inc. on August 27, 1993. It was selected by MMES for technology-transfer potential and a U.S. Patent application was prepared in August, 1994.

LICENSES

None

INDUSTRIAL INPUT and TECHNOLOGY TRANSFER

Air Products was interested in Fe_3Al and FeAl alloys for the MOLTOX process several years ago. They built a pilot plant as well as tested FeAl alloys in a molten nitrate/nitride salt environment. Air Products participated in meetings and in alloy development with ORNL and with Timken.

Work began with Devasco International, Inc. of Houston, TX in FY 1993 for the development of shielded-metal-arc (SMA) electrode formulations for the FA-385 FeAl type alloy composition. Such production of weld-electrodes is an important step in enabling FeAl for weld-overlay cladding applications or any other application that involves welding. A CRADA to develop SMA electrodes was signed with Devasco in FY 1994.

Work also began in FY 1993 with Haynes International (Kokomo, IN) to produce filler-metal weld wires via aspiration casting methods based on the most weldable FA-385 series alloy compositions. Weld wires of several compositional variants have been produced and weld-overlay cladding deposits have been made to test these alloys. Initial results are good, and analysis and evaluation of the weld-clad test pads is in progress. Production of weld wires with Haynes will continue, both to directly support the weld-overlay studies and to provide core wires to develop SMA electrodes in the CRADA with Devasco.

Efforts to commercially develop weld-consumables is also directly relevant to the development of castable FeAl alloys, because casting defects are usually repaired by welding as well. Commercial FeAl powder production by AMETEK Specialty Metal Products Division, Eighty-Four, PA, is being evaluated to enable other kinds of FeAl coating technology (ie. powder extrusion) to be developed.

COST SHARING

Timken and Latrobe are estimated to have spent about 150 $K on melting and processing of FeAl alloys. Air Products contributed about 150 $K in their testing efforts on FeAl alloys.

ESTIMATED ENERGY SAVINGS

The high-temperature strength of FeAl alloys has been shown to be signifanctly better than type 316 stainless steel at 650-750°C. This, combine with their inherent oxidation resistance, can improve the energy efficiency of a variety of systems. FeAl alloys have unique corrosion-resistance to molten salts (sodium nitrate salts at 650°C, and sodium carbonate salts at 900°C) that will enable applications that not possible with conventional materials. Improved high-temperature strength, good weldability and sufficient room-temperature ducility of as-cast material saves significant processing energy relative to heavily processed and heat-treated materials. FeAl has a density of only 5.7-6 g/cm^3, and which can be important for large structures at high-temperatures as well as advanced automotive applications. These FeAl alloys have good weldability, so them can be considered for weld-overlay cladding on conventional structural steels and alloys, or applications that require joining to similar or dissimilar metals.

HIGHLIGHTS

WELDABLE FEAL ALLOYS CAN BE USED AS WELD-OVERLAY CLAD ON STEELS - Recent work has shown that weldable FeAl alloys, with appropiate welding-technique modifications, can be used to produce overlay weld-deposits on commercially available structural steel substrates. Hydrogen cold-cracking has been a problem that must be overcome for this technique to be used in industry. Neutron diffraction methods were used to measure residual strains in FeAl weld-overlay cladding on 2¼Cr-1Mo steel, and finite-element-method (FEM) modeling was used to understand the data. These analysis tools showed that the FeAl weld-clad deposit had a tensile stress state while the steel underneath was in compression. The residual stresses in the steel are small, primarily due to stress-relaxation that takes place during post-weld heat-treatment at 700°C. The residual stresses in the FeAl weld-clad, however, are substantial and close to the yield strength of that material. They arise due to the mismatch in thermal expansion between the FeAl and the steel as they cool together after the post-weld heat-treatment. This knowledge should help to design better welding methods to produce crack-free weld-deposits.

Table 1 - Compositions of Developmental FeAl Cast Filler-Metals

Wire and description		Composition (wt.%) Al	Cr	Nb	Ti	Mo	Zr	C	B	Comments
ORNL Weldable FeAl Alloy Reference Materials										
FA-385		21.1				0.42	0.1	0.03		
FA-385M1		21.1				0.42	0.1	0.03	0.0025	
FA-385M2		21.1				0.42	0.1	0.03	0.005	
FA-385M3		21.1	2.3			0.42	0.1	0.03		
FA-385M4		21.1		1.0		0.42	0.1	0.03		
Haynes Wires, aspiration-cast, 0.125 in. diam.										
I-01,	aim	30	5	0.5	0.5	0.25	0.2	0.1		
	actual	31.2	3.3	0.5	0.7	0.3	0.2	0.12	0.007	
	weld-deposit	21.2	2.9	0.4	0.4	0.5	0.2	0.13	0.007	no cracks
(1 pass, 2¼Cr-1Mo)										
I-02,	aim	30	5	0.5	0.5	0.25	0.2	0.1	0.0025	
	actual	31.3	3.2	0.5	0.7	0.3	0.2	0.12	0.009	
	weld-deposit	26.8	3.2	0.4	0.5	0.4	0.2	0.12	0.012	
(2 passes, 2¼Cr-1Mo)										
I-03,	aim	30	5	0.5	0.5	0.25	0.2	0.1	0.005	
	actual	31.5	3.5	0.5	0.6	0.3	0.2	0.11	0.017	
	weld-deposit	26.2	3.2	0.4	0.4	0.4	0.2	0.11	0.015	2nd layer cracked
(2 passes, 2¼Cr-1Mo)										
Haynes Wire, aspiration-cast, 0.25 in diam.										
II,	aim	30	7	0.6			0.2	0.1		
	actual	27.3	7	0.6			0.25	0.13		
	(weld deposits were not made because the wire was too brittle to use)									
ORNL Wire, aspiration-cast, 0.125 in. in diam.										
I-01,	aim	30					0.2	0.1	0.005	
	weld-deposit on 2¼Cr-1Mo and 304L steels									cracked
I-02,	aim	30	7				0.2	0.1	0.005	
	weld-deposit on 2¼Cr-1Mo and 304L steels									cracked
I-03,	aim	30				0.4	0.1	0.1	0.005	
	weld-deposit on 2¼Cr-1Mo and 304L steels									cracked

Table 1 - Compositions of Developmental FeAl Cast Filler-Metals (continued)

Wire and description		Composition (wt.%) Al	Cr	Nb	Ti	Mo	Zr	C	B	Comments
II-01,	aim	30	5	0.1	0.1	0.2	0.2	0.1	0.005	
	actual weld-deposit on 2¼Cr-1Mo, 9Cr-1MoVNb and 304L steels									cracked
II-02,	aim	25	5	0.1	0.1	0.2	0.2	0.1	0.005	
	actual weld-deposit	18	1.6			0.6	0.1			cracked
(1 pass on 2¼Cr-1Mo, 9Cr-1MoVNb and 304L steels)										
II-03,	aim	20	5	0.1	0.1	0.2	0.2	0.1	0.005	
	actual weld-deposit	11.9	2.2	0.1		0.5	0.1			no cracks
(1 pass on 2¼Cr-1Mo, 9Cr-1MoVNb and 304L steels)										
		Haynes Wires, aspiration-cast, 0.156 in. in diam								
III-01	aim	30	7	0.6	0.5	0.25	0.2	0.1		
	actual weld-deposit									no cracks
(1 pass, 2¼Cr-1Mo steel)										
III-02	aim	30				0.4	0.1	0.03		FA-385 repeat
	actual weld-deposit									no cracks
(1 pass, 2¼Cr-1Mo steel)										

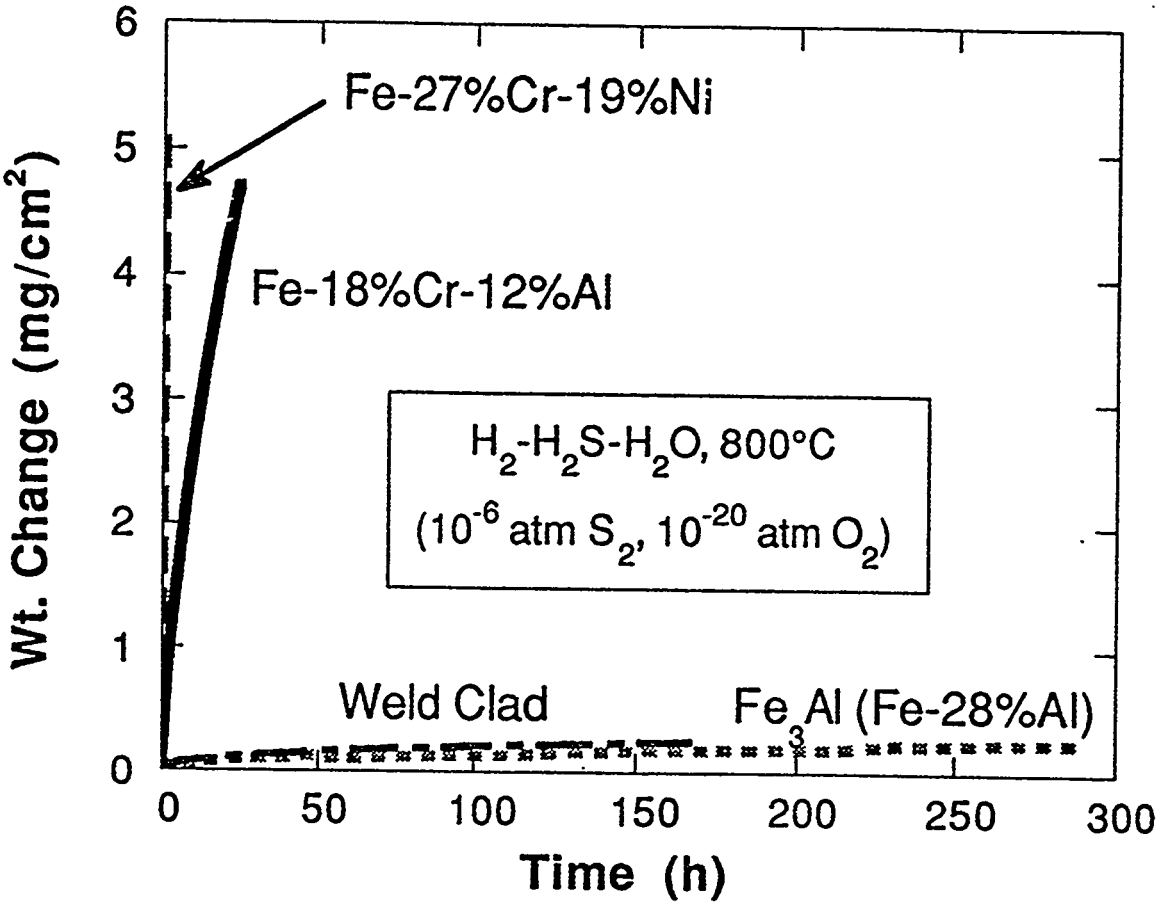

Figure 1. Corrosion test data of weight gain as a function of exposure time in highly sulfidizing gases at 800°C to simulate a coal gas environment. The weld-clad specimen is an FeAl weld-deposit made with Haynes I-01 wire on a 2¼Cr-1Mo steel substrate, and cut off for testing.

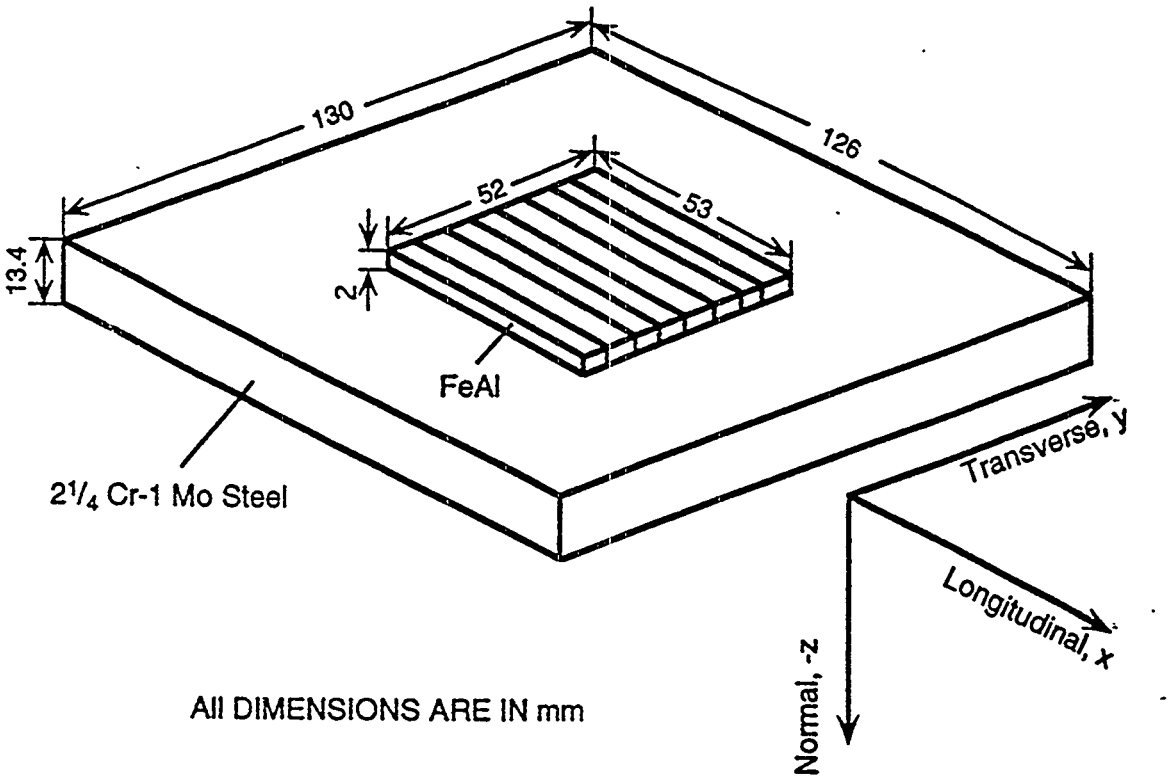

Figure 2. A schematic drawing of the FeAl weld-overlay on 2¼Cr-1Mo steel specimen used for neutron-diffraction measurements of residual stress analysis.

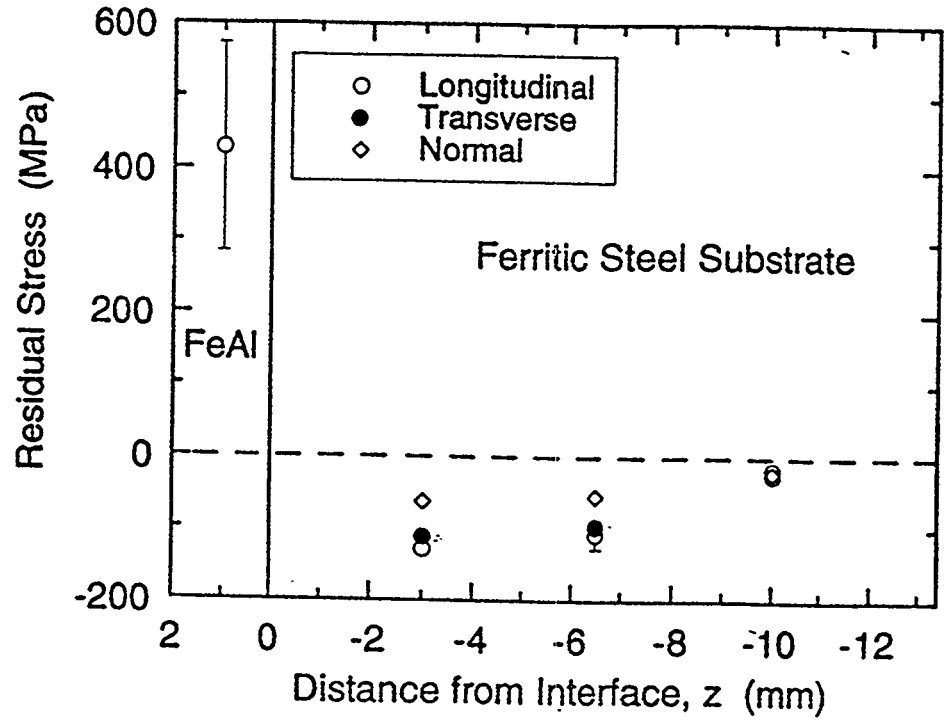

Figure 3. Residual stress in the longitudinal direction as a function of depth in the FeAl weld-overlay cladding and in the 2¼Cr-1Mo steel substrate. Stresses are calculated from the actual strains measured using neutron-diffraction techniques, as described in-text.

Ni_3Al TECHNOLOGY TRANSFER

V. K. Sikka, M. L. Santella, and D. J. Alexander

Metals and Ceramics Division
Oak Ridge National Laboratory
P. O. Box 2008
Oak Ridge, Tennessee 37831

P. R. Howell and W. A. Pratt

The Pennsylvania State University
Department of Materials Science and Engineering
University Park, Pennsylvania 16802

R. P. Martukanitz

Applied Research Laboratory
P.O. Box 30
State College, Pennsylvania 16804

INTRODUCTION

Ductile Ni_3Al and Ni_3Al-based alloys have been identified for a range of applications. These applications require the use of material in a variety of product forms such as sheet, plate, bar, tubing, piping, and castings. Although significant progress has been made in the melting, casting, and near-net-shape forming of nickel aluminides, some issues still remain. These include the need for (1) high-strength castable composition for turbochargers, furnace furniture, and hot-die applications; (2) castability (fluidity, hot-shortness, porosity, etc.); (3) weld reparability of castings; and (4) hot fabricability of cast ingots. All of the issues listed above can be "show stoppers" for the commercial application of nickel aluminides. This report describes work completed to address some of these issues during the fourth quarter of FY 1994.

TECHNICAL PROGRESS

Summary

A nickel-aluminide composition with a stronger oxidizing element than zirconium was identified. This composition showed no reaction with the shell material during investment casting of the test bars and turbochargers at PCC Airfoils, Inc. (Douglas, Georgia). The composition is known as DC-221HP. Three large heats of this composition were procured from Cannon Muskegon Corporation (Muskegon, Michigan). Several batches of turbochargers were cast from these large heats as melt stock. The turbochargers were supplied to Cummins Diesel (Columbus, Indiana) for friction welding and engine testing. The friction welding has been completed at Holset Engineering Company, Inc. (a division of Cummins) [Madison, Indiana]. The engine testing has yet to begin pending the availability of equipment.

As part of a General Motors-Saginaw Division (GM-Saginaw) [Saginaw, Michigan] Cooperative Research and Development Agreement (CRADA), testing continued on the nickel-aluminide coupons in both the batch and pusher carburizing furnaces. The coupons were removed periodically and evaluated for microstructural changes at ORNL. Results of the microstructural evaluations were presented to GM-Saginaw at quarterly review meetings. In addition to test coupons, testing continued on a nickel-aluminide tray along with an HU tray in a production batch carburizing furnace. Further casting trials of trays, fixtures, and posts also continued at Alloy Engineering & Casting Company (Champaign, Illinois), the primary supplier of furnace components for GM-Saginaw.

A significant effort was made towards solidification modeling of nickel-aluminide test bars and trays. The solidification modeling results revealed the insights into the metal flow into the mold and potential areas to watch for casting defects.

Two weld wire compositions (IC-221W and IC-221LA) were identified for both welding and weld repair of nickel-aluminide castings. Two 100-lb batches of weld wire were procured from a commercial vendor. The weld wire measuring 1/16 and 1/8 in. diam

are available to use at ORNL and for potential new application development at industrial locations. The evaluation of hydrogen embrittlement during laser welding of nickel-aluminide alloys was completed at The Pennsylvania State University.

Many interactions occurred with industry. The most significant interactions were with Cummins Engine Company, Inc. (Columbus, Indiana); PCC Airfoils; GM-Saginaw; Alloy Engineering & Casting; Rapid Technologies, Inc. (Newnan, Georgia); Metallamics, Inc. (Traverse City, Michigan); Sandusky International (Sandusky, Ohio); The BIMAC Corporation (Dayton, Ohio); B.C. Industries, Inc. (Kalamazoo, Michigan); Steeltech Ltd. (Grand Rapids, Michigan); Ametek Specialty Metal Products Division (Eighty Four, Pennsylvania); Ford Motor Company (Detroit, Michigan); Bethlehem Steel-Burns Harbor Plant (Burns Harbor, Indiana); and Weirton Steel (Weirton, Pennsylvania).

Milestones

1. Optimize alloy composition/casting parameters to reduce casting defects. Start 10/93, End 9/94.

The IC-221M alloy is the high-strength, castable alloy optimized for its castability through a joint program between ORNL, PCC Airfoils, and Cummins. One of the nagging problems in the use of IC-221M alloy for production-quantity turbochargers has been the surface reaction between the alloy and the ceramic shell material. A closely coordinated joint program between ORNL, PCC Airfoils, and Cummins has made significant progress to eliminate the surface reaction during this year. Detailed metallography and microprobe analysis have confirmed that the reaction is from the oxidation of zirconium in the alloy to ZrO_2. The extent of reaction is dependent on the zirconium content of the alloy. No reaction is observed for zirconium content of $\leq$0.85 wt %. However, the lower zirconium content also introduces porosity in the casting. A further examination revealed that the reaction can be reduced by: (1) eliminating the grain refiner, (2) minimizing the contact time at $\geq$1000°C between the casting and the shell, and (3) controlling the zirconium

content of the alloy. All three approaches were investigated. For each approach, ORNL supplied the melt stock. The test bars were cast at PCC Airfoils, and who also conducted the initial metallography with follow-up metallography and fatigue testing performed at ORNL. The metallography and fatigue data were used to make decisions for the follow-up experimental condition.

The IC-221M alloy composition was modified by the addition of a stronger oxidizer than zirconium to eliminate the surface reaction. After several casting trials, metallography, and mechanical properties testing, a composition designated as IC-221HP was been identified to be free of reaction with the mold shell material. This composition not only eliminates the reaction with the shell material but also gives optimum mechanical properties, with fatigue properties still significantly better than the currently used alloy IN-713C .

A set of turbochargers were cast from the IC-221HP composition. The turbochargers showed no surface reaction and an acceptable level of microporosity. However, some shrinkage of porosity was observed in the hub section of the turbocharger. The shrinkage of porosity in the hub section was eliminated by a slight modification of the mold and pouring temperatures. A large batch of alloy IC-221HP was procured from Cannon Muskegon Corporation. The alloy cast was paid for by Cummins. The melt stock prepared by Cannon Muskegon Corporation was cast into several sets of turbochargers. A few turbochargers that were examined metallographically confirmed the results of the experimental heats with commercially melted larger batch of IC-221HP. A set of turbochargers of IC-221HP were supplied to Cummins for engine testing at Holset Engineering Company, Ltd. (Huddersfield, England). The turbochargers were successfully friction welded to the connecting rod. However, the engine testing is awaiting the availability of the test rigs.

2. Castability of nickel aluminides, Start 10/93, End 9/94.

A computer software was procured to model the mold design for proper mold filling with minimum shrinkage areas. The software was used for solidification modeling

of test bars and heat-treating trays for GM-Saginaw. The computer modeling results were shared with GM-Saginaw and Alloy Engineering & Casting who is casting the trays and fixtures for GM-Saginaw. The modeling work has received high praise from GM-Saginaw and Alloy Engineering & Casting.

3. Weld reparability of castings, Start 10/93, End 9/94.

Efforts continued in several areas which include: (a) optimization of filler-wire composition for weld repair of sand castings and the fabrication of components, (b) obtaining commercial quantities of weld wire of selected compositions, (c) preparation of weld overlays, (d) preparation of simulated welds and training, and (e) weld metal mechanical properties. Significant progress has been made in all of these areas, and a brief highlight for each activity is listed below:

A. Optimization of Filler-Wire Composition for Weld Repair of Sand Castings and the Fabrication of Components. The previously developed filler-wire composition (IC-221W) was found to produce cracks during the weld repair of castings, especially under severe restraint conditions. At this point, it was identified that limited high-temperature ductility of IC-221W was the primary cause for such cracking. In order to improve the ductility, a filler wire of lower aluminum content was identified. This composition is known as IC-221LA and contains sufficient aluminum to provide the desired oxidation and carburization resistance needed for many applications. This composition has sufficient ductility to not only prevent weld cracking but also to allow its wire fabrication through normal ingot metallurgy route. A patent disclosure was submitted for the new composition.

B. Obtaining Commercial Quantities of Weld Wire of Selected Compositions. The encapsulating of prealloyed powder in a nickel strip has been identified as the most economical method for the fabrication of nickel-aluminide weld wire of both IC-221W and IC-221LA compositions. The powder compositions are properly compensated for in the nickel content of the strip. Using this method, spools of 1/8- and 1/16-in.-diam wire of

IC-221W weighing 25 lb each were procured from Ametek Specialty Metal Products Division (Eighty Four, Pennsylvania). The performance of the wire produced by this method was so good that an additional 50 lb of the 1/16-in.-diam wire in two 25-lb spools are currently on order. Since the performance and the price of the IC-221W were so good by the prealloyed encapsulation method, 100 lb of the IC-221LA wire were also procured from Ametek.

C. *Preparation of Weld Overlays.* The availability of 1/16-in.-diam wire has made possible the automated, high-deposition-rate weld deposits of IC-221W and IC-221LA compositions. The initial trials have shown that up to 1/4-in.-thick layers of IC-221W composition can be successfully weld-overlay deposited on base materials such as mild steel, 2-1/4Cr-1Mo, 9Cr-1Mo, steel, and type 304 stainless steel. The success of weld overlays opens up an opportunity of using nickel aluminides as high-quality and inexpensive coatings on other materials to take advantage of their oxidation and carburization resistance. Metallography and hardness testing of the weld overlays was completed.

D. Preparation of Simulated Welds and Training. The roller assemblies manufactured as part of Metallamics' CRADA at Sandusky required a great deal of welding. In order to minimize problems during commercial fabrication, several steps were taken at ORNL. The first step was to obtain a 4-in.-long ring from each of the centrifugally cast pipe from Sandusky. Sections were cut from one of the rings to machine-weld configurations that simulated the actual assembly design. The welding of the sections from the ring was carried out to finalize the weld-wire composition and the welding parameters. The IC-221LA composition was identified as the best filler-wire composition and gas tungsten arc as the best welding method. The IC-221LA wire for this application was prepared at ORNL through the making of the ingot, extrusion, and cold-swaging process combinations. The wire was produced in 3/32- and 1/8-in.-diam sizes. Sufficient wire was produced for the welding of two roller assemblies.

The welding technology including the process parameter and weld-wire requirements were transferred to Sandusky through two visit by the welder experienced in welding nickel aluminide at ORNL. The major step in transferring the welding technology was to train Sandusky in the use of the gas tungsten arc process as opposed to the stick electrode process that is used frequently in industry. The welder at Sandusky was sufficiently trained to weld repair some defects that were observed in the trunnion shaft during machining.

E. Weld Metal Mechanical Properties. During the filler-wire optimization, sheets were fabricated from four different compositions. Tensile tests were conducted on specimens from the sheets at temperatures ranging from room temperature to 1000°C. The composition with the best combination of strength was chosen for the fabrication of weld wire and the welding trials.

4. Hot workability of IC-218LZr, Start 10/93, End 9/94.

The IC-218LZr alloy is selected for use as aerospace fasteners and for other applications where cast components cannot be used. It is essential that a commercial source be developed for the production of wrought product from this alloy. One possible route for commercial rod can consist of casting 3- to 4-in.-diam ingots, encapsulating the ingots in a mild steel can, and hot extruding to a ratio exceeding 16:1. The hot-extrusion temperature for the alloy is 1100°C. The extrusion ratio of 16:1 results in a complete breakdown of cast structure into an equiaxed, fine-grain structure. The bar produced is machined or acid cleaned to remove the can. The procedure just described was used commercially for a 100-lb batch of IC-218LZr. The bar produced could be cold swaged to different sizes.

Although the procedure described above has been used, a commercial source for bar needs to be established. This source needs to coordinate the activities of an ingot producer, extruder, machining, and cold working. Efforts continued to establish such a source.

5. Hydrogen embrittlement during laser welding of nickel-aluminide alloys. Start 10/93, End 9/94.

The progress made during the first year of study of hydrogen embrittlement during laser welding of nickel aluminide is outlined below:

Examination of the base IC-221M, IC-221W, IC-396M, and IC-396W alloys confirmed that the Ni_5Zr eutectic constituent was presented in all of the castings. Microhardness testing showed that the centers of the 25- × 25- × 75-mm castings were significantly softer than the outer edges. This variation in hardness was attributed to a transition from columnar to equiaxed grains found near the centers of the castings.

Welds produced by ORNL with metal-powder-cored wire of the IC-221W composition were analyzed in some detail. Weld deposits were made with as-fabricated wire, and with wire which had been vacuum heat treated in an effort to reduce possible contamination from undesirable trace elements such as hydrogen. Weld beads made with both wires cracked in a similar manner, and both exhibited similar microstructures. The appearance of the cracks was consistent with a solidification cracking mechanism, and all were associated with zirconium enrichment, as found in previous studies. Indications about a possible influence of hydrogen on the cracking were inconclusive. Initial laser-beam welding indicated that there was no evidence of hydrogen-assisted cracking under ambient conditions.

During the second quarter of FY 1994, studies at The Pennsylvania State University focused on four areas of experimentation: (1) final development of the cathodic hydrogen charging parameters, (2) calibration of the welding fixture and final welding parameter adjustments, (3) development of nondestructive evaluation procedures for measuring cracking severity in the welds, and (4) homogenization of the EDM samples.

Results from experiments in the first quarter of FY 1994 indicated that insufficient levels of hydrogen were present in the material after charging. It was uncertain whether the charging parameters were inadequate. In order to determine which was the case, another

sample was charged and tested as soon as possible after charging. As in the previous quarter, it was noted that the charging process darkened the surface of the sample. The dark surface layer was thought to be an iron compound. This determination was made by removing some of the surface layer with a file and examining the filings. The filings were found to be magnetic. The iron may have been dissolved from the anodic stainless steel beaker and deposited on the cathodic sample, or, the iron may have originated from the wire used to suspend the sample in the beaker.

It was anticipated that this dark layer may affect laser beam absorption during welding and may affect cracking susceptibility. In fact, this was the case. During the first quarter of FY 1994, experiments indicated that laser coupling efficiency may be lower on samples with the iron surface layer. Laser welding parameters that produced full penetration welds on the clean EDM samples did not produce full penetration welds on the samples with the dark surface layer. It was decided that the best way to alleviate this problem was to carefully remove the dark layer from the surface. The surface layer was easily removed using wet 600 grit SiC paper. This process removed only the surface layer, so the hydrogen levels in the material should not be affected.

In continuing experiments, the charging time and voltage were increased to attain a hydrogen level approximately equal to that of the powder cored filler wire. A single sample was charged for 3000 min as in previous experiments, and immediately packed in dry ice and transported to UEC Analytical Chemical Laboratory (Monroeville, Pennsylvania) for hydrogen analysis. Prior to testing, the dark surface layer was removed by filing and cleaning with acetone. The results of these tests were nearly equivalent to the prior results indicating that no diffusion of hydrogen out of the material occurs. Further samples were tested without removing the dark surface layer. These samples produced hydrogen levels greater than the cleaned samples. A consequence of the charging process is a higher level of hydrogen near the surface than near the center of the sample. It was speculated that the filing removes a significant amount of the surface material, and hence, a large portion of the

hydrogen in the sample. The results of these experiments indicated that a longer charging time was required to attain a hydrogen level of 12.5 ppm as found in the powder cored filler wire during the first quarter of FY 1994. Another sample was charged for 12 h at 4.5 V and 1.84 A, and tested using the same technique. A hydrogen level of 11.75 ppm was achieved. This is comparable to the 12.51-ppm level found in the powder-filled welding wire.

The second area of work was the calibration of the welding fixture. The strain bolts acquired from Omega Engineering, Inc. (Stamford, Connecticut) were calibrated for much higher loads than necessary for our experiments. In order to ensure accurate measurement of the load applied during welding, the bolt was recalibrated using an Instron tensile tester. A fixture, as developed to ensure a uniaxial load, was applied to the strain bolt. The bolt was connected to the data acquisition system so that the entire system would be calibrated. Various loads were applied to the strain bolt, and the output (in millivolts) was recorded. These data were then plotted to establish a calibration curve for small loads. This calibration curve, including the experimental and calculated calibration points from Omega, is included below as Figure 1. From this curve, we were able to derive a second order polynomial equation to fit the low-load data points. This equation was used to determine the required millivolt output for a desired load on the sample.

In addition to calibration of the welding fixture, the laser welding parameters were adjusted to fine tune the welding. It was believed that the prior welds were not completely representative of an efficient laser weld. In order to narrow the weld, the travel speed was increased to 2.5 cm/s, and shielding as was reduced to 60 CFH helium. Preliminary welds were produced using the welding fixture to apply a transverse stress to the sample. Initial welds were stressed to 10 ksi; however, these welds simply pulled apart during welding. The stress was reduced to approximately 5.1 ksi, and the welding speed was increased.

The increased welding speed resulted in a weld penetration depth of approximately 80% of the plate thickness. Although this was not a full penetration weld, it allowed us to

test the data acquisition system in practice. A sample of the data attained during welding is included below as Figure 2. These data illustrate the drop in stress during welding followed by the gradual in stress which occurs during cooling. In further experiments, the stress will be reduced to 2 ksi, and full penetration welds will be produced.

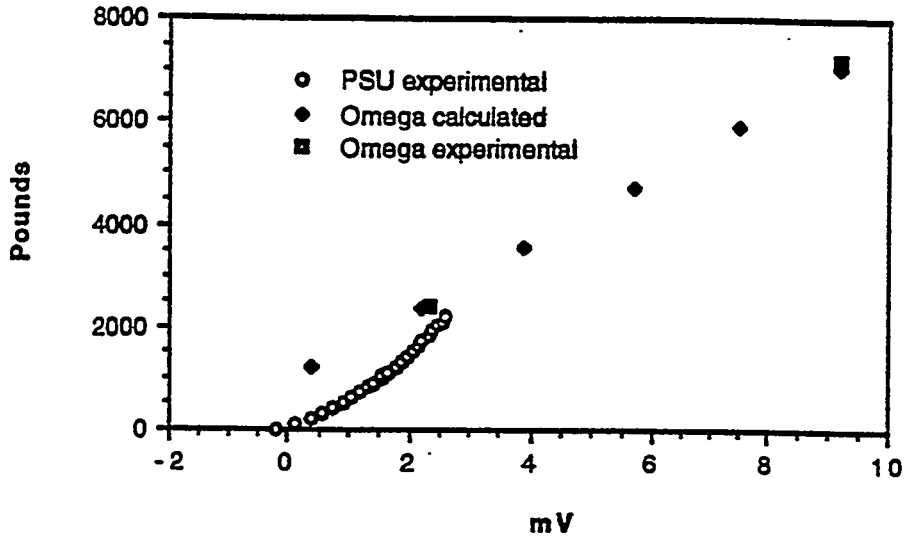

Figure 1. Calibration curve for the Omega strain bolt.

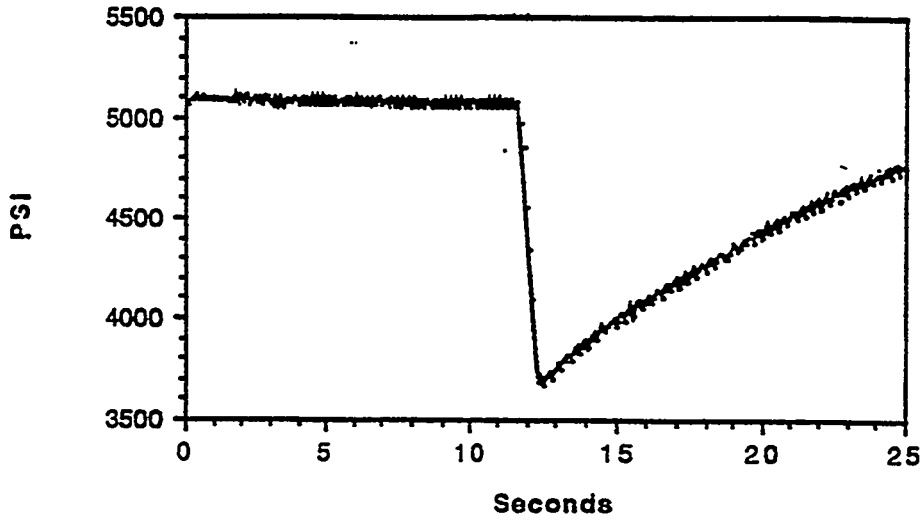

Figure 2. Data acquired during autogeneous laser welding of alloy IC-221M.

The third area of work was experimentation with nondestructive evaluation techniques for locating cracks in the material after welding. In the final welding experiments it will be necessary to quantify the number of cracks in each weld that is produced. Hence, it was necessary to find a technique that would accurately, inexpensively, and quickly reveal cracks in the material. Four techniques were examined: (1) visual inspection using a stereoscope, (2) dye-penetrant inspection, (3) radiographic analysis, and (4) C-scan ultrasonic imaging. Each powder cored filler wire weld, produced during the first quarter of FY 1994, was examined using each of these four techniques. The results were analyzed and compared. It was decided that dye-penetrant testing is the most acceptable technique. It offered quick and accurate analysis for surface cracks and porosity, and revealed cracks that were not observed during visual examination. Although both X-ray and ultrasonic testing revealed limited internal porosity, neither revealed cracks in the samples. This was thought to be a result of the "tightness" of the cracks. After the final welds were produced, each was examined using dye-penetrant testing. Each crack was examined to determine orientation, position, and overall crack length. These results were quantified and used as an indicator of the relative success of each weld.

The last area of experimentation was the attempted homogenization of the EDM specimens. As described in the first quarterly progress report, experiments were conducted to determine sufficient homogenizing parameters. The experiments indicated that annealing the material for at least 300 h at 1000°C would be adequate. During this reporting period, one sample of each composition was annealed in air for 312 h at 1000°C, and furnace cooled. As reported in the last quarterly report, high-temperature heat treatment resulted in the formation of a dark greenish oxide of the sample surface. This oxide was examined to determine its characteristics and the potential effects on weldability. Microhardness tests were performed on an inhomogeneous EDM sample, a homogenized sample with the oxide removed, and on the oxide itself. Although the homogenized sample appeared to be slightly softer than the inhomogeneous material, it was not a significant amount. Optical

microscopic examination of the surface revealed small clusters of what appeared to be triangular and irregularly shaped crystals. Research seemed to indicate that the oxide layer was Cr_2O_3. In order to alleviate any problem with weldability, the oxide layer will be removed by grinding the sample surface prior to welding.

6. Technology transfer activities. Start 10/93. End 9/94.

The purpose of this milestone was to undertake activities that will promote the transfer of nickel-aluminide technology to industry. These activities included visiting potential producers and users of materials and describing the technology in detail, training industry personnel either at ORNL or at the industrial facilities, and holding technology transfer meetings at ORNL. As a result of these activities, several additional applications have been identified for these materials.

Many interactions occurred with industry. The most significant interactions were with Cummins Engine Company, Inc. (Columbus, Indiana); PCC Airfoils; GM-Saginaw; Alloy Engineering & Casting; Rapid Technologies, Inc. (Newnan, Georgia); Metallamics, Inc. (Traverse City, Michigan); Sandusky; The BIMAC Corporation (Dayton, Ohio); B.C. Industries, Inc. (Kalamazoo, Michigan); Steeltech Ltd. (Grand Rapids, Michigan); Ametek Specialty Metal Products Division (Eighty Four, Pennsylvania); Ford Motor Company (Detroit, Michigan); Bethlehem Steel-Burns Harbor Plant (Burns Harbor, Indiana); and Weirton Steel (Weirton, Pennsylvania).

PUBLICATIONS

1. M. N. Srinivasan, S. Manjigani, A. Wofenden, and V. K. Sikka, "Elastic Moduli of Nickel and Iron Aluminides," *Proceedings of Seventh Annual Conference on Fossil Energy Materials*, Oak Ridge, Tenn., May 11-13, 1993.
2. V. K. Sikka and H. R. Shih, "Cold Rollability of A Ni_3Al-Based Alloy," 1994 (to be published).

3. R. M. Cooper, V. K. Sikka, and R. D. Noebe, "Mechanical Properties of Extruded NiAl Powder Produced by Reaction Synthesis," (to be published).
4. V. K. Sikka, "Processing of Intermetallic Aluminides," to be published in *Physical Metallurgy and Processing of Intermetallic Compounds*, ed. N. S. Stoloff and V. K. Sikka (Chapman & Hall, New York, NY, 1995).
5. V. K. Sikka, "Intermetallics for Structural Applications," to be published in *Corrosion and Oxidation of Intermetallic Alloys*, ed. G. Welsch and C. Y. Ho, (Purdue University, West Lafayette, Indiana, 1995).

PRESENTATIONS

1. M. N. Srinivasan, A. Wofenden, V. K. Sikka, and S. Manjigani, "Elastic Behavior of Iron and Nickel Aluminides," Seventh Annual Conference on Fossil Energy Materials, Oak Ridge, TN, May 11-13, 1993.
2. V. K. Sikka, "Nickel and Iron Aluminides for High-Temperature Aggressive Environments," Materials Week '93: Heat Resisting Materials Session II, Pittsburgh, PA, October 20, 1993.
3. V. K. Sikka, "Status of In-Service Testing of Ni_3Al Coupons in Batch Furnace," GM-Saginaw Nickel-Aluminide CRADA Review Meeting, Oak Ridge National Laboratory, Oak Ridge, TN, February 23, 1994.

PATENTS/DISCLOSURES

None.

LICENSES

A licensing agreement with Rapid Technologies, Inc. was signed.

COST INFORMATION

PERSONNEL INFORMATION

None.

INDUSTRIAL INPUT AND TECHNOLOGY TRANSFER

CRADA with GM-Saginaw on Use of Nickel Aluminides in Heat-Treating Furnace:

The nickel-aluminide tray has completed 12 months of testing in the batch carburizing furnace at GM-Saginaw. The tray has not shown any sign of damage and is expected to continue in test during 1995. The HU tray in test as a companion in the same furnace has undergone extensive surface cracking. Test coupons continued in test in the batch and pusher carburizing furnaces at GM-Saginaw. Test coupons were removed at several intervals from both the batch and pusher furnaces. All of the exposed coupons were metallographically examined, and the results were presented at the periodic meeting with GM-Saginaw and Alloy Engineering & Casting Company. Several casting trials continued. The pusher furnace tray, lower fixture, upper fixture, and posts have been cast at least five times during the year. Based on these results, the set of fixtures will be cast during February 1995, for test in the pusher furnace starting mid March 1995.

CRADA with Metallamics. The objective of the CRADA with Metallamics was to centrifugally cast the nickel aluminide for roller applications. Two centrifugally cast 14-1/2-in. OD by 1-in.-wall rollers, connected to sandcast trunnions of nickel-aluminide alloy IC-396M, were installed at Bethlehem Steel-Burns Harbor Plant during January 1994. The weld on one of the rollers had cracked after a service of four months. The weld was replaced with the pins and reinstalled in the furnace during July 1994. Both of the rolls are currently operating in the furnace under actual production conditions.

COST SHARING

A cost savings from industry during FY 1994 include: Cummins ($20K for production of melt stock of IC-221HP); Rapid Technologies ($100K in support of walking-beam rail manufacturing); Bethlehem Steel ($25K in support of roll manufacturing); and GM-Saginaw and Metallamics are 50:50 cost-share programs, and they have met their obligations.

PRECIPITATION-STRENGTHENING EFFECTS IN IRON-ALUMINIDES

P.J. Maziasz, C.G. McKamey, G.M. Goodwin, and R.W. Swindeman

Metals and Ceramics Division
Oak Ridge National Laboratory
P.O. Box 2008, Oak Ridge TN 37831

INTRODUCTION

The purpose of this work is to produce precipitation to improve both high-temperature strength and room-temperature ductility in FeAl-type (B2 phase) iron-aluminides. Previous work has focused on primarily wrought products, but stable precipitates can also refine the grain size and affect the properties of as-cast and/or welded material as well. New work began in FY 1994 on the properties of these weldable, strong FeAl alloys in the as-cast condition. Because the end product of this project is components for industry testing, simpler and better (cheaper, near-net-shape) processing methods must be developed for industrial applications of FeAl alloys.

TECHNICAL PROGRESS - FY 1994

Summary

1. Mechanical Properties Behavior - FeAl alloys:

Initial weldability studies (SIGMAJIG hot-cracking) narrowed a group of twelve FeAl alloys to three with the best weldability, namely the FA-385, FA-385-M1 and -M2 alloys. Mechanical properties testing, including tensile-testing at room-temperature (22°C) in various environments (air, vacuum and dry oxygen) (Table 1) and 600°C in air (Table 2), and creep-rupture testing at 600°C/207 MPa (30 ksi) (Table 3) were completed during FY 1994. The most weldable FeAl alloys, FA-385-M1 and -M2, were also the strongest at 600°C (Table 2), and had the best creep-strength at 600°C/207 MPa (Table 3), with rupture lives ranging from 260 to 430 h in the as-hot-rolled plus stress-relieved condition. These two heats of FeAl show creep-strength comparable to type 304 austenitic stainless steel.

All of these FeAl alloys had poor ductility in air at room-temperature in the as-hot-rolled condition, and heat-treatments did little to improve the ductility in air. Most specimens exhibited only a fracture stress with no plastic strain. However, visual inspection also revealed that hot-rolling induced cracks in the sheet-stock, and it is well known that moisture-induced embrittlement in air can be severe in FeAl alloys. Earlier we found a modest improvement in room-temperature ductility (1-2%) when identical FeAl specimens were tested in vacuum. Tensile tests at room temperature in dry oxygen eliminated hydrogen embrittlement effects, and revealed inherent plasticity ranging from 2-15% total elongation. When tested in oxygen, these alloys exhibited large effects of alloy composition and heat-treatment on ductility. As before, the most weldable alloys, FA-385, -385-M1, -385-M2 and -385-M3, also showed the best room temperature ductility in oxygen (>10%). Tensile tests in dry oxygen also revealed heat-treatment effects on the room temperature ductility that were not revealed in air. For hot-rolled (900°C) sheet, heat-treatment at 800-900°C produced the best ductility, whereas the best YS was found after heat-treatments of 900-1100°C. The FA-385-M1 and -M2 alloys had the highest YS (500-540 MPa).

Tensile testing at 600°C showed that heat-treatments at 1000-1050°C reduced the YS of FA-385-M1 and FA-385-M2 somewhat. Heat-treatments at 900-1050°C slightly reduced the creep-rupture lives of these alloys at 600°C/207 MPa (FA-385-M1 < FA-385-M2), while heat-treatments at 1100°C and above were worse for creep-rupture resistance.

In FY 1993, larger (15 lb) heats of the most weldable FeAl/FA-385 alloy compositions (FA-385, -385-M1, -M2, were made to determine scale-up effects. However, due to the very poor results during hot-rolling to produce thin sheet, these alloys were simply extruded at 900°C into rod-stock from which mechanical properties specimens were machined. Room-temperature tensile data for these specimens obtained during FY1994 are shown in Table 4, while tensile and creep data at 600°C are included in Tables 2 and 3, respectively. The as-extruded materials showed much higher strengths and ductilities

compared to the as-hot-rolled materials when tested in air (8-10%), and all were somewhat better when tested in dry oxgyen (12-14%). Extrusion produced a much finer, uniform grain size relative to the hot-rolled material (about 1 μm compared to 1-60 μm, respectively). Heat-treatment at 1200°C also improved the strength, but reduced ductility at room-temperature. However, as expected, the fine-grained as-extruded materials showed less creep-rupture strength and more strain-to-failure at 600°C. The extruded FeAl material and the machined round buttonhead specimens were more flaw-free relative to the hot-rolled material and punched sheet specimens. Extrusion is definitely one of the attractive simple fabrication methods for FeAl alloys.

2. Mechanical Properties Behavior - As-Cast FeAl alloys:

New work began during FY 1994 to produce larger (15 lb) heats of the B2-FeAl/Fe-30Al and /Fe-36Al alloys and to measure the ambient and high-temperature mechanical properties of as-cast material. The best FeAl/FA-385 alloy compositions found to date (weldability/ductility/strength) were chosen. This study included as-cast properties as well as heat-treatment effects on properties. Our plan for FY 1995 is to determine the effects of additional simple processing (ie. forging, extrusion) of as-cast material. Austenitic stainless steel components initially of interest to MOLTOX (molten salt pump impellor) were produced by casting. Critical components for the Kraft black-liquor recovery boilers in the pulp-and-paper industry are also made from cast austenitic stainless steels. Castable FeAl iron-aluminides are therefore an important alternate processing avenue that needs to be explored to enable industrial applications of FeAl.

At the beginning of FY 1994, as-cast ingots were cut into coupons from which large, round, threaded-shoulder mechanical properties specimens were machined. Room-temperature tensile data and higher-temperature creep data at 600°C/207 MPa were obtained on as-cast material during FY 1994 (Tables 5 and 6, respectively). In addition, some heat-treatment effects on room-temperature and elevated-

temperature properties were also measured.

Heat-treatment for 1h at 750°C increased the ductility (in oxygen) of the Fe-36Al alloys relative to as-cast materials, most likely by relieving residual stresses present after machining. A heat-treatment for 1h at 900°C made the alloys stronger at room-temperature, and slightly reduced their ductility. At 600°C, the FA-385 series alloys (Fe-36Al) were significantly stronger than the Fe-30Al alloys. The FA-385 series alloys maintained about the same YS found at room-temperature (see Fig. 1). A significant discovery this year was that the micro-additions of boron made these Fe-36Al alloys significantly stronger at 650-800°C than the boron-free alloy (FA-385) (Fig. 1). The YS is greater than 400 MPa at 700°C and does not significantly fall until above 750°C. Heat-treatments of 1h at 900°C and 1200°C did not have much affect on the YS of these alloys at 600°C.

Creep-rupture tests at 600°C/207 MPa showed the as-cast FA-385 alloy to have better creep-rupture resistance than wrought material (compare Tables 3 and 6), but rupture lifetime was only 11-12 h. The FA-385 alloys with micro-additions of boron had significantly better creep-rupture resistance in the as-cast condition relative to wrought material, especially the FA-385-M2 material (rupture lifetime - 674 h, minimum creep rate - 0.0025 %/h). Heat-treatment for 1h at 1200°C improved the creep resistance of the FA-385 base alloy slightly, but was not beneficial for the boron-doped alloys. The FA-385-M2 alloy with 50 wt.ppm B showed the least effect of heat-treatment at 1200-1250°C. The excellent combination of properties of the B-doped FeAl alloys in the as-cast condition makes them very attractive for such applications.

3. Phase/Structure/Fracture Studies:

Wrought FeAl sheet specimens tensile-tested in air at room temperature were shown last quarter to have a brittle transgranular cleavage fracture mode. The fracture mode after tensile testing at 600°C remains similar. The as-cast materials tested in air at room-temperature showed fracture initiation in a brittle-transgranular mode, but the remaining fracture was intergranular along the cast grain structure. In oxygen at room temperature, the fracture initiation portion becomes smaller and less brittle, consistent with the higher uniform elongation measured. The as-cast FeAl (FA-385 series) specimens tested this quarter at 600-800°C showed a mixture of ductile intergranular and transgranular-cleavage at 600-700°C, and exhibited purely transgranular ductile-dimple failure at 800°C. The specimens showed some necking at 600-750°C, and complete necking to a chisel-point failure at 800°C. These tensile properties suggest that processing in the ductile failure regime (ie. >850°C) should be good.

TEM and AEM examination of as-cast and of extruded specimens of the FA-385 series alloys reveals that they are entirely B2 phase without any detectable $D0_3$ (entirely non-magnetic). The as-cast specimens of FA-385M1 and -385M2 with micro-additions of boron contain significant concentrations of fine Zr-rich MC precipitates and 2-fold superdislocations within the grains, which may help explain both their room temperature YS/ductility and their elevated temperature strength. The as-extruded specimens of these same materials with recrystallized, fine-grained structures have almost no detectable fine precipitates and low matrix dislocation contents. These microstructural factors are consistent with the as-cast material being more creep-resistant than the as-extruded material at 600°C, while the as-extruded material is much more ductile at room temperature.

PUBLICATIONS

Journals

1. P.J. Maziasz and C.G. McKamey, "Microstructural Characterization of Precipitates Formed During High-Temperature Testing and Processing of Iron-Aluminide Alloys," *Materials Science and Engineering,*

A152 (1992) 322-334.

2. C.G. McKamey, P.J. Maziasz, and J.W. Jones, "Effects of Addition of Molybdenum or Niobium on Creep Rupture Properties of Fe_3Al," *Journal of Materials Research*, 7 (Aug., 1992) 2089-2106.

3. C.G. McKamey, P.J. Maziasz, G.M. Goodwin and T. Zacharia, "Effects of Alloying Additions on the Microstructures, Mechanical Properties and Weldability of Fe_3Al-Based Alloys," *Materials Science and Engineering A* 174, 59-70 (1994).

4. W.D. Porter and P.J. Maziasz, "Thermal Expansion Data on Several Iron- and Nickel-Aluminide Alloys," *Scripta Metallurgica et Materialia* 29 (1993) 1043-1048.

5. S. Viswanathan, C.G. McKamey, P.J. Maziasz and V. Sikka, "Tensile Properties of As-Cast Fe_3Al-Based Alloys," submitted to *Materials Science and Engineering A* in 1993.

Other Publications

1. P.J. Maziasz, C.G. McKamey and C.R. Hubbard, "Designing Precipitate-Strengthened Iron-Aluminides For High-Temperature Applications," Alloy Phase Stability and Design, eds. G.M. Stocks, D.P. Pope and A.F. Giamei, Mat. Res. Soc. Symp. Proc. Vol. 186, Materials Research Society, Pittsburg PA (1991) pp. 349-355.

2. P.J. Maziasz, C.G. McKamey, O.B. Cavin, C.R. Hubbard and T. Zacharia, "Some Effects of Composition and Microstructure on the $B2 \leftrightarrow D0_3$ Ordered Phase Transition in Fe_3Al Alloys," in High-Temperature Ordered Intermetallic Alloys-V, eds. I. Baker, R. Darolia, J.D. Whittenberger, and M.H. Yoo, Mat. Res. Soc. Symp. Proc. Vol. 288, Materials Research Society, Pittsburgh, PA (1993) p. 209.

3. C.G. McKamey and P.J. Maziasz, "Effect of Heat-Treatment Temperature on Creep-Rupture Properties of Fe_3Al-Based Alloys," pp. 147-58 in Processing, Properties and Applications of Iron Aluminides, eds. J.H. Schneibel and M.A. Crimp, TMS, Warrendale, PA (1994).

PRESENTATIONS

Oral Presentations

1. P.J. Maziasz, "Designing Precipitate-Strengthened Iron-Aluminides For High-Temperature Applications," Symposium on Alloy Phase Stability and Design, Spring 1990 MRS Meeting, San Francisco, CA, April 16-20, 1990.

2. C.R. Hubbard, "Phase Equilibria of Fe-28Al Alloys by High Temperature XRD," 39th Annual Denver X-ray Conference, Steamboat Springs, CO, July 30 - August 3, 1990.

3. P.J. Maziasz and C.G. McKamey, "Microstructural Characterization of Precipitates Formed During High-Temperature Testing and Processing of Iron-Aluminide Alloys," presented at the International Conference on High-Temperature Aluminides and Intermetallics, sponsored by ASM-International, held in San Diego, CA, Sept. 16-19, 1991.

4. O.B. Cavin, C.R. Hubbard and P.J. Maziasz, "High Temperature X-ray Diffraction Determination

of Phase Transitions in Large Grain Alloys," presented at Accuracy of Powder Diffraction II, held at NIST in Gaithersburg, MD, May 25-29, 1992.

5. W.D. Porter, P.J. Maziasz and J.A. Cook, "Physical Properties Measurements of Iron and Nickel Aluminide Alloys," presented at the Technology Transfer Conference and Workshop on Nickel and Iron Aluminides, held in Oak Ridge, TN, August 4-5, 1992.

6. P.J. Maziasz and W.D. Porter, "Physical Properties Measurements of Ni_3Al Alloys," oral presentation at the GM-Saginaw/ORNL CRADA (ORNL 92-0076) Meeting on Ni_3Al for Heat-Treating Assemblies, held at ORNL, Oak Ridge, TN, Nov. 9-10, 1992.

7. P.J. Maziasz, C.G. McKamey, O.B. Cavin, C.R. Hubbard and T. Zacharia, "Some Effects of Composition and Microstructure on the $B2 \leftrightarrow D0_3$ Ordered Phase Transition in Fe_3Al Alloys," poster presented at Symposium L - High-Temperature Ordered Intermetallic Alloys-V, Fall 1992 MRS Meeting, held in Boston, MA, Nov. 30 - Dec. 4, 1992.

8. C.G. McKamey, P.J. Maziasz and S. Viswanathan, "Microstructure and Fracture Behavior of As-Cast Fe_3Al-Based Ordered Intermetallic Alloys," poster presented at the International Metallographic Society Meeting in Charleston, SC, July 18-21, 1993.

9. C.G. McKamey and P.J. Maziasz, "Effect of Heat-Treatment Temperature on Creep-Rupture Properties of Fe_3Al-Based Alloys," presented at the Symposium on Processing, Properties and Applications of Iron Aluminides, held during the 1994 TMS Annual Meeting, San Francisco, CA, (Feb. 27 - Mar. 3, 1994).

10. P.J. Maziasz and C.G. McKamey, "Precipitation-Strengthening for Creep Resistance in Fe_3Al and FeAl Alloys," oral presentation at the 3rd International Conference on High-Temperature Intermetallics, held in San Diego, CA, May 16-19, 1994.

HONORS AND AWARDS

First Place - Scanning Electron Microscopy Catagory for the poster "Microstructure and Fracture Behavior of As-Cast Fe_3Al-Based Ordered Intermetallic Alloys," (C.G. McKamey, P.J. Maziasz and S. Viswanathan) presented at the International Metallographic Society Meeting in Charleston, SC, July 18-21, 1993.

PATENTS/DISCLOSURES

An invention disclosure was filed with Martin Marietta Energy Systems, Inc. (MMES) on "High-Temperature, Corrosion Resistant Iron-Aluminides Exhibiting Improved Weldability," (P.J. Maziasz, G.M. Goodwin and C.T. Liu) on August 27, 1993. It was selected by MMES for its technology-transfer potential, and a U.S. Patent application was filed in August, 1994. The new data obtained on improved high-temperature mechanical properties of weldable FeAl-type B2-phase alloys, particularly the as-cast material, was included as additional claims and combined with the above patent disclosure.

LICENSES

None

INDUSTRIAL INPUT and TECHNOLOGY TRANSFER

FeAl work was directly related to the MOLTOX project that was supported in the past by DOE and Air Products, Inc. as part of this program. This work is also connected to technology transfer efforts for iron-aluminides being pursued by ORNL/MMES. In FY 1993, the physical properties data on iron- and nickel-aluminides generated in this program were important input into CRADA's with General Motors (ie, GM-Saginaw AIM/CRADA on Ni_3Al). The specific FeAl alloys developed in this program have potential for metals processing applications (ie., hot dies, rolls, furnace furniture, etc.), pulp and paper applications due to their corrosion/erosion resistance, and may be good candidates for natural-gas burner nozzles in a wide variety of industrial applications due to their outstanding oxidation/sulfidation resistance. FeAl alloys are also 25% less dense than steels or nickel-base alloys, and could be beneficial for applications where lighter weight is a serious consideration.

COST SHARING

The Fossil (AR&TD) Materials Program has included extruded pieces of the FA-385 alloys for evaluation in a coal-liquifaction plant in joint testing between DOE and Japan.

ESTIMATED ENERGY SAVINGS

The high-temperature strength of FeAl alloys has been shown to be signifanctly better than type 316 stainless steel at 650-750°C. This, combine with their inherent oxidation resistance, can improve the energy efficiency of a variety of systems. FeAl alloys have unique corrosion-resistance to molten salts (sodium nitrate salts at 650°C, and sodium carbonate salts at 900°C) that will enable applications that are not possible with conventional materials. Improved high-temperature strength, good weldability and sufficient room-temperature ducility of as-cast material saves significant processing energy relative to heavily processed and heat-treated materials. FeAl has a density of only 5.7-6 g/cm^3, which can be important for large structures at high-temperatures, as well as advanced automotive applications. These FeAl alloys have good weldability, so they can be considered for weld-overlay cladding on conventional structural steels and alloys, or for applications that require joining to similar or dissimilar metals.

HIGHLIGHT

MICRO-ADDITIONS OF BORON TO FEAL ALLOYS SIGNIFICANTLY IMPROVES WELDABILITY AND HIGH-TEMPERATURE STRENGTH OF AS-CAST MATERIAL: New modified FeAl/Fe-36 at.%Al alloys have been developed with significantly improved weldability. The hot-cracking resistance during welding is comparable to that of type 316 austenitic stainless steel. Micro-additions of boron were found to improve the strength and ductility at room temperature, and to dramatically improve the strength at 600-750°C in the as-cast condition. At 600-750°C, these new FeAl alloys are almost 3 times stronger than type 316 stainless steel. These new FeAl alloys retain their outstanding oxidation/corrosion resistance to >1100°C, whereas type 316 oxidizes badly above 700°C.

Table 1 - Room Temperature Tensile Data on Wrought (hot-rolled) FeAl Alloys

Alloy	Fabrication/ Heat-Treatment Condition	Strength (MPa) Yield	Ultimate	Total Elongation (%)	Test Environment
FA-324	1h/800°C+1h/700°C	355	409	2.2	air
FA-385	1h/800°C+1h/700°C	336	519	4.4	air
	1h/800°C+1h/700°C	357	483	3.3	air
	HR/900°C+1h/800°C	404	755	13.5	oxygen
	HR/900°C+1h/900°C	450	782	10.5	oxygen
	HR/900°C+1h/900°C	337	337	<0.1	air
		440	440	<0.1	air
	HR/900°C+1h/1000°C	420	809	14.7	oxygen
	HR/900°C+1h/1000°C	417	465	1.8	air
		304	304	<0.1	air
		401	480	1.6	vacuum
	HR/900°C+1h/1050°C	481	481	<0.1	air
		464	521	0.9	vacuum
	HR/900°C+1h/1100°C	408	662	7.8	oxygen
FA-388	1h/800°C+1h/700°C	318	406	1.8	air
	1h/800°C+1h/700°C	315	355	1.3	air
	HR/900°C+1h/1000°C	434	434	<0.1	air
FA-385-M1	HR/900°C+1h/800°C	381	801	12.3	oxygen
	HR/900°C+1h/900°C	536	867	11.7	oxygen
	HR/900°C+1h/1000°C	439	703	7.5	oxygen
		518	518	<0.1	air
		511	566	1.5	vacuum
	HR/900°C+1h/1050°C	504	504	<0.1	air
		499	554	0.8	vacuum
	HR/900°C+1h/1100°C	518	826	10.1	oxygen
FA-385-M2	HR/900°C+1h/800°C	421	780	13.8	oxygen
	HR/900°C+1h/900°C	492	943	14.7	oxygen
		382	382	<0.1	air
	HR/900°C+1h/1000°C	508	663	3.8	oxygen
		467	533	2.0	air
		525	525	<0.1	air
		515	523	0.7	vacuum
	HR/900°C+1h/1050°C	198	198	<0.1	air
		519	596	2.3	vacuum
	HR/900°C+1h/1100°C	501	720	7.2	oxygen
FA-385-M3	HR/900°C+1h/800°C	339	739	14.1	oxygen
	HR/900°C+1h/900°C	512	812	8.7	oxygen
	HR/900°C+1h/1000°C	486	634	4.3	oxygen
		461	473	1.1	air
		192	192	<0.1	air
	HR/900°C+1h/1050°C	321	321	<0.1	air
		429	471	1.2	vacuum
	HR/900°C+1h/1100°C	448	720	8.4	oxygen
FA-385-M4	HR/900°C+1h/800°C	335	580	6.4	oxygen
	HR/900°C+1h/900°C	400	424	1.2	oxygen
	HR/900°C+1h/1000°C	359	395	1.2	air
		414	420	1.8	oxygen
	HR/900°C+1h/1100°C	383	539	3.9	oxygen
FA-385-M5	HR/900°C+1h/1000°C	340	364	0.8	air

Table 1 - (continued)

Alloy	Fabrication/ Heat-Treatment Condition	Strength (MPa) Yield	Ultimate	Total Elongation (%)	Test Environment
FA-385-M6	HR/900°C+1h/1000°C	339	339	<0.1	air
FA-385-M7	HR/900°C+1h/1000°C	325	342	2.0	air
FA-385-M8	HR/900°C+1h/1000°C	241	281	0.5	air
FA-385-M9	HR/900°C+1h/800°C	307	417	4.0	oxygen
	HR/900°C+1h/900°C	363	388	1.2	oxygen
	HR/900°C+1h/1000°C	221	221	<0.1	air
		342	342	<0.1	vacuum
		429	444	2.0	oxygen
	HR/900°C+1h/1100°C	246	246	<0.1	air
		380	560	5.1	oxygen
FA-385-M10	HR/900°C+1h/1000°C	349	358	0.6	air
FA-385-M11	HR/900°C+1h/1000°C	324	324	<0.1	air

Table 2 - Tensile Data on Wrought FeAl Alloys Tensile Tested at 600°C

Alloy	Fabrication/ Heat-Treatment Condition	Strength (MPa) Yield	Ultimate	Total Elongation (%)
FA-324	HR@900°C+1h/750°C	312	353	49.3
	1h/800°C+1h/700°C	332	394	20.1
FA-385	1h/800°C+1h/700°C	346	495	20.9
	HR@900°C+1h/750°C	400	493	11.0
	HR@900°C+1h/750°C	422	510	8.3
	HR@900°C+1h/750°C	389	481	10.1
	extruded/900°C+1h/750°C	413	471	41.4
	HR@900°C+1h/1000°C	357	451	14.6
		350	387	17.8
FA-388	1h/800°C+1h/700°C	359	475	9.3
	HR@900°C+1h/750°C	418	487	9.9
	HR@900°C+1h/1000°C	357	453	9.9
FA-385-M1	HR@900°C+1h/750°C	487	592	7.9
	HR@900°C+1h/750°C	481	558	5.6
	extruded/900°C+1h/750°C	437	518	40
	HR@900°C+1h/1050°C	364	382	1.1
FA-385-M2	HR@900°C+1h/750°C	484	555	8.2
	HR@900°C+1h/750°C	480	567	9.6
	extruded/900°C+1h/750°C	445	529	31.6
	HR@900°C+1h/1000°C	475	578	14.0
		408	468	1.3
FA-385-M3	HR@900°C+1h/750°C	478	542	2.1
	HR@900°C+1h/750°C	489	590	3.2
	HR@900°C+1h/1000°C	404	536	17.0
	HR@900°C+1h/1050°C	405	485	4.6
FA-385-M4	HR@900°C+1h/750°C	390	482	9.1
	HR@900°C+1h/750°C	395	503	6.9
	HR@900°C+1h/1000°C	370	476	14.7
FA-385-M5	HR@900°C+1h/750°C	416	521	11.4
	HR@900°C+1h/750°C	389	487	4.4
	HR@900°C+1h/1000°C	351	466	13.6
FA-385-M6	HR@900°C+1h/750°C	402	482	18.5
	HR@900°C+1h/750°C	401	477	12.2
	HR@900°C+1h/1000°C	333	449	10.7
FA-385-M7	HR@900°C+1h/750°C	398	482	24.5
	HR@900°C+1h/750°C	335	482	4.5
	HR@900°C+1h/1000°C	328	461	5.4
FA-385-M8	HR@900°C+1h/750°C	384	477	5.7
	HR@900°C+1h/750°C	369	473	4.1
	HR@900°C+1h/1000°C	365	475	9.1
FA-385-M9	HR@900°C+1h/750°C	379	458	13.2
	HR@900°C+1h/750°C	375	405	0.9
	HR@900°C+1h/1000°C	289	369	3.7
FA-385-M10	HR@900°C+1h/750°C	393	456	3.1
	HR@900°C+1h/750°C	420	521	3.3
	HR@900°C+1h/1000°C	397	535	7.5
FA-385-M11	HR@900°C+1h/750°C	347	447	3.4
	HR@900°C+1h/750°C	313	315	2.5

Table 3. Creep-rupture properties of new modified FA-385 FeAl-type alloys (wrought)

Alloy	Processing/Heat-Treatment Condition	Creep Conditions Temp. (°C)	Stress (ksi)	Rupture Time (h)	Elongation (%)	Minimum Creep-rate (%/h)
FA-385	HR-900°C/1h-750°C	600	30	11	62.8	1.7
		600	30	10.3	56.3	3.1
	HR-900°C/1h-900°C	600	30	4.5	35	4.1
	HR-900°C/1h-1000°C	600	30	8.8	38	3.0
		600	30	60	40	
		600	30	4.6	31	4.3
	HR-900°C/1h-1050°C	600	30	5.5	30	2.7
	HR-900°C/1h-1100°C	600	30	1	26.4	42
	HR-900°C/1h-1150°C	600	30	3.5	45	5.7
	HR-900°C/1h-1200°C	600	30	4	29	4.2
	HR-900°C/1h-1200°C	600	30	2.1	16.1	5.5
	extruded at 900°C	600	30	5.75	90	
FA-388	HR-900°C/1h-1000°C	600	30	7.8	47.5	3.7
		600	30	6.5	40.5	3.8
		600	30	4.4	9.2	2.25
FA-385 -M1	HR-900°C/1h-750°C	600	30	295.7	15.7	0.02
		600	30	434	14.5	0.01
	HR-900°C/1h-900°C	600	30	102	44	0.44
	HR-900°C/1h-1000°C	600	30	48	37	
		600	30	129	35	0.24
	HR-900°C/1h-1050°C	600	30	138.7	33	0.1
	HR-900°C/1h-1100°C	600	30	29	45	1.2
	HR-900°C/1h-1200°C	600	30	84.4	30.3	
	HR-900°C/1h-1250°C	600	30	54.1	23.4	
	extruded at 900°C	600	30	61.9	77	
FA-385 -M2	HR-900°C/1h-750°C	600	30	271	9.5	0.015
		600	30	267	16.3	0.015
	HR-900°C/1h-900°C	600	30	70	51	0.5
	HR-900°C/1h-1000°C	600	30	216.2	43	0.15
		600	30	165	45	0.2
		600	30	118	60	0.3
	HR-900°C/1h-1050°C	600	30	184	35.3	0.13
	HR-900°C/1h-1100°C	600	30	92	39	0.5
	HR-900°C/1h-1150°C	600	30	131	26.3	0.2
	HR-900°C/1h-1200°C	600	30	131	25.6	0.2
	HR-900°C/1h-1250°C	600	30	51.1	33.5	0.6
	extruded at 900°C	600	30	65		
	extruded at 900°C/1h-1200°C	600	30	292	48	0.081
FA-385 -M3	HR-900°C/1h-750°C	600	30	20.1	56.4	0.9
	HR-900°C/1h-1000°C	600	30	21.6	43.6	0.8
	HR-900°C/1h-1150°C	600	30	14.3	30.2	0.74
	HR-900°C/1h-1200°C	600	30	15.9	43.8	0.8
	HR-900°C/1h-1250°C	600	30	8.2	42.2	1.7

Table 3. (continued)

Alloy	Processing/Heat-Treatment Condition	Creep Conditions: Temp. (°C)	Creep Conditions: Stress (ksi)	Rupture: Time (h)	Rupture: Elongation (%)	Minimum Creep-rate (%/h)
FA-385 -M4	HR-900°C/1h-750°C	600	30	11.2	24.3	2.2
		600	30	16	32.5	1.4
	HR-900°C/1h/1000°C	600	30	17.8	20.1	0.7
	HR-900°C/1h-1150°C	600	30	17.6	28.1	0.6
	HR-900°C/1h-1200°C	600	30	18	21	1
	HR-900°C/1h-1250°C	600	30	16.6	9.4	0.2
FA-385 -M5	HR-900°C/1h-750°C	600	30	12.3	33	1.0
		600	30	26.3	32.4	0.6
	HR-900°C/1h-1000°C	600	30	19.2	27.6	2.2
FA-385 -M6	HR-900°C/1h-750°C	600	30	11.4	33.5	1.9
		600	30	13.1	38.8	1.6
	HR-900°C/1h-1000°C	600	30	8	36	2.3
FA-385 -M7	HR-900°C/1h-750°C	600	30	14.6	47	1.9
		600	30	8	29	2.3
	HR-900°C/1h-1000°C	600	30	7	23	1.9
FA-385 -M8	HR-900°C/1h-750°C	600	30	15.9	29	1.1
		600	30	5	12.3	1.3
	HR-900°C/1h-1000°C	600	30	20.3	23	0.55
FA-385 -M9	HR-900°C/1h-750°C	600	30	8.1	38.1	2.8
	HR-900°C/1h-1000°C	600	30	5.8	35.7	1.8
	HR-900°C/1h-1150°C	600	30	7.7	22.9	1.6
	HR-900°C/1h-1200°C	600	30	7	25.3	1.9
	HR-900°C/1h-1250°C	600	30	12.1	22.6	1.1
FA-385 -M10	HR-900°C/1h-750°C	600	30	24.4	35	0.8
	HR-900°C/1h-1000°C	600	30	58.6	27.6	0.2
FA-385 -M11	HR-900°C/1h-750°C	600	30	7.9	21.4	1.6
	HR-900°C/1h-1000°C	600	30	56	20	0.2

Table 4 - Room Temperature Tensile Data on Hot-Extruded FeAl Alloys

Alloy	Fabrication/ Heat-Treatment Condition	Strength (MPa) Yield	Ultimate	Total Elongation (%)	Test Environment
FA-385	extruded/900°C	426	900	12.5	oxygen
	+1h/750°C	412	759	8.4	air
	extruded/900°C +1h/1200°C	505	636	4.4	air
FA-385-M1	extruded/900°C	439	974	13.9	oxygen
	+1h/750°C	435	850	10	air
	extruded/900°C +1h/1200°C	502	656	4.5	air
FA-385-M2	extruded/900°C	429	910	11.8	oxygen
	+1h/750°C	436	861	10.2	air
	extruded/900°C +1h/1200°C	515	622	4.1	air

Table 5 - Room and Elevated Temperature Tensile Data on Cast FeAl Alloys

Alloy	Fabrication/ Heat-Treatment Condition	Test Temp (°C)	Strength (MPa) Yield	Ultimate	Total Elongation (%)	Test Environment
FA-385	as-cast	22	383	494	2.1	air
		22	403	504	2.4	air
		22	434	688	6.8	oxygen
		600	381	472	29.6	air
		650	330	352	54.7	air
		700	247	253	49	air
		750	173	185	50	air
	(+1h/1150°C)	800	87	93	88	air
	(+1h/750°C)	22	375	701	8.2	oxygen
	(+1h/900°C)	22	456	483	1.4	air
		22	465	494	1.8	air
		22	328	553	5.8	oxygen
	(+1h/900°C)	600	393	469	26.9	air
	(+1h/1200°C)	600	384	473	22.7	air
FA-385-M1	as-cast	22	422	509	2.2	air
		22	421	508	2.9	air
		22	453	527	2.5	oxygen
		600	417	531	22	air
		650	451	530	21	air
		700	415	452	23	air
		750	371	379	32	air
	(+1h/1150°C)	800	188	216	55.5	air
	(+1h/750°C)	22	406	666	6.2	oxygen
	(+1h/900°C)	22	508	531	1.6	air
		22	511	549	2.0	air
		22	419	651	5.4	oxygen
	(+1h/900°C)	600	431	522	22.5	air
	(+1h/1200°C)	600	434	532	22	air
FA-385-M2	as-cast	22	420	514	2.5	air
		22	418	493	1.3	air
		22	449	507	2.0	oxygen
		600	420	530	23.2	air
		650	437	511	20.2	air
		700	406	433	17.2	air
		750	362	369	15.5	air
	(+1h/1150°C)	800	189	224	49.6	air
	(+1h/750°C)	22	484	782	7	oxygen
	(+1h/900°C)	22	459	489	0.4	air
		22	518	550	1.8	air
FA-30-M1	as-cast	22	511	580	1.6	air
		22	516	594	1.3	air
		22	539	608	1.6	oxygen
		650	320	348	26.7	air
		700	233	261	33.6	air
		750	159	187	33.6	air
	(+1h/1150°C)	800	124	140	41.2	air
	(+1h/750°C)	22	486	666	5	oxygen
	(+1h/900°C)	22	491	558	0.9	air
		22	507	551	0.9	air
		22	453	638	3.8	oxygen

Table 5 (Continued) - Room and Elevated Temperature Tensile Data on Cast FeAl Alloys

Alloy	Fabrication/ Heat-Treatment Condition	Test Temp (°C)	Strength (MPa) Yield	Ultimate	Total Elongation (%)	Test Environment
FA-30-M2	as-cast	22	487	550	1.0	air
		22	482	551	1.1	air
		22	508	508	1.1	oxygen
		800	125	140	34.6	air
	(+1h/750°C)	22	457	606	4.2	oxygen
	(+1h/900°C)	22	475	534	0.7	air
		22	486	528	1.8	air
FA-30-M3	as-cast	22	509	588	1.3	air
		22	512	587	1.2	air
		22	527	606	1.8	oxygen
		650	314	385	31	air
		700	223	290	35	air
		750	206	225	39	air
	(+1h/1150°C)	800	144	158	36	air
	(+1h/750°C)	22	517	723	5.5	oxygen
	(+1h/900°C)	22	533	569	2.7	air
		22	528	567	1.2	air
		22	500	727	6.0	oxygen

Table 6. Creep-rupture properties of new modified FeAl-type alloys (as-cast)

Alloy	Processing/Heat-Treatment Condition	Creep Conditions Temp. (°C)	Creep Conditions Stress (ksi)	Rupture Time (h)	Rupture Elongation (%)	Minimum Creep-rate (%/h)
FA-385	as-cast	600	30	12	70	
	as-cast/1h-900°C	600	30	11	64.4	
	as-cast/1h-1200°C	600	30	31.2	84.4	0.67
	as-cast/1h-1250°C	600	30	12	72.5	2.4
FA-385 -M1	as-cast	600	30	454	47.5	
	as-cast/1h-900°C	600	30	380	28	
	as-cast/1h-1250°C	600	30	404	45	0.07
FA-385 -M2	as-cast	600	30	674	44.2	0.0025
	as-cast/1h-1200°C	600	30	388	46.6	0.062
	as-cast/1h-1250°C	600	30	520	48.4	0.04
FA-30 -M1	as-cast	600	30	96.3	40?	
	as-cast/1h-1200C	600	30	90	79.5	0.47
FA-30 -M2	as-cast	600	30	53.6	37.6	
	as-cast/1h-1200°C	600	30	117	50.5	0.23
FA-30 -M3	as-cast	600	30	160	30?	
	as-cast/1h-900°C	600	30	121.4	62	
	as-cast/1h-1200°C	600	30	329	45.8	0.05
	as-cast/1h-1250°C	600	30	285	42	0.05

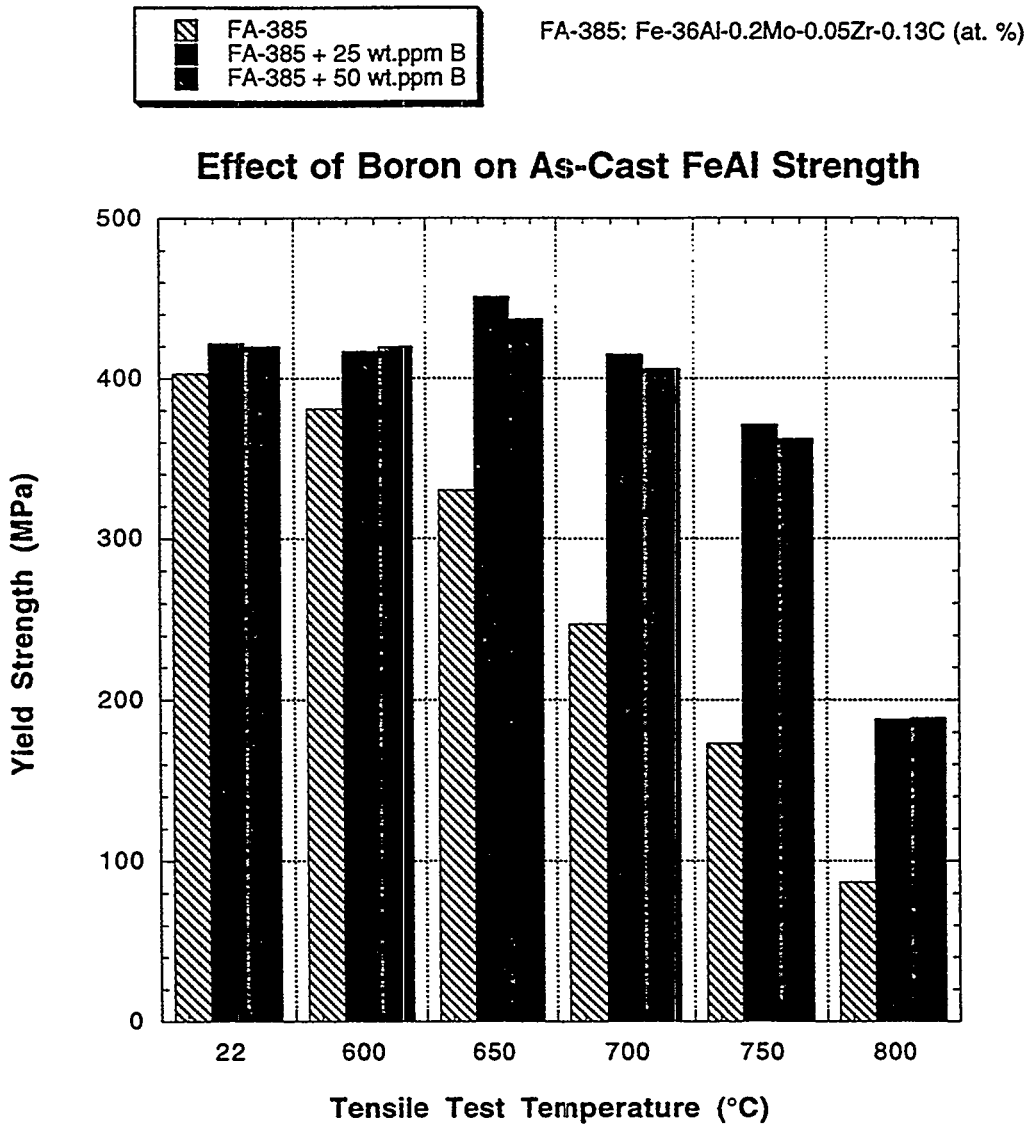

Figure 1 - Yield strength as a function of tensile test temperature for as-cast FeAl alloys (FA-385, -385M1 and -385M2).

SUPERIOR METALLIC ALLOYS THROUGH RAPID SOLIDIFICATION PROCESSING (RSP) BY DESIGN

John E. Flinn

Idaho National Engineering Laboratory
Lockheed Idaho Technologies Co.
P.O. Box 1625
Idaho Falls, Idaho 83415-2218

INTRODUCTION

Rapid solidification processing using powder atomization methods and the control of minor elements such as oxygen, nitrogen, and carbon can provide metallic alloys with superior properties and performance compared to conventionally processing alloys. Previous studies on nickel- and iron-base superalloys have provided the baseline information to properly couple RSP with alloy composition, and, therefore, enable alloys to be designed for performance improvements.

The RSP approach produces powders, which need to be consolidated into suitable monolithic forms. This normally involves canning, consolidation, and decanning of the powders. Canning/decanning is expensive and raises the fabrication cost significantly above that of conventional, ingot metallurgy production methods. The cost differential can be offset by the superior performance of the RSP metallic alloys. However, without the performance database, it is difficult to convince potential users to adopt the RSP approach. Spray casting of the atomized molten droplets into suitable preforms for subsequent fabrication can be cost competitive with conventional processing. If the fine and stable microstructural features observed for the RSP approach are preserved during spray casting, a cost competitive product can be obtained that has superior properties and performance that cannot be obtained by conventional methods.

TECHNICAL PROGRESS

Summary

The information from the research activities has shown that properties and performance of metallic alloys can be substantially improved through effective control and utilization of the interstitial elements carbon, oxygen, and nitrogen in conjunction with rapid solidification processing. The RSP approach has involved the atomization of a melt stream to fine molten droplets that are

convectively gas cooled. The powders are consolidated, primarily by hot extrusion, into suitable monolithic forms for evaluation.

The RSP studies on austenitic stainless steels and nickel-base alloys have shown positive effects from the presence of the interstitial elements. The alloys, A286, Ni-20Fe-20Cr, and 718, have shown fine and stable grain sizes compared to their conventionally processed counterparts (e.g., 0.01 versus 0.100 mm grain size after a 1 h-1100°C heat treatment). The origin of the fine grain size for these RSP alloys has been traced to the solidification microstructure in the particles. Although the details of the mechanism(s) for the grain size stability in these alloys are not understood, it does appear that oxygen is playing a major role. Also, it has been observed that oxygen is responsible for stabilizing nanometer size cavities in certain RSP alloys, and these in turn provide potent nucleation sites for carbides. This dispersion configuration is responsible for substantial improvements in creep resistance for RSP alloys. The positive effects of nitrogen on the properties of austenitic stainless steels is well documented. For these alloys, it is the most potent solid solution strengthening element. However, there is very little information available on the effects of nitrogen in nickel-base alloys. The importance of nitrogen with respect to nickel-base alloys is primarily associated with its use for gas atomization. It is much cheaper than argon or helium.

The fundamental information obtained from the earlier RSP studies has been applied to the design of a series of nickel-base alloys for high temperature, energy efficient applications. The series consists of two nickel-base, stainless types (one for aqueous corrosion and the other for oxidation resistance), and a precipitation-hardenable superalloy. For each set of alloys, five variations in the powder processing parameters were involved as well as a conventionally-processed counterpart (CPC). The primary variable in processing was the nitrogen level. The powders and CPC for each alloy were consolidated and formed into bars by hot extrusion. Analysis of the bar materials showed that nitrogen levels as high as 0.18 wt% had been achieved with some of the alloys. Since nitrogen is virtually insoluble in nickel, the high nitrogen levels are due to the high chromium contents in this nickel-base alloy series. Microstructural response to high temperature/1 h heat treatments as well as aging was determined for the RSP and CPC materials. For the precipitation-hardenable alloy series, the aging evaluation was fairly extensive in order to establish peak hardening/strengthening. For the two nickel-base stainless alloys, the aging efforts were mainly to evaluate the stability of nitrogen in solution.

Testing of the nickel-base alloys included mechanical properties (tensile and creep) and corrosion resistance (electrochemical polarization measurements in acid solutions and supercritical water oxidation exposures). All test results indicate that the RSP alloys are significantly superior to their conventionally processed counterparts, as well as to many of the commercially available nickel-base alloys.

A substantial effort has been devoted to Cooperative Research and Development Agreements (CRADAs) with U.S. industrial partners. Four CRADA studies have been completed. These involved potential use of the RSP technology for photovoltaic, high-temperature electrical, corrosion and wear, and high strength-high fatigue applications. Three additional CRADA studies are underway involving the possible use of the RSP technology for high temperature oxidation resistance, hard-magnetic materials, and molding applications.

Milestones

The milestones for this project are associated with completion of the RSP studies on the alloys by design (ABD) and technology transfer activities (i.e., information dissemination and CRADA participation).

RSP Applications to Alloys by Design

Results from the RSP studies on the superalloys (Ni-20Fe-20Cr, A286, and 718) provided the basis for the design of a series of nickel-base alloys with a base composition of Ni-25Cr-15Fe-0.06C. Additions to the base alloy included Mo, V, Nb, and/or Si; the nominal compositions of the alloys are shown in Table 1. Twenty batches of powder (~5 kg/batch) were processed by gas atomization for the three alloys. Processing variables included melt-cover gas and the gas used for melt-stream breakup (atomization) and cooling of the molten droplets. Both helium

Table 1. Nickel-Base Alloys by Design

	Composition (wt%)								
Designation	Ni	Cr	Fe	Mo	V	Nb	Si	C	General Applications
ABD1	Bal.	25	15	3	0.5	0.5	–	0.06	Corrosion
ABD2	Bal.	25	15	3	–	5.5	–	0.06	Superalloy
ABD3	Bal.	25	15	–	–	–	2.5	0.06	Oxidation

and nitrogen were used in the processing. Metallographically-prepared cross sections for a range of screened particle size fractions were examined for porosity and solidification microstructure features. The alloys processed with nitrogen showed no evidence of porosity, whereas significant porosity was observed in the powder particles processed with helium. These observations confirm that the ABD, nickel-base series were able to entrain, in solution, significant levels of nitrogen. The highest nitrogen levels (in wt%) achieved for the three alloys were ABD1-0.18, ABD2-0.18, and ABD3-0.12. The high nitrogen levels are attributed to the Cr, Nb, and Mo contents in the alloys.

The solidification microstructure for all three alloys was dendritic. The secondary dendrite arm spacing (SDAS) increased with particle size, but showed no evidence of any cooling rate effects from helium versus nitrogen gases for atomization and convective cooling. The compositions of the alloys did have a significant effect on the SDAS size. For ABD1, an increase in nitrogen content appeared to reduce the SDAS. However, this effect was not discernable in ABD2. The SDAS behavior as a function of particle size is shown in Figure 1 for low and high nitrogen levels in ABD1 and ABD2.

The powders, five batches per alloy, as well as an ingot of each alloy were extruded into bars. The extrusion temperature for the powder was 900°C; the temperature for the ingot was 1100°C. An extrusion ratio of ~10 to 1 was used. Heat treatment evaluations were performed on the extruded powders and conventionally processed counterparts. Both grain size/growth behavior and aging effects were correlated with mechanical properties. In addition, corrosion assessments on the RSP alloys were performed in acid solutions. The tests involved electrochemical-polarization and supercritical water oxidation (SCWO) with HCl.

1. Grain Size Behavior: Grain sizes were determined for the extruded powders and CPCs after 1-h heat treatments. Results for the 1100 and 1200°C heat treatments of the low- and high-nitrogen content RSP alloys are shown in Figure 2. It is apparent from this figure that fine and stable grain sizes are produced from RSP compared to CPC. Also, it appears that increasing the nitrogen content reduces the grain size. The high-nitrogen ABD2 alloy resulted in the smallest grain sizes observed to date from RSP, i.e., 3 μm (1100°C) and 4 μm (1200°C). Microstructural examinations revealed a very high population of niobium nitride precipitates for this alloy.

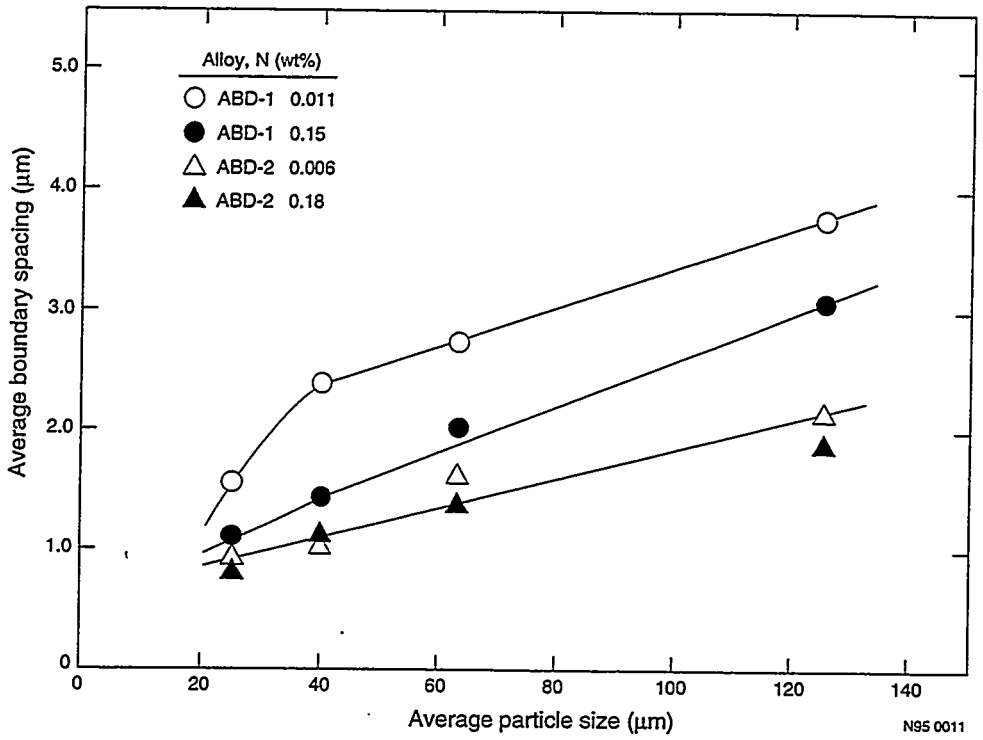

Fig. 1 – Influence of particle size on the solidification boundary spacing for ABD1 and ABD2 powders with different nitrogen contents.

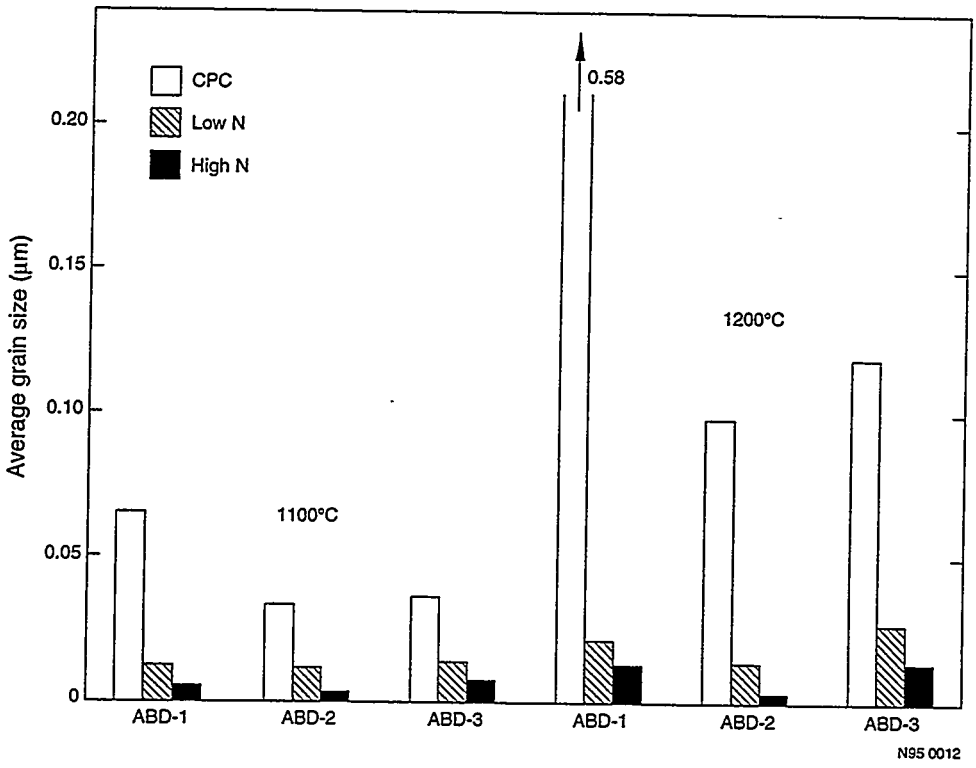

Fig. 2 – Grain sizes after 1 h heat treatments at 1100 and 1200°C for the RSP ABD alloys with high- and low-nitrogen contents, and CPC comparisons.

2. Tensile Properties – Before Aging: The tensile properties were affected by grain size and nitrogen, in addition to the nominal compositional differences shown in Table 1. The fine grain sizes obtained from RSP produced very significant increases in yield and ultimate tensile stresses compared to the larger grained CPCs. This effect is illustrated in Figure 3 along with the nitrogen influence on strengthening shown by tests at room temperature, 600, and 800°C for the ABD1 series. It is apparent from these results that significant improvements in tensile strengthening can be obtained from nitrogen. Although not shown, the ductilities for this alloy series were good, ranging from 40 to 60% for these test temperatures. It should be noted that ABD2 and ABD3 showed similar tensile behavior to ABD1 with respect to grain size and nitrogen influences in the unaged conditions.

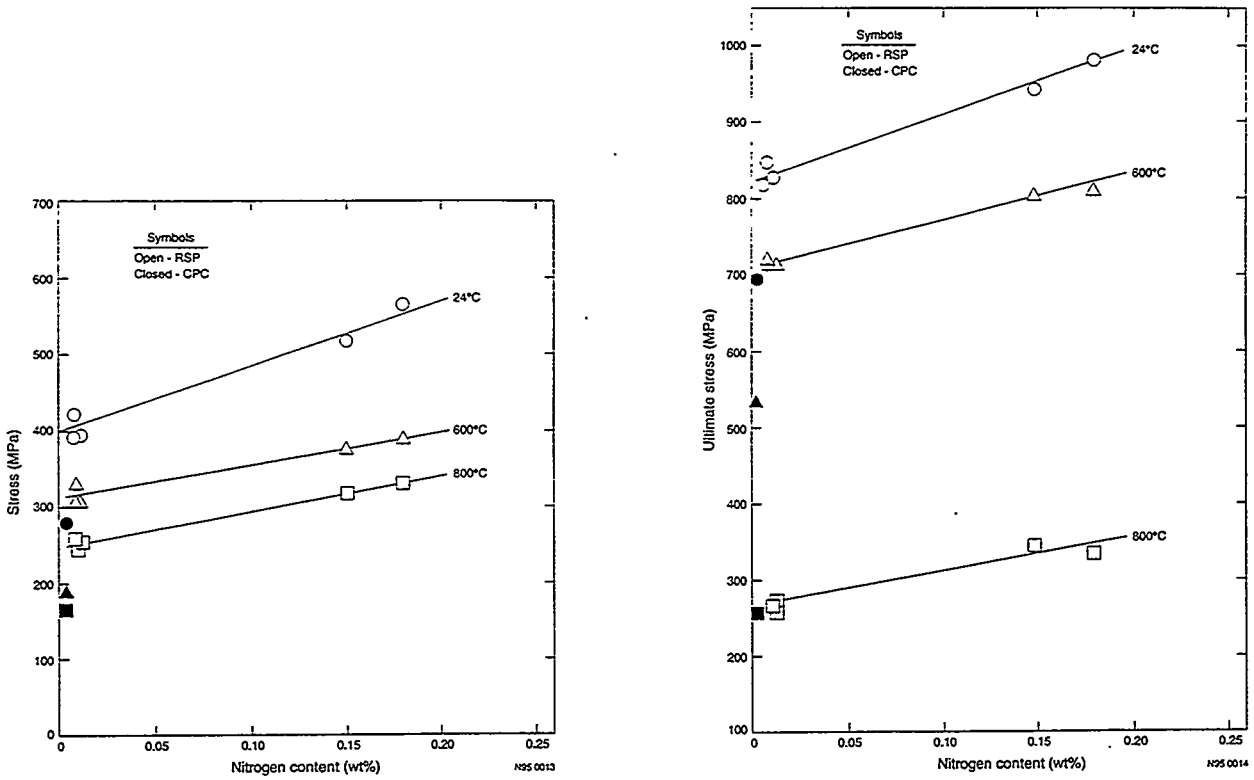

Fig. 3 – Influence of nitrogen content on the tensile stresses for the ABD1 alloy series: (a) yield and (b) ultimate.

3. Tensile Properties – After Aging: The aging behavior for the ABD alloys was examined to determine the effects of nitrogen on retention of strengthening without significant losses in ductility. In addition, aging is necessary for ABD2

since it represents a potential superalloy that relies on precipitation strengthening from γ" (Ni_3Nb). The ABD2 alloy is an alternative to the more common superalloys, 718 and 625.

The ABD2 alloys were given a series of solution anneals and aged for various times at temperatures between 650 and 750°C. Hardness measurements were performed to determine the combination of aging time and temperature producing maximum hardness. The results showed that maximum hardness was achieved after a 1000°C anneal followed by a 675°C-50 h age. The room temperature tensile properties after this heat treatment cycle are shown in Figure 4, along with results reported for Alloys 718 and 625. It is apparent that the RSP ABD2 alloy has superior strengthening compared to the 718 and 625 superalloys. However, it should be noted that high nitrogen content appears to be detrimental to development of an effective γ" precipitate in the ABD2 alloy. This is not surprising since a significant amount of Nb would be lost to nitride formation during the aging treatment and not available for γ". The tensile strengths shown in Figure 4 have the same trend at higher test temperatures, i.e., at 600 and 800°C. Although not shown, the ductilities for the ABD2 alloys are comparable to those reported for Alloys 718 and 625.

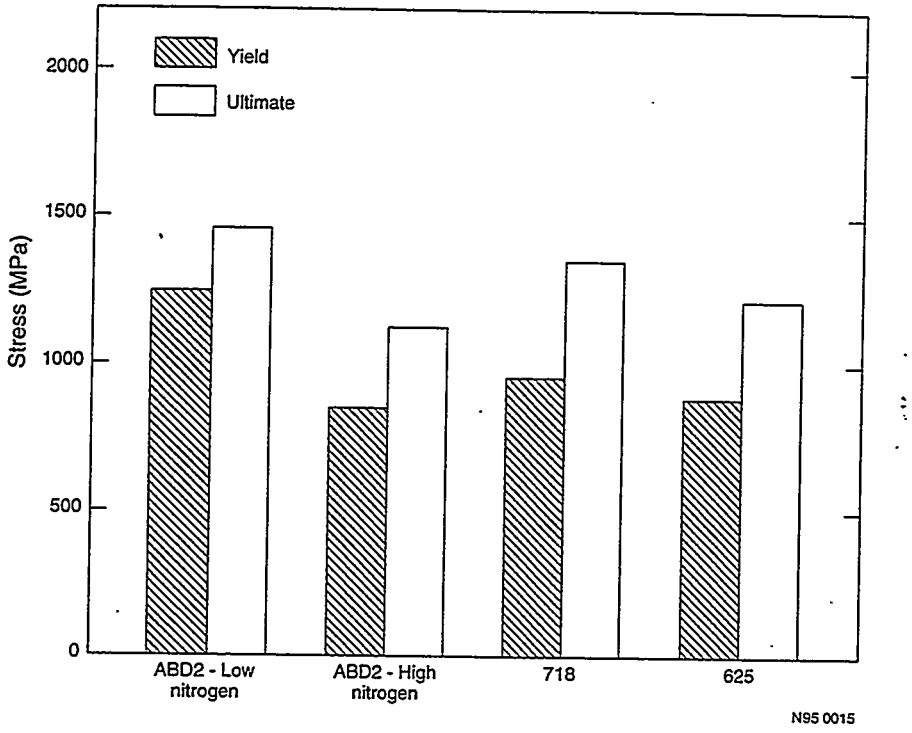

Fig. 4 – Tensile stress comparisons for age-hardenable ABD2, 718, and 625 nickel-base alloys.

Aging exposures at 700°C for up to 2000 h were given to the ABD1 and ABD3 alloy series. The room temperature tensile properties before and after aging for low- and high-nitrogen contents are shown in Table 2. These results indicate a no loss in strengthening and only a slight reduction in ductility from the aging treatment; hence, there is no obvious indication of a detrimental effect from nitrogen in these nickel-base alloys.

4. Creep Properties: Creep testing for the ABD alloys is underway. For the ABD1 and ABD3 series, nitrogen appears to have a positive effect on creep resistance. For ABD2 series, the creep resistance appears to be lower for the high-nitrogen alloys after aging at 675°C for 50 h than for the low-nitrogen alloys. This behavior is not unexpected since full strengthening from aging was not achieved for the high-nitrogen alloys (see Figure 4).

5. Corrosion – Electrochemical: Polarization corrosion tests on the ABD alloy series were performed in room temperature solutions of HCl, NaCl, and H_2SO_4. The polarization characteristics were compared to test results observed for nickel-base Alloys 718, 625, C22, and C276. The test results show that ABD2 corrosion resistance should be comparable to that of the higher molybdenum and lower iron alloys (625, C22 and C276), but superior to that of Alloy 718. The corrosion indications for the ABD1 series suggest that its resistance should be very good, slightly better than that of Alloy 718. Based on the results from the

Table 2. Tensile Properties for the ABD1 and ABD3 Alloys Before and After Aging at 700°C for 2000 h

Condition	Nitrogen (wt%)	Yield (MPa)	Ultimate (MPa)	Total Elong. (%)	Reduction in Area (%)
ABD1					
Unaged	0.011	394	825	47	64
Aged	0.011	413	841	43	53
Unaged	0.18	565	975	41	54
Aged	0.18	558	944	32	50
ABD3					
Unaged	0.014	350	785	48	63
Aged	0.014	380	801	45	54
Unaged	0.12	475	882	37	52
Aged	0.12	490	877	33	37

HCl and NaCl tests, the ABD3 specimens appeared to be quite sensitive to the chloride ion. This finding is not surprising since the alloy's composition was designed more for oxidation resistance than for aqueous corrosion resistance.

6. Corrosion – SCWO: An opportunity arose to place some of the RSP alloys into a supercritical, water oxidation experiment. The test environments were selected to simulate chlorinated hazardous wastes. The conventionally-processed nickel-based alloys included C22, 625, and C276. The RSP alloys included C22, ABD2, and ABD3 with the lower nitrogen contents. The parameters for the test involve 240 atm pressure, temperatures to 650°C, pH as low as 0.65, and a total exposure time of 240 h. Weight loss determinations and visual examinations were performed after 60 and 120 h exposures. The weight loss results are shown in Figure 5. The RSP alloys had lower weight losses. It should be noted that the two ABD alloys were not designed for the rather harsh conditions of the SCWO experiment. Compositional adjustments to the alloys in combination with RSP could significantly improve the performance shown in Figure 5.

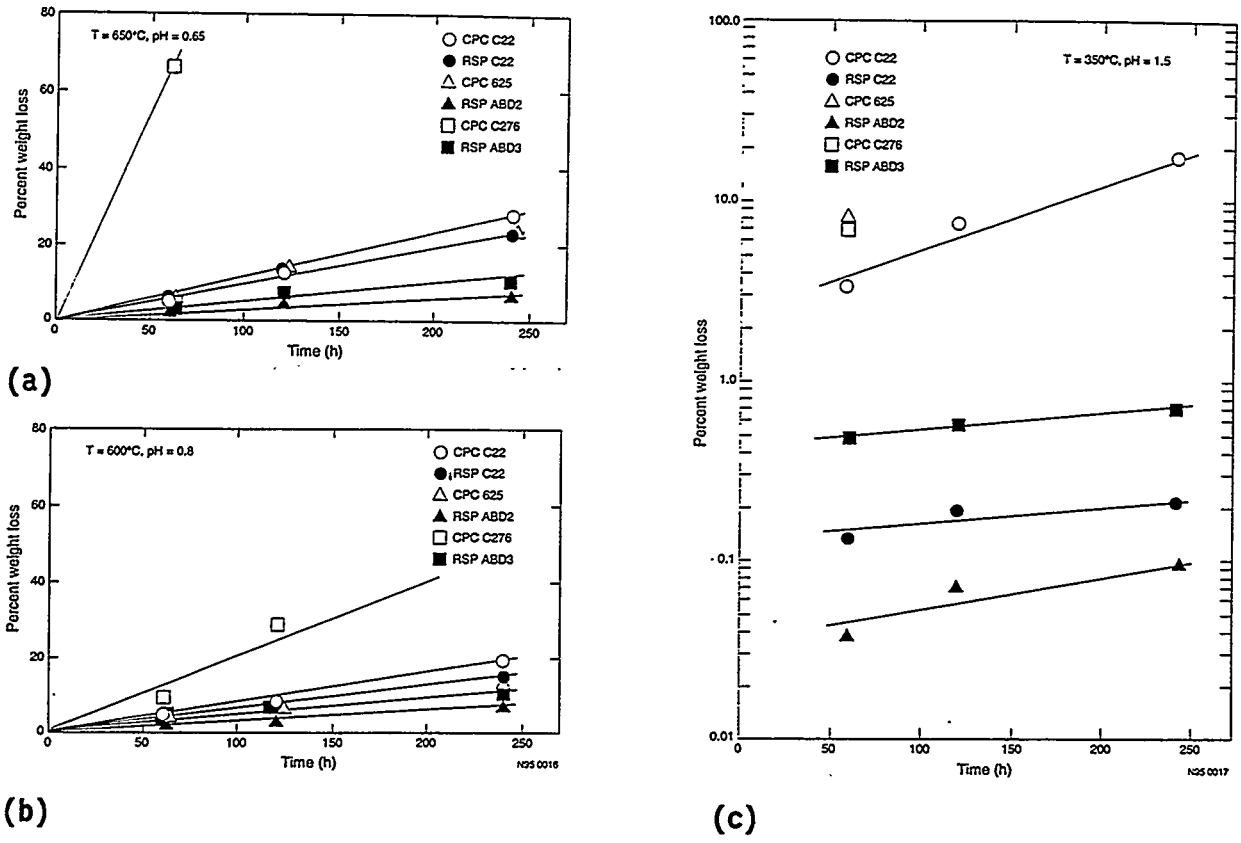

Fig. 5 – Corrosion weight loss of nickel-base alloys for SCWO tests at 240 atm pressure: (a) T = 650°C, pH = 0.65, (b) T = 600°C, pH = 0.8, and (c) T = 350°C, pH = 1.5.

Spray Casting of RSP Preforms

RSP produces powder that requires consolidation into the appropriate monolithic forms. For high-value applications, the consolidated form requires full densification and bonding of the particles. As a result, pressing and sintering of the powders may not provide sufficient integrity for most applications. The more conventional powder consolidation practices rely on canning (under hermetic conditions) the powders, consolidation, and decanning. The canning/decanning operation represents about 60% of the cost for powder consolidation. Although the properties and performance of the RSP alloys will in general be superior to those of their conventionally-processed counterparts, the differences in manufacturing costs must be reduced in order to attract industrial interest to the RSP technology. A task associated with this project is to demonstrate that an effective preform can be produced by spray casting the molten droplets on to a substrate to produce a bar or plate. This approach would eliminate the expensive canning/decanning operation, and permit the RSP approach to be competitive. Several items need to be successfully demonstrated with the spray casting approach. These include: (a) retention of the fine and stable microstructural features; (b) deposition of nearly 100% dense product; and (c) minimization of wastage, e.g., overspray. These three issues will be addressed in FY 1995 using Type 316 SS for the spray casting.

Technology Transfer

The primary activity for this task has been interaction with U.S. industries interested in utilizing the RSP technology. The effort has involved joint studies, via seven CRADAs, to improve the properties and performance of metallic alloys. The areas of application include high-temperature electrical (conduction and resistance), corrosion and wear, high strength-high fatigue resistance, photovoltaic devices, and hard magnetic alloys for small motors. All of these applications have very significant implications for improving energy efficiency and conservation.

Four of the studies have been completed, and three of those remaining have evolved into a Phase 2 evaluation. One of the CRADA partners will be evaluating some rod products produced from the ABD nickel-base alloy powders. Successful demonstration of the spray casting approach will nearly ensure the adoption of the RSP technology by this industrial partner as well as others.

ACKNOWLEDGMENT

This work was supported by the U.S. Department of Energy, Assistant Secretary for Energy Efficiency and Renewable Energy, under DOE Idaho Operations Office Contract No. DE-AC07-94ID13223.

PUBLICATIONS (1994)

None.

PRESENTATIONS (1994)

TMS Annual Meeting (San Francisco, CA)
J. E. Flinn and T. F. Kelly. "Rapid Solidification Processing of Metallic Alloys: Issues and Opportunities" (invited).

PATENTS/DISCLOSURES (1994)

Five invention disclosures are being prepared. The subjects include:

1. Strengthening of Metallic Alloys from Nanometer-Size Oxide Dispersions
2. Spray Casting of Metallic Preforms
3. Combined Effects for Strengthening of Metallic Alloys Through Fine and Stable Microstructural Control
4. High Strength, Corrosion Resistant Austenitic Stainless Steel
5. High Strength, Corrosion Resistant Nickel-Base Alloy.

INDUSTRIAL INPUT AND TECHNOLOGY TRANSFER (1994)

1. CRADAs involving the RSP technology: seven, four of which are complete. The remainder have entered into Phase 2 evaluations. One of the industrial partners will be testing the nickel-base alloys by design (ABD) for high-temperature applications.

COST SHARING (1994)

1. CRADA activities involved cost-in-kind contributions of ~$150,000 for the year from industrial partners
2. Cost share from Bureau of Mines for the Idaho National Engineering Laboratory CRADA participation was ~$50,000
3. Internal funding was obtained for the purchase of a new chamber, vacuum system, and power supply for the spray-casting effort
4. Two of the nickel-base alloys by design (ABD) were tested without cost to the project in a very unique supercritical water oxidation experiment.

HIGHLIGHTS (1994)

1. The experimental research on three nickel-base alloys by design has shown that proper use of the interstitial elements O, N, and C can provide fine and stable microstructures and very significant improvements in properties and performance.

2. Studies have begun on the spray casting of preforms to reduce the costs associated with powder consolidation. Initial results on Type 316 SS are quite promising.

3. Four CRADA studies with industrial partners were completed.

SYNTHESIS AND DESIGN OF INTERMETALLIC MATERIALS - MOLYBDENUM DISILICIDE

J. J. Petrovic, R. G. Castro, D. P. Butt, I. E. Reimanis, H. Kung, A. Bartlett, M. Sandlin, M. Pena, and S.-P. Chen

Los Alamos National Laboratory
Los Alamos, NM 87545

EXECUTIVE SUMMARY

INTRODUCTION

The objective of this program is to develop structural silicide-based composite materials with optimum combinations of elevated temperature strength/creep resistance, low temperature fracture toughness, and high temperature oxidation resistance for applications of importance to the U.S. processing industry. A further objective is to develop silicide-based prototype industrial components. The ultimate aim of the program is to work with industry to transfer the structural silicide materials technology to the private sector in order to promote international competitiveness in the area of advanced high temperature composite materials and important applications in major energy-intensive U.S. processing industries. The program presently has a number of developing industrial connections, including a CRADA with the advanced materials company Advanced Refractory Technologies Inc. and interactions targeted at developing industrial gas burner and metal and glass melting/processing applications.

Current experimental emphasis is on the development and characterization of SiC reinforced-$MoSi_2$ matrix composites, plasma sprayed

$MoSi_2$-based materials and microlaminate composites, and $MoSi_2$ reinforced-Si_3N_4 matrix composites. We are developing processing methods for $MoSi_2$-based materials, such as plasma spraying/spray forming and electrophoretic deposition. We are also pursuing the fabrication of prototype industrial gas burner and injection tube components of these materials, as well as prototype components for glass processing.

SUMMARY OF TECHNICAL PROGRESS IN FY-1994

1. Industrial Interactions.

In FY-1994, a significant interaction has been developed between LANL and Schuller International, a major U.S. fiberglass manufacturer. In April 1994, Los Alamos personnel visited Schuller International Mountain Technical Center in Lakewood, Colorado. As a result of this visit, a bilateral proprietary information agreement was established, and this then lead to a meeting held at Los Alamos in September 1994 to discuss the details of an interaction between LANL and Schuller International, to address the materials needs which Schuller has for fiberglass manufacturing. A program plan for the interaction was developed and specific milestones were formulated. Activities based on this program plan will be initiated in FY-1995.

Los Alamos personnel also visited Libby-Owens-Ford in July 1994 as part of the materials assessment activity for the glass industry. Libby-Owens-Ford is a flat glass producer located in Toledo, Ohio. The materials needs for this industry were shown to vary considerably, from improvements in the basic design of regenerative furnaces for glass melting to an understanding of the flow characteristics of glass. This visit set the stage for a visit by Libby-Owens-Ford personnel to the Los Alamos National Laboratory in early October 1994, for further discussions of areas of potential interactions.

In May 1994, a meeting took place at LANL with personnel from the Radian Corporation, who have an interest in the use of $MoSi_2$ components for high temperature industrial environmental process sensors A bilateral proprietary information agreement was established with Radian, and LANL will pursue prototype tube components for emissivity measurements. In June 1994,

an interaction took place with personnel from Precision Combustion Inc. This company has an interest in developing a miniature $MoSi_2$ electric, catalytic heated tube for gas turbine applications.

The Exotherm Corporation is currently producing composite powders of $MoSi_2$ containing SiC and Si_3N_4 additions, using a self-propagating high temperature synthesis (SHS) process. Advantages of this process over current production methods for $MoSi_2$ powders are high productivity and low cost, the ability to process multi-element compounds of a given composition, control of reinforcement size in composite powders, and self-refinement of the composite material by tailoring of the combustion wave. Exotherm has provided LANL with $MoSi_2$-SiC and $MoSi_2$-Si_3N_4 powders, for evaluations of the plasma spraying of these materials.

2. $MoSi_2$-Based Prototype Industrial Components.

Research activities during FY-1994 focused on fabricating and characterizing plasma-spray formed prototype components of $MoSi_2$ and $MoSi_2$-Al_2O_3 composites. Prototype fuel burner nozzles and gas injection tubes have been produced for industrial on-site testing at Air Products and Chemicals Inc. during this fiscal year. An integral part of the prototype fabrication has been the understanding of the process-structure-properties associated with plasma-sprayed material. Optimization and improvement of the plasma-spraying process was done to minimize the cracking which occurred during the fabrication of tubular components. Understanding the effects of residual stresses during tube fabrication was initiated during this fiscal year. Processing techniques such as transferred-arc spraying, which can improve the temperature uniformity of the spray-formed $MoSi_2$ and $MoSi_2$ composite tubes, will be pursued in the next fiscal year.

Extensive TEM characterization and phase identification has been performed on plasma-sprayed $MoSi_2$ and $MoSi_2$ composites in the as-deposited condition and after elevated temperature exposures. In particular, post-mortem analysis on composite $MoSi_2$-Al_2O_3 gas injection tubes, which were immersed in molten Fe, Al-4%Mg and Cu, were characterized. The superior performance of the composite $MoSi_2$-Al_2O_3 gas injection tubes in the molten Cu and Al-4%Mg

was directly related to the microstructural stability of the composite tubes at the use temperatures. Microstructural analysis is an important research tool for providing information on the performance and compatibility of $MoSi_2$ and $MoSi_2$-oxide composites for high temperature applications. TEM and SEM will be used extensively to characterize the compatibility of $MoSi_2$ with glass compositions as part of our collaboration with Schuller Mountain Technical Center during the next fiscal year..

3. $MoSi_2$-Al_2O_3 Microlaminate Composites.

The mechanical behavior of plasma-sprayed $MoSi_2$ was extensively investigated at room and elevated temperatures (up to 1400°C). Characterization of monolithic $MoSi_2$ and laminated beams of $MoSi_2$-Al_2O_3 which were produced by plasma-spray forming have been performed. A database of plasma-sprayed $MoSi_2$ and Al_2O_3 is being produced to provide baseline information on the mechanical behavior of the as-sprayed material which can be compared to $MoSi_2$-Al_2O_3 laminated material produce by plasma-spraying. Laminated composites are being investigated as a way of improving the room temperature fracture toughness through delamination and separation of individual layers. Results during this fiscal year have shown that a strong bond exists between the $MoSi_2$ and Al_2O_3 in the as-deposited condition. Investigations are being performed to weaken the interface using refractory metal interlayers. Deformation of the composite $MoSi_2$-Al_2O_3 material at elevated temperatures has been described by a number of mechanisms, namely, plastic deformation of the $MoSi_2$ with multiple cracking in the Al_2O_3 and large scale interface delamination.

Optimizing the mechanical behavior of the laminated material to improve the fracture toughness at room temperature, allowing for non-catastrophic failures, while at the same time maximizing the elevated temperature strength and creep behavior were principal objectives in the research conducted during FY1994.

4. CRADA with Advanced Refractory Technologies.

In FY-1994, SiC whisker-$MoSi_2$ powder blends were received from Advanced Refractory Technologies (ART), and a number of composites were consolidated from these blends. Additions of up to 30 vol.% SiC whiskers markedly improved the room temperature bend strength. Additions of 1-2 wt.% carbon lead to substantial room temperature strengthening in the absence of any SiC whiskers. This is due to the formation of in-situ SiC from reaction of the carbon with silica present in the microstructure. Indentation creep studies on SiC whisker-$MoSi_2$ matrix composites indicated a complex behavior associated with effects of the SiC whiskers on the $MoSi_2$ grain size, as well as the density of the composites at higher whisker volume fraction loadings.

The bend strength of ART SiC whisker-$MoSi_2$ matrix composites was determined at room temperature and 1200°C, for composites containing Grade M SiC whiskers, as well as carbon additions. In general terms, bend strength increased with increasing SiC whisker content, and with carbon additions, although higher SiC contents can result in reduced strength. In-situ SiC produced by carbon additions to pure $MoSi_2$ significantly improved both room temperature and 1200°C strength.

Experimental results have indicated that the elevated temperature mechanical properties of the ART SiC whisker-$MoSi_2$ matrix composites are strongly affected by the grain size of the $MoSi_2$ matrix. High temperature strength and creep resistance increase with increasing $MoSi_2$ grain size.

5. $MoSi_2$ Reinforced-Si_3N_4 Matrix Composites.

A series of $MoSi_2$ reinforced-Si_3N_4 matrix composites containing 0, 10, 20, 30, 40, and 50 vol.% $MoSi_2$ phase were consolidated to high density using a 5 wt.% MgO addition. The microstructure of the 50 vol.% $MoSi_2$-50 vol.% Si_3N_4 composite indicated that the Si_3N_4 appeared as the matrix phase.

Electrical resistivity measurements on the $MoSi_2$-Si_3N_4 composites showed values as low as 980 ohm-cm for the 50 vol.% $MoSi_2$ phase composite. The feasibility of Electro-Discharge Machining (EDM) of the 50 vol.% $MoSi_2$-50

vol.% Si_3N_4 composite was definitely and positively established. However, optimized EDM behavior requires composites with resistivity values of 100 ohm-cm or less, and this is our next objective in developing these composites.

Initial indentation flaw fracture toughness measurements indicated that toughness increased with increasing $MoSi_2$ phase content at both room temperature and 1200°C, although there may be a toughness reduction at the 50 vol.% $MoSi_2$ level. Initial interface studies have indicated two types of interfacial species in the $MoSi_2$-Si_3N_4 composites, pure silica and a magnesium silicate. Room temperature bend strength values have been observed to be in the range of 690-270 Mpa, decreasing with increasing $MoSi_2$ phase content.

6. Micromechanical Modeling.

In FY-1994, the micromechanical modeling activities have focused on the modeling of microlaminate composite structures, to provide insights into the $MoSi_2$-Al_2O_3 microlaminates produced by plasma spraying. Using a spring-network model, the modeled microlaminates with weak interfaces were seen to be 50% stronger and 300% tougher than their monolithic counterparts. Fracture paths and stress-strain curves obtained by the models were consistent with experimental results, and the toughening and strengthening effects were due to the extensive debonding at the interfaces. Due to the shift of our programmatic thrusts to more applied aspects of industrial interactions and prototype components, the micromechanical modeling activities will not continue into FY-1995.

TECHNICAL PROGRESS: July-September 1994

Industrial Interactions

<u>Schuller International Mountain Technical Center</u>

On September 8-9 a kick-off meeting was held between LANL (Rich Castro, John Petrovic, Gerry Maestas and Harriet Kung) and Schuller International Mountain Technical Center (Dr. Walter Johnson) to identify and establish a collaborative working arrangement to address the materials needs for

the fiberglass industry. The meeting focused specifically on the use of $MoSi_2$ in the fiberglass industry but also addressed other technologies in which Schuller was interested (i.e., microwave processing, alloy development, and sensor technology). Areas of collaboration were identified along with a draft program plan/milestones for achieving the research objectives. Proprietary drawings of components used in the fiberization process at Schuller were discussed with LANL personnel. A copy of these drawings were left with LANL to begin formulating the process methodology to fabricate prototype components. Schuller was very excited about the prospects of establishing this collaborative research effort with LANL and was eager to begin testing of prototypes and coated components fabricated at LANL.

The following lists potential areas of collaboration and a draft program plan with milestones and estimated delivery dates which were formulated during this meeting.

I. Identified Areas of Potential Collaborations:

1. Monolithic center section component of $MoSi_2$ (or a $MoSi_2$ composite) to replace existing precious metal center section used in fiberization. $MoSi_2$ may also find application in replacing precious metal bushings.

2. Coatings on existing Mo components (i.e., vertical 29" electrode arm and dwell tank components) with $MoSi_2$ or ceramic oxides.

3. Wear resistant coatings for "Bagger Spout" used in packaging fiberglass.

4. Spray-forming of $Mo/MoSi_2$ composite electrode arms and mounts, and melter needle head assembly.

5. Materials performance and characterization:

   a. wetting of glass on $MoSi_2$

b. compatibility of $MoSi_2$ and $MoSi_2$ composites with fiberglass composition
c. interaction and stability of $Mo/MoSi_2$ composite material
d. corrosion and erosion of $MoSi_2$ in glass.

6. Monolithic $MoSi_2$ electrode heads made by various processing techniques (i.e., HIPing, spray-forming, conventional PM).

7. Inserts made from $MoSi_2$ for use in fiberization spinner disc. $MoSi_2$ as a coating in the fiberization spinner disc could also find application to reduce wear and increase spinner lifetime.

8. Modeling of thermal and mechanical stresses, glass flow and fiberization in spinner disc designs.

II. Program Plan and Milestones:

Year 1. FY 1995

Task 1: Develop $MoSi_2$ coatings for molybdenum electrodes

a. LANL provides Schuller with plasma-sprayed coatings	Dec 1994
b. Schuller tests coated components in molten glass	May 1995
c. Characterization and performance evaluation LANL/Schuller	Sept 1995

Task 2: Develop wear resistant coating for "Bagger Spout"

a. Select wear resistant coating LANL/Schuller	Nov 1994
b. LANL coat stainless steel "bagger spout"	Jan 1995
c. In-house performance test of component, Schuller	May 1995

Task 3: Fabricate $MoSi_2$ inserts for fiberglass spinner disc

a. LANL fabricate $MoSi_2$ inserts blanks (1.25" dia x .125" thick):	
– hot press, HIP, plasma-spray form	Mar 1995
b. Schuller establish insert design and laser drill hole pattern	June 1995

Task 4: Materials Characterization

a. wettability studies at LANL
b. $MoSi_2$ and $MoSi_2$ composites-(Si_3N_4, SiC, ZrO_2, Al_2O_3 and Y_2O_3) / glass interactions at LANL Sept 1995

Task 5: Mo/$MoSi_2$ sprayformed components

a. LANL begin fabrication of small test samples Sept 1995

<u>Year 2. FY 1996</u>

Task 1. Optimize $MoSi_2$ coatings on molybdenum electrodes

a. Schuller/LANL evaluate coating performance and glass interactions
b. Schuller design modification of electrodes
c. LANL design and tailor $MoSi_2$ coatings for optimum performance Sept 1996

Task 2. Continue developing wear-resistant coatings for glass processing applications

a. LANL provide material selection and coated prototypes Sept 1996

Task 3. Test and evaluate $MoSi_2$ inserts in fiberization spinner disc

a. Schuller perform in-house testing of $MoSi_2$ inserts Dec 1995
b. Schuller/LANL evaluate performance of inserts Sept 1996
c. LANL model stress, and glass flow in spinner Sept 1996

Task 4. Continue materials characterization of composite $MoSi_2$ systems

a. Select and characterize promising composite systems Sept 1996

Task 5. Fabricate full-scale monolithic $MoSi_2$ electrode arm and mount

a. LANL fabricate electrode using hot pressing/HIP
b. Investigate feasibility of spray-forming $Mo/MoSi_2$ electrode
c. Schuller perform in-house testing of electrode Sept 1996

Year 3. FY 1997

Task 1. Continue optimization of electrode arm and mount

a. LANL develop processing envelope for industrial fabricator
b. LANL/Schuller technology transfer Sept 1997

Task 2. Optimize $MoSi_2$ insert design for fiberglass spinner disc

a. Schuller optimize fiberglass spinner disc design
b. Schuller/LANL material selection and optimization
c. LANL prototype fabrication and Schuller testing Sept 1997

Task 3. Continue developing spray-forming of $Mo/MoSi_2$ composites

a. LANL provide prototype components for industrial testing Sept 1997

Task 4. Continue materials characterization and applications modeling

a. LANL provide characterization support and modeling of prototype components Sept 1997

Completion of many of these task will depend on the ability to coat large scale components in the existing vacuum plasma-spray chamber which can be tested at Schuller MTC. A request for capital equipment funding ($63K) to purchase a two-axis motion mechanism with a CNC motion controller and a spindle axis for part rotation is being submitted. This will allow the ability to coat longer $MoSi_2$ tubes (approx. 36" long) and larger flat plate samples (approx. 36" x 24"). The manipulation capability of the existing vacuum plasma-spraying

chamber is currently limited to a toggle switch operation for positioning the plasma-spray torch over the part to be coated.

Libby Owens Ford

A visit to the Libby-Owens-Ford plant (a flat glass producer) in Toledo, Ohio was done on July 14, 1994, as part of the Materials Assessment activity for the Glass Industry. The materials needs for this industry was shown to vary considerably from improvements in the basic design of the regenerative furnaces to understanding the flow characteristics of the glass. Following are areas in the float glass process which were identified by LOF where expertise at the National Laboratories may be used.

Melting:

- Water-cooled stainless steel was used extensively in various applications (i.e., pushers, paddles, burner-tips). In some cases, a need to extend the life of these components was of interest to LOF. New coatings and possibly new alloys may find applications in this area and should be explored.

- A drive towards oxygen enrichment of the combustion air (i.e., O_2/fuel) was discussed and seemed to be an expanding technology at LOF. Although there were no in-depth discussions of specific materials needs and applications, it was clear that materials related problems will be a major issue in the development of this technology. The need to lower NO_x emissions, improve combustion efficiency, and possibly eliminate the regenerators on both sides of the furnace are driving forces for this new technology. Areas of concern will be the compatibility of the existing materials (i.e., refractories, stainless steel components, etc.,) with the enriched O_2 environment. Degradation of other furnace parts will occur due to the higher H_2O and CO_2 vapor. Oxygen resistant materials and/or coatings will be required for many applications. Erosion and corrosion of the refractory walls will also be a problem. Advanced wear-resistant or environmentally resistant coatings will need to be developed for specific applications.

- An interest in developing improved electric boost elements used to assist in the melting of the patch portion of the glass furnaces was mentioned. The material which is currently used is molybdenum and has a fairly good performance record although it can use some improvements, maybe a possible technology for $MoSi_2$.

- Submerged bubbling of the glass using advanced tubular materials is also needed at LOF. Melt homogeneity and thermal stirring are the driving force for this development. Currently, H_2O-cooled high carbon steel bubblers are used which can last up to 5 years.

- The need for modeling and computational support from the DOE labs to understand the flow patterns, and compositional and thermal gradients in glass was of interest. As a result of our visit, Dr. Zhu Ming Chu from LOF has requested to visit LANL sometime during September. He is very interested in utilizing our computational expertise to help LOF understand glass flow and glass properties during processing.

Float Glass Process:

- Glo-bar heating was used extensively over the glass ribbon to maintain temperature uniformity as the glass progressed through the furnace. Problems with debris falling into the glass as a result of flaking and blistering of the glo-bars was discussed. New burner technology may find applications in this area. Radiant burners, and/or gas fired burner panels may be of interest.

- Controlling the desired thickness of the glass is accomplished by using a "Tweel" which stretches the glass to a desired thickness. Sensor technology to control and monitor the glass thickness during processing is needed. The performance of the stainless steel Tweel seemed to be adequate for this application.

Annealing Lehrs:

- The function of this part of the process was to stress-relieve the glass ribbon through controlled cooling. Rolls used to transport the glass during this operation were made from asbestos. LOF is in the process of converting all the asbestos rolls to another material and was interested in suggestion for new materials which would serve the same function as asbestos but would also minimize the abrasion/marking of the glass ribbon due to roll contamination with glass particles. Development of a replacement material would result in the elimination of asbestos and improve the quality of the glass.

Glass Bending/Forming:

- The finishing side of the float glass process was associated with the bending and forming of glass to the required shape. At LOF, 85% of their operation is supplying glass plate to the automotive industry. The major issue associated with the bending and forming of glass plate was the introduction of scratches and artifacts into the finished glass. The need for new roller material and/or ceramic or metal fiber covers was of interest to LOF.

Sensor Development:

- Sensor technology for monitoring and controlling the float glass process was mentioned during our visit to LOF. On-line real time monitoring of the CVD process, and non-contact diagnostics for compositional and thermal determination of the float glass were two areas which were of interest to LOF.

Exotherm Corporation

Composite powders of $MoSi_2$ containing SiC and Si_3N_4 additions are currently being produced by Exotherm Corporation using a self-propagating high temperature synthesis (SHS) process. Advantages of this process over current production methods for $MoSi_2$ powders are:

- High productivity and low cost
- Ability to process multi-element compounds of a given composition,

- Control of reinforcement size in composite powders.
- Self-refining of the composite material by tailoring the combustion wave.

Exotherm has provided LANL with the following powder composition made by the SHS process:

$MoSi_2$-10% SiC	$MoSi_2$ -18%Si_3N_4	$MoSi_2$- 20% SiC-18%Si_3N_4
$MoSi_2$-20% SiC	$MoSi_2$ -30%Si_3N_4	
$MoSi_2$-30% SiC	$MoSi_2$ -46%Si_3N_4	

Powder size distribution, morphology, and phase identification using x-ray diffraction have been performed on this powders. TEM characterization of the starting SHS powders and the resulting plasma-sprayed deposits will be done during the next quarter.

Penn State: O-ring and C-ring tests.

Ten $MoSi_2$ spray formed tubes approximately 8.00" long with a inside diameter of .250" and a wall thickness of roughly .125" were plasma-spray formed. Two of the tubes were produced using reactive plasma-spraying. O-ring and C-ring sections (200 total) will be machined from these tubes by McKee Carbide Machining for testing the tube strength at room and elevated temperatures (1000 ^{o}C and 1200 ^{o}C). Samples will be shipped to Penn State (John Hellmann) to determine the characteristic strength and the Weibull modulus of the spray-formed tubes. Test results will be reported next quarter.

CRADA with Advanced Refractory Technologies (ART)

New ART Blends

Results obtained on the CRADA have suggested that the elevated temperature mechanical properties of the ART SiC whisker-$MoSi_2$ matrix composites are strongly influenced by the grain size of the $MoSi_2$ matrix. The data suggest that the high temperature strength and creep resistance increase with increasing $MoSi_2$ grain size.

Based on these observations, it was suggested to ART that they make modifications to the processing of their SiC whisker-$MoSi_2$ powder blends. First, a recommendation was made to introduce a SiC whisker beneficiation step into their fabrication sequence for the SiC whisker-$MoSi_2$ blends. The purpose of this beneficiation step was to remove fine particulate SiC detritus which was intermixed with the SiC whiskers and which might stabilize the $MoSi_2$ grain size at a level smaller than optimum. The second recommendation was to use three different types of $MoSi_2$ powders, so that definite $MoSi_2$ grain size trends could be established.

Using this input from LANL, ART fabricated the following SiC whisker-$MoSi_2$ matrix blends and supplied them to LANL in late August 1994:

Lot No.	$MoSi_2$	SiC Whiskers	Vol.% SiC(w)
SC-026S	Starck Grade C	Grade R	20
SA-026S	Starck Grade A	Grade R	20
CC-026S	Cerac M-1103	Grade R	20

A SiC whisker beneficiation step was incorporated in the processing of these new blends. In addition, ART also developed a new Aqueous Dispersion/Flocculation (AD/F) process for making these blends, which has replaced the original blend process. This new processing approach appears to produce blends that are superior to the old solvent evaporation process in terms off whisker deagglomeration, dispersion, and homogeneity throughout the blend. The new process had advantages in terms of performance, scalability, and environmental, since it is aqueous based.

We will hot press composites from these new, improved ART SiC whisker-$MoSi_2$ matrix blends. We will then evaluate the microstructures and mechanical properties of these new composites, and compare them to the results already obtained on the first generation ART materials. Particular emphasis will be placed on characterizing and optimizing $MoSi_2$ grain size effects for optimum properties.

$MoSi_2$-Al_2O_3 Microlaminates

Work in three areas will be described. The first is a summary of the pertinent results of the in-service tests of the tested gas injection tubes by Air Products Inc. Next, some results of high temperature mechanical testing of laminated $MoSi_2/Al_2O_3$ beams will be shown. Finally, preliminary results of a new technique for measuring interface fracture resistance will be presented.

Air Products Laminated Tubes

SEM characterization of the $MoSi_2/Al_2O_3$ laminated tubes tested by Air Products Inc. in an in-service test has been done. Because tubes immersed in an Fe melt did not survive the test, any discussion of their post-mortem microstructure will be postponed until the thermochemical stability of $MoSi_2$ in molten Fe can be assessed.

Tubes immersed in molten Cu survived the test essentially intact. A variety of reactions occurred, most predominantly the apparent loss of Si to the Cu melt, resulting in the formation of Mo_5Si_3 precipitates throughout the tube. Fig. 1 shows the morphology found on the inner surface of the tube. Standardless EDS of the region showed it to be a mix of Mo_5Si_3 and possibly silica. In the bulk of the tube, Fig. 2 shows a typical region in which Mo_5Si_3 precipitates are found in the $MoSi_2$ matrix. The mechanism of Si loss is not understood; however, controlled tests to study the reaction between a Cu droplet and bulk $MoSi_2$ are currently underway. Apparently the loss of Si did not decrease the tube's integrity during the test. Some limited cracking was observed, Fig. 3, but there was no gross reaction nor loss of effectiveness associated with these few cracks.

The tube immersed in molten Al showed no signs of Si depletion, nor any structural damage that would seriously decrease its effectiveness. Reactions between the Al and Al_2O_3 were undetectable, owing to the well known compatibility of the two materials.

In both cases, the superior structural performance of the laminated tubes is believed to be in part a result of the relatively high thermal conductivity of

$MoSi_2$, which tends to decrease the transient thermal stresses occurring immediately upon immersion in the melt.

4-Point Bending of $MoSi_2/Al_2O_3$ Laminated Beams

A series of 4-point bend tests of layered $MoSi_2/Al_2O_3$ beams has been conducted at 1400°C, 1200°C and 1000°C. Fig. 4 is a micrograph of the 1400°C beam after testing. The large deformation of the beam was accommodated by a combination of mechanisms, namely, plastic deformation of the $MoSi_2$, multiple cracking of the Al_2O_3, and large scale interface delamination. Fig. 5 is a higher magnification micrograph showing interface failure and cracking in the Al_2O_3. Stress-time(displacement) curves for the 1200° beams are shown in Fig. 6, with the curve for a pure $MoSi_2$ beam shown for comparison. The stiffness of the laminated beams are comparable with the monolithic $MoSi_2$, likely due to the similar moduli in the as-sprayed condition of both alumina and $MoSi_2$. Post-spray consolidation will be attempted in order to increase the stiffness of the beams.

The stress-displacement behavior of the laminated beams shows an increase in both yield strength and ultimate strength compared to monolithic $MoSi_2$. The higher yield stresses of the laminated beam could be due to the higher stresses that a constrained ductile layer can experience, while the higher ultimate strengths are due in part to the layering preventing catastrophic failure. Fig. 7 show a typical region in the laminated beam after testing. Non-linear stress-displacement behavior is apparently accommodated by yielding in the $MoSi_2$ as well as by extensive interface debonding.

Fig. 8 shows a major crack advancing through the same beam. Crack advance is not accompanied by interface debonding, as compared with the behavior seen in Fig. 7 in which extensive interface debonding occurred. Apparently there are two distinct mechanisms for deformation, with and without the presence of a dominant crack. Modeling of this behavior will be carried out, and is essential in understanding the high temperature behavior of these layered structures.

Interface Mechanical Testing

Interface fracture toughness is a critical property in the performance of the $MoSi_2/Al_2O_3$ system, as well as in any composite system. A major difficulty is measuring this value easily and accurately. A new technique for measuring mode I interface toughness is being developed, and preliminary results will be shown.

Fig. 9 shows the geometry used for testing. In this scheme, a wedge is driven into a split sleeve, which in turn fits into a hole drilled at the interface of the sample to be tested; application of a load drives a crack along the interface. Analytic analysis of the sample shows that the fracture toughness of the interface is given by

$$K = \frac{-P}{2\sin\theta\,(\pi a)^{1/2}} \times (\tan\phi\,\sin\theta - \cos\theta)\,2a^{-i\varepsilon}\cosh(\pi\varepsilon) \qquad (1)$$

where
P = applied load
a = crack half length
ε = a constant describing the elastic mismatch between the materials being tested
θ and ϕ = constants describing geometry and friction.

The only unknown in Eq. (1) is the friction between the wedge and the sleeve; consequently, tests on a material of known fracture toughness are being carried out in order to evaluate the coefficient of friction, μ. In addition, a separate method for directly measuring μ is being developed.

Fig. 10 is a plot of crack length vs. load^2 for a preliminary test on a monolithic material, soda-lime glass. Using Eq. (1) and assuming a value of $K_I = 1.0$ MPa$(m)^{1/2}$, gives a value of $\mu = 0.15$. This will be compared with direct data when it is available.

Transmission electron microscopy (TEM) was employed to examine the microstructure of $MoSi_2$-Al_2O_3 microlaminate tubes after immersion exposure to molten Cu. The composite exhibited excellent performance in the molten copper

but showed reaction and dissolution in the molten steel. A detailed summary was reported in the previous quarterly progress report. The objective of this study is to determine the mechanisms which influence such behavior.

TEM specimens were made from the tip of the tubes after the immersion test. The structure and chemistry characterization were carried out on a Philips CM30 microscope operating at 300 kV. The microscope is also equipped with a Kevex EDX detector and a GATAN parallel electron energy loss spectrometer. The structure of the composite tubes, prior to the immersion test, has been characterized and the results were summarized in the January-March quarterly report and will be published in ref. [1].

Fig. 11 shows a cross-sectional TEM micrograph of the microlaminate tube in the as-sprayed condition. The layers with the darker contrast are C11b-$MoSi_2$, while the ones with the lighter contrast are g-Al_2O_3. Fig. 12 (a) shows the microstructure after the immersion test. As compared to the as-sprayed case (Fig. 11), significant changes in microstructure can be observed. No alternating layer structure can be found throughout the whole sample. Instead, the structure consists of a light background and a second phase with a distinct rod shape and darker contrast. Fig. 12(b) shows a selected area diffraction (SAD) pattern taken from the background. The pattern can be matched with a-Al_2O_3 in the $<6\bar{8}2\bar{1}>$ orientation. Corresponding EDX spectrum shows that the background contains two major peaks which can be identified as Al and O. From the results of the SAD pattern and EDX spectrum, it can be concluded that the light background observed in Fig. 12(a) is a-Al_2O_3. The only possible source for the formation of a-Al_2O_3 is from the original g-Al_2O_3 layers in the microlaminate tubes. Apparently, the temperature of the immersion test (~1200°C) is high enough for the g-Al_2O_3 in the as-sprayed form to transform to the more stable a structure. Apart from the phase transformation, the Al_2O_3 has also undergone changes in grain shape and size. The columnar (column width ~0.5 μm) grain structure in the as-sprayed form has been changed into a more equiaxed structure with an average grain size ~5 μm.

SAD patterns taken from the dark rod-shaped phase were shown in Fig. 13(a,b). The patterns can not be matched with any of the following structure: $MoSi_2$, Mo_5Si_3, a-Al_2O_3, or g-Al_2O_3. Fig. 13(c) shows the corresponding EDX

spectrum taken from the dark phase. In addition to the two major peaks, Al and O, a small Mo peak can be identified from the spectrum. Further examination of the patterns in Fig. 13(a,b) reveals the possible match to a metastable structure of Al_2O_3, k-Al_2O_3. It is possible that $MoSi_2$ reacted with molten Cu, dissolving the Si and most of the Mo into the Cu, the small amount of Mo left behind was then incorporated into the Al_2O_3 and form a metastable form of Al_2O_3.

In summary, a postmortem structure/chemistry characterization of the molten Cu immersion tested $MoSi_2$-Al_2O_3 microlaminate tubes has been performed. Apparently, the Al_2O_3 layers have successfully survived the molten Cu immersion test . Due to the high temperature involved in the test, the g-Al_2O_3 was found to transform into the more stable form, a-Al_2O_3. Significant change in grain shape and grain growth were also observed. No trace of $MoSi_2$ layers can be found at the tip of the tube. It is suspected that the $MoSi_2$ layers have dissolved into the molten Cu, with only a trace of Mo retained possibly through incorporation into a metastable Al_2O_3 phase. These results suggest that even though $MoSi_2$ may not be resistant to the corrosive molten Cu, however, the Al_2O_3 layers, having gone through phase transformation and grain growth, have formed a protective layer at the tip of the tube, which has prevented the reaction from progressing further. This also explains the rounded shape observed near the tip of the tube after the immersion test.

$MoSi_2$-Si_3N_4 COMPOSITES

Si_3N_4/$MoSi_2$ material (0, 10, 20, 30, 40, and 50% $MoSi_2$) containing 5% MgO in the Si_3N_4 was made by hot pressing the powders of these materials. Optical microscopy of these materials clearly shows both of the Si_3N_4 and $MoSi_2$ grains. Indentation by a Vickers diamond was used to find the fracture toughness values for these materials. Due to a question on stress-corrosion cracking in these materials, observation of cracks for each material was made for a period of one month. The pure Si_3N_4 was the only material which exhibited growth after indentation, which was about 20 to 30 microns. The other materials did not exhibit this behavior. The fracture toughness values for these materials is shown in Figure 14. These values were measured from crack lengths made from 20 kg Vicker indents. The error bar shows one standard deviation for the data. Each point is a fracture toughness value for each crack in the indents. (Five

indents were made for each % $MoSi_2$, thus, twenty fracture toughness values were calculated for each sample.) Some outliers are observed due to error in the crack patterns of the indents. Figures 15 and 16 show data on the indentation fracture morphology in the $MoSi_2$-Si_3N_4 composites.

Room temperature fracture strengths of hot pressed $MoSi_2$-Si_3N_4 composites containing 0 to 50 volume percent $MoSi_2$ were measured using the 4-point bend method. Figure 17 shows the test results. The sample containing 10 volume percent $MoSi_2$ had the highest bend strength. Specimens containing more than 10 volume percent $MoSi_2$ showed a monatomic strength decrease as a function of $MoSi_2$ volume fraction. The reason for the high fracture strength of the composite containing 10 volume percent $MoSi_2$ is currently not known; however, it is possible that the Si_3N_4 grain size is smaller in this sample compared to the monolithic material due to boundary pinning by $MoSi_2$ during hot pressing. In addition, residual thermal stresses may play a role in increasing the fracture resistance of the 10 volume percent material. Future work to determine strengthening mechanisms will be performed.

Assessing the electro discharge machining (EDM) characteristics of $MoSi_2$-Si_3N_4 composites is an important part of the overall investigation of $MoSi_2$-based ceramics. To this end, an informal collaboration with Texas A&M University has been established. Areas of focus within the EDM Machinability assessment include resistivity measurements as a function of composition, mechanism evaluation after wire cutting experiments, and machining optimization. Dr. Nancy Faulk at Texas A&M has had extensive experience in all of these areas, and with her help our group will have an opportunity to tailor $MoSi_2$-Si_3N_4 composites for this fast and efficient machining technique.

ELECTROPHORETIC DEPOSITION OF $MoSi_2$

(1) Literature Search

An extensive literature search on the process of electrophoretic deposition (ED) has been carried out. Information regarding the electrophoretic deposition of beta-alumina has been particularly helpful in providing information about the dynamics and limitations of ED. Research on the fundamental aspects of ED,

and on the deposition of magnesium oxide and superconductors have provided additional information about the importance of particle size, surface chemistry, and solvent properties. The most recent research on ED describes methods for tailoring laminated microstructures in oxide ceramics. This literature, along with literature regarding the surface chemistry of silicon oxides, has helped in the design of a plan of action for developing ED for $MoSi_2$-based ceramics.

(2) Initial Experiments

Since June of 1994, we have been examining ED as a process to deposit $MoSi_2$-based ceramics. There has been success in deposting oxide and nitride ceramics; however, deposition of $MoSi_2$ has proven to be difficult. Factors contributing to the difficulty of depositing $MoSi_2$ include its high density (> 6 g/cc), and large particle size (Starck Grade A: 5-20 μm). Both of these factors lead to rapid settling of particles in suspension. In addition, the surface chemistry of the commercial $MoSi_2$ powders used in these experiments is not well characterized, which makes it difficult to generate appreciable surface potentials.

Recently, deposition of fine layers of $MoSi_2$ (Starck grade C: ≈ 2 μm) has been achieved for powders washed in concentrated aqueous NaOH. The deposition medium was a 0.001 M KCl aqueous solution adjusted to a pH of ≈ 10 with NaOH, and the deposition electrode was Mo metal. Deposition was attributed to increased surface hydroxyl group density on the washed NaOH; however, the surface hydroxylation has not been quantified. Problems with deposition in aqueous media include electrolysis of water and electrode corrosion. Also, because of the high dielectric constant of water (≈ 80), particle surface potentials are limited.

(3) Summary of Plan of Action

Experiments performed to date have provided adequate information to formulate a thorough plan of action to be carried out within the next several months. The plan comprises three aspects: surface characterization and surface modification of $MoSi_2$ powders, deposition medium and dispersant (electrolyte) optimization, and deposition process optimization.

Surface modification of $MoSi_2$ powders will be performed in order to generate high surface potentials. Surface hydroxylation by EDTA or strong base is a straightforward surface modification, and will be the process used initially. Hydroxylation increases the density of chemisorption sites, thus increasing the likelihood that the surface will generate high potentials. Future techniques for surface modification include aluminum alkoxide treatment to increase surface adsorption activity. Zeta-potential measurements are an important method for determining the success or failure of surface modification. Zeta-potential measurement devices from several manufacturers have been assessed. Purchase of an instrument is forthcoming.

Proper solvent and electrolyte selection are important to this study. A good solvent should have low toxicity and low cost, and should facilitate the generation of high surface potentials when coupled with the right dispersant. Solvents with dielectric constants between 10 and 30 such as amyl alcohol, ethyl alcohol, and methyl isobutyl ketone will be investigated initially. Because the active sites (SiOH) on $MoSi_2$ surfaces are highly acidic, the best electrolyte dispersants are basic amines and amides. Several dispersants of this type will be investigated initially.

The final aspect of this initial plan of action is process optimization in the $MoSi_2$ system. Ideally, ED of $MoSi_2$ will be a rapid method of forming dense (< 40% porosity) green structures with desired dimensions. Processes such as sintering of deposited coatings, and sample removal (from the deposition electrode) of deposited multilayer composites may determine the overall feasibility of the technique in the end. For the optimization of the ED process, deposition electrode design, measurement of current-voltage relationships during ED, and sample removal and firing require thoughtful consideration for process optimization.

Development of Joining Technology for $MoSi_2$-based Components:

During our collaboration with Air Products, where $MoSi_2$-Al_2O_3 laminate composites were exposed to molten metals, we were told that one of their needs was a technology that would allow them to join $MoSi_2$-based materials to

commercial gas fittings. Therefore, we are responding to this request by initiating a study to develop joining technology. This effort will begin late in the next quarter. The primary focus of the initial research will be to join $MoSi_2$-based components to stainless steel fittings. Some preliminary work has been done to determine if it is possible to join $MoSi_2$ to Pyrex. A crack free bond was produced, but some MoO_3 gas evolution occurred at the interface.

Corrosion/Oxidation of $MoSi_2$-based Materials in Industrial Environments:

Studies were initiated in the previous quarter to obtain base-line information on the oxidation kinetics of $MoSi_2$, $MoSi_2$-5wt% Al_2O_3 particulate, and $MoSi_2/Al_2O_3$ laminate composites in pure O_2. In particular we found that the $MoSi_2$-5wt% Al_2O_3 particulate composite was more resistant to pesting, but had a higher oxidation rate at elevated temperatures compared with pure $MoSi_2$. It was found that the $MoSi_2/Al_2O_3$ laminate composite was significantly more susceptible to pesting compared with pure $MoSi_2$, most likely due to the presence of residual stresses. This quarter we began setting up the Materials Corrosion and Environmental Effects Laboratory for simulated combustion environments. Some initial studies were performed in pure CO_2. We learned that the susceptibility of $MoSi_2$-based materials to pest in CO_2 is significantly less than that in O_2. Studies in the next quarter will focus on CO_2 and SO_2-based environments.

In order to understand the effects of combustion environments on the corrosion of $MoSi_2$-based materials we will model the thermodynamics of the complex reactions. We recently procured a highly refined version of SOLGASMIX[1] which allows data input using EXCEL spread sheets. This will significantly improve the effectiveness with which we can modify and improve data bases. Figure 1 shows a portion of the data base we in the process of developing.

Impression Creep Behavior of $MoSi_2$-based Materials:

Impression creep testing of $MoSi_2$-based materials was not performed this quarter. The impression creep rig is currently being moved to the Materials Science Laboratory where it will be located outside the fence enabling direct

collaborations with industry and universities. The system will also be refurbished. Finite element modeling of the impression creep method is now complete. We will communicate the results of the experimental and theoretical studies performed to date in a major publication tentatively to be submitted to *J. Am. Ceram. Soc.*

PUBLICATIONS

1. R. G. Castro, H. Kung and P. W. Stanek, "Reactive Plasma Spraying of $MoSi_2$ using an Ar-10%CH_4 Powder Carrier Gas" Matl Sci. Eng A185 (1994) 65-70.

PRESENTATIONS

1. D. P. Butt, S. A. Maloy, D. A. Korzekwa, and J. J. Petrovic, "Impression Creep of $MoSi_2$-SiC Composites," to be presented at the International Conference on Composites Engineering, ICCE/1, New Orleans, 1994.

2. D. P. Butt, S. A. Maloy, D. A. Korzekwa, and J. J. Petrovic, "Creep Behavior of $MoSi_2$-SiC Composites," *Proceedings of the International Conference on Composites Engineering*, ICCE/1, pp 72-73, New Orleans, 1994.

3. M. S. Sandlin, D. P. Butt, and J. J. Petrovic, "Electrophoretic Forming of Non-Oxide Ceramics," to be presented at *97th Annual Meeting of the American Ceramic Society*, Cincinnati, OH, 1995.

HONORS AND AWARDS

None.

PATENTS, LICENSES AND DISCLOSURES

None.

REFERENCES

1. H. Kung, R. G. Castro, A. H. Bartlett and J. J. Petrovic, Scripta met et Materialia (accepted for publication).

2. L. D. Trowbridge and J. M Leitnaker, "SOLGAS Refined: A Computerized Thermodynamic Equilibrium Calculation Tool," Martin Marietta Utility Services, Inc. Rept. No. K/ETO-140. Oak Ridge, TN, Nov. 1993.

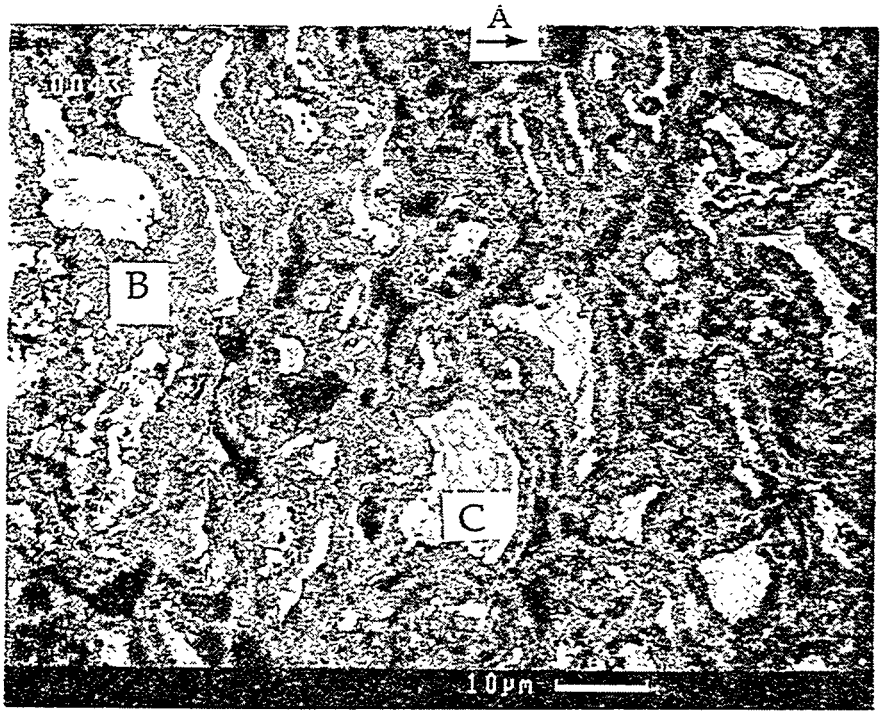

Fig. 1 Inner surface of tube immersed in Cu. 'A' is mounting resin, 'B' is silica, and 'C' is Mo_5Si_3.

Fig. 2 Interior of tube immersed in Cu. Dark region of $MoSi_2$, lighter precipitates are Mo_5Si_3.

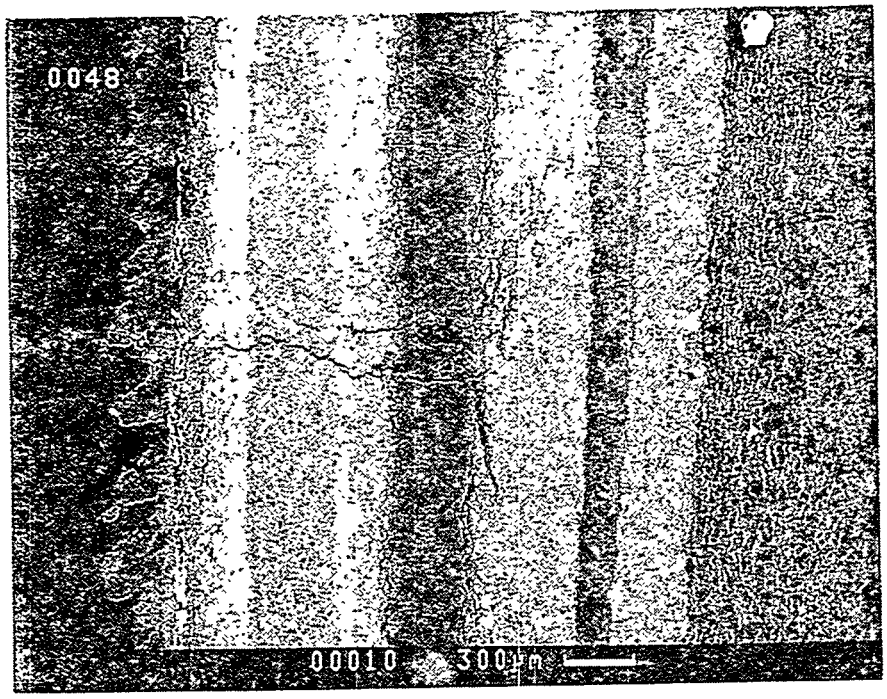

Fig. 3 A non-catastrophic crack originating on the inner surface of the tube immersed in Cu.

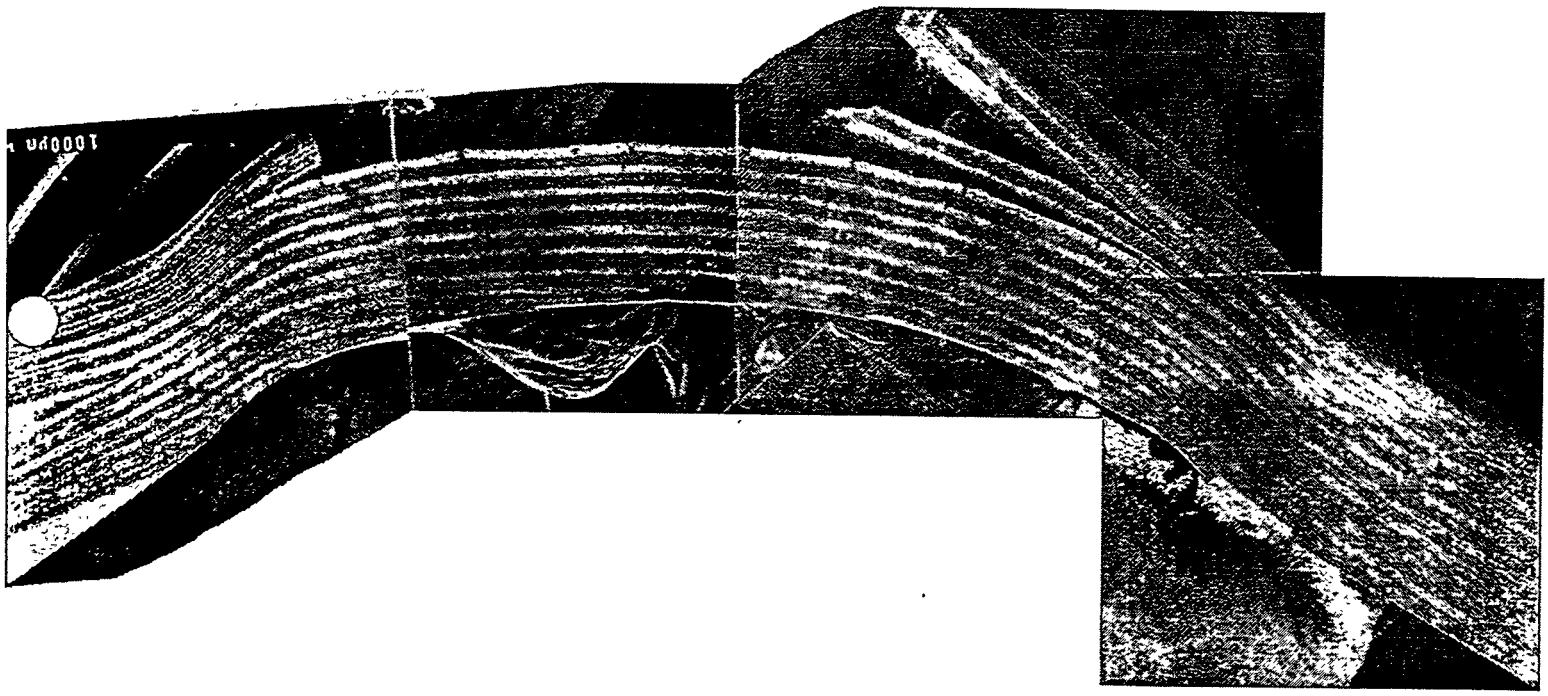

Fig. 4 Layered $MoSi_2/Al_2O_3$ beam after 4-point test at 1400°C

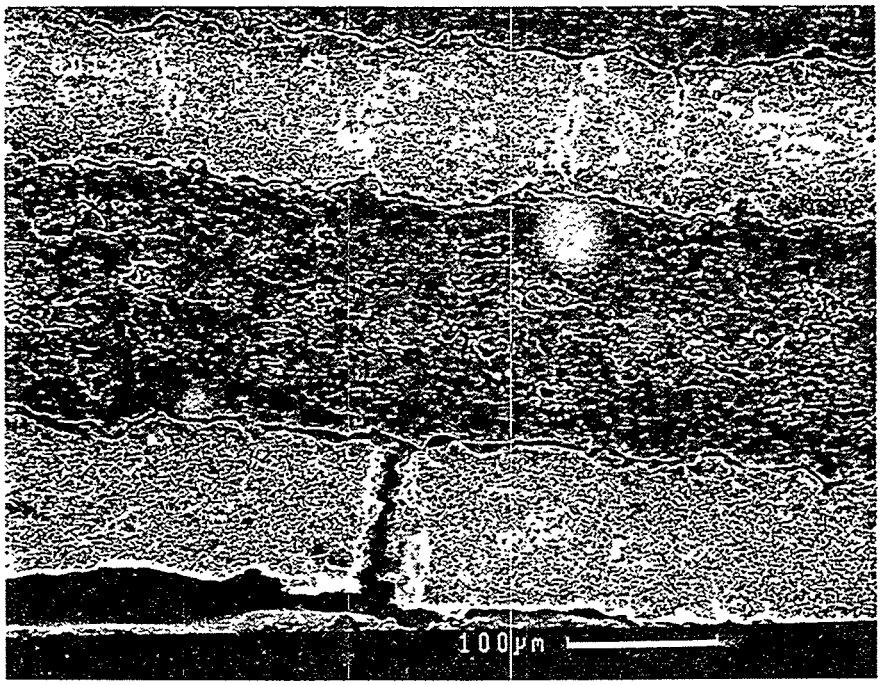

Fig. 5 Interface failure and Al_2O_3 cracking of a layered $MoSi_2/Al_2O_3$ beam after testing at 1400°C.

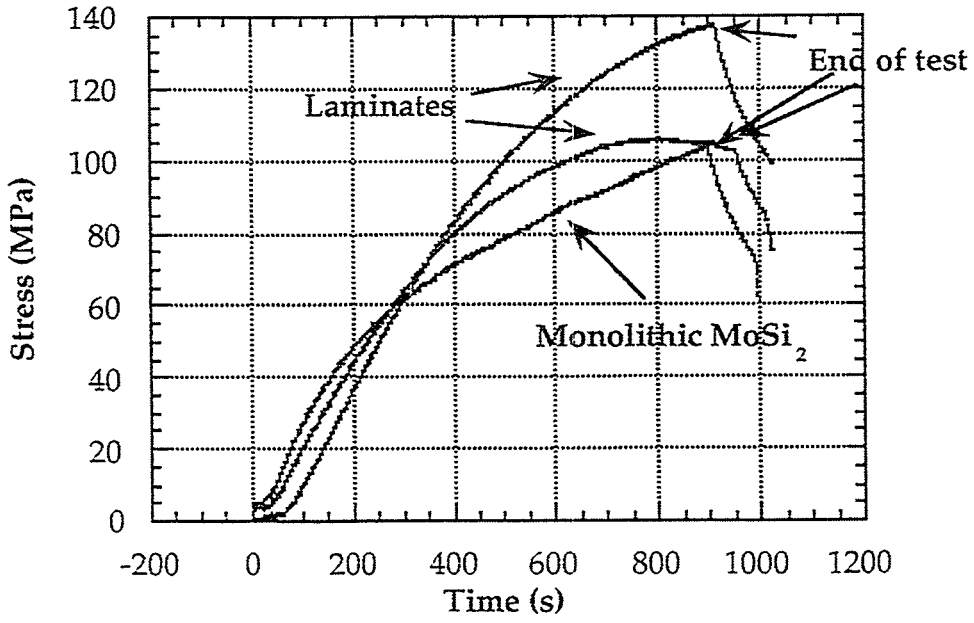

Fig. 6 Stress-time curves for $MoSi_2/Al_2O_3$ beams tested at 1200°C. A curve for monolithic plasma sprayed $MoSi_2$ is shown for comparison.

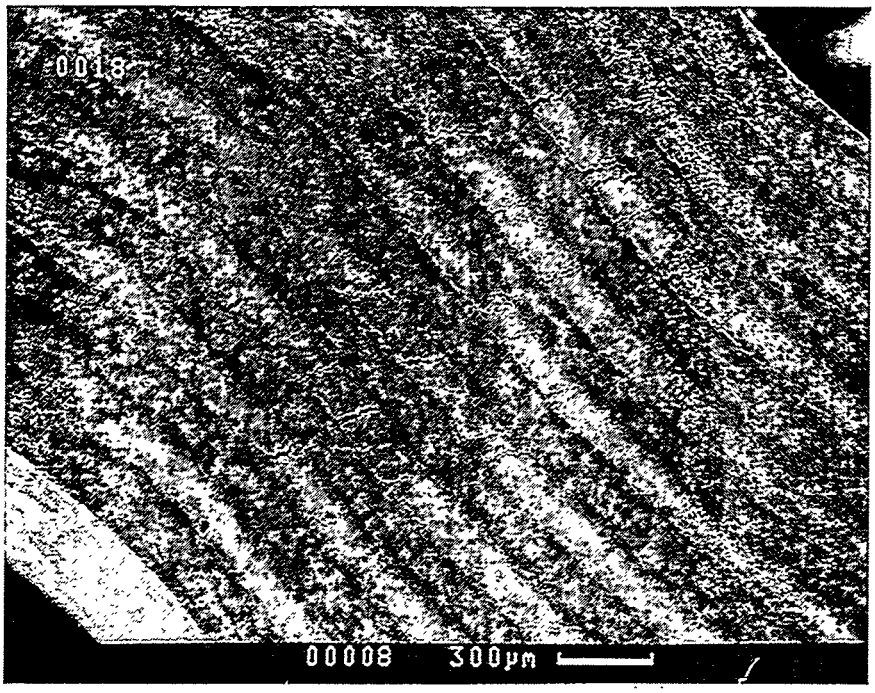

Fig. 7 Extensive interface debonding observed in the $MoSi_2/Al_2O_3$ beam tested at 1200°C

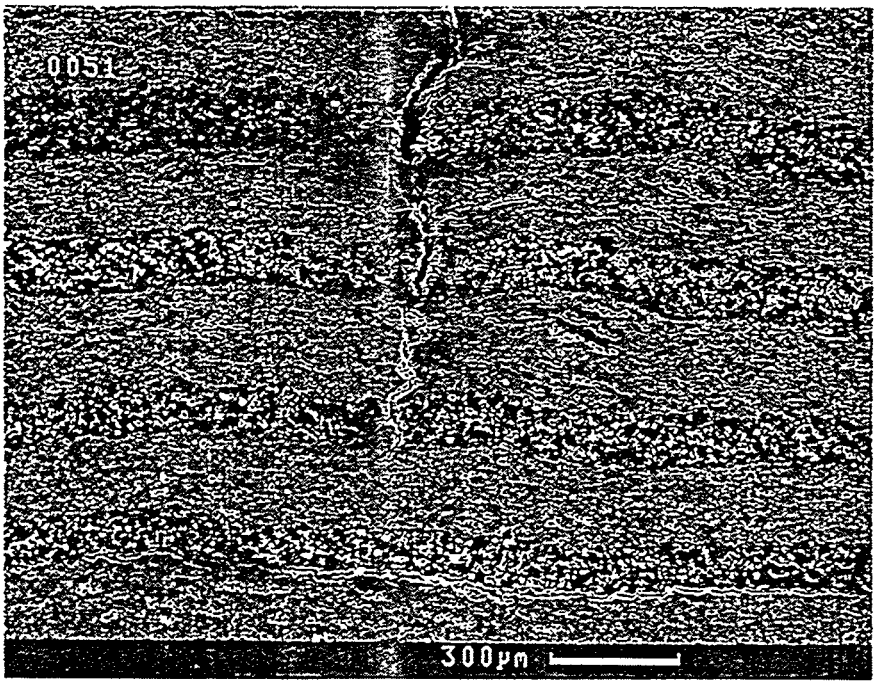

Fig. 8 Dominant crack advancing in the $MoSi_2/Al_2O_3$ beam teted at 1200°C. Note that interface debonding does not accompany crack growth.

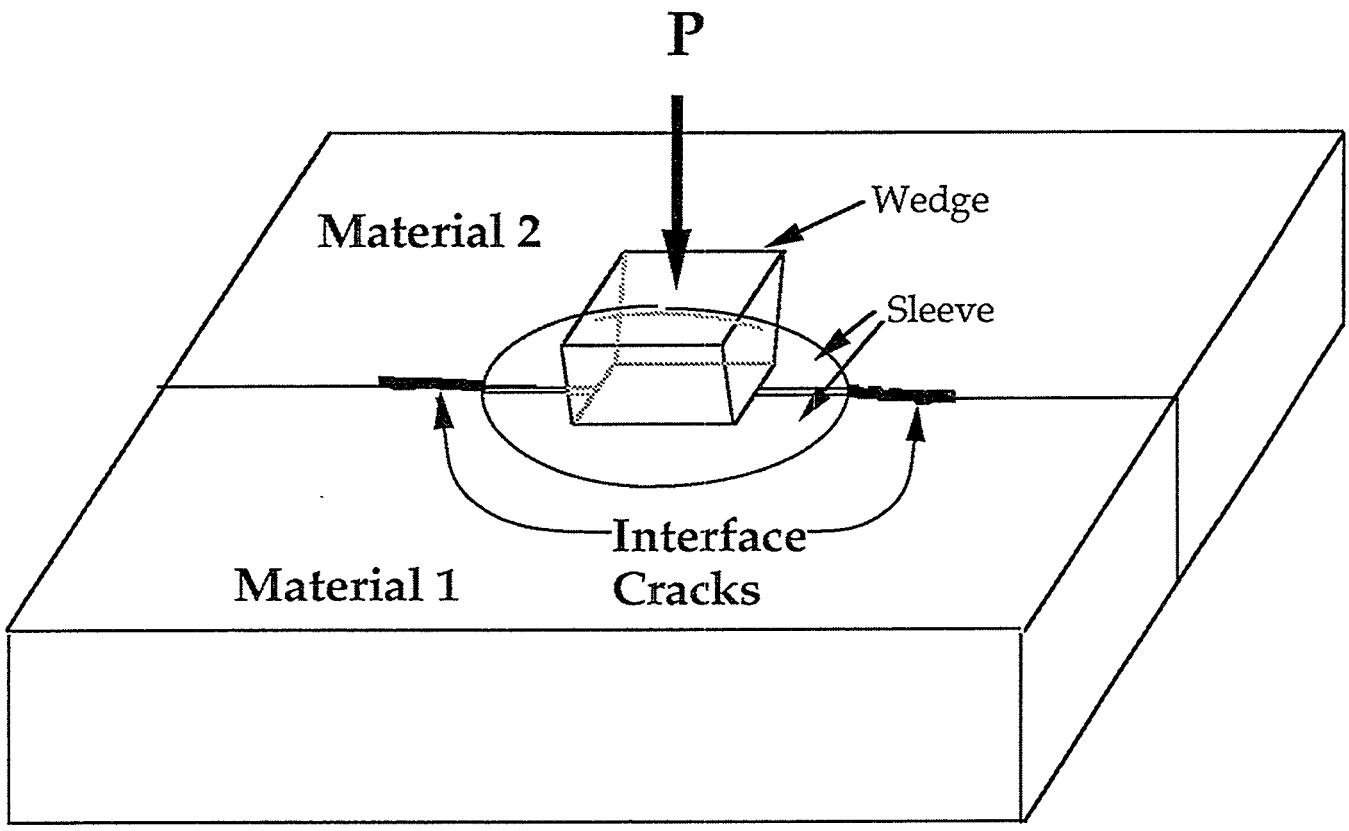

Fig. 9 Experimental set-up used in novel wedge interface toughness test.

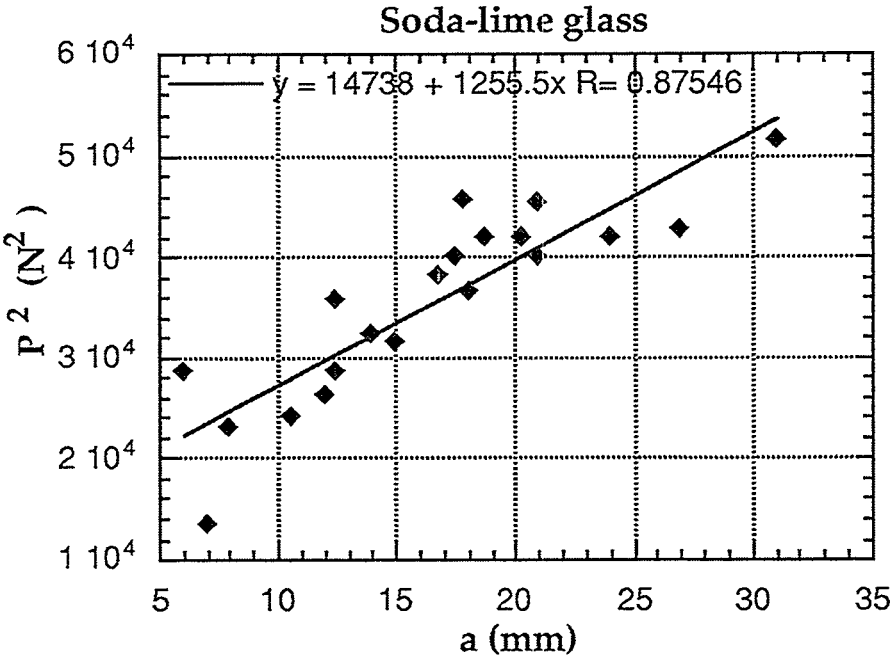

Fig. 10 Load^2 vs. crack length results for soda-lime glass tested by wedge method.

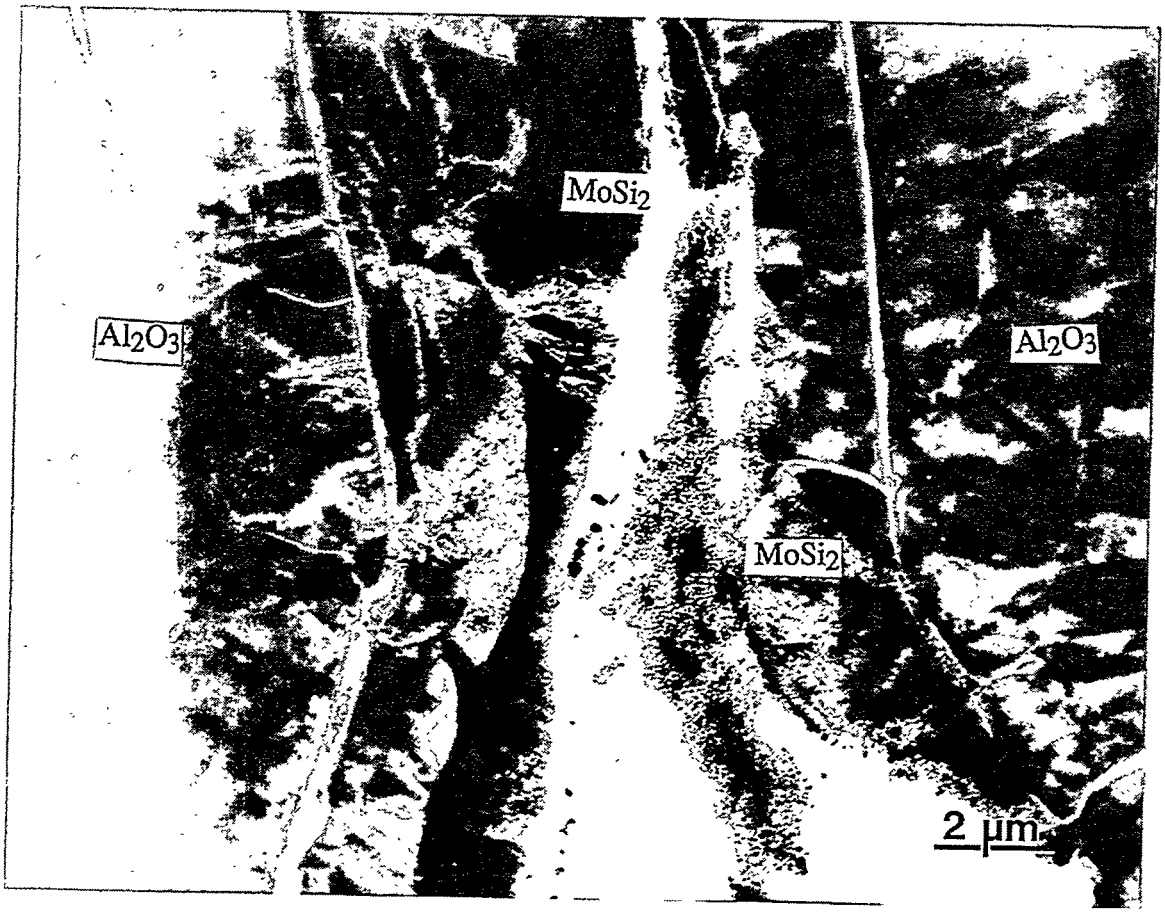

Fig. 11 TEM micrograph of the as-sprayed $MoSi_2$-Al_2O_3 composites.

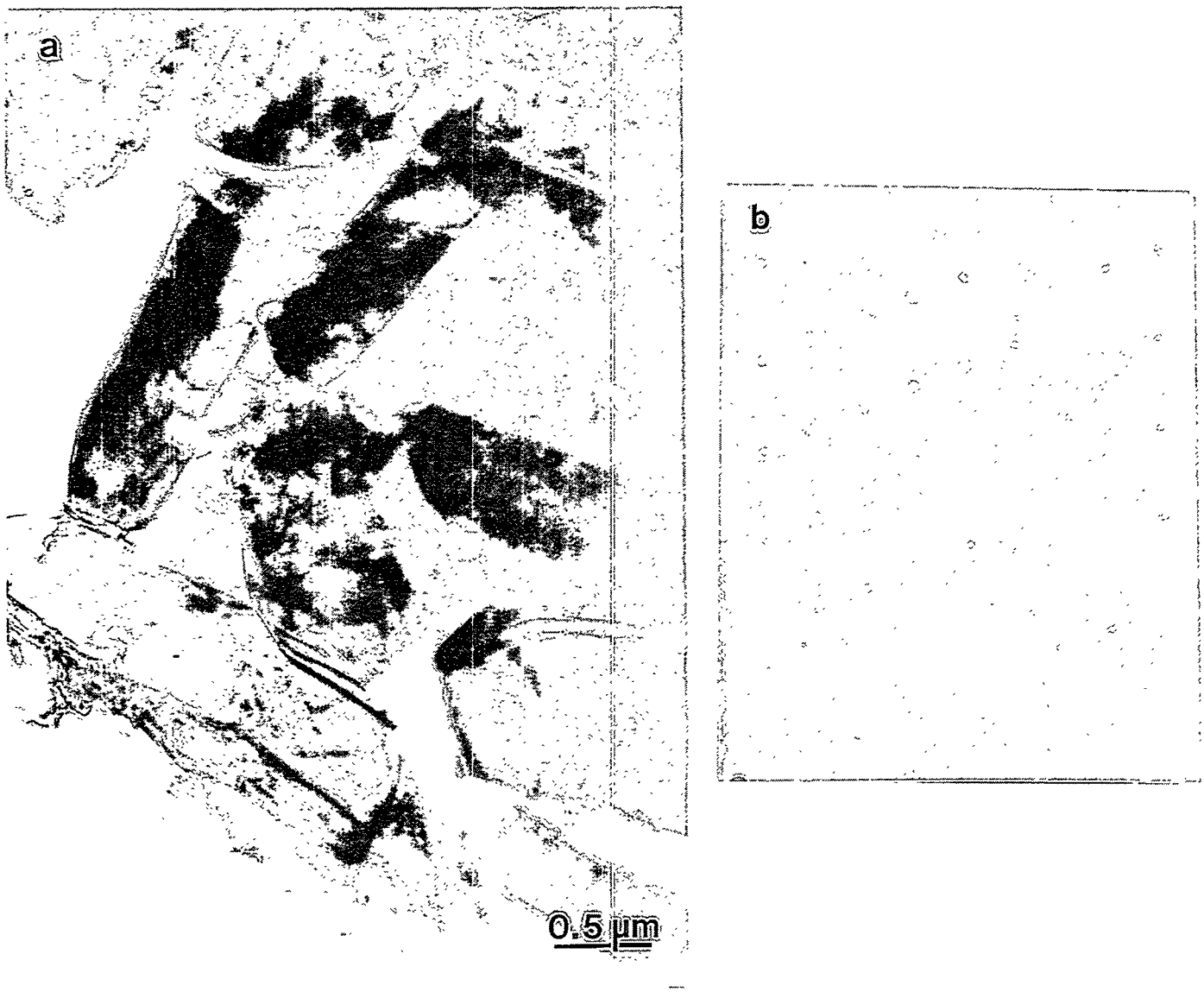

Fig. 12 (a) TEM micrograph of the microlaminate tube after immersed into molten Cu.
(b) Corresponding SAD pattern from the light background phase.

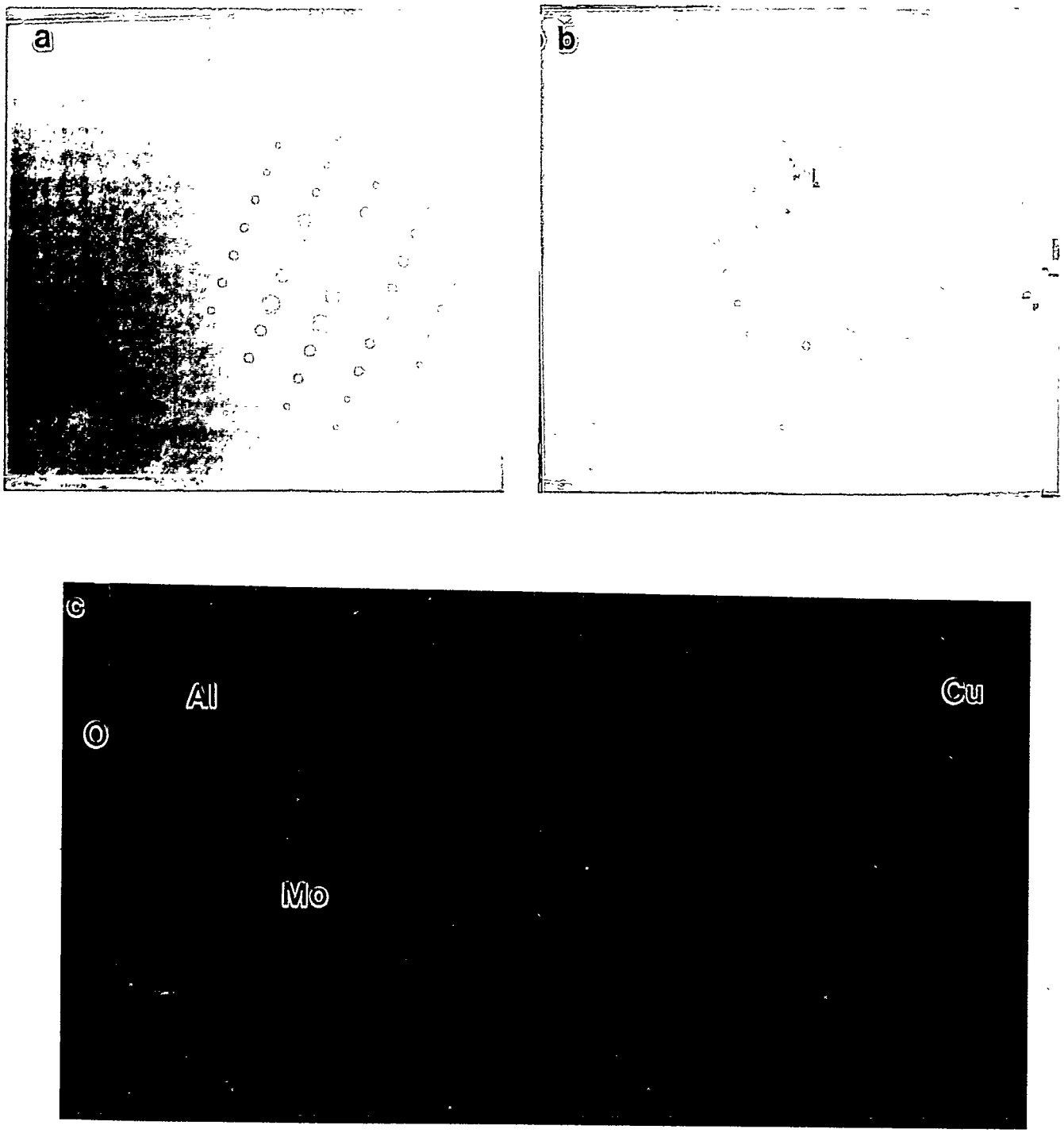

Fig. 13 (a,b) SAD patterns taken from the dark phase in Fig. 2 (a).
(c) Corresponding EDX spectrum taken from the dark phase.

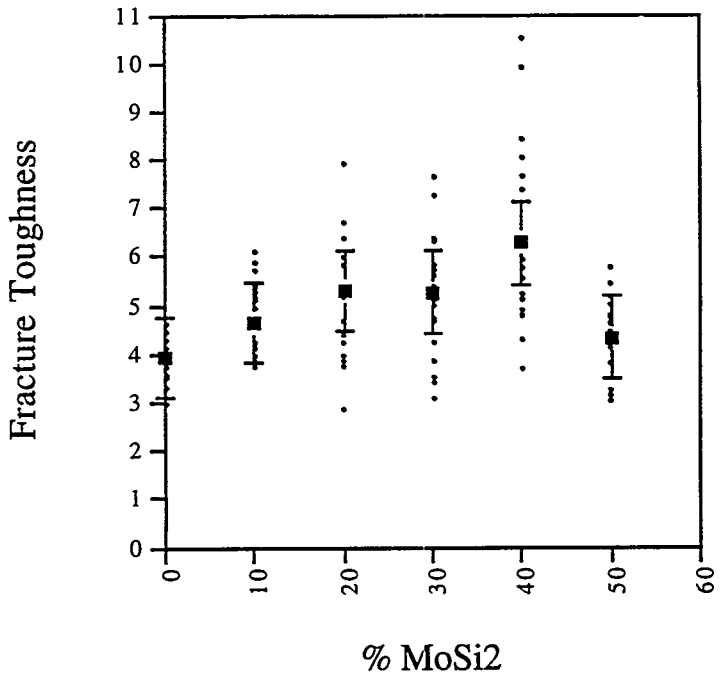

Fig. 14 Fracture toughness of $Si_3N_4MoSi_2$ materials for 20 kg load indents.

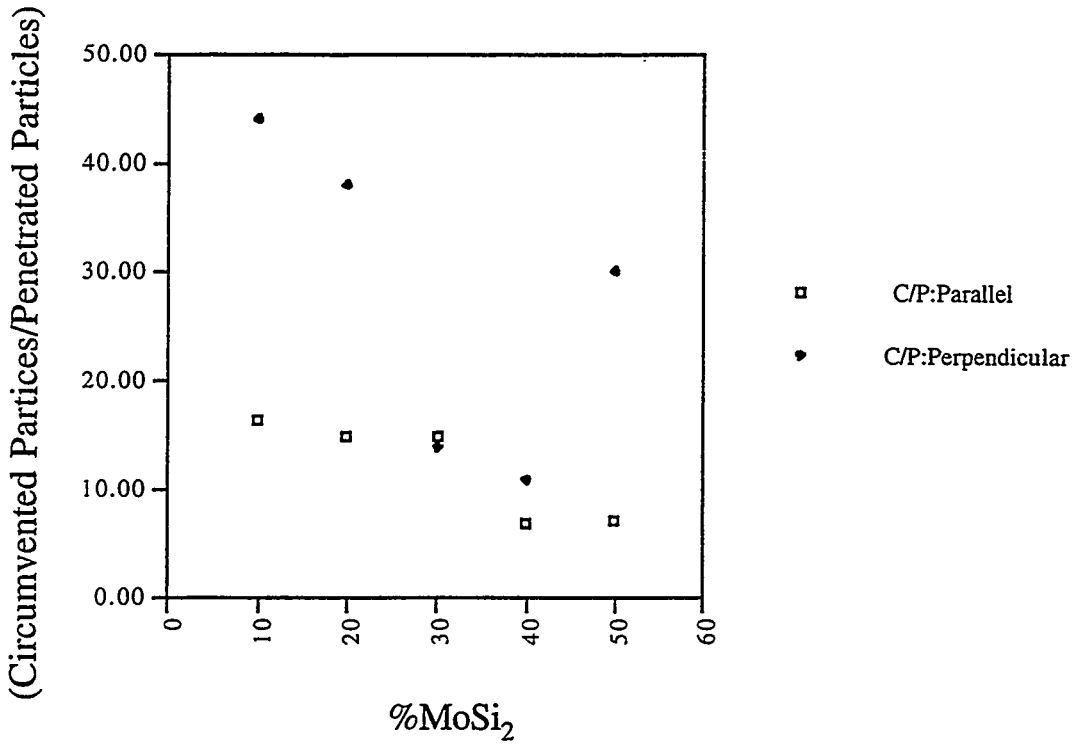

Fig. 15 Ratio of circumvented $MoSi_2$ particles and penetrated $MoSi_2$ particles for each direction.

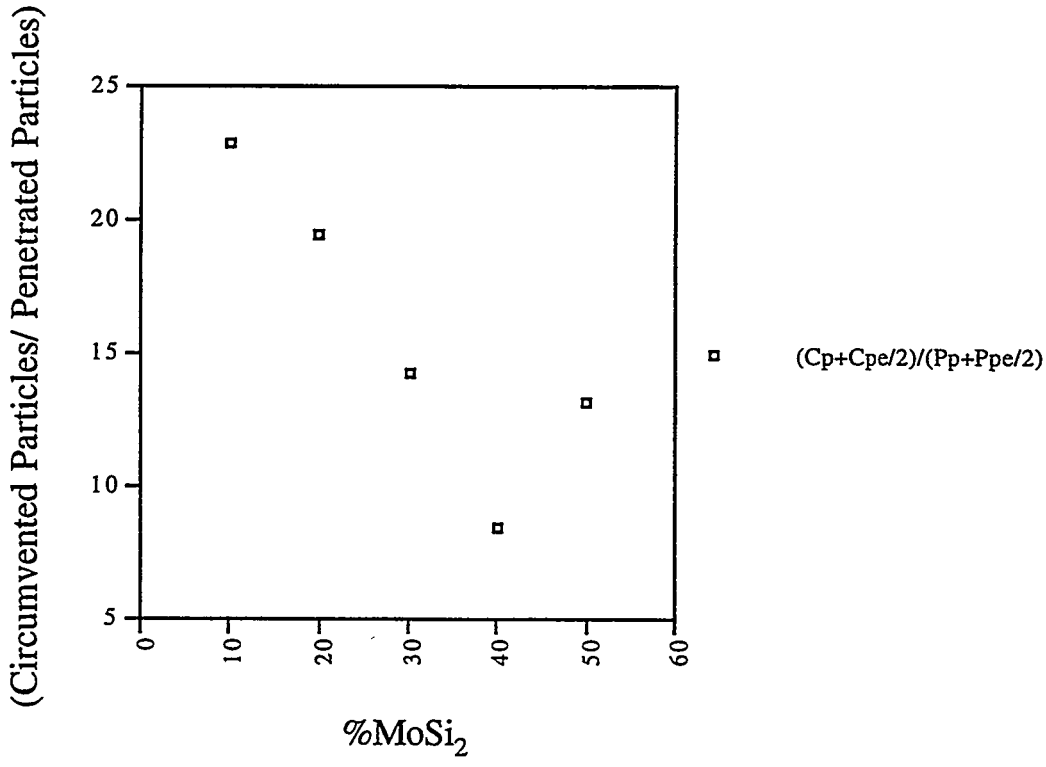

Fig. 16 Overall C/P ratio.

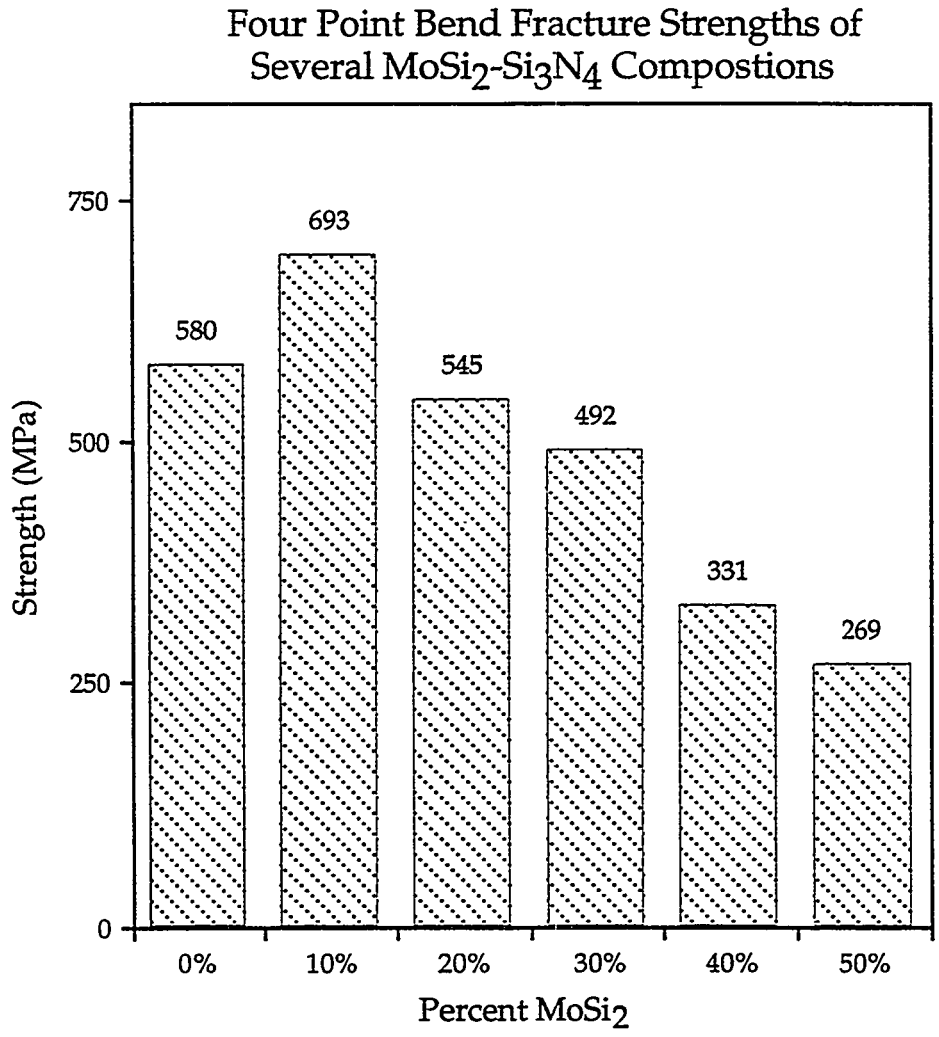

Fig. 17 Four point modulus of rupture for several Si_3N_4-$MoSi_2$ Composites.

ADVANCED CERAMICS AND COMPOSITES

ADVANCED METHODS FOR PROCESSING CERAMICS

W.B. Carter
School of Materials Science and Engineering
Georgia Institute of Technology
Atlanta, GA 30332-0245

Contract 19X-SM063C

INTRODUCTION

Combustion chemical vapor deposition (CCVD) is a flame assisted, open air chemical vapor deposition (CVD) process. The process is capable of producing textured, epitaxial coatings on single crystal substrates using low cost reagents. Combustion chemical vapor deposition is a relatively inexpensive, alternative thin film deposition process with potential to replace conventional coating technologies for certain applications. The goals of this project are to develop the CCVD process to the point that potential industrial applications can be identified and reliably assessed.

This project was initiated in October, 1992 under the direction of Brent Carter as an add-on to a project directed by Joe Cochran. This annual progress report covers work conducted from April 15 1994 through September 30, 1994.

TECHNICAL PROGRESS - FY 1994

Summary

1.Zirconia - Yttria Coatings:

Zirconia-yttria coatings were produced using liquid fuel combustion chemical vapor deposition. Four deposition conditions were investigated: two solution compositions each

deposited at two total cation concentrations (total moles of Zr + Y in solution). Table I lists the process parameters used.

Table I. - Process Parameters Used for Depositing Zirconia - Yttria Coatings

Solvent	Toluene
Reagents	2-Ethylhexanoates of Zr & Y
Reagent Stoichiometry	2.5 &7.5 mol % Y 2-Ethylhexanoate
Solution Cation Conc.	0.005 and 0.02 mol/l
Solution Flow Rate	~0.1 ml/s
Oxidizer	Oxygen
Oxidizer Flow Rate	~0.05 l/s
Deposition Temperature	1100 - 1400°C
Substrates	Polished, a-axis sapphire

Substrates were held in a holder fashioned from Kanthal wire. One flat side of a substrate faced the vertical flame at an angle of about 45° with respect to horizontal. A substrate was initially heated by lowering it slowly into the upper end of a flame produced with pure solvent (no reagents). After the deposition temperature was reached, reagent containing solvent was substituted for the pure solvent. Deposition began when this solution reached the flame. Depositions were terminated by switching from the reagent containing solution to pure solvent. After only pure solvent was being burned, the substrate was slowly removed from the flame.

All coatings were nodular as shown in an SEM micrograph of a coating produced from a 2.5 mole % $YO_{1.5}$ - 0.005 M total cation concentration solution (Fig. 1). Average grain sizes were larger for the lower $YO_{1.5}$ content coatings than for the higher $YO_{1.5}$ content coatings (0.74 ± 0.14 μm compared with 0.38 ± 0.08 μm; 0.005 M total cation concentration). Figure 2 is an SEM micrograph of a fracture cross section of a coating produced from a 2.5 mole % $YO_{1.5}$ solution of 0.005 M total cation concentration. All coatings appear dense.

The x-ray diffraction patterns indicate that the phase compositions of the coatings differ with the $YO_{1.5}$ composition of the precursor solution. Figure 3 displays such a pattern for a

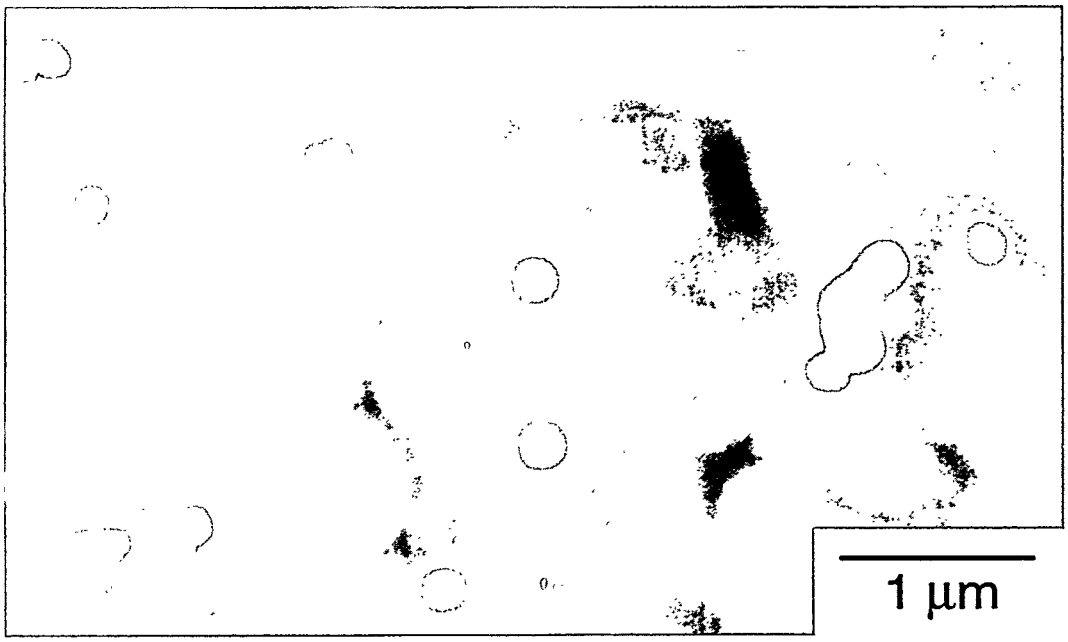

Figure 1 - Plan view SEM micrograph of coating produced with 2.5 mole % $YO_{1.5}$ solution and total reagent concentration of 0.005 M.

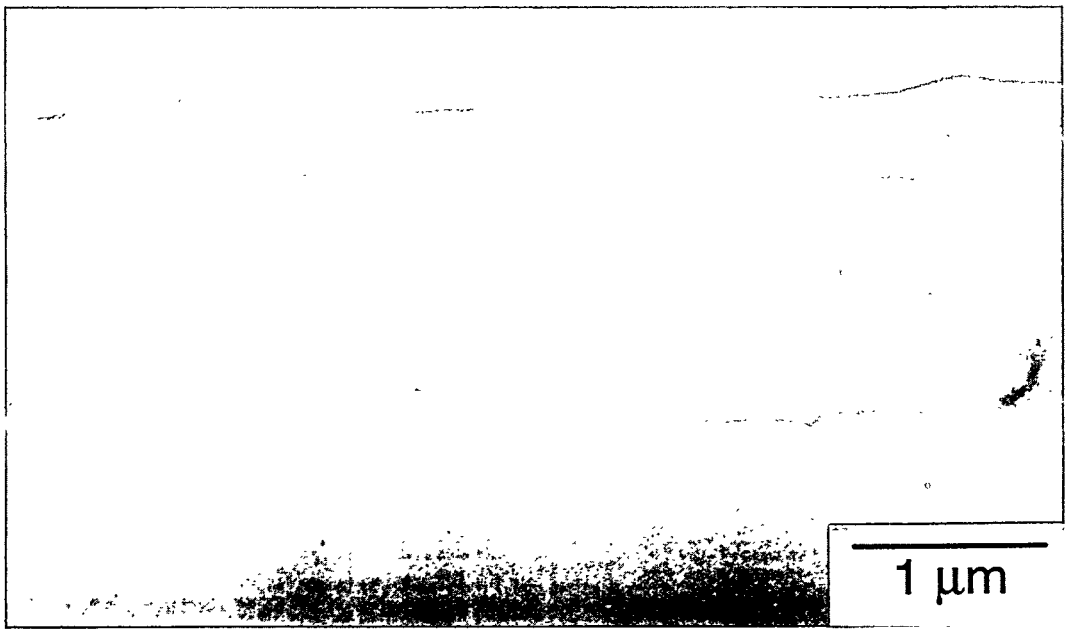

Figure 2 - SEM micrograph of fracture cross section of a coating produced with 2.5 mole % $YO_{1.5}$ solution and total reagent concentration of 0.005 M.

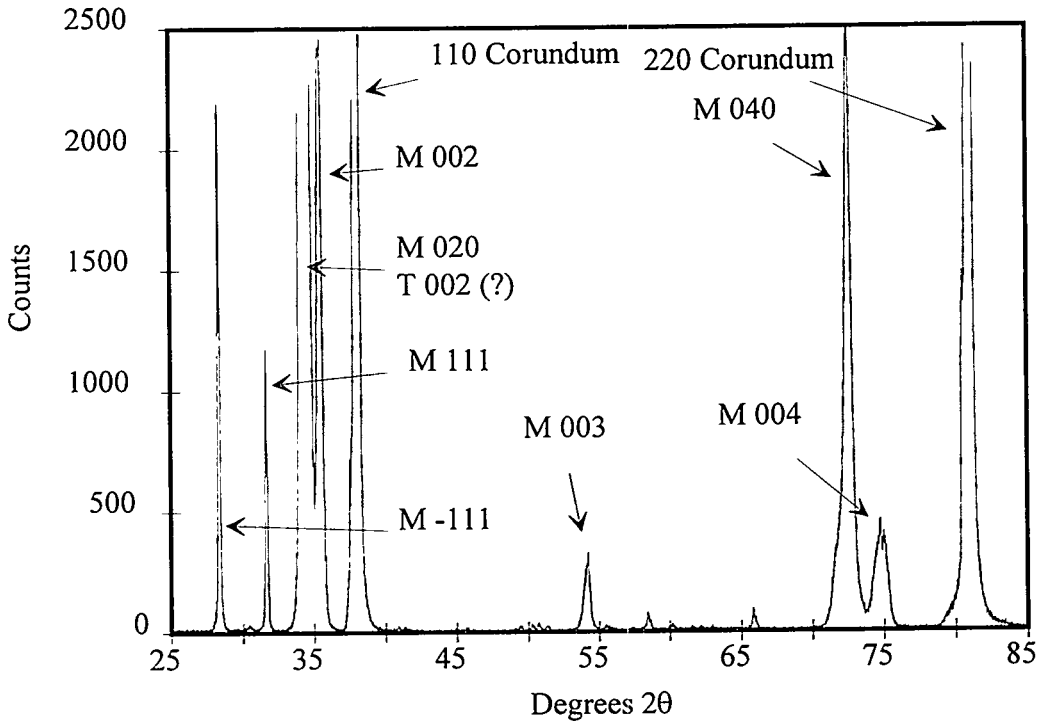

Figure 3 - X-ray diffraction pattern of coating produced with 2.5 mole % $YO_{1.5}$ solution and total reagent concentration of 0.005 M.

coating produced from a 2.5 mole % $YO_{1.5}$ - 0.005 M total cation concentration solution. This pattern indicates the unambiguous presence of the monoclinic phase. This is consistent with the ZrO_2 -$YO_{1.5}$ phase diagram if we assume that the coating has a composition near that of its precursor solution and that all of the tetragonal material that forms during deposition converts to monoclinic upon cooling to room temperature. However, the evidence to support this is incomplete as the possible additional presence of the tetragonal phase cannot be ruled out.

Figure 4 displays an x-ray diffraction pattern of a coating produced from a 7.5 mole % $YO_{1.5}$ -0.005 M total cation concentration solution. This pattern indicates the unambiguous presence of monoclinic and cubic phases. This is consistent with the ZrO_2 -$YO_{1.5}$ phase diagram assuming that the coating has a composition near that of the precursor solution and that all of the tetragonal material that forms during deposition converts to monoclinic upon cooling to room

temperature. As for the lower $YO_{1.5}$ content coating, the possible presence of the tetragonal phase cannot be excluded.

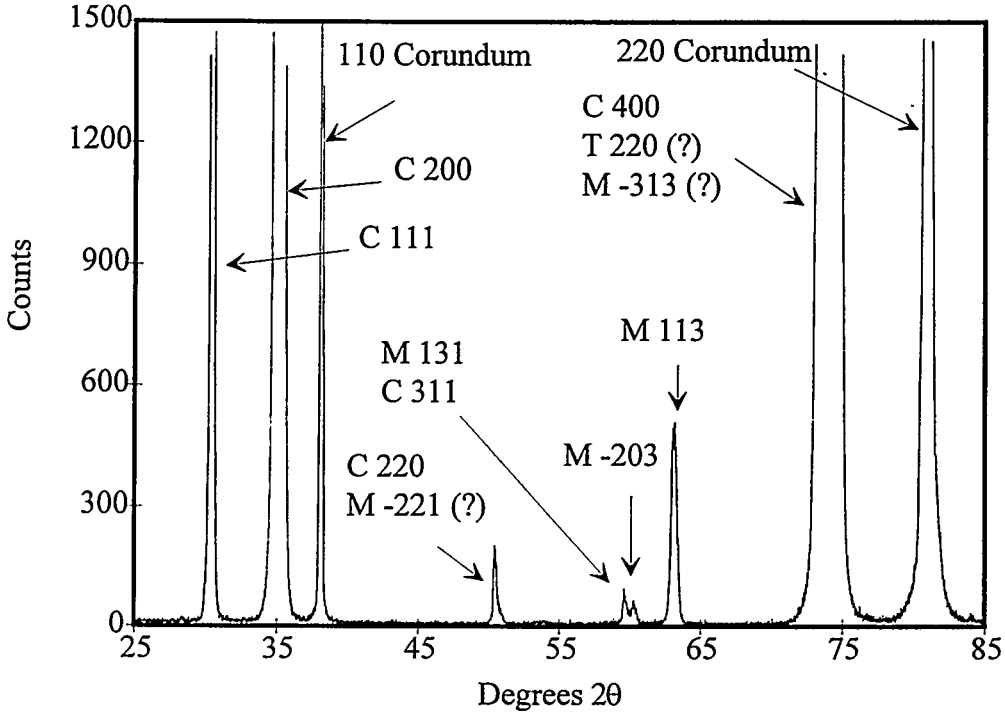

Figure 4 - X-ray diffraction pattern of coating produced with 7.5 mole % $YO_{1.5}$ solution and total reagent concentration of 0.005 M.

Figure 5 is a bright field TEM micrograph of a coating produced under similar conditions. Selected area diffraction (SAD) indicates that the dark, circular shaped features located near the centers of several grains are produced by material that is either monoclinic or tetragonal in structure. A selected area diffraction pattern obtained from an area including many grains of this coating indicates that most of the diffracting material is of cubic structure and epitaxially aligned.

The higher $YO_{1.5}$ content coatings thus appear to consist of cubic grains aligned epitaxially with respect to the substrate, and thus with respect to each other. If tetragonal material forms as expected, it apparently grows near the centers of these cubic grains. Some of this tetragonal material may transform to monoclinic upon cooling to room temperature. It is not known if all of the non-cubic material is located within cubic grains.

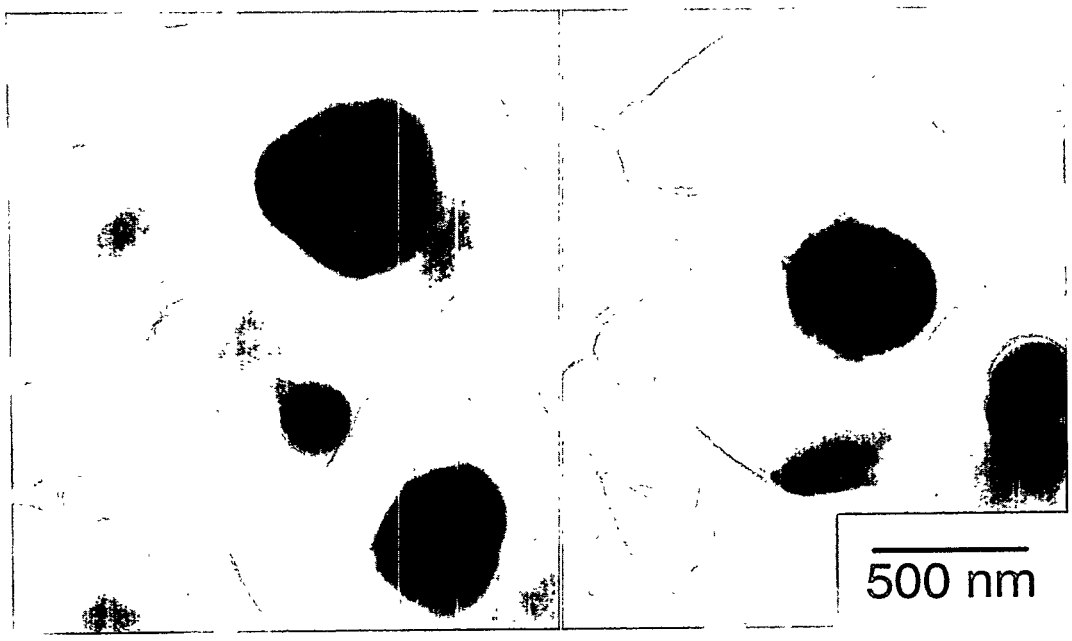

Figure 5 - Bright field TEM micrograph of coating produced with 7.5 mole % $YO_{1.5}$ solution and total reagent concentration of 0.005 M.

2. Development of Hybrid CCVD Process:

In order to produce a more stable deposition environment and to simplify scaleup, an investigation of a hybrid CCVD process using a fuel gas, a premixing burner, and a flammable solvent was initiated. The flames produced appeared to contain primarily laminar flow, unlike the flames produced with the liquid fuel CCVD process, which are turbulent. This hybrid CCVD process was used to deposit a zirconia-yttria coating.

A standard Bunsen burner with a 1 inch diameter head was modified such that an aerosol of toluene containing coating precursors in solution mixed with the fuel and oxidant gases in the barrel of the burner immediately prior to combustion. Table II lists the process parameters used.

The temperature of the deposition zone, as determined with the use of a thermocouple, was stable to within ±10°C. The temperature variations in the turbulent diffusion flames used in the liquid fuel CCVD process are significantly larger, on the order of ±100-200°C.

Table II. - Process Parameters Used with Hybrid CCVD Process for Depositing Zirconia - Yttria Coatings

Solvent	Toluene
Fuel Gas	Methane
Oxidizer Gases	Oxygen and Air
Diluent Gas	Argon
Reagents	2-Ethylhexanoates of Zr & Y
Reagent Stoichiometry	5.2 mol % Y 2-Ethylhexanoate
Solution Cation Conc.	0.015 mol/l
Solution Flow Rate	0.0028 ml/s
Methane Flow Rate	40.0 ml/s
Oxidizer Flow Rates	
Oxygen	13.3 ml/s
Air	Vent Open*
Deposition Temperature	~1200°C
Substrates	Polished, a-axis sapphire

* Vent at base of bunsen burner.

Figure 6 is an SEM plan view micrograph of a dense coating about 0.3 μm thick that was deposited in 60 minutes. X-ray diffraction patterns taken of the coating show it to be composed of cubic and monoclinic phases.

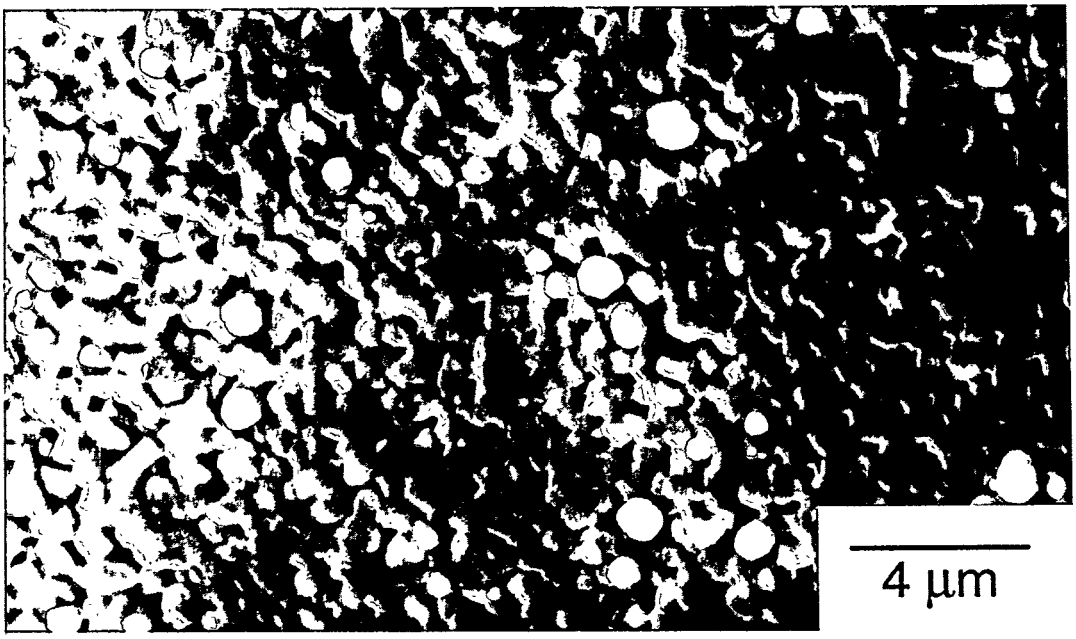

Figure 6 - Plan view SEM micrograph of coating produced with hybrid CCVD process using 5.2 mole % $YO_{1.5}$ solution and total reagent concentration of 0.02 M.

MILESTONES DURING FY 1994

The achievement of significantly greater control over the deposition environment within the flame by the development of the hybrid CCVD process constitutes a milestone accomplished during this reporting period.

PUBLICATIONS

Conference Proceedings

1. J.M. Hampikian, A.T. Hunt, and W.B. Carter, "CCVD of Silica Coatings on Ni-20 Cr," Processing and Fabrication of Advanced Materials III, eds. V.A. Ravi, T.S. Srivatsan, and J.J. Moore, TMS, PP. 345-354, 1994. Proceedings of the TMS Fall Meeting, held in Pittsburgh, PA, Oct. 17-21, 1993).

PRESENTATIONS

Oral Presentations

1. W.B. Carter, A.T. Hunt, and G.W. Book, "Combustion Chemical Vapor Deposition," presented at the Eight CIMTEC - World Ceramic Congress - Forum on New Materials, Florence, Italy, June 28 - July 4, 1994.

2. A.T. Hunt and W.B. Carter, "Deposition of Oxide and Metal Thin Films in the Open Atmosphere Using Combustion Chemical Vapor Deposition," presented at the 1994 International Conference on Metallurgical Coatings and Thin Films, San Diego, CA, 25 April 1994.

3. W.B. Carter, A.T. Hunt, and G.W. Book, "Combustion Chemical Vapor Deposition of Oxide Coatings," presented at the 1994 International Conference on Metallurgical Coatings and Thin Films, San Diego, CA, 28 April 1994.

HONORS AND AWARDS

None

LICENSES

None

INDUSTRIAL INPUT and TECHNOLOGY TRANSFER

A spin-off company, CCVD, Inc., was formed to perform research and development of the CCVD process with the eventual goal of marketing one or more products produced with the process. CCVD, Inc. has been awarded two phase 1 SBIR contracts, one of which is going to phase 2, and is expecting a third shortly.

A contract between Georgia Tech and the Department of Energy was signed in FY 1994 to produce thermal barrier coatings (TBCs) modified with the CCVD process. Subcontract negotiations are in progress with General Electric Power Generation (GEPG). This effort to produce enhanced TBCs for use in land based gas turbines is being supported by the Advanced Gas Turbine Systems Research Program, a component of DOE's Advanced Turbine Systems Program. The initial work on the CCVD process supported by the Advanced Industrial Materials Program was crucial in obtaining this additional project.

COST SHARING

None

ESTIMATED ENERGY SAVINGS

The combustion chemical vapor deposition process being developed promises to reduce energy consumption for certain coating applications currently being performed by conventional methods. The consumption of inexpensive organic solvents and fuel gases should more than offset the elimination of furnace and vacuum hardware and their concomitant energy requirements. The substantially smaller capital investment anticipated for the CCVD process relative to conventional techniques will also entail less energy expenditure up front in equipment production. As the process is presently in the early stages of development and those applications to which it may ultimately be applied are uncertain, it is not possible to produce a quantitative estimate of potential energy savings.

HIGHLIGHTS

The initial success of CCVD, Inc., a new spin-off company performing government and industry sponsored R&D, highlights this reporting period. The principal of CCVD, Inc. performed the original development work on the CCVD process while a student at Georgia Tech with support from the DOE-EE-AIM Program.

AEROGEL NANOCOMPOSITE MATERIALS

A. J. Hunt, M. Ayers, W. Cao, P. Stevens, and S.Q. Zeng

Energy and Environment Division
Lawrence Berkeley Laboratory
Berkeley, CA 94720

INTRODUCTION

Aerogels are porous, low density, nanostructured solids with many unusual properties including very low thermal conductivity, good transparency, high surface area, catalytic activity, and low sound velocity. This research is directed toward developing new nanocomposite aerogel materials for improved thermal insulation and several other applications. A major focus of the research has been to further increase the thermal resistance of silica aerogel by introducing infrared opacification agents into the aerogel to produce a superinsulating composite material. Opacified superinsulating aerogel permit a number of industrial applications for aerogel-based insulation. The primary benefits from this recently developed superinsulating composite aerogel insulation are: to extend the range of applications to higher temperatures, to provide a more compact insulation for space sensitive-applications, and to lower costs of aerogel by as much as 30%. Superinsulating aerogels can replace existing CFC-containing polyurethane in low temperature applications to reduce heat losses in piping, improve the thermal efficiency of refrigeration systems, and reduce energy losses in a variety of industrial applications. Enhanced aerogel insulation can also replace steam and process pipe insulation in higher temperature applications to substantially reduce energy losses and provide much more compact insulation. Our insulation research has been extended to a broader range of nanostructured aerogel compositions. A number of new composite materials with unusual properties were prepared. These properties arise from the very fine dimensions of the aerogel structure and the deposited material. The deposited material can produce enhanced or unusual behavior such as quantum size effects and super plasticity in metal matrix composites. These new composite materials may be useful for light weight metals reinforcement, air separation, magnetic cooling cycles, and electroluminescent sources.

TECHNICAL PROGRESS - FY 1994

Summary

1. Development and Testing of Enhanced Aerogel Insulation

This year thermally enhanced aerogel insulation based on silica/carbon composites was produced and evaluated for application as insulation. Infrared radiation is responsible for a substantial portion of the thermal conductivity in aerogel at ambient and higher temperatures. Blocking the radiant transfer by putting an opacifier into the aerogel substantially increases its thermal resistance. At higher temperatures (200° to 500°C), the radiative component of heat transfer in aerogel becomes dominant and must be suppressed for the aerogel to be a useful insulator. The radiative component is blocked by adding a second phase with a high absorption coefficient in the infrared (3 to 8 micrometers). Theoretical and experimental research established that carbon was one of the best additives for applications not requiring visual transparency.

We have developed new methods to add carbon to silica aerogel that have advantages over the earlier methods based on particle slurry addition to the sol. Chemical vapor infiltration (CVI) was used to produce nanocomposite carbon aerogel. A silica or other composition aerogel is infiltrated with a gas that is catalytically decomposed by the aerogel. The nanometer scale decomposition products are left inside the aerogel resulting in a fairly uniform solid deposit (although we have observed a low density of carbon nanotubules, rings and fibers in TEM). Deposition using the CVI method increases the strength of the aerogel and allows for much higher carbon doping levels. The samples were studied using infrared transmission and high resolution transmission electron microscopy (HREM). Nitrogen adsorption measurements were used to determine surface area and pore size distribution of the composite aerogel. Patent applications covering the CVI-aerogel nanocomposite production process were filed in FY 1994.

An precision instrument to measure the thermal conductivity of aerogel as a function of pressure and temperature was built and tested in FY 1994. The Vacuum

Insulation Conductivity Tester (VICTOR) utilizes a thin gold-film heater between identical samples clamped between temperature-controlled plates. The known input heat flux and the temperatures measured with an array of thermocouples allow an absolute determination of the thermal conductivity of the sample. The entire assembly is placed in a vacuum chamber with a variable pressure capability to determine the dependence of thermal conductivity on gas pressure. Thermocouples were calibrated against a traceable standard during the first quarter of FY 1994. Thermal resistance measurements with VICTOR showed substantial increases in the thermal resistance at all pressures at temperatures from 20° C to 100° C. It also revealed that aerogels with smaller pore sizes had improved thermal resistance at ambient pressure.

The thermal behavior of aerogel is very complex due to the presence of and the interaction among three different modes of heat transfer. Heat transfer calculations accounting for the interaction among radiation, conduction, and gas conductivity inside aerogel were carried out to predict thermal conductivity of opacified aerogel as a function of temperature, and gas pressure. The calculations predict that carbon doping significantly improves the thermal performance of aerogel at ambient temperatures. They also indicate that opacified aerogel will be an outstanding insulating material in the temperature range from 200° to 500° C.

Development of New Nanocomposite Materials using CVI

A family of new and unusual nanoporous composite materials were prepared based on the gas phase CVI and decomposition in aerogel. Various gases were infiltrated into the open pore aerogel structure that were thermally decomposed by the catalytic action of the aerogel. Composites of silica aerogel with iron, silicon, carbon, tungsten, and sulfur were prepared. Silane, trichlorsilane, ferocene, iron pentacarbonyl, tungsten hexacarbonyl, furfuryl alcohol, xylene, methane, and acetylene were used to deposit metals and carbon in the aerogel. Temperatures for the decomposition varied from room

temperature to 800° C. Various post-deposition heat and chemical treatments were used to produce compounds of the deposited materials or react with gases to form new compounds. Post processed composites of silica aerogel were prepared containing silicon carbide, magnetite, hematite, silicon, nickel oxide, tungsten sulfide, and tungsten nitride. The photoluminescent spectrum of silicon/silica composites was measured as a function of processing time and temperature. The magnetic and optical properties of the iron- and iron oxide- silica aerogels were measured. Transmission electron microscopy was used extensively to characterize the nanostructure and crystallinity of the new composites.

These nanophase materials have potential applications in metal matrix composites, magnetic cooling cycles, electroluminescent displays, and as electrodes for batteries or capacitors. Silicon-silica composites exhibit photoluminescence that our measurements confirm is due to quantum well confinement effects. The iron and iron oxide composites exhibit magnetic properties that appear useful for magnetic cooling cycles.

MILESTONES DURING FY 1994

1. Develop and Characterize enhanced aerogel insulation and publish results (August 1994).

2. Develop and characterize new non-carbon nanocomposite aerogel materials and publish results (September 1994).

These milestones were completed. Sixteen papers were published on the basis of this work and a patent application was filed for the CVI produced nanocomposite aerogels (see list).

PUBLICATIONS

Journals

1. W. Cao and A.J. Hunt, "Thermal Annealing of Photoluminescent Si Deposited on Silica Aerogels," Solid State Commun. *91* 645-648, 1994.

2. W. Cao and A.J. Hunt, "Photoluminescence of Chemically Vapor Deposited Si on Silica Aerogels, Applied Physics Letters, *64* 2, 1994.

3. D. Lee, P.C. Stevens, S.Q. Zeng and A.J. Hunt "Thermal Characterization of Carbon Opacified Silica Aerogels," accepted for publication in J. Non-Crystalline Solids.

4. S.Q. Zeng, A.J. Hunt, W.Q. Cao, and R. Greif, "Pore Size Distribution and Apparent Gas Thermal Conductivity of Silica Aerogel," J. of Heat Transfer *116*, 756-759, 1994.

5. W. Cao, and A.J. Hunt, "Improving the Visible Transparency of Silica Aerogels," J. Non-Crystalline Solids, *176*, 18, 1994.

6. Hunt, A.J. Ayers, M. "New Route to Aerogel Composites using Chemical Vapor Infiltration," accepted for publication in the J. of Non-Crystalline Solids.

7. S.Q. Zeng, A.J. Hunt, R. Greif, and W.Q. Cao, "Approximate Formulation for Coupled Conduction and Radiation Through a Medium with arbitrary Optical thickness," J. of Heat Transfer, in press.

8. S.Q. Zeng, A.J. Hunt, R. Greif, and W.Q. Cao, "Mean Free Path and Apparent Thermal Conductivity of a Gas in a Porous Medium," Accepted for publication in J. of Heat Transfer.

9. S.Q. Zeng, A.J. Hunt, and R. Greif, "Calculation of Coupled Conduction and Radiation Through an Aerogel Slab," accepted for publication in J. of Heat Transfer.

Conductivity of Gas in Aerogel," accepted for publication in J. of Heat Transfer.

11. S.Q. Zeng, A.J. Hunt, and R. Greif, "Geometric Structure and Thermal Conductivity of Porous Medium Aerogel," accepted for publication J. of Heat Transfer.

Other Publications

1. A.J. Hunt and W. Cao, ''New Routes to Nanocomposite Materials Using Aerogels,'' Proc. of the Materials Research Society, Spring 1994.

2. X.Y. Song, W. Cao, and A.J. Hunt and "AEM and HREM Evaluation of Carbon Nanostructures in Silica Aerogels," Novel Forms of Carbon II, C.L. Renschler, D.M. Cox, J.J. Pouch, and Y. Achiba Eds. *349* Materials Research Society, Pittsburgh, 269-274, 1994.

3. X.Y. Song, W. Cao, M.R. Ayers, and A.J. Hunt and ''Carbon Nanostructures in Silica Aerogel Composites,'' in press, Journal of Materials Research.

4. W.Cao, X.Y Song, and A.J. Hunt, "Preparation and Characterization of Aerogel-Based Carbon Nanocomposites," Novel Forms of Carbon II, C.L. Renschler, D.M. Cox, J.J. Pouch, and Y. Achiba Eds. *349* Materials Research Society, Pittsburgh, 87-92, 1994.

5. W. Cao and A.J. Hunt and ''Sol-gel Processing using Organo-Functional Silanes,'' Proc. of the Materials Research Society, Spring 1994.

PRESENTATIONS (by Arlon Hunt)

"Aerogel, an Unusual Low Density Solid," Department of Physics Colloquium, University of Arizona, Tucson, 23 March 1994.

''New Routes to Nanocomposite Materials Using Aerogels,'' Materials Research Society, April 12, 1994.

"Aerogel, Properties and Packaging'" 3M Central Research, St. Paul, Minnesota May 24, 1994.

"Aerogel, A Multi-use Material," Wright Patterson AFB, Dayton, Ohio, May 25, 1994.

"Commercialization Aspects of Aerogel," GenCorp, Akron, OH, May 26, 1994.

"Development of Improved Aerogel Superinsulation," Advanced Industrial Materials Meeting, Annual Information and Review Meeting, LANL, Los Alamos, NM June 1-3, 1994.

"Aerogel - Improvements, Composites, and Applications," Materials and Structures Workshop, Vienna, VA 12 July 1994.

"New Route to Aerogel Composites using Chemical Vapor Infiltration," International Symposium on Aerogels, Berkeley, California, September 21, 1994.

HONORS AND AWARDS

PATENTS/DISCLOSURES

"Aerogel Composites and Method of Manufacture," Wanqing Cao and Arlon Hunt, patent pending.

LICENSES

A license was given to Aerojet Corporation CRADA for the infrared opacification process to improve the thermal properties of aerogel for the commercialization of aerogel

INDUSTRIAL INPUT AND TECHNOLOGY TRANSFER

A CRADA was signed in FY 1994 with Aerojet Corporation to commercialize the production of silica aerogel using the carbon dioxide substitution process and opacification methods developed at LBL. The CRADA has several industrial partners to evaluate potential applications; included are General Motors, Cadillac Division, and Boeing, Maytag, Benteler, and Glacier Bay Corporations.

An industrial pipe system manufacturer has expressed interest in incorporating improved aerogel insulation into heated pipes and a CRADA for the commercialization of aerogel-based materials is under discussion.

CRADAs are under discussion with a gas separations company for potential commercialization of an aerogel based device.

COST SHARING

Cost sharing occurred on some development aspect of aerogel technology as part of the CRADA with Aerojet Corporation.

HIGHLIGHTS

The Chemical Vapor Infiltration technique discovered earlier was further developed to produce a variety of new nanocomposite materials. Materials were prepared to explore applications for thermal insulation with greater heat resistance at ambient and higher temperatures. New nanocomposite aerogels were produced with unusual properties including photoluminescence, magnetism, and high conductivity and surface area.

CHARACTERIZATION OF CVI Ddensification OF CERAMIC COMPOSITES

T.L. Starr, S.R. Stock and S. Lee
School of Materials Science and Engineering
Georgia Institute of Technology
Atlanta, Georgia 30332-0245

Subcontract #19X-SL260C

INTRODUCTION

Ceramic matrix composites promise higher operating temperature and better thermodynamic efficiency in many energy conversion systems. In particular, composites fabricated by the chemical vapor infiltration (CVI) process have excellent mechanical properties and, using the forced flow-thermal gradient variation, good processing economics in small scale demonstrations. Scale-up to larger, more complex shapes requires understanding of gas flow through the fiber preform and of the relationship between fiber architecture and densification behavior. This understanding is needed for design of preforms for optimum infiltration.

The objective of this research is to observe the deposition of matrix material in the pores of a ceramic fiber preform at various stages of the CVI process. These observations allow us to relate local deposition rates in various regions of the composite to the connectivity of the surrounding network of porosity and to better model the relationship between gas transport and fiber architecture in CVI preforms. Our observation of the CVI process utilizes high resolution X-ray tomographic microscopy (XTM) in collaboration with Dr. John Kinney at Lawrence Livermore National Laboratory with repeated imaging of a small preform specimens after various processing times. We use these images to determine geometry and

dimensions of channels between and through layers in cloth lay-up preform during CVI densification and relate these to a transport model.

TECHNICAL PROGRESS-FY 1994

Summary

Our progress in FY 1994 includes both additional CVI/XTM experiments and further analysis of previously obtained data. New experimental efforts investigate the effects of cloth orientation and fiber diameter on densification. In addition, permeability measurements at different densification times will guide development of a gas transport model. The analysis effort has produced quantitative measurements of pore surface area during the final stages of densification. This information - not obtainable by any other technique - is critical to design of fiber architectures for rapid, complete densification.

1. Imaging CVI Samples with Density Gradients

In order to reduce the possibility of "edge effects" in our experiments we now use larger graphite CVI reactors - 8.0 mm in diameter versus the previous 6.0 mm. These reactors have 175% of the volume of the earlier reactor design. Nine of these reactors were prepared with fiber architecture variations include 0/30/60° lay-up using square-weave Nicalon and Tyranno cloths with and without controlled hole alignment, and 0/90° and 0/45° lay-ups with Tyranno cloth.

XTM characterization was begun during a June test period at the Stanford Synchrotron Radiation Laboratory (SSRL) and will be

completed during the next available test period in January 1995. Three of these specimens were returned after imaging, partially infiltrated and imaged again.

Gas permeability of these specimens was measured at two levels of densification. These results will be compared to pore structure measurements developed from the XTM images. Such correlations will provide a quantitative understanding of gas flow during CVI.

In addition to these specially fabricated specimens, we machined specimens from larger samples of CVI composite and sent these for XTM imaging. These included 3-D weave, 3-D braid and filament wound Nicalon preforms.

2. Model Development

Detailed calculation of pore surface area has been completed for the 0/90 cloth lay-up preform previously imaged. The calculation involves identifying the boundary between the tow and channel regions in the image, fitting triangular elements to this boundary and summing the areas of these elements. The local fractional density also is calculated from the image data including material both within and between the fiber tows.

These results are plotted in Figure 1 and represent the only known experimental measurement of pore surface area in CVI composites. This property controls the densification process, particularly as the composite approaches full density. These measurements and analyses of image data from other preform architectures will be used to develop a preform microstructure model that allows design of fiber architecture for rapid, complete CVI densification.

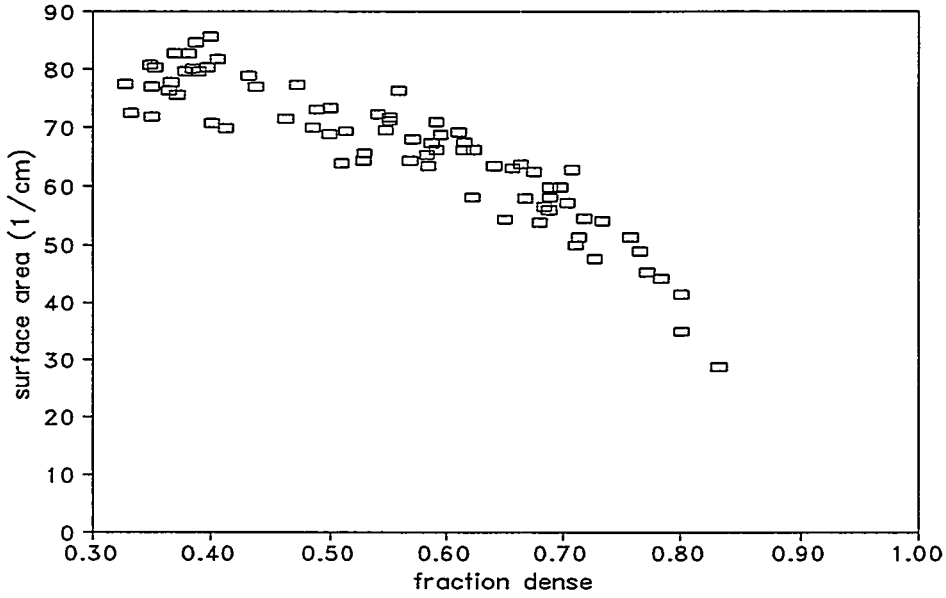

Figure 1. Pore surface area measured from XTM images decreases as density increases. Solid line is the estimate used previously in CVI process modeling.

MILESTONES DURING FY 1994

Progress was made toward completion of milestones, (1) Imaging CVI Samples with Density Gradients and (2) Model Development. These milestones will be completed in FY 95.

PUBLICATIONS

1. J.H. Kinney, D.L. Haupt, T.M. Breunig, M.C. Nichols, T.L. Starr and S.R. Stock, "Time Evolution of Microstructure During Forced Flow Chemical Vapor Infiltration of a Continuous-Fiber Ceramic Matrix Composite," Ceramic Engineering & Science Proceedings 14(9-10) 1028-1037 (1993)

PRESENTATIONS

1. T.L. Starr, S.R. Stock and S. Lee, "Microstructure Evolution During CVI Densification," at the American Ceramic Society 18th Annual Conference on Composites and Advanced Ceramics, January 9-14, 1994

2. S.R. Stock, T.L. Starr and S-B. Lee, "Microstructure Evolution During CVI Densification," Materials Research Society Fall Meeting, Nov. 28-Dec. 2, 1994

HONORS AND AWARDS

None

PATENTS/DISCLOSURES

None

LICENSES

None

INDUSTRIAL INPUT AND TECHNOLOGY TRANSFER

The 3M Company has a strong interest in CVI and is using the process for pilot-scale fabrication of prototype hot gas filters. A visit by 3M personnel to Georgia Tech planned for the end of CY 1994 was postponed until CY 1995 due to prototype production deadlines at 3M. CVI process and preform structure models developed at Georgia Tech could help 3M design future full-scale processing systems.

We had a couple of discussions with BP/Hitco concerning their use of the CVI process for aircraft brake pads. They currently use the isothermal CVI process for this product. While there is

interest in better understanding of their process, ongoing corporate reorganization of their parent company inhibited specific actions.

COST SHARING

None

ESTIMATED ENERGY SAVINGS

The development of low-cost, ceramic matrix composites will enable their incorporation into systems for energy conversion and use. Hot gas filters and high temperature heat exchangers are key components in advanced energy conversion systems, such as combined cycle power generation, that offer significant energy savings over current systems. Radiant heaters and burner tubes made of ceramic matrix composites offer significant energy savings in a wide range of industrial processes that involve heating or drying.

HIGHLIGHTS

Pore surface area was calculated from the image data over a range of fractional density. These results represent the only known experimental measurement of pore surface area in CVI composites. This property controls the densification process, particularly as the composite approaches full density. These measurements and analyses of image data from other preform architectures will allow development of a preform microstructure model for use in design of fiber architecture for rapid, complete CVI densification.

CHARACTERIZATION OF THREE-WAY AUTOMOTIVE CATALYSTS

E.A. Kenik, K.L. More
Oak Ridge National Laboratory
Metals and Ceramics Division
Oak Ridge, TN 37831-6376

W. LaBarge, R.F. Beckmeyer, J.R. Theis
General Motors - AC Delco Systems
Flint, MI 48556

INTRODUCTION

This has been the second year of a CRADA between General Motors - AC Delco Systems (GM-ACDS) and Martin Marietta Energy Systems (MMES) aimed at improved performance/lifetime of platinum-rhodium based three-way-catalysts (TWC) for automotive emission control systems. While current formulations meet existing emission standards, higher than optimum Pt-Rh loadings are often required. In addition, more stringent emission standards have been imposed for the near future, demanding improved performance and service life from these catalysts. Understanding the changes of TWC conversion efficiency with ageing is a critical need in improving these catalysts. Fresh specimens of different TWC formulations can have very different catalytic performance even for similar levels of noble metal (Pt, Rh) loading and relative ranking can change with even mild ageing. The efficiency, selectivity, and robustness of a catalyst system reflects the state of the chemically active material; including morphology, structure, elemental and chemical form. The ageing behavior and lifetime of the catalyst are determined by the evolving state of the catalyst, which in turn is a function of the chemical environment (both reactants and poisons) and exposure time and temperature. Reactivation of a catalyst requires at least partial reversal of the microstructural evolution responsible for the degradation in catalytic performance. Initially in a fresh catalyst, the active material is often distributed on a very fine scale, approaching single atoms or small atomic clusters. As such, a wide range of analytical techniques have been employed to provide high spatial resolution characterization of the evolving state of the catalytic material.

TECHNICAL PROGRESS

Summary

Technical progress meetings between GM-ACDS and MMES were held in Flint, MI on December 7, 1993 and August 15, 1994 and in Oak Ridge on April 13, 1994 to report current results on characterization of as-prepared, thermally aged, and dynamometer-aged catalyst monoliths received at ORNL during the latter half of FY 1993 and the first half of FY 1994. This included three dynamometer-aged convertors with high Rh levels, single metal model catalysts (Rh/CeO_2 and Rh/Al_2O_3) and as-prepared convertors from a process variation study. Characterization emphasizes the application of scanning electron microscopy, electron microprobe analysis, analytical electron microscopy, and X-ray diffraction.

Milestones

1. AEM characterization of catalysts.

The successful preparation of transverse monolith specimens permitted AEM measurements of the washcoat to be performed which preserved the spatial correlation with the substrate. Large (>1 μm) clumps of fine-grained (<20 nm diameter) alumina were observed in the washcoat. The clumping is taken as evidence of poor separation and blending of the alumina and ceria during milling of the washcoat powders. For as-prepared material, there was no evidence for precious metals within the alumina clumps. Between the clumps of fine alumina grains, there was a mixture of ceria and alumina with varying low levels of precious metals. Detection limit for both Pt and Rh in a GM-ACDS washcoat were determined as 0.05 wt% (minimum mass fraction) for long acquisition times (~1000 s).

Both AEM and EMPA analyses indicated that the precious metals in the as-prepared material were mal-distributed on several length scales, including monolith inlet/outlet, washcoat depth, and

local microstructural inhomogeneities such as the alumina clumps discussed above. The more porous region between the alumina clumps may provide a preferential path for infiltration of the precious metal loading solution relative to the denser alumina clumps.

2. Characterization of dynamometer-aged (10:1 Pt:Rh) catalysts.

Current AEM studies on crushed washcoat samples of conventionally loaded GM-ACDS monoliths indicated that coarse (~80 nm) precious metal clusters (Pt/Rh~12) were observed in heavily-aged material. There was a large size range for the clusters (30-120 nm) with an attendant loss of active catalyst surface area per unit volume associated with the larger crystallites. The alumina and ceria in the heavily-aged material exhibited even more grain growth and sintering than the moderately-aged material. In the former material, most recrystallized alumina grains observed in AEM were greater than 0.3 μm in diameter with some grains being larger than 1 μm. In addition, fine (5-25 nm diameter) embedded particles were observed in these large alumina grains. If these particles are precious metal clusters they represent an additional loss of catalytic surface area, as the exhaust gases cannot reach these encapsulated clusters.

In regions which had undergone significant grain growth during dynamometer ageing, especially near the cordierite substrate, most of the grain boundaries exhibited bright contrast in the SEM, indicative of segregation of high atomic number elements to the boundaries during ageing. Significant segregation of cerium (~50 wt%) was detected at such grain boundaries by high spatial X-ray microanalysis in the AEM, along with moderate concentrations of silicon (~5 wt%) and titanium (~4 wt%). The nearby cordierite ($Al_2O_3/SiO_2/MgO$) substrate is a ready source of silicon and titanium is a trace impurity in the washcoat alumina as well as an impurity in the cordierite. At high temperature, this segregation at grain boundaries may result in a liquid phase that induces the high grain growth observed.

There is a progressive evolution in the size and Pt/Rh ratio of the precious metal clusters

from the as-prepared material (where no clusters are observed) to the dynamometer-aged catalyst materials. Average cluster size ranges from 20 nm to 80 nm and the Pt/Rh ratio ranges from 25 to 12 in going from lightly to heavily dynamometer-aged material. The Pt/Rh ratio for clusters in the heavily-aged material approached the loading ratio. Material aged for 1 h in air at 850°C exhibited 20 nm clusters with a high Pt/Rh ratio (~100). This high ratio was attributed to the oxidizing environment. In order to confirm this correlation, a similar ageing was performed in a reducing environment (N_2/4% H_2). The precious metal clusters (~3 nm diameter) in this material exhibited an average Pt/Rh = 21, similar to that of the dynamometer-aged materials. Presumably, in an oxidizing environment, the rhodium is oxidized and can not diffuse to the growing precious metal clusters as rapidly as the platinum. In both the reducing portion of the dynamometer tests and the hydrogen ageing, rhodium remains unoxidized and can diffuse to the clusters.

Degradation of the washcoat in the form of cracking and spalling was observed after dynamometer-ageing by both optical and scanning electron microscopy, especially after the most severe ageing treatment. Grain growth and sintering of the alumina and ceria were observed in both the moderately- and heavily-aged materials. These changes were most evident in the washcoat close to the cordierite and near the exhaust inlet side of the monolith. The microstructure of the washcoat near the outlet side was closer to that of the as-prepared washcoat. However, in the heavily-aged material, AEM indicated relatively fine (~20 nm diameter) Pt/Rh particles in the alumina near the outlet side. On the inlet side of the same monolith, coarse (≤50 nm) Pt/Rh particles were evident near the free surface of the washcoat and finer (20-50 nm) particles were present in the sintered washcoat near the cordierite. On the basis of X-ray microanalysis, there was little difference in the Pt/Rh ratio for particles close to the inlet versus the outlet. After dynamometer-ageing both Pt and Rh exhibited less of a composition gradient through the thickness in the washcoat. Coarse (~100 nm) Pt/Rh particles were also found at grain boundary triple points in the cordierite near the washcoat

of the heavily-aged material. These two observations are consistent with the diffusion of the precious metals into the washcoat/substrate. The particles deeper in the washcoat and in the cordierite are presumed to be isolated from the flow of exhaust gases and constitute a loss of catalytic surface area.

X-ray diffraction studies confirmed the changes in both the grain size and internal strain present in the washcoat oxide components. The peaks for both γ-alumina and ceria were broad and diffuse in the as-prepared material, indicating either small particle size, high internal strain, or some combination of these two effects. In the moderately-aged material, the ceria peaks sharpened and increased in height and sharp α-alumina peaks appeared in addition to the broadened γ-alumina peaks. Strong, sharp α-alumina and ceria peaks were present for the heavily-aged material, with little evidence for any significant amount of residual γ-alumina. Distinct peaks for crystalline Pt/Rh were observed for all three dynamometer-aged materials. There were differences in peak position (lattice parameter) of the Pt/Rh clusters, which were consistent with higher Rh levels in the heavily-aged material, in agreement with earlier AEM results.

In-situ X-ray diffraction studies were performed during isochronal annealing of the as-prepared washcoat in air up to 1200°C. The material was heated in contact with a platinum strip heater and, as such, peaks for metallic platinum are always present and the evolution of the precious metal clusters could not be followed. Gradual sharpening of the diffuse peaks for γ-alumina and ceria is observed at >800°C with sharp peaks for α-alumina appearing at >1000°C. After annealing at 1200°C, the diffraction data is typical of a mixture of α-alumina and ceria with little or no evidence of retained γ-alumina.

3. Characterization of dynamometer-aged (1:1 Pt:Rh) catalyst.

In the moderately-aged high Rh (1:1 Pt:Rh) material, the distributed Rh levels in the washcoat were easily detected by AEM of crushed washcoat specimens. Fine (~10 nm) precious metal clusters of both alloy (Pt/Rh ~2) and Rh-rich (>95% Rh) compositions were observed. These

clusters tended to form in association with specific oxides in the washcoat in a manner similar to that observed for the conventional 10:1 Pt/Rh materials. Some grain growth of the alumina was observed for this material. Contaminants, such as S, P, Fe, and Si, were present inhomogeneously. These contaminants may play some role in the observed nucleation and growth of α-alumina.

4. Characterization of as-prepared catalysts from process variation study.

A program plan has been developed for future CRADA research which includes parallel microstructural characterization and dynamometer-testing of a series of process variation specimens. The as-prepared monoliths were prepared at GM-ACDS and received at ORNL in June 1994 for characterization. Different processing parameters were identified which permitted significant differences in precious metal loading and uniformity of distribution. Dynamometer-ageing of selected duplicate monoliths was initiated to determine what process variations and associated precious metal distributions resulted in improved catalytic performance. AEM and X-ray diffraction indicated that no precious metal clusters were present in the as-prepared process variation materials.

5. Characterization of model Rh/CeO_2, Rh/Al_2O_3 catalysts.

Characterization of model Rh/CeO_2, Rh/Al_2O_3 catalysts were performed to demonstrate the ability to follow the evolution of rhodium during cyclic oxidation/reduction ageing and to explain the loss in active catalytic area with ageing. Significant microstructural evolution was observed during ageing of these model catalysts. In the fresh/reduced condition, the catalysts exhibited fine grain size (~10 nm for CeO_2 and ~20 nm for Al_2O_3) and no observable precious metal clusters, though the average rhodium concentration was ~0.5 wt%. The aged CeO_2 material exhibited a significantly larger (~1 μm) grain size, low dislocation density and cavities in the 5-15 nm diameter. These cavities are the remnants of the originally interconnected porosity which was sealed off by the sintering and grain growth of the ceria. Most, if not all, the metallic rhodium clusters were in the 2-20 nm diameter range and were oriented with respect to the ceria. It is possible that some of these rhodium

clusters are internal to the ceria, similar to the cavities observed, and not on the free surface, where they would be available for catalytic reactions.

There were several types of microstructural inhomogeneity in the aged/reduced 1% Rh/Al_2O_3 model catalyst. The majority of the alumina was fine-grained, similar to the fresh catalyst. Though the average rhodium concentration was ~0.5 wt%, no heavy metal clusters were observed in such regions. However, other regions of the catalyst exhibited larger alumina grain size (100-200 nm) and significantly higher rhodium levels (~11 wt%). Coarse (10-100 nm diameter) rhodium clusters were observed in these regions. Many of these clusters were facetted and some were internally twinned. The localized grain growth in such regions may be associated with a higher local concentration of rhodium and a higher amount of chemical energy released as heat locally.

PUBLICATIONS

None for CRADA at this time.

PRESENTATIONS

Seven presentations have been made at periodic progress report meetings between GM-ACDS and MMES personnel working on this CRADA. A poster was presented at the AIM annual information and review meeting held on June 1-3, 1994 in Los Alamos.

HONORS AND AWARDS

None for CRADA at this time.

PATENT/DISCLOSURES

A record of invention has been prepared by GM-ACDS for a joint patent application on the GM-ACDS process for preparing catalyst monoliths. The application utilizes microstructural characterization from the CRADA to support the record of invention.

LICENSES

None for CRADA at this time.

INDUSTRIAL INPUT AND TECHNOLOGY TRANSFER

Joint work proceeding under CRADA titled "Improved Catalyst Materials and Emission Control Systems" between General Motors Corporation, AC Delco Systems and Martin Marietta Energy Systems.

COST SHARING

CRADA specifies matching levels of effort and support between GM-ACDS and MMES.

HIGHLIGHTS

1. The successful preparation of transverse monolith specimens has permitted AEM measurements of the washcoat to be performed which preserve the spatial correlation with the substrate. Variation of precious metal distribution can be related to position, depth, and associated microstructure of the washcoat and substrate.

2. Both AEM and X-ray diffraction indicate the transformation from γ to α alumina and significant grain during ageing of the catalysts. These processes can degrade mechanical and catalytic performance of the convertors. Segregation of cerium, silicon, and titanium to grain boundaries may promote grain growth via a liquid phase assisted diffusion.

3. Precious metal clusters evolve during ageing, with both cluster size and composition (Pt/Rh ratio) depending on the severity of the ageing. An oxidizing ageing environment promotes the formation of high Pt/Rh ratio clusters; whereas a reducing environment favors Pt/Rh ratios closer to the loaded ratio of precious metals. Oxidation of rhodium is presumed to inhibit diffusion of Rh to growing clusters.

CHEMICAL VAPOR INFILTRATION OF TiB_2 COMPOSITES

T. M. Besmann

Metals and Ceramics Division
Oak Ridge National Laboratory
P.O. Box 2008, MS 6063
Oak Ridge, TN 37831-6063

INTRODUCTION

This program is designed to develop a Hall-Heroult aluminum smelting cathode with substantially improved properties. The carbon cathodes in current use require significant anode-to-cathode spacing in order to prevent shorting, causing significant electrical inefficiencies. This is due to the non-wettability of carbon by aluminum which causes instability in the cathodic aluminum pad. It is suggested that a fiber reinforced-TiB_2 matrix composite would have the requisite wettability, strength, strain-to-failure, cost, and lifetime to solve this problem. The approach selected to fabricate such a cathode material is chemical vapor infiltration (CVI). This process produces high purity matrix TiB_2 without damaging the relatively fragile fibers. The program is designed to evaluate potential fiber reinforcements, fabricate test specimens, and test the materials in a static bath and lab-scale Hall cell.

TECHNICAL PROGRESS - FY 1994

Summary

Efforts this period were devoted to preparing improved specimens for testing at the Alcoa Technical Center and reducing processing times. Previous tests revealed that wetting of the electrode surface was non-uniform, and thus efforts were focussed on solving this problem. Samples were produced and tested in molten aluminum at ORNL. Two sets of samples were provided to Alcoa and were tested in their bench-scale Hall cell. The ORNL test results were promising, however, Alcoa has yet to report their work. Processing times were successfully

reduced to less than 6 h from over 20 h.

A set of samples were produced with varying reactant gas composition that is expected to result in varying matrix composition. Specimens with reactant flows in Table I were produced:

Table I. Reactant flows for the FCVI of carbon preforms (cm^3/min).

$TiCl_4$	BCl_3	Hydrogen
16	32	600
16	16	600
16	64	600

The FCVI runs were performed at a top surface temperature of 1050°C and ambient pressure. The final weight gains ranged from 13.7-18.2 g. A lower density sample had one or two poorly infiltrated bottom layers. The samples were also overcoated with TiB_2 to provide a more uniform initial surface. The above described samples were provided to the Alcoa Technical Center for evaluation in their bench-scale Hall cells.

Modeling work has revealed that the slow infiltration rate and difficulty in reaching high uniformity is due to the low overall flow rates. Increasing the $TiCl_4$ flow would allow an increase in flow while maintaining adequate concentrations. The major limitation in the flow of $TiCl_4$ is in the cooling water temperature of the injector. Because that temperature is limited by the process water temperature (40-50°C), the $TiCl_4$ vessel cannot be heated above that temperature. This causes the vapor pressure of the $TiCl_4$ to be low, preventing high concentrations in the carrier hydrogen. Improvements to the system were pursued via coolant restriction to the injector. Temperatures approaching 100°C were attained using a restricting valve on the injector coolant line.

Samples were produced under the new, nominal conditions: 70 cm^3/sec $TiCl_4$; 140 cm^3/sec BCl_3; 1600 cm^3/sec H_2; Hot surface temp. 1050°C. Infiltration times as low as 5.7 h were achieved to produce 6-cm thick specimens which were well-infiltrated. Tests in molten aluminum at ORNL indicated good wetting characteristics. A sample was provided to Alcoa for evaluation.

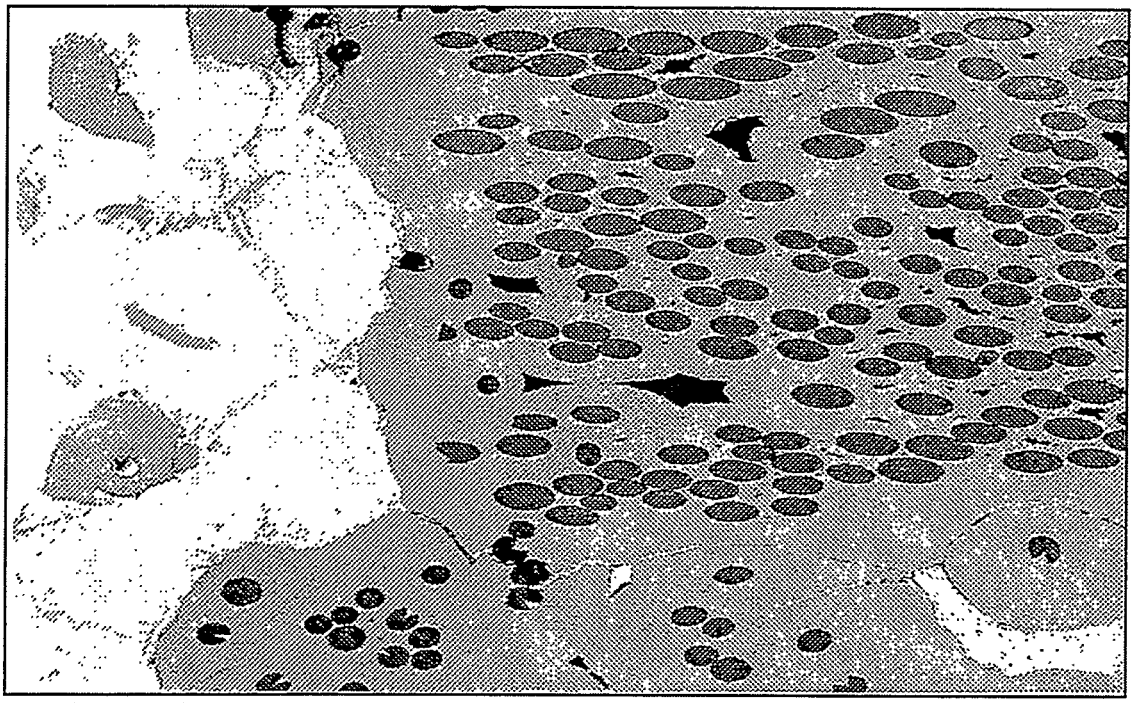

Polished surface of a composite specimen after exposure to molten aluminum displaying both good wetting and stability.

Additional discussions were held with Alcoa this period with regard to their needs for TiB_2-matrix composites. They indicated a desire to test larger plates in their DOE-funded evaluation program, and a willingness to pay for these components. Discussions were also held with AMERCOM with regard to supporting their CFCC Program efforts with modeling and

kinetics research at ORNL, SNL, and the Georgia Institute of Technology. AMERCOM has provided a written response indicating their eagerness to work with the AIM program and are currently developed a proposed statement of work.

MILESTONES:

1. Demonstrate scale-up of TiB_2 matrix composites to 8-in^2 plates, supply specimens to Alcoa for Hall-cell evaluation, and prepare letter report (August 1995)

PUBLICATIONS

1. Letter report in fulfillment of milestone 94CC-52: "Composition-Controlled TiB_2
2. "Chemical Vapor Infiltration of TiB_2 Composites," T.M. Besmann, J.H. Miller, K. M. Cooley, R.A. Lowden, and T.L. Starr, J. Am. Ceram. Soc. 77 [9] 2395-400 (1994).

PRESENTATIONS:

1. T.M. Besmann, K.M. Cooley, and T.L. Starr, Chemical Vapor Infiltration of TiB_2 Fibrous Composites, Advanced Industrial Materials Program Annual Information and Review Meeting, June 1-3, 1993, Los Alamos, NM.

HONORS AND AWARDS

None.

PATENTS/DISCLOSURES

None.

LICENSES

None this period.

INDUSTRIAL INPUT AND TECHNOLOGY TRANSFER

The Alcoa Technical Center provided specifications for large-scale specimens to be fabricated at ORNL. Several specimens have been forwarded to Alcoa for bench-scale Hall cell at testing.

COST SHARING

None.

HIGHLIGHTS

TiB_2-matrix composites were fabricated in a modified infiltration system and were prepared in less than 6 h.

HIGH-DEPOSITION-RATE CERAMICS SYNTHESIS

M. D. Allendorf, T. H. Osterheld, D. A. Outka, and D. R. Hardesty

Combustion Research Facility
Sandia National Laboratories
Livermore, California 94551-0969

INTRODUCTION

Parallel experimental and computational investigations are conducted in this project to develop validated numerical models of ceramic synthesis processes. Experiments are conducted in the High-Temperature Materials Synthesis Laboratory in Sandia's Combustion Research Facility. A high-temperature flow reactor that can accommodate small preforms (1-3 cm diameter) generates conditions under which deposition can be observed, with flexibility to vary both deposition temperature (up to 1500 K) and pressure (as low as 10 torr). Both mass spectrometric and laser diagnostic probes are available to provide measurements of gas-phase compositions. Experiments using surface analytical techniques are also applied to characterize important processes occuring on the deposit surface. Computational tools developed through extensive research in the combustion field are employed to simulate the chemically reacting flows present in typical industrial reactors. These include the CHEMKIN and Surface-CHEMKIN suites of codes, which permit facile development of complex reaction mechanisms and vastly simplify the implementation of multi-component transport and thermodynamics. Quantum chemistry codes are also used to estimate thermodynamic and kinetic data for species and reactions for which this information is unavailable.

Three tasks were defined for FY94, as follows:

1. Chemical and Physical Mechanisms of Deposit Formation
2. Computational Modeling of Ceramic Synthesis Processes
3. Synergistic Coatings Formed by Flame Spray Technology

TECHNICAL PROGRESS FY94

Summary

The primary technical accomplishments for FY94 are: 1) Experiments in Sandia's high-temperature flow reactor (HTFR) were performed to measure the decomposition rate of methyltrichlorosilane (CH_3SiCl_3; MTS), the most widely used industrial silicon carbide (SiC) precursor. A mass spectrometer was used to detect both MTS and its decomposition products. Hydrogen chloride, methane, and silicon tetrachloride were identified as major products. Measurements as a function of reactor temperature, flow rate, and carrier gas were performed. The measured MTS decomposition rate is within a factor of two of the theoretically predicted rate. A 24-step gas-phase decomposition mechanism was developed that predicts the formation of products. 2) Experiments in ultrahigh vacuum were performed to determine the adsorption and desorption kinetics of HCl on polycrystalline SiC surfaces. The sticking coefficient for hydrogen chloride at 298 K was determined to be 0.11. 3) A version of our turbulent reacting flow code compatible with a Sun SPARC-10 work station was developed this year, reducing the computational time required to run simulations of flame-spray technologies used for the formation of wear-resistant coatings. In addition to these technical specific accomplishments, discussions

were held with several manufacturers and potential end-users of ceramic composite materials in FY94 with the objective of developing a DOE lab/manufacturer/end-user consortium to promote process development and increase the use of ceramic composite materials in industrial settings.

Milestones and Progress

Task 1

High-temperature flow reactor studies of silicon carbide precursor decomposition. The primary FY94 objective of this task was to conduct an experimental investigation of the gas-phase decomposition of methyltrichlorosilane (CH_3SiCl_3; MTS), which is the precursor most commonly used by industry to manufacture SiC ceramics. Prior studies by other investigators established that gas-phase chemistry plays an important role in determining the efficiency of SiC deposition and the quality of the deposit. Since the overall objective of this work is to develop generic process models of SiC deposition, it is essential to have a quantitative understanding of the chemical reactions affecting the precursor.

Experiments were conducted in Sandia's high-temperature flow reactor (HTFR), which is equipped with a mass spectrometer for detecting MTS and its stable decomposition products. The method for obtaining the experimental data is shown schematically in Figure 1. The middle portion of the figure shows a diagram of the reactor, showing the movable injector through which MTS enters the HTFR and the mass spectrometer probe used to measure MTS and product concentrations. The upper box shows the HTFR temperature profile and the decay of the MTS concentration from its initial value $[MTS]_0$ (equal to the concentration after complete mixing with the carrier gas, but before reaction). The residence time of MTS is varied by moving the injector relative to the probe tip, a distance between 20 and 50 cm. At the temperatures, pressures, and flow rates of these experiments, this translates into a residence time (τ_{reac}) for the MTS/carrier gas mixture in the flat-temperature zone (temperature = T_{reac}) of the HTFR of 50-250 msec. The corresponding temperature and concentration profiles used in plug-flow and 2-D boundary layer modeling (see Task 2 below) are shown in the lower box.

Key results of the work conducted this year are outlined below.

- It was established that, under the low conversion conditions used in these experiments, CH_4, HCl, and $SiCl_4$ are the major stable products of the gas phase decomposition of MTS in either helium or hydrogen carrier gas. No evidence for other possible products, such as $HSiCl_3$, CH_3Cl, CH_2SiCl_2, C_2H_6, and H_2SiCl_2, was found. The global reaction stoichiometry is $CH_3SiCl_3 + 2HCl \rightarrow SiCl_4 + CH_4 + HCl$.

- The MTS decomposition rate in helium bath gas (maintained at 26.5 torr) was measured over a range of temperatures from 1183 K to 1263 K, which was chosen to maintain MTS decomposition at < 10% and thereby minimize the effects of secondary reactions. The purpose of these experiments was to determine the temperature dependence of MTS decomposition in an inert, rather than potentially reactive, carrier gas such as hydrogen. The measured rates as a function of temperature are shown in Figure 2.

- Also shown in Figure 2 is a comparison between the predicted unimolecular MTS decomposition rate obtained from RRKM theory and the experimental results. The

experimentally determined rate constant is roughly a factor of two faster than the RRKM rate. Although the uncertainty in the RRKM rate constants is at least a factor of two, the fact that the experimental rate is faster than the predicted rate suggests that secondary, bimolecular reactions of radicals with MTS are also contributing to the measured rate (this is also consistent with the products observed, which are likely formed in bimolecular reactions such as $CH_3SiCl_3 + CH_3 \rightarrow CH_2SiCl_3 + CH_4$). We conclude from the large observed activation energy (81.3 kcal/mol) that decomposition in helium is rate-limited by the unimolecular reaction of MTS. The somewhat higher overall rate observed suggests that a small contribution from secondary reactions increases the overall decomposition rate somewhat, which is consistent with model predictions (Task 2).

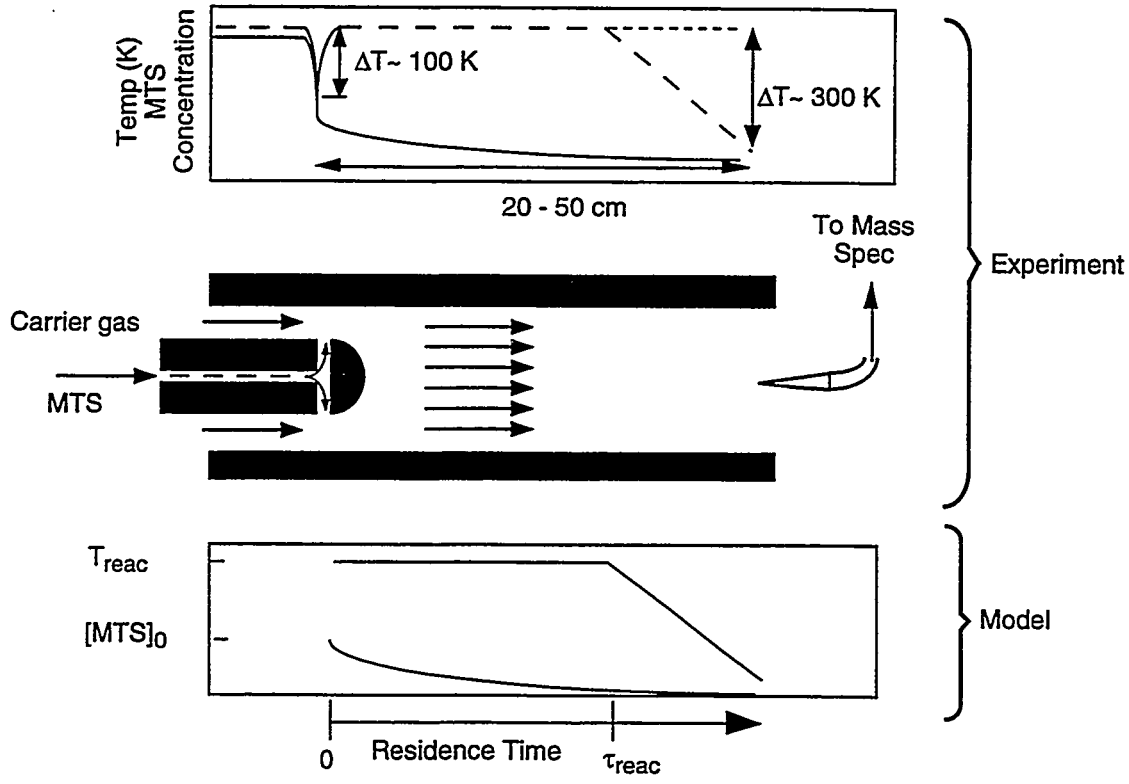

Figure 1: Schematic diagram of the HTFR experiment and comparison with the temperature profile used in the numerical model. Solid curves represent MTS concentration profiles, dashed curves are the temperature profiles.

- Measurements of MTS decomposition rate as a function of MTS concentration indicate that the MTS decomposition rate is independent of the MTS concentration, i.e., that first-order, non-chain reaction kinetics exist in the dilute regime used in these experiments. To further establish this, radical scavengers were added to the reaction mixture to see if the rate constant decreased. Addition of 6-10% of acetylene, ethylene, or propylene to the reaction mixture actually increases the MTS decomposition rate slightly, suggesting that bimolecular reactions are not a major factor in determing the rate. Experiments in which the reactor surface area was increased by 48% also indicate that wall reactions do not make a significant contribution to the decomposition rate in these experiments, as shown in Table I.

- MTS decomposition in hydrogen carrier gas is substantially faster than in helium. At 1193 K, an MTS decomposition rate of 2.1 s^{-1} was measured, which is almost 6 times the rate measured at the same temperature in helium bath gas (0.36 s^{-1}). The MTS rate is found to increase asymptotically with exposure of the reactor to hydrogen and MTS, requiring the reactor to be "conditioned" for approximately two hours prior to making rate measurements. This behavior is suggestive of the formation of a surface intermediate on the reactor walls, implying a heterogeneous mechanism for the increase in reaction rate. However, the addition of radical scavengers such as ethylene, propylene, and acetylene decreases the decomposition rate markedly, indicating that a gas-phase chain reaction may also be involved. Thus, MTS decomposition in a hydrogen carrier gas involves different mechanisms from those observed in helium. Further experimental and theoretical work is necessary before process model development can proceed.

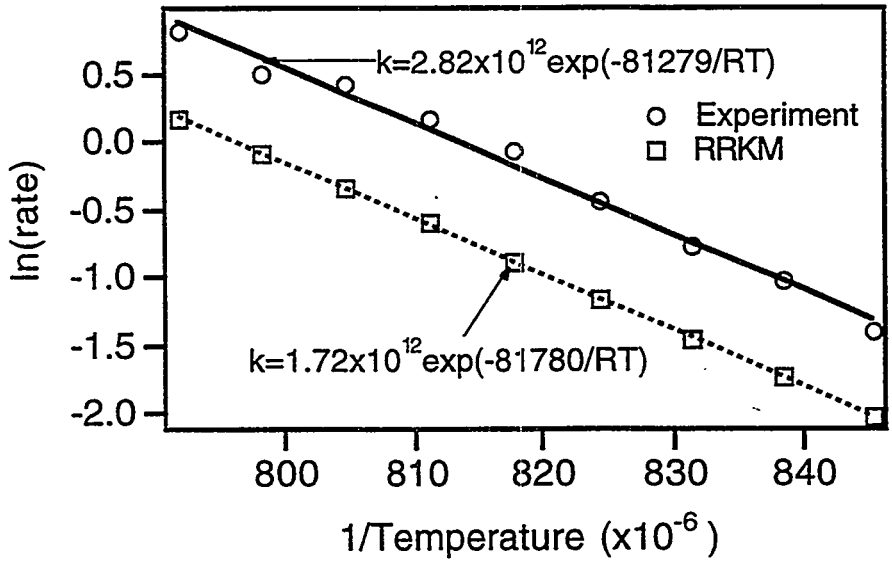

Figure 2: Comparison of MTS decomposition rates measured in the HTFR compared with the predictions of RRKM theory.

Measurements of hydrogen chloride adsorption/desorption on polycrystalline silicon carbide surfaces. A second objective of Task 1 is to obtain quantitative information concerning key surface processes affecting deposition that is needed for model development. Prof. Michelle Schulberg of the Chemistry Department at Chatham College, Pittsburgh, PA, provided valuable expertise on surface chemistry during a visit to Sandia during the summer of 1994 as an AIM-sponsored visiting scientist. She completed experiments concerning the reaction of hydrogen chloride with SiC surfaces that were begun under AIM sponsorship in 1992. Results of these experiments suggest that our earlier interpretation of HCl desorption data is incorrect due to a (at that time unknown) xenon impurity in the chamber with the same mass as $SiCl_3^+$, the major cracking fraction of $SiCl_4$. This lead to the erroneous conclusion that HCl could etch the surface of SiC via loss of $SiCl_4$. Key results of the latest study, which is being submitted to *Surface Science* for publication, are given below.

- HCl is adsorbed by the SiC surface. Auger electron spectroscopy (AES) shows that, for samples exposed to much larger than saturation coverage doses, the amount of chlorine adsorbed increases with the proportion of silicon on the surface. After the adsorption, the silicon Auger signal decreases sharply, while the signal due to carbon remains fairly stable. This provides indirect evidence that chlorine is adsorbed by surface silicon sites. To calculate the surface coverage, assumptions must be made regarding the stoichiometry of the surface layer. Two limiting cases give saturation coverages of 0.13 to 0.92 monolayers.

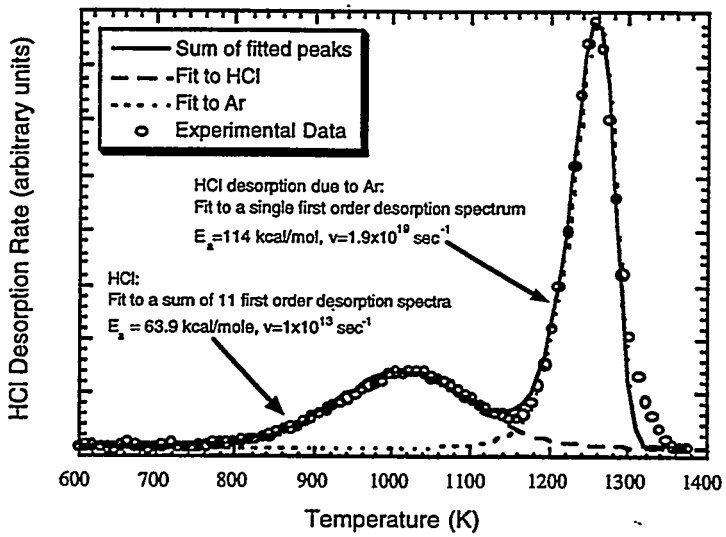

Figure 3: Temperature-programmed desorption profiles showing the desorption of HCl and Ar from a polycrystalline SiC surface.

- When the SiC sample is heated to temperatures in the 700-1100 K range, chlorine desorbs from the surface, as shown by a decline in the Cl AES signal. All chlorine leaves the surface as HCl; no surface etching occurs. HCl desorbs in a peak centered at 1020 K (Figure 3), corresponding to the decrease in the AES signal. No other desorption products are found in this temperature range. In particular, no silicon-chlorine or carbon-chlorine species are detected. At higher temperatures (1150-1300 K), argon that remains on the surface after sputter cleaning desorbs, removing HCl adsorbed on chamber walls and producing a second HCl desorption peak located at 1260 K.

- The HCl desorption peak can be fit to a first order desorption model (Figure 3). Since the surface of polycrystalline SiC is heterogeneous, with a variety of accessible binding sites, a multiple-site desorption model is used. We assume that there are eleven different sites with evenly spaced binding energies and that their initial populations are described by a Gaussian distribution. The total desorption spectrum is then the sum of the desorption from each site. The pre-exponential factor for each site is held fixed at the "normal" value of 10^{13} sec^{-1}. The

best fit to the experimental data is found when the mean activation energy for desorption is 63.9 kcal/mol and the width of the Gaussian distribution is 4.9 kcal/mol.

- By comparing the incident flux and the desorption flux, the initial sticking probability of HCl on a clean SiC surface is found to be 0.11, similar to values measured on Si(111) surfaces. A first-order adsorption model provides a good fit to the experimental data (Figure 4).

These observations throw an entirely new light on our understanding of the effect of HCl on SiC formation. Our previous study of HCl surface kinetics suggested that strongly bonded surface chlorine could inhibit SiC deposition by blocking surface sites. The latest results indicate that the bonding is not so strong and that HCl surface residence times may be too short at process temperatures to account for the inhibition effect observed by Besmann et al.*

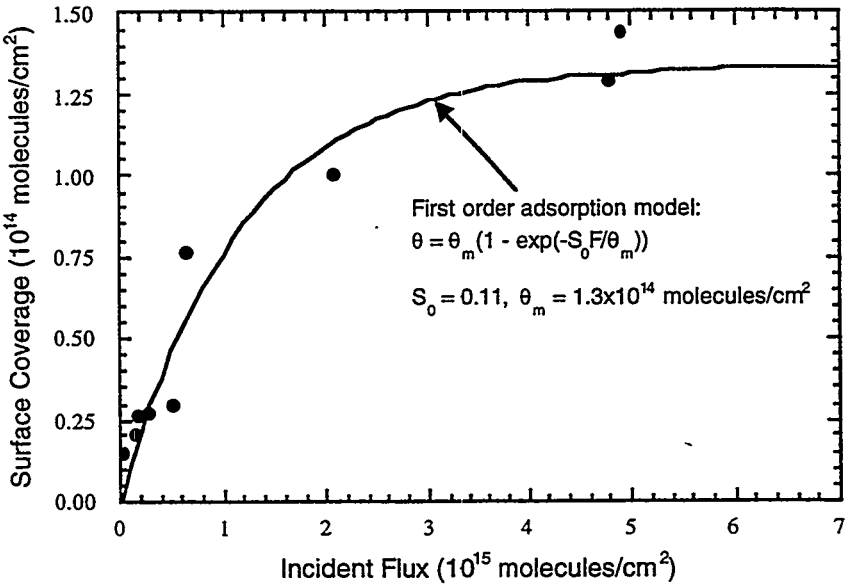

Figure 4: Comparison of the amount of desorbed HCl (as determined from the surface coverage) as a function of incident HCl flux. A first-order adsorption model indicates that the HCl sticking coefficient is 0.11 at 298 K.

Task 2

Modeling the gas-phase decomposition of silicon carbide precursors. Gas-phase chemistry is an important aspect of SiC deposition processes. Experiments by several investigators show that the precursors, MTS and hydrogen, react under processing conditions to yield gas-phase products including HCl, CH_4, and $SiCl_4$. Our own experiments in the HTFR (see Task 1) confirm this. Thus, an essential part of process simulation is the development of a mechanism that predicts the temperature and pressure dependence of MTS decomposition. We have made important progress during FY94 toward developing an experimentally verified model for this chemistry. Key results are summarized below.

---

* T. M Besmann, B. W. Sheldon, T. S. Moss III, M. D. Kaster *J. Amer. Ceram. Soc.* **75**, 2899 (1992).

- A reaction mechanism including 78 gas-phase reactions and 45 species assembled during FY93 was used to predict MTS decomposition and product formation rates measured in the HTFR. Using estimated reaction rates, reasonable agreement was achieved with experimental results for 1200-1300 K reactor temperatures. Sensitivity analysis, which identifies those reactions having the greatest influence upon species concentrations, allowed this reaction set to be condensed to 24 reactions and 17 species.

- Both plug-flow and boundary-layer codes were tested for their ability to simulate HTFR data. Good fits to experimental data could be achieved using a plug-flow model, which is simple (it includes no fluid mechanics) and fast. The more sophisticated CRESLAF (Chemically Reacting Shear-Layer Flow) code, which assumes boundary-layer flow and includes multicomponent mass and thermal diffusion, heat transfer, and buoyancy, predicts that substantial radial concentration gradients exist for some species in the HTFR reaction zone. Future modeling studies will therefore use the CRESLAF code rather than the plug flow model currently in use. An advantage of CRESLAF is that it can also predict the axial and radial temperature and velocity profiles for the reactor if the wall temperature is known. For example, Figure 5 shows the predicted axial velocity obtained by fitting the reactor wall temperature to match thermocouple measurements of the axial gas-temperature.

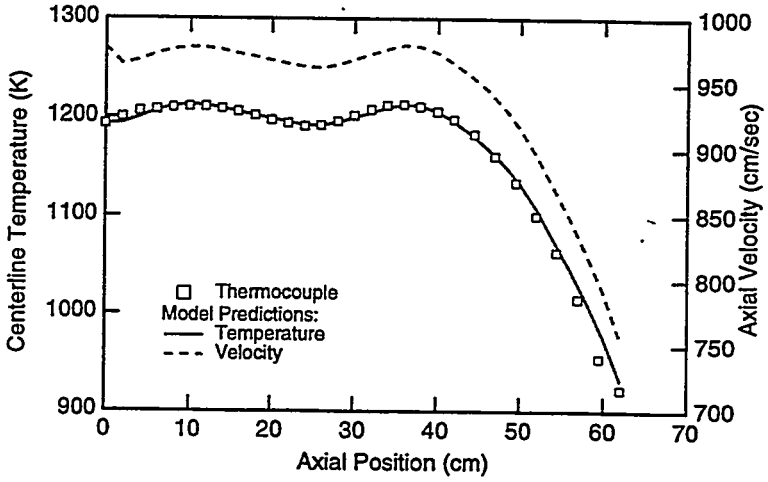

Figure 5: CRESLAF prediction of axial velocity in the HTFR based on a fit of the reactor wall temperature axial temperature measurements. Data (squares) correspond to Pt/Rh thermocouple measurements.

- Rate constants for many of the reactions within the reduced set are not well known. Using data from HTFR experiments, these rate constants were adjusted to achieve the best fit to the data. Predictions for one set of experimental conditions (helium carrier gas, total flow rate of 5000 sccm) are compared in Figure 6 with measured concentrations. A good fit to the MTS concentration data was achieved and the predicted concentrations of CH_4 and $SiCl_4$ are generally within 20% of the measured values. Although the model includes several bimolecular routes by which MTS can decompose, it predicts that decomposition is independent of MTS concentration, in agreement with the experimental observation.

computation make it difficult to obtain convergence. Since the SPARC-10 is at least a factor of five faster than the VAX, larger grids (more elements) can be used, providing finer resolution in those areas where steep gradients occur. The VAX version of the code only allowed the calculation space to be divided into a 40 x 40 grid, while the faster SPARC-10 allows the code to be redimensioned to a 55 x 55 grid. The code was tested and shown to give results that are in agreement with those produced in previous simulations on the VAX.

PUBLICATIONS

1. M. D. Allendorf and T. H. Osterheld "Computational Modeling of the Decomposition of Methyltrichlorosilane, a Silicon Carbide Precursor," *Chemical Vapor Deposition of Refractory Ceramics III*, Proceedings of the Materials Research Society, submitted, 1994.
2. M. Schulberg, M. D. Allendorf, and D. A. Outka "Adsorption and Desorption Kinetics of Hydrogen Chloride on Polycrystalline Silicon Carbide Surfaces," *Surface Science.*, submitted, 1994.
3. T. H. Osterheld and M. D. Allendorf, "Low-Pressure Kinetics of Methyltrichlorosilane Decomposition," *Chemical Vapor Deposition of Refractory Ceramics III*, Proceedings of the Materials Research Society, submitted, 1994.
4. T. H. Osterheld, M. D. Allendorf, and C. F. Melius,"Unimolecular Decomposition of Methyltrichlosilane: RRKM Calculations," *J. Phys. Chem.*, **98** (1994), 6995.
5. M. D. Allendorf, T. H. Osterheld, and C. F. Melius "The Decomposition of Methyltrichlorosilane: Studies in a High-Temperature Flow Reactor," *Gas-Phase and Surface Chemistry in Electronic Materials Processing*, The Materials Research Society, Pittsburgh, **334** (1994), 105.

PRESENTATIONS

1. M. D. Allendorf, T. H. Osterheld, C. F. Melius "The Decomposition of Methyltrichlorosilane: Studies in a High-Temperature Flow Reactor," Materials Research Society Fall Meeting, Boston, November 1993.
2. M. D. Allendorf, T. H. Osterheld, C. F. Melius "The Decomposition of Methyltrichlorosilane: Studies in a High-Temperature Flow Reactor," AIChE Annual Meeting, St. Louis, December 1993.
3. M. D. Allendorf "High Deposition Rate Chemical Vapor Deposition," presented at the Advanced Industrial Concepts Materials Program Review Meeting, Los Alamos, June 1994.

HONORS AND AWARDS: None during this reporting period.

PATENTS/DISCLOSURES: None during this reporting period.

LICENSES: None during this reporting period.

INDUSTRIAL INPUT AND TECHNOLOGY TRANSFER: Technical discussions were conducted during FY94 with ceramic materials manufacturers and potential end-users in the glass industry to provide an overview of Sandia capabilities in process simulation and materials science. Discussions are continuing and will be broadened to include paper manufacturers in FY95. The FY95 objective is the development of a DOE lab/manufacturer/end-user consortium (with cost sharing) whose focus is to reduce costs and identify new industrial markets for ceramic composite materials.

COST SHARING: None.

METALLIC AND INTERMETALLIC-BONDED CERAMIC COMPOSITES

K. P. Plucknett, T. N. Tiegs,
K. B. Alexander, S. B. Waters, and P. F. Becher
Metals and Ceramics Division, Oak Ridge National Laboratory
P. O. Box 2008, Oak Ridge, TN 37831-6068

INTRODUCTION

The purpose of this task is to establish a framework for the development and fabrication of metallic-phase-reinforced ceramic matrix composites with improved fracture toughness and damage resistance. The incorporation of metallic phases that plastically deform in the crack tip region, and thus dissipate strain energy, will result in an increase in the fracture toughness of the composite as compared to the monolithic ceramic. It is intended that these reinforced ceramic matrix composites will be used over a temperature range from 20°C to 800-1200°C for advanced applications in the industrial sector. In order to systematically develop these materials, a combination of experimental and theoretical studies must be undertaken.

TECHNICAL PROGRESS

Summary

1. Intermetallic-Bonded Oxide Ceramic Composites

As reported earlier, the addition of TiC to an Al_2O_3 matrix improves wetting of the matrix by Ni_3Al during densification resulting in an interpenetrating Ni_3Al microstructure. The addition of TiC is also used to increase the hardness and thermal conductivity of Al_2O_3 ceramics, factors that have lead to the extensive use of Al_2O_3–TiC composites in wear and cutting tool applications. Examples of the thermal and mechanical properties of dense Al_2O_3-TiC based composites are illustrated in Table I. In addition, the rise in

fracture resistance with crack extension has also been determined for the $65Al_2O_3$-25TiC-$10Ni_3Al$ composition, Figure 1. As noted in Figure 1, the fracture resistance of the intermetallic-bonded composite rises rapidly with crack extension while the fine grained alumina and the alumina-TiC composite exhibit lower toughness values which show little change with crack growth. A rising fracture resistance response is required for improving mechanical reliability and damage resistance.

Table I. Thermo-mechanical properties of fine grained Al_2O_3 based composites.

Composition Volume %	Flexure Strength, MPa	E, GPa	Hardness, GPa	Thermal Diffusivity, cm^2/s	Thermal Expansion Coefficient, $10^{-6}/°C$
$65Al_2O_3$-25TiC-$10Ni_3Al$	580	375	17	0.08	9.5
$65Al_2O_3$-25TiC-10Ni	580		17.5	0.075	
$65Al_2O_3$-35TiC	450	430	15	0.075	8.2

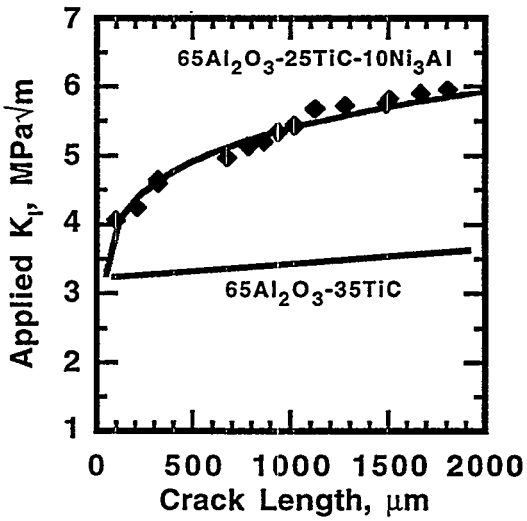

Figure 1. The fracture resistance rises rapidly with crack extension in the intermetallic-bonded composite. In comparison, neither the alumina nor the alumina-TiC composite exhibit significant fracture resistance.

2. Pressureless-Sintering of TiC–Ni_3Al Composites

Initial SEM observations of the wetting behavior of hot-pressed TiC substrates have demonstrated that not only does Ni_3Al wet TiC with a low wetting angle, but it also

penetrates into the TiC substrate to a significant depth (~100 μm after 15 minutes at 1550°C). This obviously is a favorable condition for (pressureless-) liquid phase sintering. Initial work has been performed with samples utilizing TiC + 20 vol. % Ni_3Al (IC-50; -60, +325 mesh) powders that were cold-pressed to a green density of ~47% of theoretical density (T. D.). Initial sintering trials at 1650°C (with a 4 hour hold time) resulted in densities of ~ 90 % T. D. Examination of the pore morphology and size indicates that they may be formed at the original site of the Ni_3Al powder in the green body, as the Ni_3Al is removed from this region by capillarity during liquid phase sintering leaving a void (a common observation when the 'liquid' phase powder size is much greater than the matrix powder, as in the present case). Finer Ni_3Al powder has been obtained, and initial results show a reduction in the retained pore size in sintered materials, though the as-sintered densities were similar to those obtained with the coarser Ni_3Al powder. Future work is aimed at refining this approach to obtain higher sintered densities.

3. Intermetallic-Bonded Non-Oxide Ceramic Composites

Fabrication of Composites - As reported previously, the effects of processing on the densification and mechanical properties of WC-Ni_3Al and TiC-Ni_3Al composites were examined in a systematic series of tests. An experimental array (based on the Taguchi method) was formulated to assess the impact of processing (e.g., hold time at maximum hot pressing temperature, powder milling medium and powder milling time) on the composite properties (Tables II and III). The analysis of the results for this second array are currently in progress.

Table II. Taguchi experimental design array for TiC–17 vol. % Ni_3Al composites for examination of hot-press temperature versus time at temperature, graphite die coating type, powder milling medium and powder milling time.

Test	Temperature /Hold Time (°C / min)	Powder Milling Medium	Milling Time (h)	Graphite Die Coating Type	Hardness (GPa)	Indent Toughness (MPa√m)
1	1325 / 35	Isopropanol	16	Al_2O_3	14.2	7.0
2	1325 / 35	Hexane	4	BN	12.1	6.1
3	1325 / 35	Argon	1	ZrO_2	9.8	5.5
4	1325 / 125	Isopropanol	4	ZrO_2	16.0	6.2
5	1325 / 125	Hexane	1	Al_2O_3	13.8	6.5
6	1325 / 125	Argon	16	BN	13.4	7.4
7	1350 / 35	Isopropanol	1	BN	14.4	6.0
8	1350 / 35	Hexane	16	ZrO_2	14.3	6.7
9	1350 / 35	Argon	4	Al_2O_3	14.0	7.8

Table IV. Taguchi experimental design array for WC–17 vol. % Ni_3Al composites for examination of hot-press temperature versus time at temperature, graphite die coating type, powder milling medium and powder milling time.

Test	Temperature / Hold Time (°C / min)	Powder Milling Medium	Milling Time (h)	Graphite Die Coating Type	Hardness (GPa)	Indent Toughness (MPa√m)
1	1325 / 35	Isopropanol	16	Al_2O_3	13.7	11.3
2	1325 / 35	Hexane	4	BN	13.3	16.0
3	1325 / 35	Argon	1	ZrO_2	13.9	9.5
4	1325 / 125	Isopropanol	4	ZrO_2	13.8	10.4
5	1325 / 125	Hexane	1	Al_2O_3	13.8	13.4
6	1325 / 125	Argon	16	BN	12.4	12.6
7	1350 / 35	Isopropanol	1	BN	13.4	12.4
8	1350 / 35	Hexane	16	ZrO_2	11.0	9.3
9	1350 / 35	Argon	4	Al_2O_3	14.0	11.5

Based on these and earlier studies, WC - 17 vol. % Ni_3Al composites have been developed that exhibit hardness values in the range of 14 to 17 GPa and flexure strengths of 1.3 GPa. Thus, the flexure strengths of the Ni_3Al-bonded WC composites, even at this early stage of development, approach those of the commercially available cobalt-bonded WC systems. These same composites

exhibit toughness values of 10 to 12 MPa$\sqrt{m}$ for short crack conditions and 16 to 22 MPa$\sqrt{m}$ for long crack conditions consistent with the rising fracture resistance behavior obtained in commercial cobalt-bonded tungsten carbides. From these studies, it is quite clear that the Ni_3Al-bonded carbide composites exhibit extremely promising mechanical properties suitable for a number of applications.

PATENT/DISCLOSURES

Patent application was filed on ESID 1454-X, "Multicomponent, Particle-Hardened, Alumina-Based Composites Containing Ductile Intermetallic Alloys."

PUBLICATIONS

K. B. Alexander, J. H. Schneibel, H. T. Lin, and P. F. Becher, "Fabrication and Properties of Alumina Matrix Composites Containing Nickel Aluminide Reinforcements," TMS, Pittsburgh, PA, 1994.

J. H. Schneibel and K. B. Alexander, "Processing and Mechanical Properties of Laminar Ni_3Al-Al_2O_3 Composites," pp. 255-260 in MRS Symposium Proceedings,, Vol. 350: Intermetallic Matrix Composites III, J. A. Graves, R. R. Bowman, and J. J. Lewandowski (eds.), Materials Research Society, Pittsburgh, PA, 1994.

PRESENTATIONS

Processing and Mechanical Properties of laminar Ni_3Al-Al_2O_3 Composites, J. H. Schneibel and K. B. Alexander, presented at the MRS Spring Meeting, Symposium on Intermetallic Matrix Composites, San Francisco, CA, April 4–5, 1994.

In-situ Testing of Ceramic Composites in a Scanning Electron Microscope, K. B. Alexander, P. F. Becher and J. H. Schneibel, Metals and Ceramics Division, ORNL. Invited talk, Basic Sciences Fall Meeting, American Ceramic Society, Louisville, KY, Sept. 1994.

Microstructural Design of Ceramic Composites, K. B. Alexander and P. F. Becher, Metals and Ceramics Division, ORNL., Invited talk, Pacific Coast Regional Meeting of the American Ceramic Society, Los Angeles, CA, Oct. 19–22, 1994.

LICENSES

None.

INDUSTRIAL INPUT AND TECHNOLOGY TRANSFER

Proprietary Information Agreements concerning the application of composites described in Disclosure ESID 1454-X, S-80, 624 on "Multicomponent, Particle-Hardened, Alumina–Based Composites Containing Ductile Intermetallic Alloys" have been signed by Black and Decker, Golden Technologies, Cercom, and Metallamics. A large (6 inch long by 2 inch high by 0.5 inch thick) alumina-based composite sample was shipped to Cercom Inc. for evaluation for application as a paper drawing blade. In addition, several WC–Ni_3Al blanks have been supplied to General Electric to determine if the composites are suitable for application as end milling tools for machining titanium alloy.

COST SHARING

None.

HIGHLIGHT

WC–17 vol. % Ni_3Al composites have been developed that exhibit hardness values in the range of 14 to 17 GPa and flexure strengths of 1.3 GPa. Thus, the flexure strengths of the Ni_3Al–bonded WC composites, even at this early stage of development, approach those of the commercially available cobalt-bonded WC systems. These same composites exhibit toughness values of 10 to 12 MPa$\sqrt{m}$ for short crack conditions and 16 to 22 MPa$\sqrt{m}$ for long crack conditions consistent with the rising fracture resistance behavior obtained in commercial cobalt-bonded tungsten carbides. From these studies, it is quite clear that the

Ni_3Al–bonded carbide composites exhibit extremely promising mechanical properties suitable for a number of applications.

MICROWAVE AND RF ASSISTED CHEMICAL VAPOR INFILTRATION

D. J. Devlin and R.S. Barbero

Materials Science and Technology Division
Los Alamos National Laboratory
Los Alamos, NM 87545

Work during this reporting period has focused on the development of a CVI technique for rapid production of carbon/carbon and alumina composite systems. The focus of the alumina effort is towards porous materials for membrane supports and hot gas filtration. Industrial interest in these applications include companies such as; Dow, Westinghouse, Amoco and DuPont. Applications for the carbon materials are numerous and include; brakes, sporting goods, biomedical materials, flaps and seals for thrust control, after burner nozzles, turbine engine flaps and rotors. This effort will focus on aircraft brakes. A collaboration is underway with Hitco a major producer of carbon/carbon materials.

Fiber reinforced composite materials, particularly CVI processed materials, are porous even under the best processing conditions. The objective of most processing schemes is to minimize the porosity enhancing mechanical properties and oxidation resistance. However, applications for engineered porous materials for high temperature membranes and filters has recently drawn attention to these composites. A recent DOE assessment estimates up to 2 quads of energy a year could be saved if membranes were more widely used in industry. Improved high temperature membranes could save: 1 quad/yr. in liquid/gas separations; 0.68 quad/yr. in natural gas recovery; and 0.36 quad/yr. in oxygen enrichment. Over half the distillation processes within the chemical process industry could be replaced resulting in 200 million barrels of oil saved each year. High temperature membrane reactors are being considered for on board methanol reforming for fuel cell powered vehicles. Estimates of 2 to 4 billion barrels/day with an economic benefit of $42 billion per year by 2030 have been suggested. In addition to energy savings many of these applications have important environmental benefits. Through the right choice of fiber architecture and CVI process conditions porous materials can be engineered.

Alumina is often the material of choice for these applications. Silicon based ceramics suffer from the formation of glass under oxidizing conditions, leading to pore blockage (1). Alumina on the other hand, has a higher resistance to corrosive attack and excellent high temperature properties. Fabrication of continuos fiber reinforced alumina composites by CVI techniques has been hindered by homogeneous gas has nucleation. This results in a limitation in deposition rate, inefficient use of reactant, and alumina soot with associated problems such as clogging of process lines. To avoid the problem low pressures and reduced deposition rates are employed. With the MACVI functioning as a cold wall furnace, excessive gas phase nucleation can be avoided and the deposition rate increased.

Advanced composites are becoming increasingly important in industrial technologies. The promise of greater industrial efficiencies, reduced energy consumption, greater reliability and product life has been a driving force behind this program. Continuous fiber reinforced composites such as carbon/carbon meet the requirements for many important applications, unfortunately, entry into many markets has been prohibited due to their high costs. Working with Hitco a leading manufacturer of carbon/carbon composites for both civil and defense applications we are developing a new process for the fabrication of three dimensional carbon/carbon composites. The approach reduces processing times significantly and leads to improved quality. For example,

typical carbon/carbon processing can run several months to complete a part. Consequently, it is necessary to process hundreds of parts at time to reduce costs to $ 100 /lb. Manufacturers are often left with many parts in inventory waiting for customers. Furthermore, the large scale batch processes are not advantageous to maintaining quality. Variations from batch to batch and even within batches can lead low yields and reduced reliability. Our process is capable of manufacturing single or multiple parts in 30 hours. With the short processing time the production rates of the batch process can be maintained or further increased. The ability to produce smaller quantities of parts reduces the costs incurred in maintaining large inventories. This allows the manufacturer to take orders and deliver in a "just in time" fashion, or economically manufacture custom parts. Finally, improved quality and yield with the small batch process will be possible.

The target product for this program is a brake system presently used in commercial aircraft. These materials must be qualified. For example, brakes are expected to absorb all the kinetic energy of a commercial passenger jet landing at full flight speed. Hitco has the characterization capability and knowledge of required microstructure and material properties, and will guide us on the proper choice of processing parameters. Manufacturing facilities at Hitco use the same type of RF equipment necessary for this new process. This makes the process very attractive. Our approach makes use of this familiar technology in a different way to produce, during a chemical vapor infiltration process, (CVI) inverted temperature gradients in individual parts. Since most aspects of the process i.e. chemistry and basic equipment remain the same, transfer to a real industrial process is very likely.

The objective of this program is to develop an improved chemical vapor infiltration process for the fabrication of continuous fiber reinforced composites. Specifically the aim is to exploit techniques of electromagnetic heating to establish inverted temperature gradients in porous preforms such that densifcation by CVI can occur from the inside-out. Advantages in using electromagnetic energy in CVI are the ability to couple energy directly into the substrate and the possibility of heating the substrate volumetrically. Coupling energy directly into the substrate should increase energy efficiency, compared to radiant heating methods. Volumetric heating, together with heat losses at the surfaces due to radiation and convection, gives rise to "inverted" thermal gradients. With the internal region of the substrate hot, cool reactant gases penetrate inward prior to the onset of the deposition reaction. Consequently, deposition can occur from the inside-out. Inside-out densification should minimize premature pore closure in outer regions, resulting in a more spatially uniform composite. Decreases in processing time are also expected. A cold wall reactor will also minimize unwanted deposition on the walls and fixtures thereby saving on reactant costs and minimizing waste production.

TECHNICAL PROGRESS

Summary

A process has been developed based on electromagnetic volumetric heating to rapidly densify carbon/carbon composites. The approach utilizes RF frequencies to achieve the desired inverted temperature gradients. The use of familiar industrial heating techniques makes the process attractive to manufactures. Carbon composites comprised of 3-D continuous fiber reinforcement and a pyrolitc carbon matrix have been fabricated to acceptable densities in as little as 30 hours. A collaborative effort is underway with Hitco to develop the process for the fabrication of carbon/carbon aircraft brakes. Using microwave heating methods a process for the CVI fabrication of continuous fiber reinforced alumina composites is under development. Interest in these materials for high temperature engineered porous materials has been expressed by a number of companies such as: Dow, Westinghouse, Amoco and DuPont. Crystalline alumina has been successfully deposited on nicalon fibers using the process. Issues of composite homogeneity and gas phase nucleation need to be resolved.

Milestones

Rapid densification of carbon preform by inverted temperature gradient technique

The initial efforts at processing carbon/carbon materials used 2.45 GHz microwave frequency. We reported the successful heating of 3 -D preforms to 1000C with alumna insulation. Attempts to infiltrate these materials with pyrolitic carbon met with failure. The insulation must be in contact with the preform and ultimately reaches temperatures where deposition can occur. The pyrocarbon deposited on the insulation absorbs microwaves heating the insulation with a loss of power absorbed in the preform. The preform temperature drops and infiltration ceases. The need for insulation to heat carbon materials is due to the high electrical conductivity of carbon. The skin depth or penetration of radiation at 2.45 GHz is estimated at less than a millimeter. With all the heating at the surface, insulation is required to reduce losses. Furthermore, an inverted gradient is not possible at this frequency. For carbon/carbon materials, RF frequencies are required to heat the part effectively. At 50 kHz the skin depth is estimated at 1 to 2 centimeters. This type of technology is commonly used in industrial heating. In most large scale processes, like the fabrication of carbon/carbon composites, RF induction heating is used to heat a susceptor which than radiates to the part. Using much of the same processing equipment we can heat the part directly and produce inverted gradients.

Thermal Gradients by Electromagnetic Heating.

The concept for the production of inverted gradients is illustrated in figure 1. Ordinary radiant heating in the visible light region of the spectrum results in rapid attenuation of the radiation at the surface. Moving down in frequency to the microwave and RF regions of the spectrum, dependent on the dielectric properties of the material, the penetration of the radiation into the part increases. The magnetic intensity of the electromagnetic wave decays exponentially with increasing distance into the part.

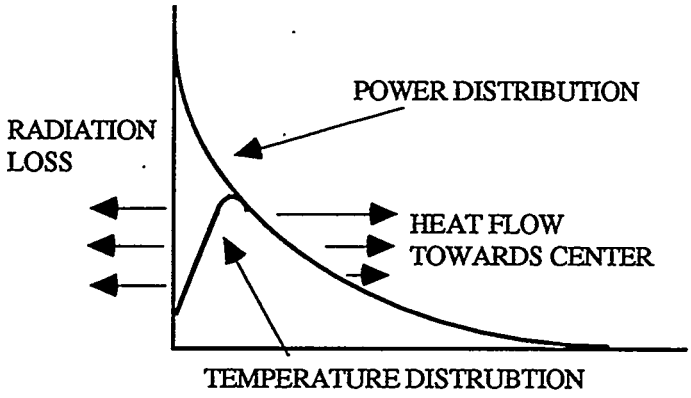

Figure 1. The effect of volumetric heating on the temperature distribution.

The current induced falls off in a similar manner and is characterized as a skin or current depth given by the following relation:

$$\delta = (1/\pi f \mu \sigma)^{1/2} \qquad \text{eq. 1}$$

where:

f is the frequency cps

μ magnetic permeability, $4\pi \times 10^{-7}$ H/m

σ is the electrical conductivity $\Omega^{-1}m^{-1}$

For a carbon fiber preform the electrical conductivity is estimated at 25,000 $\Omega^{-1}m^{-1}$(2). Using this value the variation in current depth with frequency is shown in figure 2.

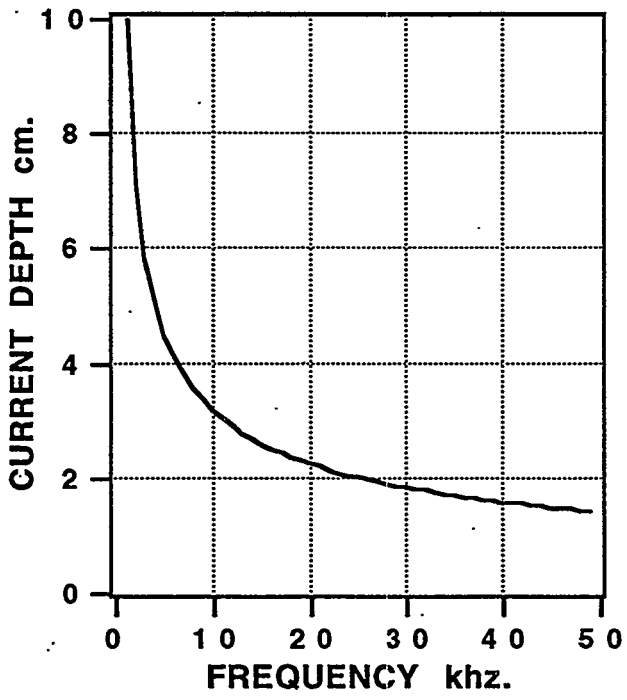

Figure 2. Variation of current depth with frequency for carbon fiber preform.

Processing parts with large dimensions will require frequencies in the 10 kHz range. As illustrated in figure 1 the power distribution, while still highest at the surface, does penetrate the interior resulting in volumetric heating. The temperature distribution falls off at the surface due to radiative and convective losses leading to an inverted gradient. For the deposition of carbon from methane, a difference in temperature of 200°C can reduce the deposition rate by a factor of 150 near the exterior surface. Thus, deposition can occur from the inside-out.

Based on the classical heat flow equation (3) for a cylinder of radius a, the temperature distribution can be expressed by the following equation :

$$\theta_r - \theta_c = \frac{P_a}{2k_c}\left[\frac{r^2}{a^2} - \frac{1}{k_2}\left(\frac{X(k_2 r/a)-1}{Z(k_2)}\right)\right] \qquad \text{eq. 2}$$

$X(k_2 r/a)=\mathrm{ber}^2(k_2 r/a) + \mathrm{bei}^2(k_2 r/a)$

$Z(k_2)$= ber(k_2)ber'(k_2) + bei(k_2)bei'(k_2)

ber and bei are the kelvin functions.

where: $k_2 = k_1 a$

$k_1 = \sqrt{2}/\delta$

P_a = the total power absorbed watts/m^2

θ_r and θ_c = the radial and centerline temperatures

k_c = thermal conductivity watt/m °K

Equation 2 can be modified to account for heat loss at the surface by defining a radiation correction factor P_n/P_a.

where: P_n is net power absorbed after radiation W/m^2

The temperature distribution through the cylindrical preform is given by:

$$\theta_r - \theta_c = \frac{P_n}{2k_c}\left[\frac{r^2}{a^2} - \left[\frac{1}{P_n / P_a}\right]\frac{1}{k_2}\left(\frac{X(k_2 r / a) - 1}{Z(k_2)}\right)\right] \qquad \text{eq. 3}$$

A dimensionless plot of equation 3 is shown in figure 3 for various values of P_a/P_n.
For the case where no radiation losses occur, $P_a/P_n = 1$ the temperature is high near the surface. As radiation loss increases the temperature at the surface drops producing an inverted temperature gradient.

The current depth is another important factor in the establishment of thermal gradients. For a given material this depends on the frequency of radiation and the part dimension. The dimensionless plot in figure 4 shows the effect of varying the ratio a/δ, on the predicted thermal profiles. As the current depth increases relative to the radius of the part, large thermal gradients result. With the proper choice of frequency and control of the radiative heat loss, thermal gradients can be predicted. This approach can be used to scale the process for a full size brake.

Experiment/results

A reactor consisting of a simple induction coil operated at 50 kHz is illustrated in figure 5. Samples were readily heated without insulation to temperatures ranging from 1100 to 1400 C. The preforms used were Hitco's 3D carbon fiber (30 volume percent fiber), cut into cylinders approximately 1 inch in diameter by 3 inches in length. The matrix was deposited via the direct pyrolysis of methane at pressures ranging from 100 to 300 torr, with a flow rate of 200 sccm. Temperature gradients were monitored with thermocouples inserted in the preform at various radial positions.

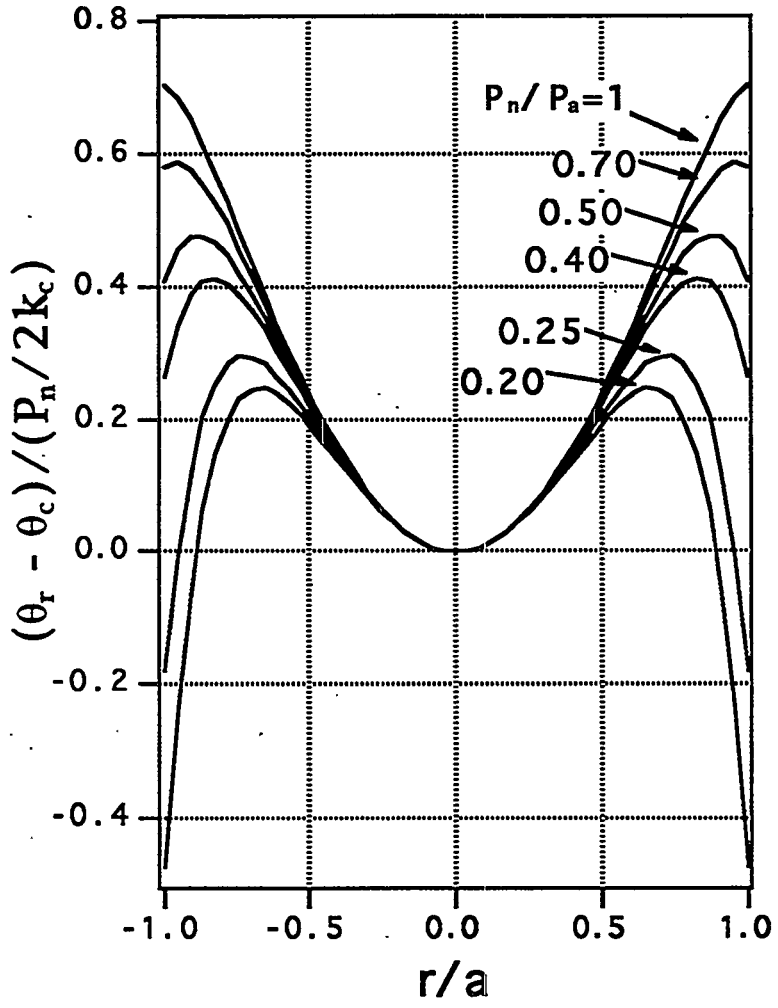

Figure 3. The effect of radiation loss on the temperature distribution

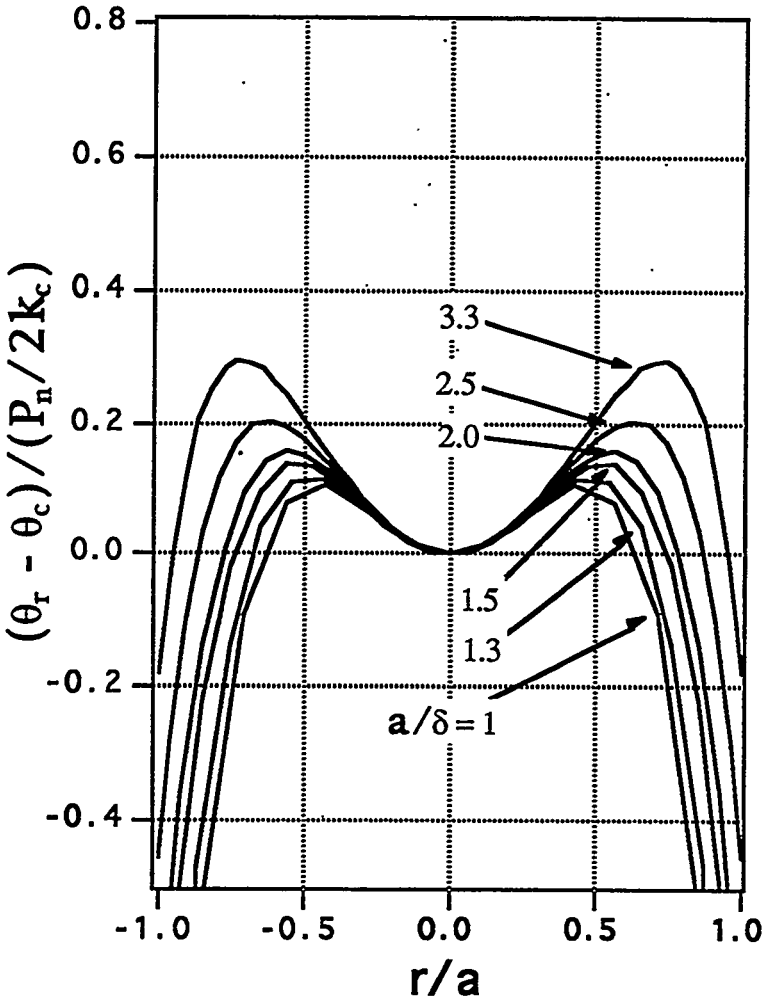

Figure 4. Effect of varying the relative curret depth on the temperature distribution

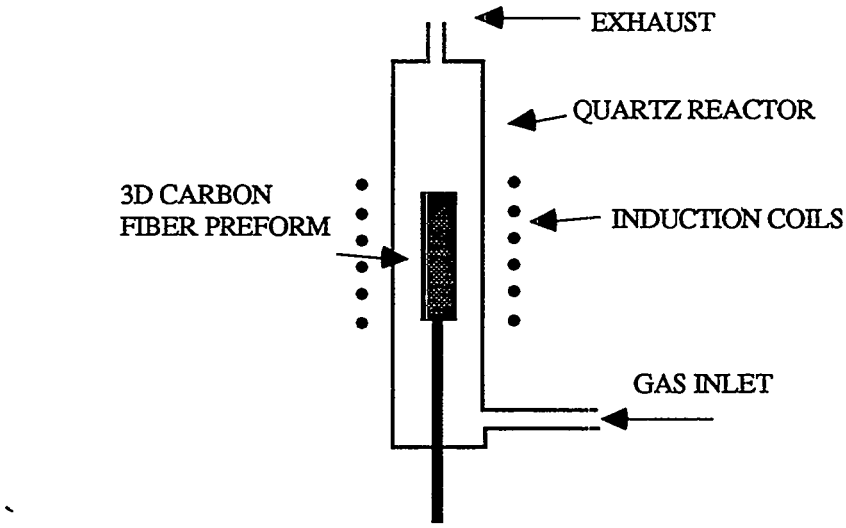

Figure 5. Schematic of the carbon/carbon composite reactor.

For the process conditions of 1330°C, 100 torr and 200 sccm of methane the evolution of the temperature gradient from the centerline to the surface was monitored. Figure 6 shows this variation with time. The initial increase in delta T is thought to be caused by preferential deposition on the interior of the preform resulting in stronger coupling to the center. The process is initially self propagating and the total absorbed power required continually decreases. Eventually as deposition near the exterior occurs the temperature gradient decreases. Materials have been processed to high densities in as little as 30 hours. Experiments were undertaken to evaluate the previously described model for the prediction of temperature gradients. A preform was infiltrated at 1100°C, 300 torr and 200 sccm of methane. Temperatures were monitored at the center of the preform, approximately half way from the center to edge and near the edge. The total power into the part was 6kW. The results of the measurements along with the predicted gradients calculated from equation 3 are plotted in figure 7. Values for the parameters used in the model are listed below:

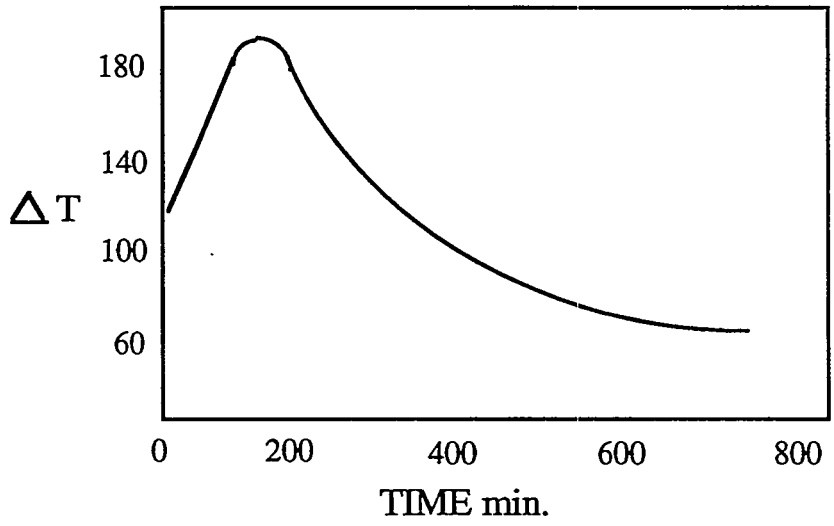

Figure 6. The variation in the temperature gradient as infiltration proceeds.

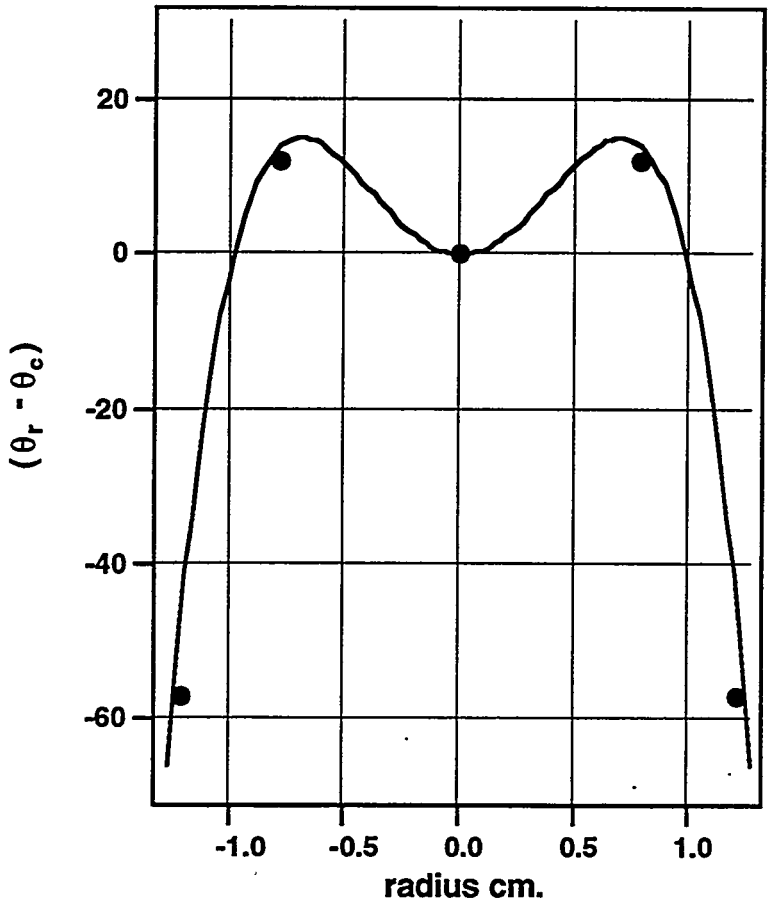

Figure 7. Comparison of experimentally measured temperature gradient to model calculations for a 3-D carbon preform

Parameters:

$f = 50$ kHz
$P_n = 26$ watt/cm^2
$P_a = 7.75$ watt/cm^2
$\sigma = 25{,}000\ \Omega^{-1}m^{-1}$
$\delta = 1.42$ cm.
$k = 10$ watt/m^2 °K
$a/\delta = 1$

Good agreement between the model predictions and the experimental data were obtained. Convective heat transfer coefficients were estimated and found to be negligible. The total emissive power was a estimated according: $E = \varepsilon\sigma_b T^4$; where ε is the emmisivity. A reasonable estimate of ε for a rough porous carbon surface is 0.9 A difficulty in the calculation is determining the correct radiating surface area. The effective radiating surface area for a carbon preform will be higher than the geometric area. A good estimate of the effect would require an adequate description of the fiber bundle and fiber bundle arrangement. Within such a model, view factors for individual fibers in the bundle, and individual bundles in the preform would need to be calculated. However, a simple model ignoring these details appears to give a reasonable result. Figure 8 describes the approximate arrangement of fibers within a bundle and the arrangement of bundles within the preform.

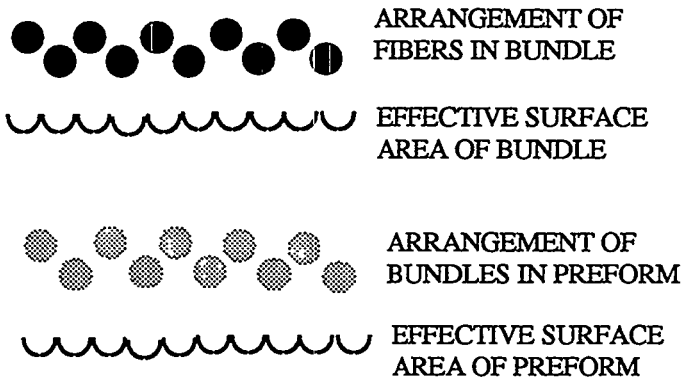

Figure 8. Approximate increase in surface area over the geometric surface area of a carbon fiber preform

The effective surface area is increased by a factor of $(\pi/2)^2 = 2.47$, over the geometric surface area. Using this value, and the total power into the part, the corresponding absorbed and net power used in the calculation are obtained. The thermal conductivity was taken as effectively the same as that reported for an epoxy/graphite fiber composite adjusted for a 30 vol. percent fiber loading (4).

The objective of the program will be to scale the process for the testing of dyno-rings at Hitco. This will require the fabrication of 4 to 5 inch diameter parts. To maintain similar temperature gradients a lower frequency will be required. The results of the above experiment allow us to predict the gradients for the larger parts at different frequencies. Calculations for 10 kHz frequency on a 10 cm. diameter part are shown in figure 9.

The predicted temperature gradients are similar to those calculated and measured for the 1 inch diameter and 50 kHz example. A scaled reactor for the fabrication of dyno-rings will be possible with a variable frequency generator (3 to 11 kHz) available at LANL. The ability to vary the frequency will allow for further control of temperature gradients.

We have demonstrated the ability to densify parts in reduced times on the order of 30 hours. Materials with densities in the range of 1.7 g/cc are easily fabricated. Upcoming efforts will be aimed at characterizing materials made by this process. The matrix shows strong sp^2 character as indicated by the raman spectra (figure10). X-ray diffraction results also indicate a strong graphitic nature to the matrix material. Further characterization at Hitco will include polarized light microscopy and thermal conductivity .

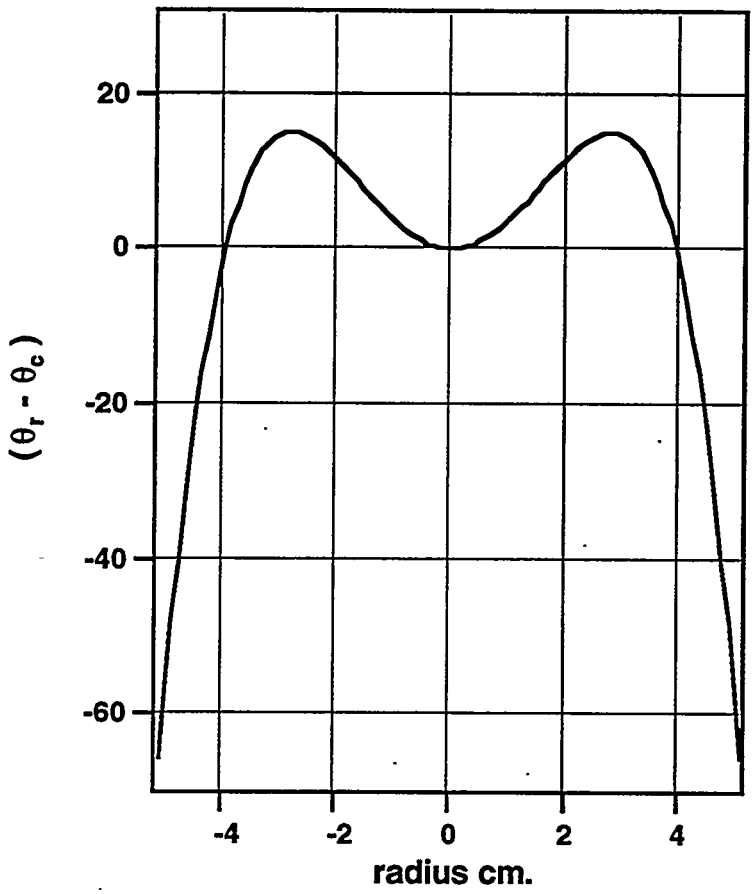

Figure 9. Predicted temperature gradients for a 10 cm. diameter carbon preform processed at 10 kHz.

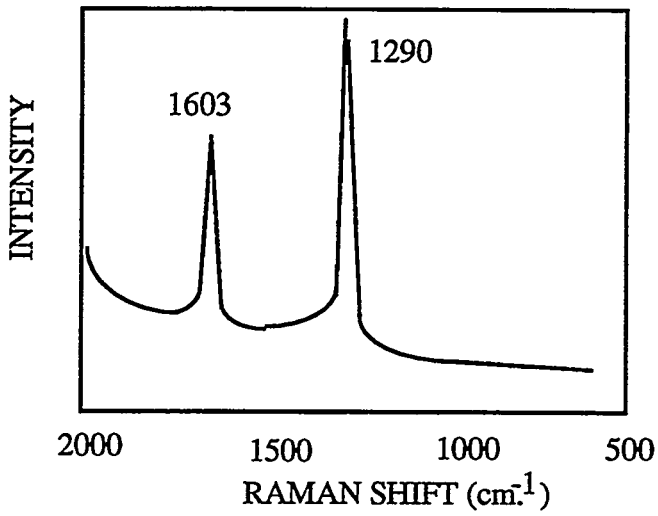

Figure 10. Raman spectra of matrix material produces by inverted gradient process.

Development of MACVI process for fabrication of continuous fiber reinforced alumina composites.

Continuous fiber reinforced alumina composites have tremendous potential for applications such as gas filtration and membrane supports. These application often involve high temperatures in excess of 1000°C; pressures in the range of 700 kPa and highly corrosive environments including; sulfur, chlorine and alkali. Fabrication of continuos fiber reinforced alumina composites by CVI techniques has been largely hindered by the homogeneous gas has nucleation of alumina. This results in a limitation in deposition rate, inefficient use of reactant and alumina soot with associated problems such as clogging of process lines.

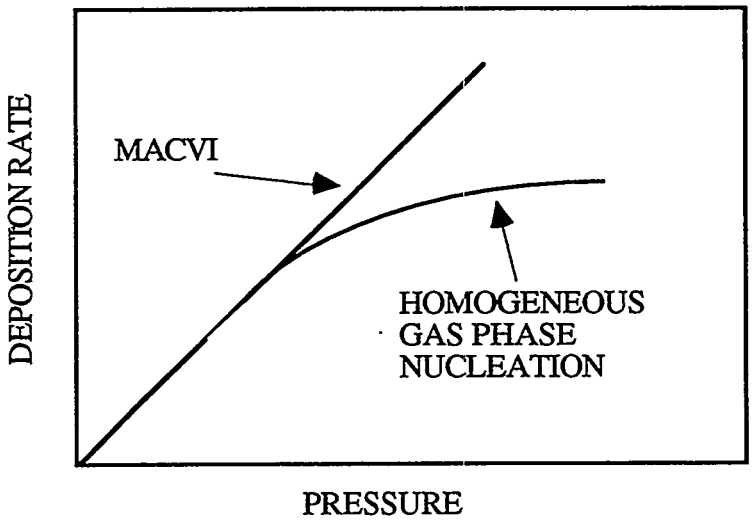

Figure 11. Effect of homogeneous gas phase nucleation on overall deposition rate

To avoid the problem low pressures and reduced deposition rates are used. Figure 11 illustrates the effect. Increasing pressures beyond 100 torr results in a reduction in deposition rate.

The conductivity of alumina and silicon carbide are such that microwave frequencies are required to efficiently heat the material. The MACVI technique has the advantage of functioning as a cold wall furnace. Excessive gas phase nucleation can be avoided and the deposition rate increased.

The deposition of Al_2O_3 occurs via the hydrolysis of $AlCl_3$:

$$H_2 + CO_2 = H_2O + CO$$

and

$$2AlCl_3 + 3H_2O = Al_2O_3 + 6HCl$$

or the overall reaction:

$$2AlCl_3 + 3H_2 + 3CO_2 = Al_2O_3 + 3CO + 6HCl$$

Spotz et.al (5), using a single mode cavity demonstrated the rapid densification of alumina by MACVI. High densities were reported for process times as short as 14 hours. We are investigating the extension of this process to a multimode cavity, thereby reducing the restrictions

on part geometry's inherent in the single mode approach. Figure 12 illustrates the experimental set up, consisting of a multimode microwave cavity and a $AlCl_3$ sublimator operated at 100°C.

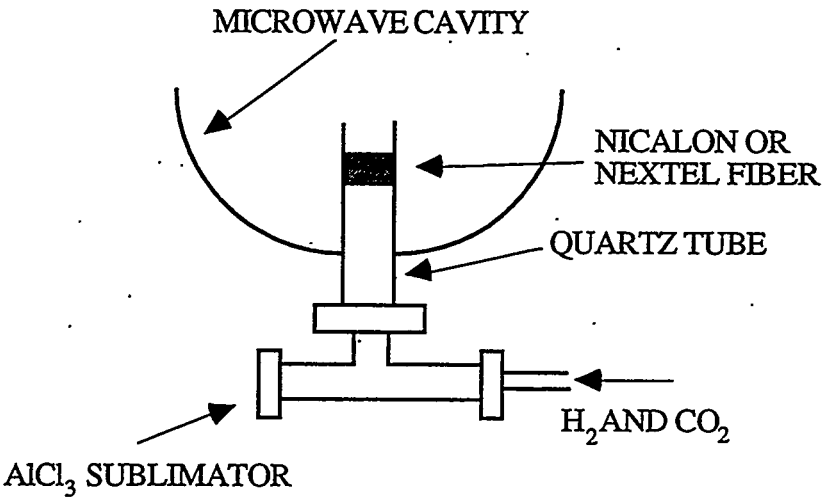

Figure 12. Schematic of the MACVI set-up for alumina infiltration.

$AlCl_3$ vapor is carried into the reactor by a gas mixture of H_2 and CO_2. The reactants are forced through a microwave heated fiber preform held in quartz tube. Both silicon carbide fibers (nicalon) and alumina fibers (Nextel) have been investigated. Micrographs of alumina coatings on nicalon fibers are shown in figure 13. Crystalline α alumina is obtained under the deposition conditions however, uniform deposition through out the preform has not yet been possible.

Figure 13. Micrographs of crystalline alumina on nicalon fiber deposited by MACVI.

PRESENTATIONS

"Microwave Assisted Chemical Vapor Infiltration" D.J. Devlin and R.S. Barbero, AIM Program, Annual Information and Review Meeting, Los Alamos NM, June 1-3, 1994

PUBLICATIONS

"Chemical Vapor Infiltration of Carbon Fiber Bundles" R.P. Currier, D.J. Devlin and R.S. Barbero. Ceramic Engineering and Science Proceedings, p 1038, vol.14, No. 9-10, 1993.

"Ceramic Matrix Composites by Microwave Assisted CVI" R.P Currier and D.J. Devlin, Microwaves: Theory and Application in Materials Processing II. Ceramic Transactions, p387,Vol 36,1993.

HONORS AND AWARDS none

PATENT/DISCLOSURES U.S. Patent No. 5254374 " Chemical Vapor Infiltration using Microwave Energy", Issued October 19,1993

LICENSES none

INDUSTRIAL INPUT AND TECHNOLOGY TRANSFER

We have developed a joint work statement with Hitco to evaluate and develop the process for the fabrication of aircraft brakes. An abbreviated task description is shown below. The early efforts will be aimed at determining the basic CVD conditions to obtain the desired microstructure/properties as dictated by Hitco. This will be followed by a scale-up to 5 inch diameter dynamometer samples for performance at Hitco. A phase II effort will involve the design and construction of a full scale reactor for the fabrication of actual brakes.

Proposed Approach to Prototyping and Testing Carbon/Carbon Aircraft Brakes Using Los Alamos Rapid Fabrication Technique.

Phase I

1.1 Small scale infiltration of required preform architecture. The objective of this task is to establish the basic chemical vapor infiltration conditions for rapid processing.

1.2 Characterization of microstructure and physical properties: mechanical properties, density density gradients, and thermal conductivity. Characterization of matrix by polarized light microscopy and raman spectroscopy.

1.3 Refinement and redefinition of process parameters. The objective of this task is to finalize the process parameters such as reactant gas composition, gas flow, preform temperature, temperature gradients and heating schedules to achieve reduced processing time and improved density with a proven matrix microstucture.

1.4 Scaling process with for 5" diameter part. The objective of this task is to scale the process using information from the previous tasks. such that dyno rings for performance and tribological testing can be fabricated.

1.5 Infiltration of dyno rings for performance testing.

1.6 Qualification of material resulting in demonstration of process. This task involves full characterization of materials as in 2.2 and performance testing at HITCO.

PHASE II

2.1 With Hitco, design process furnace for full scale brake.

2.2 Contract to vendor for furnace construction

2.3 Testing and acceptance of furnace.

2.4 Process full size brakes.

COST SHARING

The described effort will involve cost sharing, the extent of which has not yet been determined by Hitco.

HIGHLIGHTS

A process for the rapid densifcation of carbon/carbon composites using electromagnetic volumetric heating has been developed. Efforts are under way to develop the process, for the fabrication of commercial aircraft brakes with an industrial partner.

References:

1. "Assessment of Porous Ceramic Materials for Hot Gas Filtration Applications", M.A. Alvin, T.E. Lippert, and J.E. Lane, Cerm. Bull., Vol 70, No. 9, 1991.

2. "Microwave Heating for Manufacturing Carbon-Fiber Thermoplastics", A.C. Lind, L.N. Medgyesi-Mitschang, J.E Kurz, H.F. McKinney, and F.C. Wear, Mat. Res. Soc. Symp. Proc. Vol. 189, 1991.

3 "Classical Heat Flow Problems Applied to Induction Billet Heating" Trans. AIEE Vol. 77, p 106-112, 1958.

4. "High-Strength Medium-Temperature Thermoset Matrix Composites" Engineered Materials HandBook, Vol 1, p414, 1988

5. "Microwave Assisted Chemical Vapor Infiltration", M.S. Spotz, D.J. Skamser, P. S. Day, H.M. Jennings, and D.L. Johnson, Cerm. Eng. & Sci. Proc. Vol. 14, No 9-10, 1993.

SYNTHESIS AND PROCESSING OF COMPOSITES BY REACTIVE METAL PENETRATION

Ronald E. Loehman and Kevin G. Ewsuk
Sandia National Laboratories
Albuquerque, New Mexico 87185

Antoni P. Tomsia
Pask Research and Engineering
Berkeley, California 94720

William G. Fahrenholtz
University of New Mexico
Albuquerque, NM 87106

INTRODUCTION

Ceramic-metal composites are being developed because their high stiffness-to-weight ratios, good fracture toughness, and variable electrical and thermal properties give them advantages over more conventional materials. However, because ceramic-metal composite components presently are more expensive than monolithic materials, improvements in processing are required to reduce manufacturing costs. Reactive metal penetration is a promising new method for making ceramic- and metal-matrix composites that has the advantage of being inherently a net-shape process. This technique, once fully developed, will provide another capability for manufacturing the advanced ceramic composites that are needed for many light-weight structural and wear applications. The lower densities of these composites lead directly to energy savings in use. Near-net-shape fabrication of composite parts should lead to additional savings because costly and energy intensive grinding and machining operations are significantly reduced, and the waste generated from such finishing operations is minimized.

The goals of this research program are: 1) to identify feasible compositional systems for making composites by reactive metal penetration; 2) to understand the mechanism(s) of composite formation by reactive metal penetration; and 3) to learn how to control and optimize reactive metal penetration for economical production of composites and composite coatings.

TECHNICAL PROGRESS: FY 1994

Summary

We are developing a reactive metal penetration process that converts brittle ceramic preforms to tough ceramic-metal composites by direct redox reaction with molten metal. The preforms can be either dense or porous and there is little or no change in their size or shape when they are converted to the composite.

The general form of reaction between Al and oxides is

$$(2 + x)\ Al + (3/y)\ MO_y \rightarrow Al_2O_3 + Al_xM_{3/y} \qquad (1)$$

where MO_y can be either a binary or more complex oxide, and the composition of the residual metal phase is determined by the phase equilibrium relations of the system. Evidence is accumulating that reactive penetration is applicable generally to oxide-metal combinations for which there is both favorable wetting of the oxide by the molten metal (i.e., contact angle $\theta < 90°$) and a negative Gibbs energy for reaction.

In the Al/mullite system, molten aluminum reduces mullite to produce alumina and elemental silicon according to the reaction:

$$(8 + x)\ Al + 3\ Al_6Si_2O_{13} \rightarrow 13\ Al_2O_3 + 6\ Si + x\ Al \qquad (2)$$

Metal-ceramic composites have been produced both by reacting ceramic preforms with molten metal, and by sintering mixtures of ceramic and metal powders. The preforms can be either fully dense or porous. With excess aluminum present (i.e., $x > 0$), the stoichiometric reaction gives a composite of alumina, silicon, and aluminum. However, if the ceramic is in contact with a reservoir of molten Al during reaction, the Si can diffuse out of the composite, leaving only Al and alumina. Experimental results on reaction couples with different compositions indicate that reactive metal penetration may be a general route to composite synthesis.

By combining results of electron microscopy studies of microstructure development with thermodynamic and kinetic data, we have developed a model mechanism for reactive metal penetration. The concentration of oxygen in the system (P_{O_2}) during reaction seems to play a critical role. The proposed 4-stage reaction mechanism includes the following steps: 1) the metal melts and wets the ceramic preform surface; 2) oxygen diffuses out of the ceramic preform grain boundaries to lower the P_{O_2} to a range that favors wetting; 3) molten metal penetrates the ceramic preform grain boundaries; and 4) the metal on the grain boundaries reacts with the individual grains of the ceramic preform.

The metal content of composites formed by reactive metal penetration is determined by the composition of the ceramic preform. Originally we believed that higher metal contents might be achieved using porous preforms; we anticipated that the metal would physically infiltrate and fill the pores of the preform prior to further penetration and reaction with the matrix. Initial experiments found that pressureless physical penetration of porous mullite preforms is limited by the formation of an oxide layer on molten Al at the typical reaction temperature of 1200°C. Recently, however, we found that by increasing the reaction temperature to 1350°C and above the molten aluminum will physically infiltrate any pores in the preform before reacting with the mullite matrix to form the Al/Al_2O_3 composite. Thus, the metal content of composites formed by reactive metal penetration can be tailored by varying the porosity and composition of the ceramic preform as well as the reaction temperature.

Net shape or near-net shape forming can greatly reduce the cost of manufacturing finished components. Both experiments and modeling have shown that composite formation by reactive metal penetration in the Al/mullite system is a net shape process. We completed detailed molar volume calculations that model the Al/mullite reaction. The calculations show that size and shape are maintained for a wide range of process conditions by a balance among relative molar volumes of reactants and products, Al penetration of the preform, and outward diffusion of Si. The predicted metal volume fractions were confirmed experimentally using quantitative stereology.

Milestones:

Work this year has concentrated on Tasks 1, 3, and 5 of the Field Work Proposal.

1. Evaluate Reactions and Mechanisms of Composite Formation in the Al/Mullite System

Microstructure Evolution: In reactive metal penetration of mullite by aluminum, molten Al reduces polycrystalline mullite to alumina and silicon according to Reaction 2. To better understand the reaction mechanism(s) for such composite formation, the microstructures of partially infiltrated mullite specimens were analyzed using transmission electron microscopy (TEM). Previously, optical microscopic analysis showed that a reaction layer forms between the mullite ceramic and the metal ceramic composite (Figure 1). TEM analysis of the pure mullite (Figure 2) in comparison to partially infiltrated mullite (Figure 3) indicates that molten Al initially penetrates the ceramic preform along its grain boundaries. Once on the grain boundaries, molten Al reacts with individual mullite grains to produce alumina and silicon following Reaction 2 (Figure 4). An undulatory reaction front is clearly visible on the grain in the lower right corner of Figure 4, along with alumina precipitates within the Al on the grain boundary. We believe that alumina crystallites rapidly precipitate along the original mullite grain boundaries to form the rigid

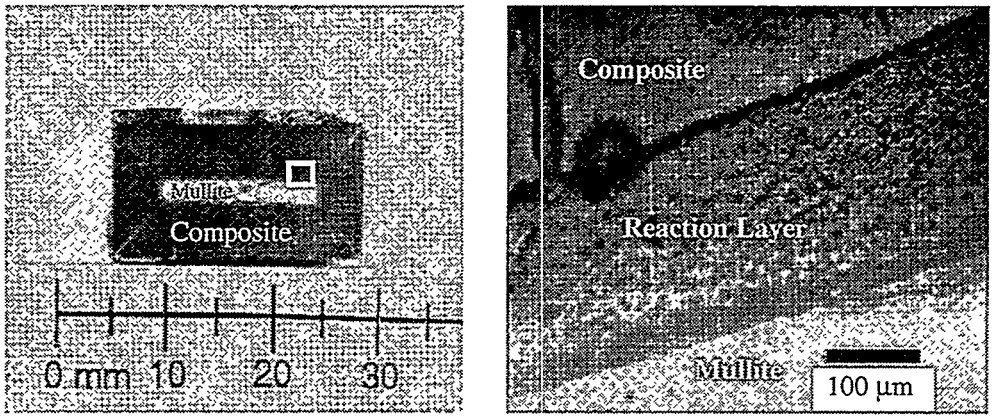

Figure 1. Optical micrographs of partially infiltrated mullite showing the reaction layer formed between mullite and the metal ceramic composite produced by reactive metal infiltration in the Al/mullite system.

Figure 2. TEM of the sintered mullite. No secondary phases are present at the grain boundaries, indicating the mullite is phase-pure.

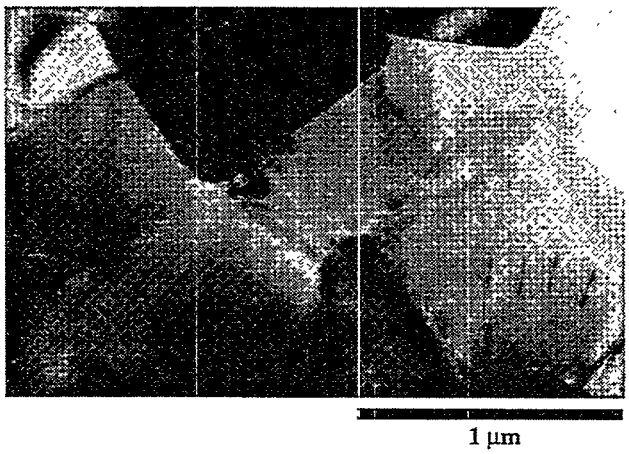

Figure 3. TEM of partially infiltrated mullite showing alumina penetration of the mullite ceramic along grain boundaries.

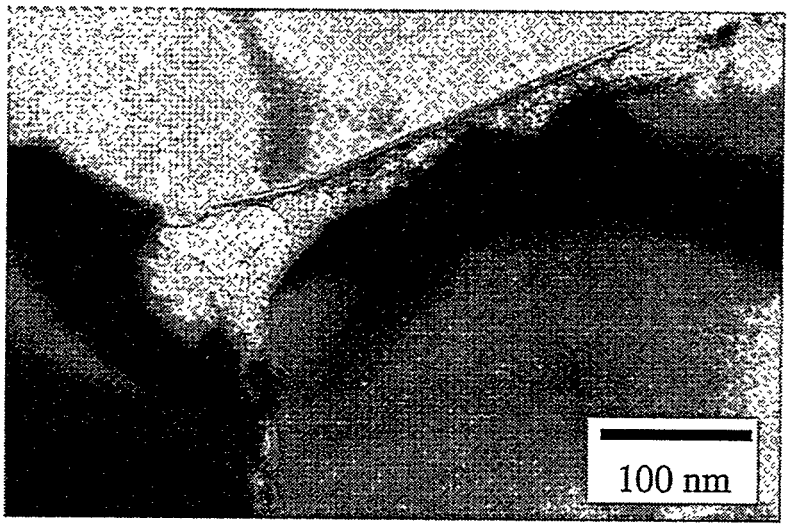

Figure 4. TEM of a partially infiltrated mullite preform showing grain boundary Al reacting with individual mullite grains. Following Reaction 2, the Al reduces the mullite grains to produce alumina and elemental silicon. Alumina precipitates form and ultimately percolate on the grain boundaries, while the silicon diffuses out of the system through the molten Al.

ceramic skeletal structure of the composite that controls many of its ultimate physical properties. It is the initial formation of this rigid grain boundary skeleton that makes reactive metal penetration an inherently net shape process.

Thermodynamics: By combining results on microstructural development obtained by TEM with previously obtained thermodynamics and kinetic data, we have been able to develop a likely reaction mechanism for reactive metal penetration. As reported previously, the concentration of oxygen in the system (P_{O_2}) during reaction plays a critical role. At 1200°C, there is a large thermodynamic driving force for Reaction 2 to proceed as written (i.e., $\Delta G_r = -905$ kJ/mole). However, there is also a large thermodynamic driving force for reaction of aluminum with atmospheric oxygen to form alumina at 1200°C (i.e., $\Delta G_r = -1163$ kJ/mole). The Ellingham diagram for Al/Al_2O_3 indicates that Al and alumina will be in equilibrium at a P_{O_2} of $10^{-28.5}$ atm. (i.e., a condition favorable for wetting). Thus, to limit Al oxidation by atmospheric oxygen and to ensure the Al/mullite reaction proceeds as written in Reaction 2, a system P_{O_2} of $\leq 10^{-28.5}$ atmospheres is required.

It seems likely that the molten Al itself acts as an O_2 getter during the reaction to reduce the P_{O_2} of the mullite grain boundaries to $\leq 10^{-28.5}$ atmospheres, which will make conditions favorable

for wetting and reaction. The optically-visible reaction layer formed during partial penetration can be attributed to the localized oxygen deficiency and initial precipitation of metal particles at the grain boundaries. The time required to reduce grain boundary oxygen concentration to $\leq 10^{-28.5}$ atmospheres can explain the 5 - 10 minute delay in penetration at the start of an experiment. Finally, localized grain boundary reduction also explains the difference in penetration of dense and porous mullite preforms. It appears that, because oxygen diffusion through grain pores is faster than along grain boundaries, it is more difficult to achieve a favorable P_{O_2} condition for wetting and reaction in a porous mullite body.

Reaction Mechanism: In Summary, TEM, thermodynamic, and kinetic analyses suggest the following 4-stage reaction mechanism for reactive metal penetration: 1) the metal melts and wets the ceramic preform surface; 2) oxygen diffuses out of the ceramic preform grain boundaries to lower the P_{O_2} to a favorable wetting condition; 3) molten metal penetrates the ceramic preform grain boundaries; and 4) the metal on the grain boundaries reacts with and reduces the individual grains of the ceramic preform.

3. Assess Near-Net Shape Fabrication By Reactive Metal Infiltration

Calculations: Molar volume calculations were used to model the reactive metal penetration process. The volume of the composite was compared to that of the original ceramic preform, as outlined in Table 1. In our calculations, we assumed that the amount of alumina is fixed by the reaction stoichiometry, and that the Si and Al contents are variable. Reaction 3 below, is a variation on Reaction 2 that allows for the possibility of Si diffusion out of the composite. The volume change on reaction was calculated as a function of Al content, x, for Si contents of y = 6 (stoichiometric reaction) and y = 0 (complete Si loss) in the composite.

$$(8 + x)\ Al + 3\ Al_6Si_2O_{13} \rightarrow 13\ Al_2O_3 + y\ Si + x\ Al \qquad (3)$$

Results for two different preform compositions are given in Table I, but the calculation is easily extended to other compositions. Reaction 3 is for a pure mullite preform, whereas Reaction 4 is for a mullite-glass preform that contains approximately 15 weight percent SiO_2.

$$(40 + 3x)\ Al + 9\ Al_6Si_2O_{13} + 12\ SiO_2 \rightarrow 47\ Al_2O_3 + 5y\ Si + 3x\ Al \qquad (4)$$

Results of the molar volume calculations are plotted in Figures 5 and 6. We predict that the Reaction 3 will be net shape for an aluminum content of x = 1 when there is no silicon loss (y = 6), and x = 7 when all the silicon lost (y = 0). From compositional analyses using energy

Table 1. Outline of the molar volume calculation used to model the reactive metal penetration of mullite according to Reaction 3.

	Preform		Composite		
	Aluminum	Mullite	Alumina	Silicon	Aluminum
Molecular Wt. (g/mole)	26.98	426.04	101.96	28.09	26.98
Formula Wt. (g/mole)	(8+x) 26.98	1278.12	1325.48	(y) 28.09	(x) 26.98
Density (g/cm^3)	2.70	3.15	3.98	2.34	2.70

$$\text{Preform Volume} = V_p = \frac{\text{Preform mass}}{\text{preform density}} = \frac{1278.12}{3.15}$$

$$\text{Composite Volume} = V_c = \frac{1325.48}{3.98} + \frac{(y)\,28.09}{2.34} + \frac{(x)\,26.98}{2.70}$$

$$\text{Volume Change (\%)} = \frac{V_c - V_p}{V_p}$$

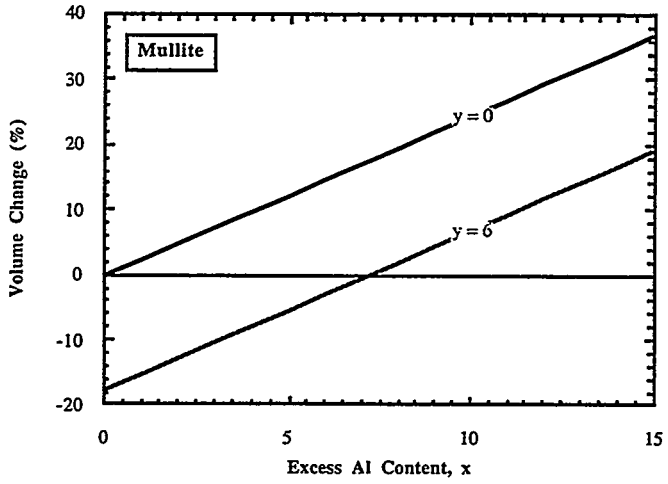

Figure 5. The calculated volume change of the mullite preform when reacted with Al to form a ceramic-metal composite. Results are plotted as a function of composite Al content, x, assuming no silicon loss (y = 6) and complete silicon loss (y = 0) following Reaction 3.

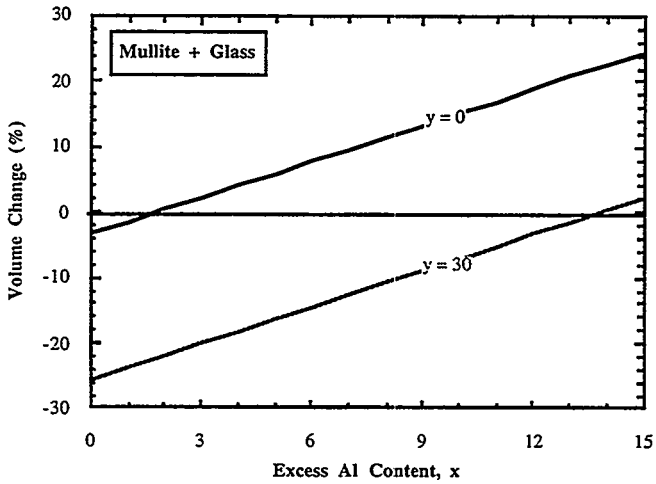

Figure 6. The calculated volume change of the mullite-glass preform when reacted with Al to form a ceramic-metal composite. Results are plotted as a function of composite Al content, x, assuming no silicon loss (y = 6) and complete silicon loss (y = 0) following Reaction 4.

dispersive spectroscopy (EDS), we know that most of the silicon diffuses out of the composite during reaction, and thus the y = 0 prediction should be most appropriate. For x = 7 and y = 0, the model predicts that the composite will contain 15 volume percent aluminum. For Reaction 4, we predict an aluminum content of x = 14 when all the silicon lost. This value corresponds to approximately 25 volume percent aluminum in the composite.

Volume Measurement: The volume changes associated with Reactions 3 and 4 were determined by directly comparing the volume of reactively formed composites to the volume of their precursor ceramic preforms. Volumes were accurately measured by liquid displacement. Results are presented in Figures 7 and 8. Mullite undergoes an average volume expansion of ~ 0.3 % while reaction of the mullite-glass preform undergoes a volume shrinkage of approximately 1.4 %. More precise control of volume may be achieved tighter control of the process variables.

Quantitative Phase Analysis: The volume fractions of the reaction products were determined using quantitative stereology of optical micrographs. This technique provided reproducible results for phase analysis. Figure 9 contains an optical micrograph of a ceramic-metal composite prepared by aluminum penetration of a mullite-glass preform. The amount of aluminum in the composite was determined to be 26 volume percent, which is in good agreement

with the molar volume calculation. Similarly, examination of micrographs of composites prepared from mullite found approximately 15 volume percent metal, also in good agreement with the model prediction.

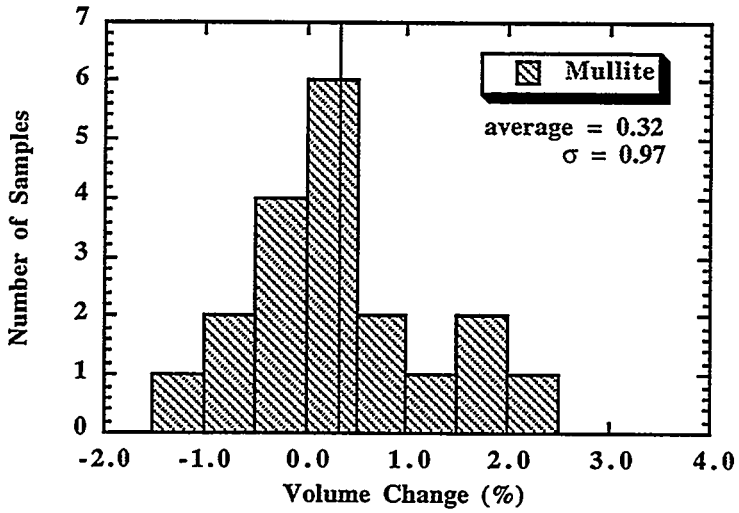

Figure 7. Measured volume changes of 17 different mullite preforms after reaction with Al to form ceramic-metal composites.

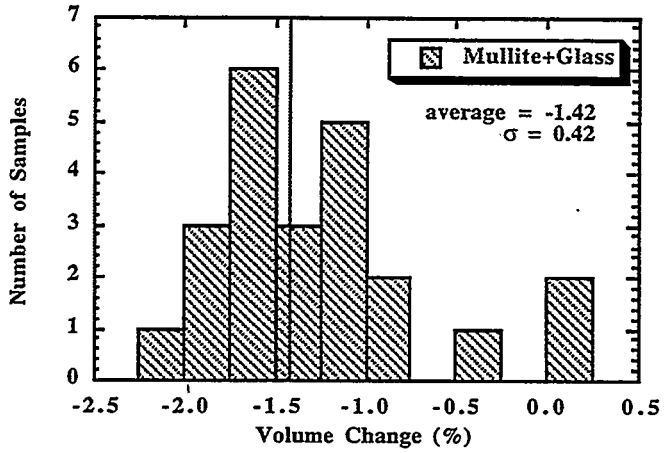

Figure 8. Measured volume changes of 21 different mullite-glass preforms after reaction with Al to form ceramic-metal composites.

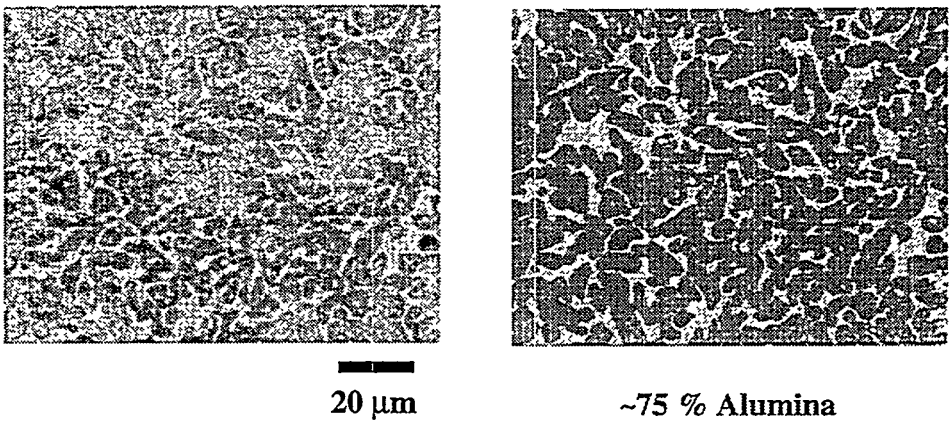

Figure 9. Optical micrograph of a ceramic-metal composite formed by aluminum penetration of and reaction with a mullite-glass preform (left). Phase concentration analysis by quantitative stereology was conducted on the digitized microstructure (right). Al_2O_3 is the darker phase.

5. Evaluate Metal-Ceramic Composite Microstructure and Properties.

Compositions and Microstructures of Porous Preforms: As stated above, composites made by reacting dense mullite preforms with an unlimited source of Al have a metal content of ~15 volume percent, or ~x = 7 (Reaction 3). The Al content of composites can be increased by adding silica to the mullite preform, as shown by Reaction 4. An upper limit of approximately 30 volume percent metal was observed for reaction of aluminum with pure silica. Below 1350°C the ability to further increase the metal content of the composite by using porous preforms is restricted by the formation of an oxide skin on the molten aluminum. Figure 10 shows a cross-section of a sample in which molten aluminum was in contact with a porous mullite preform at 1200°C for 1 hour. As can be seen, the metal did not penetrate or react with the ceramic under those conditions.

This report period, we discovered that it is possible to enhance the physical penetration of porous preforms by increasing the reaction temperature to ≥1350°C, as shown in Figure 11. Figure 12 illustrates that an aluminum drop fully infiltrates a porous mullite preform within 5 minutes at 1500°C. We believe that the enhanced physical penetration at ≥1350°C is due to the decreased equilibrium oxygen partial pressure in the oxygen-aluminum system, and the increased volatility of aluminum at the reaction temperature, which is consistent with our four-step model of reactive penetration.

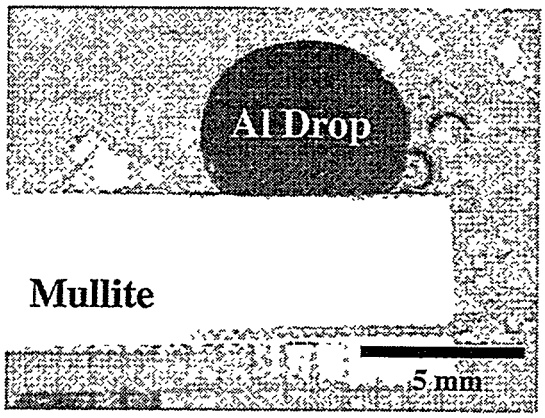

Figure 10. Cross-section of an aluminum drop on porous mullite after heating to 1200°C. There is no reaction and penetration at this temperature.

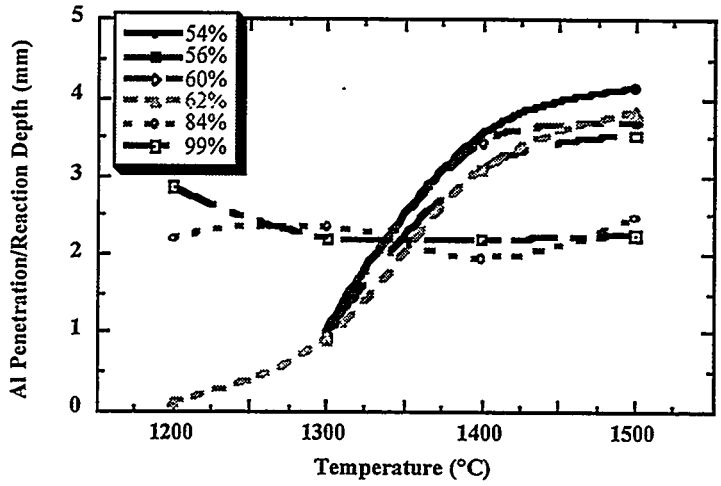

Figure 11. Al penetration and reaction depth as a function of temperature for Al reacted with mullite preforms of varying density.

Molar volume calculations similar to those presented earlier show that the metal content of composites prepared from phase-pure mullite preforms can be varied over a wide range, from 15 volume percent metal for dense mullite preforms to 65 volume percent metal for preforms that contain 50 percent porosity. This range of metal contents is illustrated in Figure 13. Presumably, the aluminum content of the composite can be increased even further if low density mullite foams or other highly porous, thermally-stable preforms are used. Similar to the case with dense preforms, the combination of physical infiltration and reactive penetration of porous

preforms leads to the formation of a two-phase, interpenetrating network in which both the aluminum and the alumina phases are continuous. The ability to physically infiltrate and reactively penetrate mullite preforms allows for compositional control without the difficulty of altering the composition of the preform.

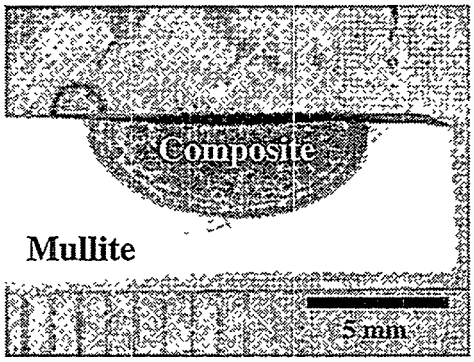

Figure 12. Cross-section of a porous mullite preform after the complete penetration of an aluminum drop at 1500°C.

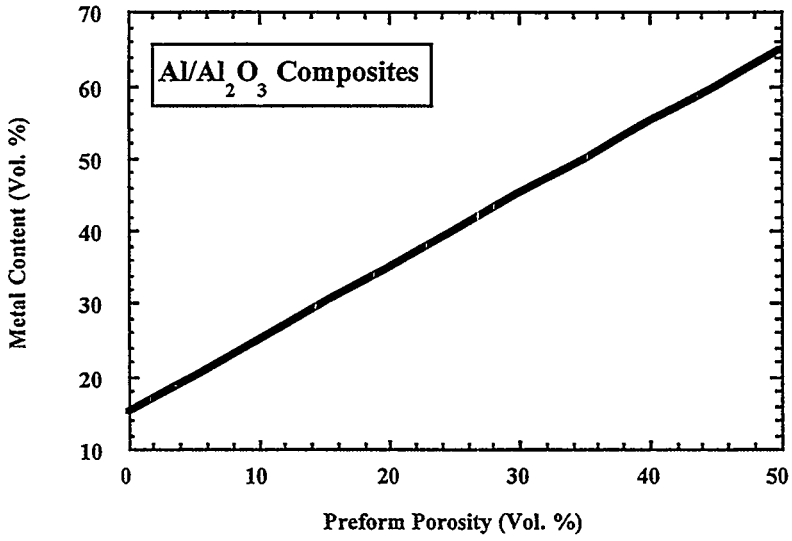

Figure 13. Predicted metal content of reactively-formed Al/Al_2O_3 composites as a function of preform porosity.

Mechanical Properties: The mechanical properties of ceramic-metal composites prepared by reactive metal penetration must be thoroughly characterized and understood for these new materials to be attractive for potential commercial applications. Reliable processing techniques have been developed to make test specimens for fracture strength and fracture toughness measurements. Composite fracture toughness is being characterized using the notched beam test and using a fractometer. To verify the reproducibility of our processing techniques we made a series of mechanical tests on bend bars prepared in our laboratory. The fracture strengths of slip cast ceramic preforms and the reacted ceramic-metal composites, which were obtained from four-point bend tests, are summarized in Figure 14. The average fracture strength of a slip cast aluminosilicate ceramic preform is 170 MPa, which is comparable to the value for mullite preforms. After reactive metal penetration, there is an appreciable increase in fracture strength to 390 MPa. The strength of the ceramic-metal composite containing ~30 volume percent metal is comparable to that of structural alumina.

In addition to the fracture strength results described above, strength values for other compositions of ceramic-metal composites produced by reactive metal penetration are also presented in Figure 14. In general, composite fracture strength increases with aluminum content.

Preliminary examination of the fracture surfaces of ceramic-metal composites produced by reactive metal penetration shows knife-edging of the ductile aluminum filaments in the composite (Figure 15). Knife-edging, which indicates ductile metal failure, is common in ductile-phase reinforced composites with improved toughness. The knife-edges in the fracture surfaces of the reactively-formed ceramic metal composites provide a microstructural explanation for their increased fracture toughness as compared to those of the ceramic preforms and alumina structural ceramics, both of which have fracture toughness in the range of 0.5 to 4 $MPa \cdot m^{1/2}$.

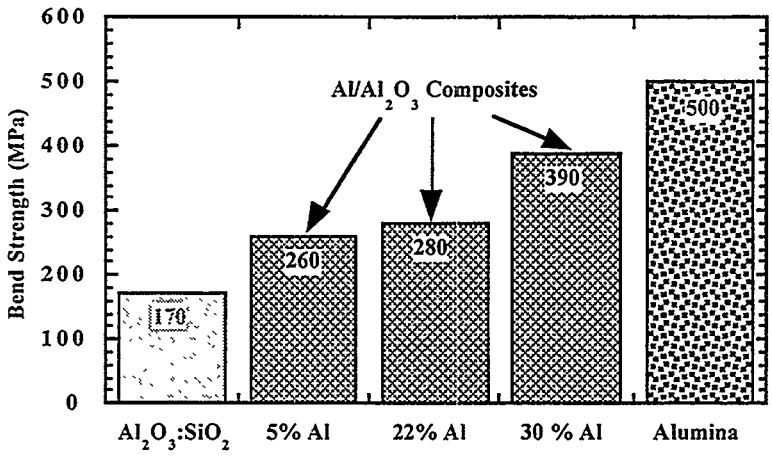

Figure 14. Bend strengths of reactively-formed ceramic-metal composites containing 5-30 volume percent aluminum compared to slip cast aluminosilicate ceramic preforms and a typical structural alumina.

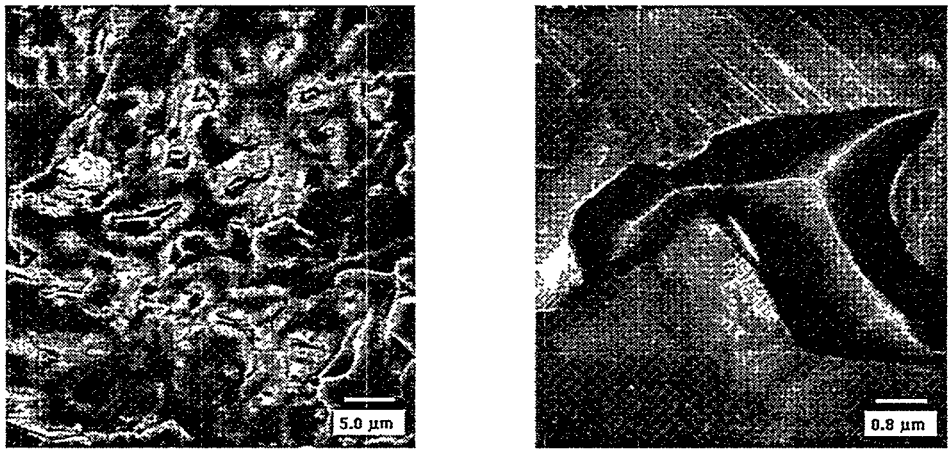

Figure 15. Optical micrographs of composite fracture surfaces showing knife-edging of the metal ligaments in a ceramic-metal composite produced by reactive metal penetration.

PUBLICATIONS

Journals

1) R. E. Loehman, K. G. Ewsuk, and A. P. Tomsia, "Synthesis of Al_2O_3/Al Composites by Reactive Metal Penetration," submitted for publication in *J. Am. Ceram. Soc.*, September, 1994.

2) E. Saiz, A. P. Tomsia, R. E. Loehman, and K. G. Ewsuk, "Formation of Al_2O_3-Al Composites by Reactive Metal Penetration of Mullite," submitted to the Journal of the European Ceramic Society, September, 1994.

3) Y. Gao, J. Jia, R. E. Loehman, and K. G. Ewsuk, "TEM Studies of Metal-Ceramic Composites Fabricated by Reactive Metal Penetration," submitted to the Journal of Materials Research, January 1995.

4) W. G. Fahrenholtz, K. G. Ewsuk, R. E. Loehman, "Formation of Structural Intermetallics by Reactive Metal Penetration of Ti and Ni," submitted for publication in *J. Am. Ceram. Soc.*, January 1995.

5) W. G. Fahrenholtz, K. G. Ewsuk, R. E. Loehman, "Near-Net Shape Processing of Metal-Ceramic Composites by Reactive Metal Penetration," submitted for publication in *J. Am. Ceram. Soc.*, January 1995.

Other Publications

1) Y. Gao, J. Jia, R. E. Loehman, and K. G. Ewsuk, "TEM Characterization of Al_2O_3-Al Composites Fabricated by Reactive Metal Penetration," submitted to the Proceedings of the 1994 Fall Meeting of the MRS, Boston, MA November 27 - December 2, 1994.

2) W. G. Fahrenholtz, K. G. Ewsuk, R. E. Loehman, "Synthesis and Processing of Al_2O_3/Al Composites by In Situ Reaction of Aluminum and Mullite," submitted for publication in "In Situ Reactions for Synthesis of Composites, Ceramics, and Intermetallics", the Proceedings of The Metallurgical Society 1995 Annual Meeting, Las Vegas, NM, February 12-16, 1995.

Master's Thesis

Jainmei Jia, "Microstructure and Mechanical Property Studies of Metal-Ceramic Composites Fabricated by Reactive Metal Penetration," Dept. of Materials Science and Engineering, New Mexico Institute of Mining and Technology, Socorro, NM, August, 1994.

PRESENTATIONS

1) K. G. Ewsuk, R. E. Loehman, A. P. Tomsia, E. Saiz, J. Ortega, W. Fahrenholtz, and Y. Gao, "Metal-Ceramic Composite Fabrication by Reactive Metal Infiltration," to be presented at the 18th Annual Conference on Composites and Advanced Ceramics, Cocoa Beach, FL, January 9-14, 1994.

2) W. Fahrenholtz, J. Ortega, R. E. Loehman, K. G. Ewsuk, and A. P. Tomsia, "Processing Near-Net-Shape Metal-Ceramic Composites by Reactive Metal Infiltration," presented at the 18th Annual Conference on Composites and Advanced Ceramics, Cocoa Beach, FL, January 9-14, 1994.

3) K. G. Ewsuk, S. Jill Glass, R. E. Loehman, and A. P. Tomsia, "Properties of Reactive Formed Metal-Ceramic Composites," presented at the 18th Annual Conference on Composites and Advanced Ceramics, Cocoa Beach, FL, January 9-14, 1994.

4) K. G. Ewsuk, (invited) "Reactive-Formed Metal-Ceramic Composites: Processing and Properties," presented at the New Mexico Institute of Mining and Technology Materials and Metallurgical Department Seminar, Socorro, NM, March 4, 1994.

5) K. G. Ewsuk, (invited) "Reactive-Formed Metal-Ceramic Composites: Processing and Properties," presented at the Argonne National Laboratory Divisional Seminar, Argonne, IL, April 22, 1994.

6) W. Fahrenholtz, J. Ortega, K. G. Ewsuk, R. E. Loehman, and A. P. Tomsia, "Kinetics of Metal-Ceramic Composite Formation by Al Infiltration of Mullite," presented at the 96th Annual Meeting of the American Ceramic Society, Indianapolis, IN, April 24-28, 1994.

7) J. Ortega, W. Fahrenholtz, K. G. Ewsuk, R. E. Loehman, and Y. Gao, "Modeling of Physical Properties of Reactive Formed Al_2O_3/Al/Si Composites," presented at the 96th Annual Meeting of the American Ceramic Society, Indianapolis, IN, April 24-28, 1994.

8) K. G. Ewsuk, S. J. Glass, R. E. Loehman, J. Jai, Y. Gao, D. Ellerby, J. Ortega, W. Fahrenholtz, and A. P. Tomsia, "Process-Microstructure-Property Relations in Reactive Formed Metal-Ceramic Composites," presented at the 96th Annual Meeting of the American Ceramic Society, Indianapolis, IN, April 24-28, 1994.

9) E. Saiz, A. P. Tomsia, R. E. Loehman, K. G. Ewsuk, and W. Fahrenholtz, "Oxygen Partial Pressure Dependence of Wetting and Penetration of Mullite by Aluminum," presented at the 96th Annual Meeting of the American Ceramic Society, Indianapolis, IN, April 24-28, 1994.

10) R. E. Loehman, K. G. Ewsuk, and W. G. Fahrenholtz, "Near Net-Shape Composite Formation by Reactive Metal Infiltration," presented at Ceramic Manufacturers and Suppliers Workshop and Exhibition, Louisville, KY, September 24-25, 1994.

11) A. P. Tomsia, K. G. Ewsuk, and R. E. Loehman, "Interfacial Reactions in Ceramics for Microelectronics Packaging," presented at the International Meeting on Metallization organized by the Ceramic Society of Japan, Kawasaki, Japan, September 21, 1994.

12) E. Saiz, A. P. Tomsia, R. E. Loehman, and K. G. Ewsuk, "Formation of Al_2O_3-Al Composites by Reactive Metal Infiltration of Mullite," presented at the Mullite '94 Conference, Irsee, Germany, September 7-9, 1994.

13) K. G. Ewsuk, S. J. Glass, R. E. Loehman, and W. G. Fahrenholtz, (invited) "Properties of Reactive Formed Metal-Ceramic Composites," presented at the Pacific Coast Regional Meeting of the American Ceramic Society, Los Angeles, CA, October 19-22, 1994.

14) A. P. Tomsia, (invited) "Ceramic/Metal Joining for Advanced Materials," presented at the Pacific Coast Regional Meeting of the American Ceramic Society, Los Angeles, CA, October 19-22, 1994.

15) W. G. Fahrenholtz, K. G. Ewsuk, R. E. Loehman, and A. P. Tomsia, "Dense Metal-Ceramic Composites by Reactive Metal Processing," presented at the Pacific Coast Regional Meeting of the American Ceramic Society, Los Angeles, CA, October 19-22, 1994.

16) D. T. Ellerby, R. K Bordia, K. G. Ewsuk, and R. E. Loehman, "Effects of Processing on the Microstructure of Interpenetrating Metal-Ceramic Composites," presented at the Pacific Coast Regional Meeting of the American Ceramic Society, Los Angeles, CA, October 19-22, 1994.

17) B. P. Hansen, W. G. Fahrenholtz, R. E. Loehman, and K. G. Ewsuk, "Temperature Effects on Aluminum Wetting and Penetration of Mullite," presented at the Ceramics and Advanced Materials Symposia at the Meeting of the New Mexico Sections of the American Ceramic Society and the Materials Research Society, Albuquerque, NM, October 31, 1994.

18) K. G. Ewsuk, S. J. Glass, R. E. Loehman, and W. G. Fahrenholtz, (invited) "Processing, Microstructure, and Properties of Reactively-Formed Al_2O_3/Al Composites," presented at the University of New Mexico, Department of Mechanical Engineering Seminar, Albuquerque, NM, November 11, 1994.

19) Y. Gao, J. Jia, R. E. Loehman, and K. G. Ewsuk, "TEM Characterization of Al_2O_3-Al Composites Fabricated by Reactive Metal Infiltration," Presented at the 1994 Fall Meeting of the MRS, Boston, MA November 27 - December 2, 1994.

HONORS AND AWARDS

None this reporting period

PATENTS/DISCLOSURES

Technical Advance

W. G. Fahrenholtz, K. G. Ewsuk, and R. E. Loehman, "Low-Cost Manufacture of Composites by Reactive Metal Penetration," Sandia National Laboratory (SD-5484) Technical Advance disclosure.

Patent Application

United States Patent Application "Composite Synthesis and Processing by Reactive Metal Penetration", filed in June, 1993

LICENSES

None this reporting period

INDUSTRIAL INPUT AND TECHNOLOGY TRANSFER

We have had on-going discussions with Golden Technologies, Golden CO, about use of reactively-formed composites for some of their applications. They are developing ceramic-metal composites using physical infiltration of porous ceramics and they wish to evaluate some of our materials for side-by-side comparison.

We have initiated a dialog with Zircoa, Inc., a ceramic component manufacturer, concerning the potential for using reactively formed, metal-ceramic composites as wear- and corrosion-resistant valves in petrochemical operations. Zircoa currently designs and manufactures ceramic valves for such applications using zirconia ceramics, which offer improved performance and life. Zirconia components can directly replace conventional metal valves in wear and corrosive environments, which can dramatically simplify market insertion.* Metal reinforced alumina composites produced by reactive metal penetration have many of the same advantages as zirconia, but at considerably lower cost. Based on mechanical properties supplied by Sandia, Zircoa has decided to evaluate the potential advantages of reactively formed, metal-ceramic composites as wear- and corrosion-resistant valves. Pending a positive evaluation, Zircoa has expressed interest in fabricating and testing prototype metal-ceramic components in collaboration with Sandia.

We also met with Clinton Bybee, the director of AB Ventures Inc. to discuss possible commercialization of ceramic-metal composites formed by reactive metal penetration. AB Ventures is a cooperative effort between Arch Venture Partners and BDM Federal. Arch Venture Partners is a venture capital firm that specializes in the commercialization of technology from DOE laboratories. AB Ventures has already been in contact with the Technology Ventures Corporation, the Martin Marietta subsidiary designed to advertise Sandia technology with possible commercial interest, and has signed a memorandum of understanding to work with TVC.

COST SHARING

Pask Research and Engineering is interested in the development of these composites, among other reasons because Dr. A. P. Tomsia, Director of Research, is a co-discoverer of the reactive metal penetration process. Over the past fiscal year, Pask R&E has contributed approximately $40, 000 to the project in in-kind labor.

---

* Due to the lower strength and toughness of alumina, alumina valve components must be larger, which also requires a redesign of the valve.

We have a continuing collaboration with Professor Rajendra Bordia of the University of Washington on toughening mechanisms in reactively-formed ceramic-metal composites. This past year Prof. Bordia assigned a graduate student to work on the project at no cost to us during the academic year. In the summer the student works in our laboratory. For the academic year this represents a cost share of approximately $25,000.

At the request of Dr. D. Alman of the U. S. Bureau of Mines in Albany Oregon we have started a collaborative program to characterize the wear properties of reactively-formed ceramic-metal composites. Dr. Alman is characterizing the wear properties of reactively-formed ceramic-metal composites we provided, and we will correlate the wear properties with composite microstructure. For the samples characterized this year, this effort represents an estimated cost share of approximately $10,000.

HIGHLIGHTS

Low-Cost Manufacturing Method for Advanced Ceramic Composites Discovered

New technology has been developed that will dramatically lower the cost of producing two-phase, interpenetrating metal ceramic composites. Al_2O_3/Al composites containing up to 30 volume percent metal can be prepared by reactive metal penetration of low-cost aluminosilicate preforms fabricated from ceramic precursors that cost less than $ 0.10/lb. Using the less expensive ceramic precursor, raw material costs for Al_2O_3/Al composites formed by reactive metal penetration are less than $ 0.50/lb. Preforms for reactive metal penetration can be prepared by standard, cost competitive techniques such as slip casting and extrusion that require no expensive additives or binders. The temperature required for densification of the preforms is also reduced significantly, to less than 1300°C. A Sandia Technical Advance disclosure has been filed on this process.

Ductile Metal Toughening Observed in Reactive-Formed Ceramic-Metal Composites

Measurements made using the indentation crack length technique reveal that, relative to the original ceramic preform (1.8 MPa $m^{1/2}$), reactive-formed ceramic-metal composites (6.4 MPa $m^{1/2}$) have significantly improved fracture toughness. This improved toughness is attributed to ductile metal toughening. Scanning electron micrographs of fracture surfaces of Al_2O_3/Al[Si] composites formed by reactive metal penetration clearly reveal ductile metal toughening, as evidenced by the characteristic "knife-edging" of the ductile metal phase of the composite.

Reactively-Formed Ceramic-Metal Reaction Mechanism Identified

In conjunction with transmission electron microscopy information on microstructural development during reactive metal penetration , thermodynamic, and kinetic analyses suggest the following 4-stage reaction mechanism for reactive metal penetration: 1) the metal melts and wets the ceramic preform surface; 2) oxygen diffuses out of the ceramic preform grain boundaries to lower the P_{O_2} to a favorable wetting condition; 3) molten metal penetrates the ceramic preform grain boundaries; and 4) the metal on the grain boundaries reacts with and reduces the individual grains of the ceramic preform. Understanding the mechanism of composite formation provides us another tool to optimize the reactive metal penetration process, and to optimize the composition and properties of reactively formed ceramic-metal composites.

THREE–DIMENSIONAL X–RAY TOMOGRAPHY OF CRACK–RESISTANT COMPOSITES: NEW PARADIGMS FOR PROCESS OPTIMIZATION

J.H. Kinney and D.L. Haupt
Chemistry and Materials Science Department
Lawrence Livermore National Laboratory
Livermore, CA 94550

INTRODUCTION

The goal of this research is to apply noninvasive, volumetric imaging technology (the x–ray tomographic microscope) to the characterization and process–modeling of ceramic matrix composites. Specifically, we propose to follow the evolution of a composite's microstructure during chemical vapor infiltration processing, and relate the microstructure to processing parameters and fiber architecture. The results will be used to provide the fundamental and practical understanding necessary for cost–effective "intelligent" processing of ceramic matrix composites.

Chemical vapor infiltration (CVI) is an important technology for fabricating continuous filament SiC ceramic matrix composites.(1) In CVI, a vapor precursor of the matrix material, such as methyltrichlorosilane (MTS), is passed through a network of reinforcing fibers at elevated temperature. The MTS dissociates, and the SiC matrix phase deposits on the fibers. As matrix growth progresses, avenues for gas transport become more tortuous and begin to close off. Infiltration and matrix consolidation eventually cease when the pores no longer form a percolating network through the composite.

Ideally, processing should be optimized so that the pores gradually close but do not seal off or become plugged until full density is achieved. CVI models have been developed that make use of the kinetics of the decomposition of MTS and the subsequent deposition of SiC.(2) These models have been used to optimize processing methods that make use of forced vapor flow and thermal gradients in the fiber preform to achieve rapid and uniform densification. However, fully dense composites fabricated with forced flow CVI methods remain an elusive goal.

Unfortunately, the same attention that has been given to the kinetics of CVI has not been given to the role that the fiber preform architecture plays in determining infiltration behavior and final density. In woven fiber composites, for example, there are many different preform architectures that have been developed. These architectures can be square weaves with sequential rotations

of the cloth layers (e.g., 0°/90°, 0°/45°); they can be two dimensional harness or satin weaves; or they can even be three–dimensional weaves. Does the architecture determine the final density of the composite; and, if so, can fiber architectures be optimized?

Part of the difficulty in assessing the role that the fiber architecture plays in densification has been the lack of a framework for quantifying the structure of the interconnected porosity and in relating the structure to measurable processing parameters such as permeability and densification. Many years ago, DeHoff, et al., developed a method for relating the topological properties of the porosity in a powder compact to its sintering behavior.(3) These researchers argued that the conducting backbone of the pore structure controls transport processes, and that topological variables provided the best description of this conducting backbone. The topological structure of the porosity, which requires a three–dimensional representation of the microstructure, could only be obtained by serial sectioning methods. The researchers developed a criterion that the sections should have a spacing no greater than 1/3 to 1/10 of the mean intercept length between the features of interest. For the case of establishing the topology of the porous networks in a CVI composite, this would require section separations of 50 μm or less over at least 5 mm—more than a hundred serial sections per sample. Each section would require photomicrographs, registration, and analysis. Such detailed sectioning would be time consuming, costly, and artifact prone. This is why, to our knowledge, there have been no attempts to quantify the topology of the percolating porous networks in ceramic composite materials.

The topology of a three–dimensional structure is completely defined by the Betti numbers β_0, β_1, and β_2.(4) β_0 is the number of individual clusters in the volume, β_1 is the number of handles (connectivity), and β_2 is the number of imbedded objects. It is the purpose of this paper to demonstrate that x–ray microtomography can cost effectively be used to completely define the topology of porous networks in woven fiber ceramic matrix composites. Furthermore, because tomographic methods are nondestructive, they can be used to study the time evolution of the pore topology in the same sample at various stages in the processing.

TECHNICAL PROGRESS IN 1994

Summary

Woven Nicalon (amorphous SiC, Nippon Carbon) fiber preforms (500 fibers per tow) were prepared with both 0°/90° and 0°/45° square weave architectures. The preforms, each 6.2 mm in diameter and 6.0 mm high, were

prepared by stacking 20 layers of Nicalon cloth into a cylindrical graphite reaction chamber. The chamber was maintained at 975C while a reactant gas of H_2, bubbled through MTS, was forced through the graphite tube and fiber preform—a method known as isothermal forced flow CVI. The 0°/45° weave was infiltrated twice to a final fractional density of 0.81 and the 0°/90° was infiltrated until vapor could no longer be forced through the sample (three times to a fractional density of 0.91).

The samples were imaged prior to infiltration with the x–ray tomographic microscope (XTM) that we designed for use at the Stanford Synchrotron Radiation Laboratory.(5) Densification of the preforms was then followed by interrupting the processing during consolidation. The XTM provides a three–dimensional digital representation of the composite's microstructure with a variable resolution between 1 and 25 μm.(6) For this experiment, the samples were partitioned into cubic volume elements (voxels) of 18 μm on each edge. This voxel size was chosen so as to minimize the amount of data while still meeting the sampling criterion required to extract topological properties. Because isothermal CVI produces significant density gradients through the length of a sample, a 2.5 mm high subset of the data was extracted from a region of uniform density in each composite. This region extended from 1 to 3.5 mm downstream from the vapor inlet, covering approximately 7 layers.

The XTM images were converted to binary data with the voxels being identified as belonging to solid material or to a void space.(6) A single pass labeling algorithm developed by Hoshen and Kopelman allowed rapid cluster analysis of the three–dimensional binary volumes.(7) Cluster labeling of the pore structures in the three-dimensional images identified the percolating pore and any closed off pores that were not connected to this volume. Cluster labeling, therefore, provided a direct measure of β_0 and β_2 (β_2 was always zero because a pore cannot contain an imbedded object).

For the interconnected cluster, the connectivity, β_1, was determined from the relationship

$$\beta_1 = \beta_0 - \chi + \beta_2$$

where χ is the Euler–Poincare' characteristic of the structure calculated with the method described by Feldkamp *et al.* (8) In this method, χ for a single occupied voxel (a volume element occupied by a pore) is used to construct the value of χ for the percolating pore network with the addition rule for sets:

$$\chi(A \cup B) = \chi(A) + \chi(B) - \chi(A \cap B)$$

The intersection is used to avoid counting elements twice. All voxels in a cluster are added, then the intersections (touching faces) are subtracted. A pore containing over 12 million voxels can be analyzed for connectivity in a few minutes.

Milestones:

1. Percolation Analysis of Pore Networks

With three–dimensional data, it is possible to count all isolated (non–connected) particles in a sample. Identifying isolated particles and correctly enumerating them in a large (>100 million voxels) volume set is a computationally intensive task. Thanks to an efficient cluster labeling algorithm developed by Hoshen and Kopelman[2], however, it is possible to label and count all of the isolated features in a large volume set quite rapidly on a standard workstation. In this method of counting, particles of type A are composed entirely of voxels containing attenuation coefficients unique to the type–A particle. The algorithm performs a single pass through the data, giving each cluster of type A voxels a unique label. In those cases where two or more previously isolated clusters merge together, the higher numbered clusters are relabled as belonging to the lowest number in the newly–merged cluster. A cluster may be considered as being face–connected only, or edge and corner connections may also be included.

We have used the HK algorithm to count the number of pores which become isolated (closed–off from the infiltration) during consolidation of a ceramic matrix composite. Prior to infiltration, there are no isolated pores, as they are all interconnected. As infiltration proceeds, pores close off and become isolated from the infiltrating vapor mixture, and their number increases gradually with composite density. Near the completion of infiltration, however, the number of isolated pores avalanches. Soon afterwards, there are no longer any percolating (continuous) clusters and infiltration ceases.

2. Topological Properties of Pore Networks

Figure 1 shows the increase in β_o, the number of isolated pores per mm^3, as a function of fractional density of the composite. For both the $0^o/90^o$ and

0°/45° architectures there is an increase in the disconnected porosity with infiltration. With this data, it is possible to calculate the strength, S, of the percolating pore volume. The strength is defined as the fraction of all voxels that belongs to the percolating network. As we spawn greater numbers of disconnected pores, the strength of the percolating pore volume will decrease. Indeed, percolation theory predicts that with random (uncorrelated) pore closure the strength should go to zero at a critical threshold (percolation threshold p_c) with an exponent β such that $S \sim (p-p_c)^{\beta}$ for $p \sim p_c$, and p is the volume fraction of pores in the composite. Furthermore, the exponent, β, depends only on the dimensionality of the lattice and not on the symmetry. For a simply connected (Bethe) lattice (i.e., has no closed loops), $\beta = 1$; whereas, for a three–dimensional lattice $\beta = 0.41$.(9)

If the percolating pore is simply connected, it is possible to derive an exact expression for the strength. This expression, for site percolation, is given by

$$S = p\left(1 - Q^{z}\right)$$

where z is the number of neighbors (branches) and Q is given by the real root of the equation

$$Q = 1 - p + pQ^{z-1}$$

Figure 2 shows the calculated values of the normalized strength (S/p) for the simply–connected lattice of z=9 and z=11 along with the measured values for the 0°/90° architecture. The CVI data exhibit a critical behavior, although the data are too widely spaced to obtain a reliable value for the critical exponent. Interpolation of the existing data indicates that the critical exponent is less than one ($\beta_{interp} = 0.72$).

Figure 3 shows the value of β_1 per total volume of percolating pore (mm^3) vs. fractional density of the composite. We call this index the connectivity index, and it provides a value for the interconnectedness of the pore (the number of multiple pathways connecting different regions of the composite). The higher the connectivity index of a given pore, the more pathways must be closed off before percolation ceases. The connectivity index of the 0°/45° is initially twice that of the 0°/90°, an indication of an initial difference between the architectures.

If deposition is uniform such that the pores close off gradually without breaking connections (plugging), then we should expect a 1/V (V=pore volume) increase in the connectivity index with infiltration. This functional relationship

is shown by the dashed and solid lines in Figure 3. It is apparent from the data that the deposition is not uniform, and that the pores close at an ever increasing rate with infiltration. The 0°/90° architecture actually shows an initial increase in connectivity due to a tendency of this weave to form bridging between plies. By about 75% density, however, the two architectures seem to have formed percolating pores with topologically equivalent structures. This is evidenced in Figure 4, which shows the connectivity per unit cell, where the unit cell size is defined as the area of a repeat pattern in the square weave times the distance between plies (0.9mm^3). Beyond 75% density, the connectivity decreases rapidly towards that of a simply connected structure. At this point, closing of a single pathway can terminate the CVI process.

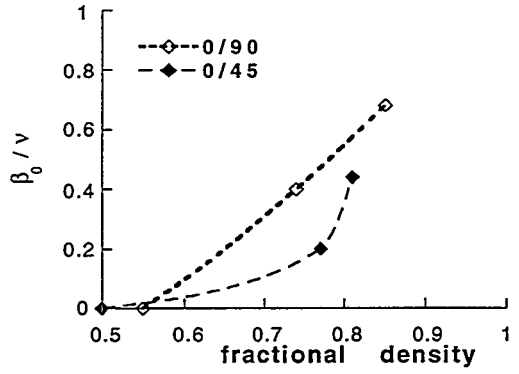

Figure 1: Increase in the number of isolated pores per cubic mm with consolidation for the 0°/45° and 0°/90° weave. Both the number and average size of the pores increases with infiltration.

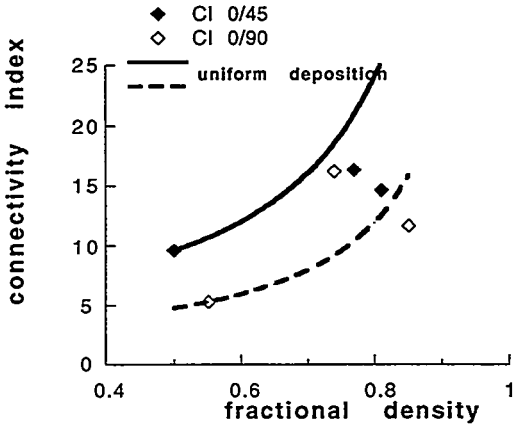

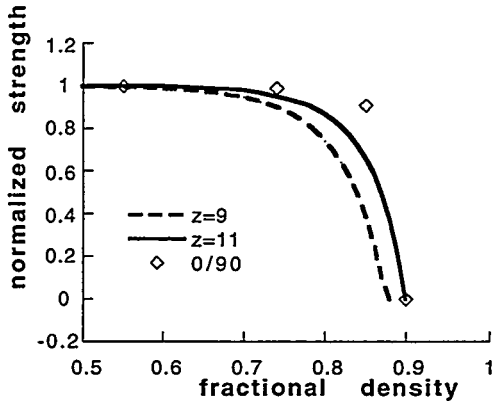

Figure 2: The normalized strength (probability of a pore belonging to the percolating cluster) for the 0°/90° weave as a function of density. The normalized strengths of a simply connected structure (Bethe lattice) are given by the dashed and solid lines.

Figure 3: Connectivity index as a function of fractional density in the 0°/90° and 0°/45° weaves.

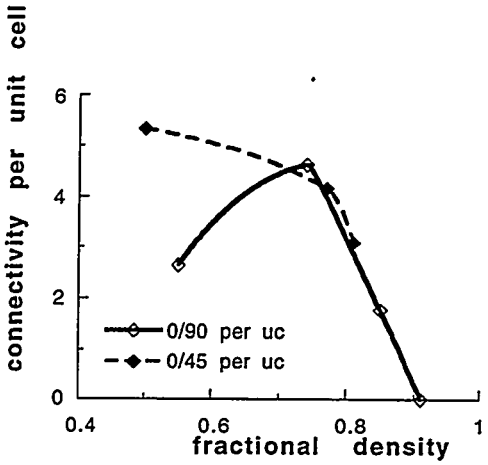

Figure 4: Connectivity per unit cell for both the 0°/90° and the 0°/45° weaves. By about 75% density, the percolating clusters have evolved to topologically equivalent structures in both weaves.

CONCLUSIONS

It is possible to quantify the topology of the percolating porous networks in woven fiber ceramic matrix composites with noninvasive x–ray microtomography. We have demonstrated the technique with two sample architectures, a 0°/45° and a 0°/90° weave. The pore topology was followed through stages of infiltration from the preform to final consolidation. β_0, the number of isolated pores, was used to measure the strength of the percolating pore. We found that the strength decreased in a manner expected for site percolation, and measured a critical exponent less than 1. β_1, the connectivity, was found to decrease in both architectures beyond 75% density as interconnecting pathways became plugged. The percolating pore structures in both architectures became topologically equivalent near final consolidation. This is the first experimental evidence of universality and critical scaling behavior in this class of materials.

The image data were acquired in about an hour. With reconstruction and data analysis, it was possible to quantify the pore topology with just a few hours of time on a conventional computer workstation. The rapidity of x–ray tomographic methods as compared with serial sectioning makes it cost effective and practical to explore the topology of percolating pore networks in advanced composite materials, and to develop new frameworks for optimizing the processing of these materials.

It is important that these observations be followed up, and if universality holds, the critical scaling exponents should be measured. The availability of these data will dramatically improve our understanding of composite processing, and provide a realistic model for residual porosity that can be used in engineering models of structures made from these materials. DOE is no longer interested in

continuing this funding, and we will not be able to continue with these measurements.

REFERENCES

1. Besmann TM, Sheldon BW, Lowden RA, Stinton DP 1991. Science **253**:1104
2. Starr TL in Chemical Vapor Deposition of Refractory Metals and Ceramics, TM Besmann, BM Gallois, and J Warren, eds. (Materials Research Society, Pittsburgh, PA, 1992), page 207.
3. DeHoff RT, Aigeltinger EH, Craig KR 1972 Experimental determination of the topological properties of three–dimensional microstructures. J Microscopy **95**:69.
4. Odgaard A, Gundersen HJG 1993 Quantification of connectivity in cancellous bone, with special emphasis on 3–D reconstructions. Bone **14**:173–182.
5. Kinney JH, Nichols MC, 1992 X–ray tomographic microscopy (XTM) using synchrotron radiation. Ann Rev Mater Sci **22**:121–152.
6. Kinney JH, Breunig TM, Starr TL, et al. 1993 X-ray tomographic study of chemical vapor infiltration processing of ceramic composites. Science **260**:789.
7. Hoshen J, Kopelman R 1976 Percolation and cluster distribution. I. Cluster multiple labeling technique and critical concentration algorithm. Phys Rev B **15**:3438–3445.
8. Feldkamp LA, Goldstein SA, Parfitt AM, et al. 1989 The Direct Examination of Three–Dimensional Bone Architecture in Vitro by Computed Tomography. J. Bone and Min Res **4**:3–11.
9. Stauffer D, Aharony A. 1992 Introduction to Percolation Theory, 2nd Edition. Taylor and Francis:London, pages 15–56.

PUBLICATIONS

Journals 94

J.H. Kinney, C.P. Henry, D.L. Haupt, and T.L. Starr, "The topology of percolating porosity in woven fiber ceramic matrix composites", Applied Composite Materials (in press).

J.H. Kinney, D.L. Haupt, M.C. Nichols, et al., "Three–dimensional perspectives of evolving microstructures". Nucl Instr. Meth. A347:480–486 (1994).

Conference Proceedings 94

T.M. Breunig, M.C. Nichols, J.S. Gruver, J.H. Kinney, and D.L. Haupt, "A servo–mechanical load frame for in situ, noninvasive imaging of damage development". Ceramic Engineering and Science Proc., 15:410–417 (1994).

T.M. Breunig, M.C. Nichols, J.H. Kinney, and D.L. Haupt, "In situ Three–Dimensional Characterization using Noninvasive X–ray Tomographic Microscopy", in The firt International Conference on Composites Engineering, D. Hui, ed., pp 63–64 (1994).

HONORS AND RECOGNITION

First Prize for Best Conference Paper, American Ceramic Society, 1994.

PATENTS/DISCLOSURES

"A Two Stage Asymmetric X–ray Magnifier for X–ray Tomographic Microscopy", patent received #5,245,861 (1993).

LICENSES

A CRADA has been signed with General Electric Corporation to transfer XTM technology and for joint development of advanced reconstruction software.

INDUSTRIAL INPUT AND TECHNOLOGY TRANSFER

COST SHARING

The technology transfer of the XTM to General Electric is being supported by a grant from Defense Programs through a technology transfer initiative. The maturation of this technology directly benefits from the AIC Materials Program efforts in ceramic matrix composites. Labor costs for maintaining the hardware and software are shared among grants from the National Institutes of Health and internal Laboratory Director's Research and Development money. A new Vax workstation for data analysis was procured by the Chemistry and Materials Science Department at Lawrence Livermore National Laboratory.

ESTIMATED ENERGY SAVINGS

HIGHLIGHTS

We have demonstrated that high–resolution x–ray tomographic microscopy can be used to analyze matrix growth quantitatively during chemical vapor infiltration. The measured parameters, such as the surface area evolution,

number of pores, and pore volume, are of great importance for validating process models. The availability of x–ray tomography systems with microscopic resolution, coupled with efficient analysis software, will aid our understanding of the generic class of problems in which microstructure changes with time. Important examples include materials synthesis and processing, crack nucleation and growth, and materials compatibility.

POLYMERS AND BIOBASED MATERIALS

Chemical Recycling of Mixed Waste Plastics by Selective Pyrolysis

K. Tatsumoto, R. Meglen, and R. Evans

Process Research Branch
Industrial Technologies Division
National Renewable Energy Laboratory
1617 Cole Blvd., Golden, CO 80401

INTRODUCTION

The goal of this work is to use selective pyrolysis to produce high-value chemicals from waste plastics mixtures. Selectivity is achieved by exploiting differences in reaction rates, catalysis, and coreactants. Target wastes are molecular mixtures such as; blends or composites, or mixtures from manufactured products such as; carpets and post-consumer mixed-plastic wastes.

The experimental approach has been to use small-scale experiments using molecular beam mass spectrometry (MBMS), which provides rapid analysis of reaction products and permits rapid screening of process parameters. Rapid screening experiments permit exploration of many potential waste stream applications for the selective pyrolysis process. After initial screening, small-scale, fixed-bed and fluidized-bed reactors are used to provide products for conventional chemical analysis, to determine material balances, and to test the concept under conditions that will be used at a larger scale. Computer assisted data interpretation and intelligent chemical processing are used to extract process-relevant information from these experiments. An important element of this project employs technoeconomic assessments and market analyses of durables, the availability of other wastes, and end-product uses to identify target applications that have the potential for economic success.

TECHNICAL PROGRESS - FY 1994

Summary

Recovery of ϵ-caprolactam from waste nylon-6 carpet is currently the most advanced application under study. A cooperative research and development agreement (CRADA) with AlliedSignal was signed in February 1994 because of the successful results of work done from 1992-1993. AlliedSignal is the major North American producer of caprolactam and nylon-6 fiber. Work sponsored by the Advanced Industrial Concepts (AIC)

Materials Program since 1990 has lead to a patent which was issued in June 1993 and is the basis for this CRADA. As a result of the AIC work, a complimentary project to develop the engineering-scale of this process was undertaken with the Waste Materials Management Division (WMM) in 1993. The WMM project includes optimizing the process at the small engineering-scale level using a 10-cm fluidized-bed reactor and obtaining data for the design and construction of a 25-50 kg/h circulating fluidized-bed reactor. The WMM project is the major DOE contributor to the CRADA. This new NREL/DOE facility will be available for subsequent applications of the AIC selective pyrolysis recycling technology.

During the past year, the yield and purity of caprolactam from the nylon-6 improved greatly and the major chemical impurity has been identified. Product containing excessive amounts of this impurity fails the accepted industrial standard. Therefore, efforts have been focussed on reducing this impurity to acceptable levels, and thereby minimizing the number of steps for caprolactam purification. Progress on using more realistic process feedstocks has also been achieved. Experiments using pure nylon, clean post-industrial carpet, and finally, dirty, post-consumer carpet have been completed. The form in which carpet is feed to the reactor has also been found to affect kinetics, yields, and product purity. Therefore, studies have been undertaken to explore the impact on process chemistry of alternate process feedstock form and feeding techniques. More emphasis has been placed on improving the catalyst, and catalyst composition and performance were studied in detail.

Although considerable time was spent on the support of AlliedSignal CRADA, progress was made in FY 1994 in the other major areas: recovering diamines from the isocyanates and high-value oxygenates from the polyols in waste polyurethane (PU); recovering dimethylterephthalate from wastes containing polyethylene terephthalate (PET); and recovering bisphenol A from waste containing polycarbonate (PC). In the PU process, there are significant safety considerations in this process because one of the products is toxic. Procedures to eliminate possible chemical exposure and to periodically test for the exposure were developed. Bench scale testing has begun so that conventional chemical analysis and material balances can be done. Procedures to improve process selectivity to produce high-value oxygenates from the polyol were investigated. A major effort in 1994 was discussion with the automotive industry about the application of selective pyrolysis to both

autoshredder residue and to potential dismantling streams. An Environmental Technology Initiative (ETI) was submitted to the EPA is September 1994 based on automotive applications of selective pyrolysis. The proposal was cosponsored by the North Star Steel Co., Minnesota Pollution Control Agency, General Motors, the American Plastics Council, and the Appliance Recycling Centers of America (ARCA). The ARCA group is interested in this technology for the use of the ridged PU foam insulation which is currently a disposal problem. In the PET application, experiments were performed to test the feasibility of recycling polyester fibers for the textile industry. The PC research continues to improve the bisphenol A yield from plastic mixtures containing polycarbonate that come from the electronics industry.

The second component to this work is the development of the intelligent chemical processing system. The primary goal of this project is to provide researchers with a suite of multivariate data analysis tools which can be used for computer-assisted interpretation of our growing MBMS database. One difficulty in multivariate data analysis has been that several steps are required to apply these tools to MBMS spectra. The objective has been to create a seamless graphical interface that would afford non-expert users easier access to these data analysis tools. A single module program to perform principal component analysis and display the graphical results has been written. A graphical user interface has been written to take a newly-acquired spectrum of an unknown substance and display its multivariate similarity to other previously stored spectra. These advances have brought us closer to the objective of a seamless on-line multivariate data analysis system. A data set of 500 experiments has been built to demonstrate quantitative analysis of carpet mixtures and to screen catalysts for converting nylon-6 to caprolactam.

Milestones

1. Operate the Fluidized-bed Reactor to Generate Scale-up Data and Produce Kilogram Quantities of Crude Caprolactam for Industrial Testing, (June 1994).

This milestone, to produce kilogram quantities of crude caprolactam for the purification process analysis by AlliedSignal, was completed in June 1994. Approximately three kilograms of pyrolyzate were produced from dirty, post-consumer carpets using the 10-cm fluidized-bed reactor. Chemical analysis showed that a major

impurity exists in the product and that it must be removed before the caprolactam will pass the industrial standard. A post-pyrolysis multistage purification unit would be required to purify the product. A study to find a low-cost, effective purification method is in progress. The 10-cm fluidized-bed reactor equipped with a hopper feeder and the electrostatic precipitator is being used to optimize the process conditions. Currently, the data are being gathered from three feeds; pure nylon 6, clean carpet, and post-consumer carpet. These data are being used for both process optimization and parameter estimates for design considerations in the scaled-up fluidized-bed reactor.

2. Assessment of the Recovery of Chemicals from Polyurethane Foam, (August 1994).

The goal of this project was to use the temperature programmed, catalytic thermal processes to convert polyurethane foams from automobile seat cushions into useful monomers or chemicals. Polyurethane comprises a major fraction autoshredder residue. The flexible foam chosen for this study was a blend of toluene-based diisocyanates and simple polyols. The products were directed toward the diamine rather than the diisocyanate because of the lower toxicity of the diamine. The primary focus of the work has been selection of a catalytic agent, catalyst support and coreactant. Additional work has been undertaken to identify a processing temperature which maximizes yields of the diamine monomer and high-value oxygenated hydrocarbons. The results from the temperature-programmed pyrolysis showed that in the presence of a catalyst/support with steam, the diamine is recovered without any contamination from the polyol. The remaining or unreacted polyol is then recovered when the temperature is raised. A bench scale study showed that approximately 80% of the potential toluenediamine was recovered. The propylene oxide based polyol produced mostly allyl alcohol. Work continues on the selectivity study on the polyol and to further improve the yield of diamine.

PUBLICATIONS

Detailed publications in this project have been delayed because U.S. and foreign patents are still in progress, and because of CRADA-protected information. Technical briefs were issued on this work by the Office of Industrial Technology, DOE, and NREL.

PRESENTATIONS

C.C. Elam, R.R. Meglen, K. Tatsumoto, R.J. Evans and H.L. Chum, "The Application of Intelligent

Chemical Processing to the Problem of Plastics Recycling." A paper and poster presentation at the ACS National Meeting, Washington, D.C., August 1994.

C.C. Elam, R.R. Meglen, K. Tatsumoto, R.J. Evans and H.L. Chum, "The Application of Molecular Beam Mass Spectrometry to the Problem of Plastics Recycling Through Intelligent Chemical Processing." A paper and poster presentation at the MBMS Workshop, Estes Park, CO, October 1994.

R.J. Evans, K. Tatsumoto, C.C. Elam and H.L. Chum, "Recycling Automotive Fabrics and Plastics Back to High-Value Chemicals by Selective Pyrolysis." An oral presentation by R.J. Evans at the Automotive Interior Conference, Detroit, MI, May 1994.

R.J. Evans, K. Tatsumoto, C.C. Elam, S.R. Czernik, and H.L. Chum, "Chemical Recycling of Mixed Waste Plastics by Selective Pyrolysis." An oral and poster presentation by R.J. Evans at the AICD Materials Program Annual Review, Albuquerque, NM, June 1994.

K. Tatsumoto, C.C. Elam, R.J. Evans, Michael Looker and H.L. Chum, "Tertiary Recycling of Mixed Waste Plastics." A paper and poster presentation by K. Tatsumoto at the ACS National Meeting, Washington, D.C., August 1994.

S. Kelley, R. Evans, K. Tatsumoto, C. Elam and H. Chum, "Innovative Approaches to the Chemical Recycling of Mixed Waste Plastics." An oral presentation by S. Kelley at the IEEE Workshop, Yorktown Heights, NY, October 1994.

R.J. Evans, "Innovative Approaches to the Chemical Recycling of Plastics." An oral and poster presentation at TechView '94, Golden, CO, September 1994.

1994 R&D 100 Nomination for "Innovative Approaches to the Chemical Recycling of Mixed Waste Plastics."

1994 American Textiles "BOBBIN" Show at Atlanta, GA, September 1994.

PATENTS/DISCLOSURES

Patent applications have been filed which are directed to the following embodiments:
Controlled catalytic and thermal sequential pyrolysis and hydrolysis of polymer waste comprising of:

I. A process of producing caprolactam from nylon 6.
II. A process for producing caprolactam and hydrocarbons from mixtures of nylon 6 and polyolefins.
III. A process for producing terephthalic acid or its esters along with by-products from PET and PE.
IV. A process for producing amines, isocyanates, etc. from polyurethanes.
V. A process for producing terephthalic acid, styrene or mixtures of these two from PVC, PET, polystyrene and polyethylene.
VI. A process for producing amines, isocyanates, HCl or mixtures of the same from PVC and PU.
VII. A process for producing styrene, phenols, etc., from polystyrene and polyphenylene oxide.
VIII. A process for producing phenols, hydrocarbons, etc. from polycarbonates and acrylonitrile butadiene-styrene polymers.

Patents were issued for I (U.S. Patent 5,216,149) and VII (U. S. Patent 5,300,704). The rest are pending.

INDUSTRIAL INPUT AND TECHNOLOGY TRANSFER

The CRADA agreement with AlliedSignal has been the major technology transfer activity this year. The CRADA has helped to better define the goals of this work sponsored by the AIC Materials Program, the

complimentary work sponsored by WMM, and the work that will be done by AlliedSignal. AlliedSignal is expected to concentrate their efforts on the better defined waste carpet collecting, sorting, and feed preparation method and the product purification process.

A meeting was held with a representative from Angelica Uniform on the polyester recovery from their cotton/polyester fabrics. More meetings are scheduled with Angelica Uniform to discuss a possible research agreement. Other technology transfer activities have come from the meetings listed above. These have generated interest from industry, and discussions are ongoing on other potential applications, in particular for PU recycling. The ETI proposal of automobile plastics recycling involved discussion with several companies. GM and the ARCA have continued to express interest in this technology. Additionally, NREL researchers have discussed this technology with representatives of the American Plastics Council in a broader context than automotive plastics.

COST SHARING

The CRADA will last three years and the $6.4 million cost will be shared 51% by AlliedSignal. Most of the DOE funding (86%) is from the Waste Materials Management Division, which is focused on the scale-up of the fluidized bed reactor. The AIC Materials Program funding that will be used for this CRADA will support efforts aimed at understanding the chemical processes and optimizing conditions, with emphasis on catalyst development.

ESTIMATED ENERGY SAVINGS

An economic impact is expected from this AIC nylon 6 carpet recycling technology. About 2 million tons of carpet waste is generated annually in the United States and about one-fourth of the total waste carpet is made of nylon-6. When successfully implemented through the year 2010, the selective pyrolysis of waste carpet could result in reducing electricity consumption by approximately 1,650 billion BTUs and reducing petroleum consumption by 340,000 billion BTUs because up to 500 million pounds of caprolactam will not have to be produced from imported oil. New plants are estimated to create 37,500 person-years of new jobs.

HIGHLIGHTS

In FY 1994, four major accomplishments were achieved:
1) the CRADA negotiations were completed with AlliedSignal for the waste nylon 6 carpet example and it was signed in February 1994;
2) the demonstration of the ability to handle the post-consumer waste carpet and to carry out day-long process experiments;
3) the demonstration of the ability to produce high value chemicals from PU foam; and
4) several programs have been written to bring us closer to the seamless on-line multivariate data analysis system.
This project continues to attract a high level of interest from industry. Future collaborations between WMM, or other DOE offices, and relevant industrial partners, such as the American Plastics Council, will likely be based on this work for the Advanced Industrial Concepts Materials Program.

Composites and Blends from Biobased Materials

Stephen S. Kelley, Principal Investigator
Industrial Technologies Division
National Renewable Energy Laboratory
1617 Cole Blvd.
Golden, CO 80401

INTRODUCTION

The program is focused on the development of composites and blends from biobased materials to use as membranes, high value plastics, and lightweight composites. Biobased materials include: cellulose derivative microporous materials, cellulose derivative copolymers, and cellulose derivative blends. This year's research focused on developing an improved understanding of the molecular features that control the permeation of gases through cellulose derivatives. We used this understanding to design cellulose based materials with improved properties for gas separation applications. Novel cellulose ester membrane composites have been developed and are being evaluated under a collaborative research agreement with Dow Chemicals Company.

TECHNICAL PROGRESS

Significant progress has been made this year in increasing our understanding of the structure-property relationships and phase behavior of cellulose esters in several complex systems. This understanding has allowed for the development of novel cellulose ester materials that may potentially be useful for gas separation membranes. In addition, NREL is leading a team of researchers from the University of Colorado and Dow Chemical Company who are studying mechanical creep and compaction in cellulose ester microporous materials.

I.) Cellulose Derivative Microporous Materials

Research efforts in the preparation and characterization of novel cellulose derivative microporous materials have focused on organic/inorganic hybrid (OIH) composites using cellulose acetate (CA) as the organic component. We have demonstrated the ability to prepare CA OIH materials with wide variations in morphologies by controlling the chemical reactions and film preparation conditions. These morphologies include microscale (nanometers) phase-separated and macroscale (microns) phase-separated materials. The relationship between the various components of a CA OIH material and the scale is illustrated in Figure 1.

Ia. Preparation of CA OIH Materials - The initial CA OIH materials where prepared with CA and tetraethyl orthosilicate (TEOS). Reactive triethoxysilane groups were grafted onto the CA backbone at two levels to promote the formation of chemical bonds between the organic CA component and the inorganic TEOS component. Reactions conditions, TEOS content (0-50 wt. %), and concentration of acid catalyst, were controlled in an attempt to prepare only microscale phase separated, dense films.

Solid state nuclear magnetic resonance (Si^{29} NMR) experiments demonstrated that silane groups covalently bonded to the organic polymer and silane groups originating from the TEOS were both extensively, but not completely reacted. Swelling experiments and dynamic mechanical analysis were used to demonstrate that all of the OIH materials were crosslinked. Small angle x-ray scattering experiments demonstrated that increasing the TOES content increased the size of the microscale phase separated inorganic domains. Modulus (MOE) and ultimate strength generally increased slightly while elongation to break decreased with increasing TEOS content. The small increase in the MOE of the composite was due to the relatively high modulus of the CA starting material.

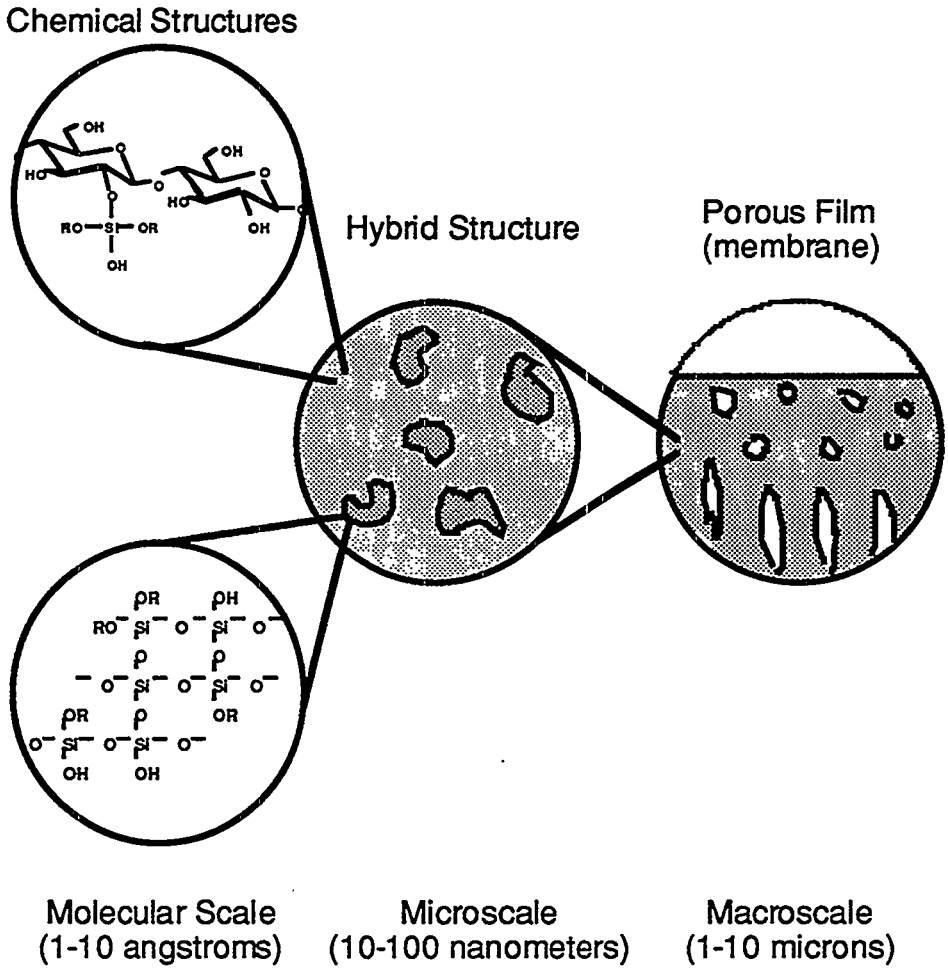

Figure 1. Schematic of the morphology of CA OIH materials.

Ib. CA OIH Membranes - The permselective properties of the CA OIH dense films were evaluated for pure gases at NREL. Improved permselective properties, along with the increased solvent resistance and mechanical properties highlighted the potential for using these materials for membrane applications. To assist with the evaluation of the potential commercial utility of these CA OIH materials, NREL has entered into a collaborative research agreement with Dow Chemical Company. Dow currently sells CA membrane systems that are used for upgrading natural gas that contains high levels of carbon dioxide and water. Dow is measuring the permselective properties of the CA OIH membranes at high pressures with mixed gas. Their initial results confirm NREL's findings that indicate these membranes offer a substantial increase in performance over the current cellulose ester membranes. This collaborative research agreement has allowed researchers at both NREL and Dow to openly discuss the details of the OIH chemistry and the plan experiments for optimizing the performance of these materials. More detailed high pressure mixed gas and gas sorption experiments are currently being conducted by Dow. If the results of these latest experiments continue to show promise NREL and Dow plan to negotiate a formal CRADA agreement for the continued development of this technology.

In a related project, NREL is working with researchers at the University of Colorado and Dow to study routes to minimize mechanical creep and compaction of microporous CA membranes. This work is being conducted at the University of Colorado under the auspices of the National Science Foundation University/Industry Cooperative Research Center for Separations Using Thin Films. The work will focus on improving the performance of CA membranes used to removed carbon dioxide from natural gas. In commercial applications these membranes perform well initially, but under high partial pressures of carbon dioxide, a plasticizing gas, they appear to fail due to mechanical creep or

compaction. The goal of this research is to develop a fundamental understanding of the relationships between the inherent properties of a material, e.g., mechanical strength and solubility properties, the processes used to form a microporous membrane, and the long-term performance of membranes under realistic use conditions, e.g., high pressure and plasticizing gases. Researchers will use very high frequency acoustical reflectometry, a unique analytical technique developed at the University of Colorado, to measure micron level changes in the thickness of the microporous membrane while simultaneously measuring the permselective properties of the membranes under an variety of experimental conditions. This project was initiated during the last few months of 1994.

II. Permselective Properties of Cellulose Mixed Esters

The goal of this work is to gain an increased understanding of the fundamental interactions that control the physical properties of cellulose mixed esters (CME), in particular the permselective properties of CME. The acyl composition, e.g., acetate, propionate, and butyrate, of CMEs is known to have a dramatic impact on the thermal and mechanical properties of these materials. However, to the best of our knowledge, there has been no systematic study on the effects of acyl composition on the permselective properties of these materials. Thus, two series of completely substituted CME were prepared and carefully characterized. Proton and carbon NMR were used to determine that these CMEs were completely substituted, i.e., a degree of substitution of 3.0, and the ester substituents were randomly located around the anhydroglucose ring. Thus, these CMEs can be treated as random copolymers.

The pure gas permeability and selectivity of these CME have been studied using dense films. Adding bulky propionate and butyrate groups to the CME increased the permeability for all of the gases used in this study: hydrogen, oxygen, nitrogen, carbon dioxide and methane. The O_2/N_2 selectivity of these CME remained relatively constant, while the CO_2/CH_4 selectivities decreased, as the propionyl and butyryl content increased. These results are shown in Table 1. Maintaining the selectivity of the CMEs while increasing the permeability suggests that these materials could have some potential for oxygen enrichment applications.

Table 1. The chemical composition and permselective properties of a series of CME.

Sample	Mole % Acetyl	Mole % Ester	Permeability (Barrers)					
			Oxygen	Nitrogen	Carbon Dioxide	Methane	O_2/N_2	CO_2/CH_4
P-0	100	0	1.2	0.4	9.5	0.3	3.0	31.6
P-8	93	7	1.3	.5	10.5	0.3	2.6	35.0
P-20	81	18	1.9	0.8	14.3	0.5	2.4	28.6
P-45	58	43	3.0	.9	20.5	0.9	3.3	22.8
P-90	11	90	5.4	1.5	34.4	2.1	3.6	16.4
P-100	0	99	6.3	1.8	44.4	2.8	3.5	15.8
B-0	100	0	1.2	0.4	9.5	0.3	3.0	31.6
B-7	93	6	1.6	0.6	11.4	0.4	2.7	27.7
B-23	80	19	2.8	0.9	19.9	0.9	3.1	22.1
B-42	64	37	3.6	1.1	27.5	1.5	3.3	18.3
B-92	10	92	11.0	4.2	90.4	7.9	2.8	11.4
B-100	0	99	13.6	4.3	104.0	8,8	3.2	11.8

Molecular modeling, using Molecular Simulations Inc. Cerius 2 software, was also used to study the effects of changing the ester type and location on the rotational energy around the anhydroglucose linkage and inter-atomic spacing. The location of the ester substituent around the anhydroglucose ring did not appear to have a systematic effect on the bond rotational energy. Increasing the content

of the more bulky ester substituent, propionyl or butyryl, increased the inter-atomic distance between cellulose ester chains. This analysis does indicate that there is a correlation between the interatomic distance of the cellulose ester chains and the permselective properties of the CMEs. However, the without detailed, independent analysis of the gas solubility and diffusivity of the CMEs, it is not clear what molecular level features are controlling the permselective properties.

III. Cellulose Acetate/Phenolic Polymer Blends

A series of miscible, single-phase, cellulose ester based blends have been prepared during the past year. Several cellulose acetates, with degree of substitution values between 1.6 and 2.7, were blended with a polyvinyl phenol (PVP), a polystyrene derivative and linear novolac resins. Polyvinyl phenol and novolac resins have very similar chemical compositions but differ in their free volume and accessibility around the phenolic hydroxyl. Thermal and spectroscopic analysis demonstrated that the CA/PVP blends are all single-phase. Preliminary analysis on some of the CA/Novolac blends indicates that they are also single phase. Infrared spectra indicated that there were shifts in the CA carbonyl stretching vibrations for all of the single phase blends.

Preparing miscible polymer blends is very unusual because of the poor compatibility of most polymers mixtures. However, in the case of CA/PVP and CA/Novolac blends, there is the potential for hydrogen bonding between the phenolic hydroxyl of the PVP or Novolac, and carbonyl or hydroxyl groups on the CA. These specific interactions are known to provide sufficient driving force for miscibility in a number of other polymer systems. The formation of miscible blends should restrict the small scale molecular motions of the CA and could provide for an increase in the gas selectivity of the CA blends for membrane application. Evaluation of the gas permselective properties of these blends is underway.

PRESENTATIONS

Invited speaker at the Kyoto Conference on Cellulosics, *Properties of Cellulose Ester Copolymers and Blends*, S. S. Kelley, presented in Kyoto, Japan, October, 1-2, 1994.

Composites and Blends from Biobased Materials, S. S. Kelley and S. S. Shojaie, presented at the IEEE Workshop on Environmentally Conscious Manufacturing for the Electronic Industry, Yorktown Heights, NY, October 20, 1994.

Properties of Cellulose Mixed Esters: A Computational Approach. T. Elder, and S. S. Kelley, presentation at the 208th national meeting of the American Chemical Society in Washington, D.C., August 21, 1994.

Preparation and Characterization of Cellulose Ester-Based Organic/Inorganic Hybrid Materials, S. S. Shojaie, S. S. Kelley, and T. G. Rials, presented at the 208th national meeting of the American Chemical Society in Washington, D.C., August 21, 1994.

Permselective Properties of Well Characterized Cellulose Mixed Ester Copolymers, S. S. Kelley and S. S. Shojaie, presented at the 208th national meeting of the American Chemical Society in Washington, D.C., August 21, 1994.

Permselective Properties of Cellulose Ester Copolymers, S. S. Kelley and S. S. Shojaie, presentation at the annual North American Membrane Society, Breckenridge, CO, May 24, 1994.

^1H Selective Excitation in Solids Using Chemical Shift Evolution, M. F. Davis, S. S. Kelley, and J. H. Iwamiya, presentation at the 35th Experimental NMR Conference, Asilomar, CA, April 13, 1994.

Preparation and Characterization of New Cellulosic-Based Organic/Inorganic Hybrid Materials Via the Sol-Gel Process, S. S. Shojaie, T. G. Rials, and S. S. Kelley, presentation at the 207th national meeting of the American Chemical Society in San Diego, CA, March 16, 1994.

Morphology of Cellulose Ester Blends, S. S. Kelley, presentation at the 207th national meeting of the American Chemical Society in San Diego, CA., March 16, 1994.

Invited lectures on *The Properties of Cellulose Ester Materials*,
Sandia National Laboratory, Albuquerque, NM, May 31, 1994.
Department of Chemical Engineering at the Colorado School of Mines, Golden, CO, October 3, 1994.
Polytechnic University, Brooklyn, NY, October 19, 1994.
Membrane Technology Research, Menlo Park, CA, October 27, 1994.

PUBLICATIONS
Preparation and Characterization of Cellulose Acetate Organic/Inorganic Hybrid Films, S. S. Shojaie, T. G. Rials, and S. S. Kelley, submitted to the Journal of Applied Polymer Science, December, 1994.

HONORS AND AWARDS - None

PATENTS/DISCLOSURES - None

LICENSES - None

INDUSTRIAL INPUT AND TECHNOLOGY TRANSFER - Collaborative research agreement signed with Dow Chemical Company to allow for the joint testing and evaluation of the potential of CA OIH materials for gas separation membranes. A joint research agreement was signed with researchers at NREL, the University of Colorado's NSF University/Industry Cooperative Research Center for Separations Using Thin Films, and Dow Chemical to study the effects of membrane material properties and the performance of microporous CA membranes subjected to mechanical creep and compaction.

COST SHARING - Characterization and analysis of the high pressure mixed gas permselective properties of CA OIH materials by Dow Chemical Company.

POTENTIAL ENERGY BENEFITS - The United States annually uses about 17,500 billion standard cubic feet (bscf) of clean burning natural gas to heat homes, produce chemicals, and for industrial power generation. To supply this energy need the United States has 95,000 bscf of known, domestic reserves of natural gas. In addition, there are an estimated 357,000 bscf of reserves of low grade, natural gas that contains carbon dioxide (CO_2) contaminates that can not be economically removed with current technology. Improved cellulose ester membranes that would allow the use of only 5 percent of the low grade natural gas in known domestic reserves, and new fields would provide more than 22,000 bscf of new domestic energy resources.

HIGHLIGHTS - Cellulose ester organic inorganic hybrid (CA OIH) materials with improved solvent resistance and mechanical properties have been prepared. The permselective properties of these materials have been evaluated for a series of gases. Initial results indicate that these CA OIH materials may be useful for gas separation applications. A collaborative research agreement has been signed with Dow Chemical Company to allow them to assist with the evaluation of these CA OIH materials for mixed gases at high pressure.

CONDUCTING POLYMERS: SYNTHESIS AND INDUSTRIAL APPLICATIONS

S. Gottesfeld, Principal Investigator

Electronics Research Group, MST-11
LOS ALAMOS NATIONAL LABORATORY
Los Alamos, NM 87545

The Conducting Polymer project funded by the AIM Materials Program is developing new methods for the synthesis of electronically conducting polymers and is evaluating new industrial applications for these materials which will result in significant reductions in energy usage or industrial waste. The applications specifically addressed during FY 1994 are electrochemical capacitors and membranes for gas separation. As an active material in electrochemical capacitors, conducting polymers have the potential of storing large amounts of electrical energy in low cost materials. Such devices are needed in electronics for power failure back-up and peak power, in power supplies for filtering, and in electric vehicles for peak power and load leveling. As a gas separation membrane, conducting polymers offer high selectivity and the potential to chemically or electrically adapt the membrane for specific gas combinations. Potential energy savings in the US. for this application are estimated at 1 to 3 quads/yr.

MILESTONES:

I. Electrochemical Capacitors Based on Conducting Polymer (CP) Films

We continued this year the development and testing of conducting polymer (CP) materials tailored for electrochemical capacitor applications. In our past work we have shown that capacitors of three types (named by us Type I, II and III) can be designed with conducting polymer active materials, with the Type III material having the highest potential energy and power density. Type III capacitors are based on unique conducting polymer materials which can be both p- and n- doped reversibly. An ideal conducting polymer would allow high-levels of both p-type and n-type doping. The advantages of such an ideal conducting polymer would be a larger voltage window and highly conducting active material on both plates at full charge.

By focusing on various derivatives of polythiophene, we demonstrated last year a new polymer, poly-3-(4-fluorophenyl)-thiophene (PFPT), which approaches this ideal behavior. We have continued this year to experiment with PFPT, aiming at optimized electrochemical system parameters that would enable highest power and longest cycle life. Accordingly, we have targeted this year the following specific milestones:

* Electrochemical conditions for highest power density and longest cycle life in electrodes based on PFPT active material

* Advance from testing of single electrodes to testing of model single cells with PFPT active material

* Synthesis of new monomers for Type III active materials with tailored side groups to facilitate charge/discharge dynamics and improve longevity under multicycling conditions.

Our achievements this year towards these milestones have been:

Enhanced power in Type III capacitors with PFPT active material: Ionic penetration into the active material is the rate limiting process in the charging and discharging of PFPT, much the same as in other conducting polymer active materials. It determines the maximum power accessible from the Type III capacitor. We have investigated this year, with ac impedance techniques, factors that affect the ionic conductivity within this novel material and examined means for enhancing it. All experiments were carried out in an inert atmosphere glove box to avoid interference of oxygen and moisture.

The ionic conductivity, R_{ion}, for a "virgin" PFPT film immersed in electrolyte was found to be very high, reaching in one typical experiment 6 kΩ. This value would completely preclude use in high power applications. However, after one electrochemical cycle of the film between -2.1 V and 1.0 V (i.e., between complete n-doped form and complete p-doped form), R_{ion} was found to dramatically decrease to about 100 Ω. The critical question we had to answer was, under which conditions is R_{ion} maintained at the lower levels required for high power applications. From our detailed experiments, we could conclude the following: A newly grown film has a reduced permeability to electrolyte and solvent (R_{ion} = 6 kΩ), but after a few "break-in" electrochemical cycles, it becomes swollen by forced influx of solvated electrolyte ions. Consequently, rapid ion transport occurs through opened solution channels in the film which do not collapse following termination of charge cycling, provided the film remains soaked in the electrolyte solution. Nearly complete collapse of the swollen structure occurs only when the electrode is washed with solvent and then dried.

These findings are significant in devising film/electrode fabrication and handling protocols for high-power polymer-based supercapacitors. We could conclude that initial "break-in" cycles covering a wider potential domain, and/or operating the capacitor with a continuously alternating polarity, could enhance ionic conductivity by forced incorporation of larger amounts of electrolyte into the volume of the active material.

We have also elucidated this year a complex dependence of the ionic conductivity within the active PEFT polymer on the nature and concentration of the electrolyte of immersion. As a typical example, for $Et_4N\ BF_4$ / acetonitrile electrolytes, we have found, as expected, an increase in the ionic conductivity within the polymer as the concentration of the salt was increased from 0.2M to 1.0 M. However, further increase in electrolyte concentration (to 2.0 M) caused a *decrease* in the ionic conductivity of the polymer, while the conductivity of the bulk electrolyte showed a further increase. We ascribe this phenomenon to an osmotically driven desolvation of the polymer which reduces the mobility of the ions remaining within the matrix. This complex dependence of polymer conductivity on external electrolyte concentration elucidates the care required in defining conditions for fastest charge/discharge dynamics.

Such studies of electrolyte incorporation and of ionic mobility within the polymer have provided us with a better basis for optimizing electrochemical conditions in Type III capacitors.

Critical Factors Affecting Long Term Cyclability: Achieving performance stability during multicycling is of highest priority in the demonstration of the viability of active materials for Type III capacitors. We have previously achieved 100,000 cycles with Type I (lower voltage) capacitors by optimizing the elctrochemical parameters of the system, but achieving prolonged cyclability with the higher voltage, Type III capacitors is more difficult. Working towards this goal, we attempted to establish a dependence of charge cyclability in PFPT on the nature of cation and anion injected into the active material during electrochemical doping. The pattern that emerged was interesting: the salts most effective for extended cycling were not the same salts that exhibit highest initial charge capacity. Insight into this pattern has allowed us to advance, for the first time, beyond the threshold of 100 cycles for electrodes with PFPT active material, while maintaining reasonable performance stability. This was achieved by growing the active film in one electrolyte and charge cycling it in another electrolyte. We suspect that the better stability observed is associated with a lower chemical reactivity of n-doped PFPT in contact with some specific cations. We are working now on further salt optimization based on this insight, to extend PFPT cyclability.

Initial Tests of Model Type III Capacitors: We ran this year some initial tests of cells with a pair of electrodes loaded with PFPT (p- and n-dopable) active material, placed together in symmetric capacitor configuration. These tests were run to obtain an estimate of energy and power densities that can be expected from a complete device based on the PFPT material, taking into account the weight of the active material as well as that of the other components of the unit building block of the capacitor, including current collectors, separator and electrolyte. The results obtained in these initial tests were encouraging, showing an energy density for the complete device (excluding casing) of 10 W/kg and a power density (calculated for 10 sec discharge) of 3.6 kW/kg of the device (excluding casing). These numbers are significantly higher than those demonstrated to date for carbon based ultracapacitors. At this point, demonstration of more extended cyclability (at least 1000 cycles) is, however, a remaining requirement for bringing our conducting polymer based Type III capacitors to the point of commercialization.

Synthesis of new monomers for Type III active materials: We continued this year work (subcontracted to UT, Dallas) on the synthesis of novel p- and n-dopable conducting polymers. Important issues to be addressed by new and further improved active Type III materials are the charging/discharging efficiency and the long term cyclability. Our choice of advanced monomer structures was based on impedance measurements which showed that both the electronic and ionic conductivities of PFPT are significantly higher in the p-doping regime compared with the n-doping regime. The lower mobility of cations in the negatively charged (n-doped) polymer is apparently the reason this behavior and has to do with strong electrostatic interactions between the cation and the negatively charged polymer. Aiming to improve ion transport in the n-doped material, we have synthesized a series of polymers which possess fixed cationic groups, requiring that anions be transported during *both* the p- and n-doping processes. This feature should allow us to capitalize on the enhanced ionic mobility of anions in such polymeric active materials.
During this year we have synthesized several such monomers with fixed positively charged sites and we are now in the process of polymerizing these new monomers to demonstrate the expected improvements in n-dopability and, hence, in energy and power density.

II. Conducting Polymer Membranes For Gas Separation

This year we have pursued strongly our activity in development and optimization of conducting polymer films for gas separation. This application of conducting polymers is particularly exciting because of its potential for large energy savings in industry. Of special interest are membrane separations of oxygen and of nitrogen from air, as well as separation of methane from CO_2.

Our FY-94 goals for this research activity have been:

* Fine-tune doping levels in films of polyaniline (PANI) to maximize selectivity in oxygen/nitrogen, as well as other gas separation processes

* Develop techniques for the fabrication of asymmetric membranes of polyaniline, aiming at a combination of high selectivity and high throughput

* Analyze fundamental gas transport properties in membranes of polyaniline (PANI), aiming at clarification of the effect of doping level on selectivity.

Our achievements this year towards these milestones have been:

Optimization of doping levels: In a series of detailed experiments performed this year, we studied the effects of doping levels in polyaniline (PANI) membranes on gas permeability and selectivity. This effort was confined to relatively thick membranes of low throughput, aiming at the intrinsic transport properties of the material. Optimized doping is the key tool for enhancing selectivity in gas separations through membranes of conducting polymers. In our experiments, as-cast membranes were immersed in solutions of different concentrations of acetic acid (CH_3COOH). The expected trend of lowered gas permeability with doping level was observed practically for all gases examined. The permeability is strongly dependent on the effective size (kinetic diameter) of the gas molecule, and relatively larger effects of doping were observed for gases with the larger kinetic diameters. As a result, a significant increase in selectivity was reached in the medium doping range for all the gas pairs examined.
The use of acetic acid was aimed at achieving specific interaction between the acetate ion and the CO_2 gas molecule. An increase of selectivity was indeed achieved in the separation of CO_2 from methane when the doping level increased but the most important reason for it was a strong unexpected drop in the permeability of methane in the medium doping range.
As to the pair O_2/N_2 which has been the main target of our efforts, the separation factors achieved following immersion in several concentrations of acetic acid were, respectively: 7.1 (0 M), 8.5 (0.005 M), 7.3 (0.050 M), 11.2 (0.080 M), and 6.7 (4.0 M). This trend with doping level is similar to that observed for the gas pair CO_2/CH_4 .
This investigation has shown that controlled doping can achieve rather strong effects on selectivity in separation of various pairs of gases through PANI membranes. The highest separation factor observed for the pair O_2/N_2 would be impressive if sustained in asymmetric membranes of high throughput.

Towards commercially acceptable throughput/selectivity combinations Until recently, we have experimented with dense, 30-40 μm thick PANI membranes which have exhibited exceptional selectivites in several gas separation processes. The flux through such membranes is, however, much too low to enable commercial applications. A central goal of our effort on conducting polymer membranes for gas separation has thus been raising of the throughput to commercially acceptable levels. Towards this goal, we have developed during this year a novel method for fabricating "integrally skinned" asymmetric membranes of PANI. Our approach yields a membrane that combines a non-

porous, ultra thin (<1 μm) top "skin" with a porous, 10-30 μm thick support. Both layers are integrated and made of polyaniline material. Key demands on such asymmetric membranes are good mechanical integrity of a porous polymeric structure and a flawless skin that preserves selectivity in the gas separation process. Limiting the thickness of the dense skin to significantly less than 1 μm enables the high throughputs.

In the novel process developed by us this year for making asymmetric PANI membranes, a volatile non-solvent for polyaniline (THF) is added to the ordinary solvent of PANI, NMP, to form a stable polyaniline (PANI) solution. This solution of PANI in NMP+THF is used to cast first a wet film of polyaniline onto a glass plate. To form the dense skin , the volatile THF is rapidly evaporated from a thin layer at the outer surface of the film by a stream of forced air. The membrane is next placed in a coagulation (water) bath which causes the bulk of the polymer below the skin to precipitate with ultraporous morphology. The asymmetric membrane is next immersed in a methanol bath to extract residual solvents and in the final step dried in a vacuum oven.

A crucial improvement in the mechanical properties of these asymmetric membranes was achieved by increasing the molecular weight of the polymer used for the preparation of the membrane. This was done by a technique of emulsion polymerization, demonstrated by us for the first time to be applicable for the synthesis of higher molecular weight PANI. The aniline monomer is dissolved, together with surfactant molecules containing an acid functional group, in $CHCl_3$ or toluene at 5°

C , while the oxidizing agent required for aniline polymerization was dissolved separately in water. The water and organic solvents form an emulsion on contact, and the aniline polymerizes within surfactant vesicles. Such spatially confined polymerization generates a polymer of higher molecular weight. This polymer was much more readily fabricated into robust asymmetric membranes.

Fig. 1a is an SEM top view of the asymmetric membrane (looking at the dense surface), Fig 1b is an SEM bottom view of the asymmetric membrane (looking at the porous surface) and Fig. 1C shows a cross-section of the membrane from which a 0.2 μm thick skin is apparent. The oxygen flux measured through the asymmetric membrane shown in figure 1, with the membrane in undoped form, was 3 x 10^{-6} cm^3 (STP) / cm^2 s cmHg. *Thanks to the thin dense skin, this flux is two orders of magnitude higher than fluxes through 40 μm thick dense PANI membranes ,with which we have experimented hitherto.* The novel assymetric PANI membranes developed by us is already approaching the flux ("productivity") levels achieved in commercial membranes -- an important requirement for commercialization. The selectivity measured for O_2/N_2 separation by our membrane in yet undoped form was also close to 6. Experiments are presently underway to utilize the expected beneficial effects of optimized doping in further enhancing the selectivity. Increasing the selectivity for O_2/N_2 separation from 6 to 10-12 (as achieved in thick dense membranes of PANI) will make this novel conducting polymer membrane very attractive for O_2/N_2, as well as other gas separations.

Analysis of Fundamental structural Properties of Polyaniline Membranes: Several collaborative efforts during this year focussed on characterization of fundamental properties of polyaniline, aimed at elucidation of key parameters that determine gas permeability in PANI membranes. As an example, ^{13}C NMR experiments were performed in collaboration with Washington University on a polyaniline (emeraldine base) sample to measure molecular motions such as ring flips. The results have suggested that, at room temperature, approximately 36% of the aromatic rings are flipping while the other 64% of the rings remain static. The rate of ring flipping is related to local free-volume, considered a key factor in determination of gas transport rates.
In another effort, a detailed study of gas solubility in PANI was completed this year by a sabbatical visitor from NIST (J. Pellegrino) . The quantitative description of the thermodynamics of gas sorption in a polymer is integral to optimizing its development and use in membrane-based gas separations. The results of this work are being now summarized.

PUBLICATIONS

(1) A. Rudge, John Davey, Francisco Uribe, "Performance Evaluation of Polypyrrole and Polyaniline As Active Materials for Electrochemical Capacitors", Proceedings of the Third International Seminar on Double Layer Capacitors and Similar Energy Storage Devices, Deerfield Beech, Florida, Dec. 6-8, 1993

(2) A. Rudge, J. Davey, I. Raistrick S. Gottesfeld and J. Ferraris, Conducting polymers as active materials in electrochemical capacitors, J. Power Sources, 47(1994) 89-107

(3) A. Rudge, I. Raistrick S. Gottesfeld and J.Ferraris, A Study of The Electrochemical Properties of Conducting Polymers For Application In Electrochemical Capacitors, Electrochimica Acta, 39(1994) 273-287

A

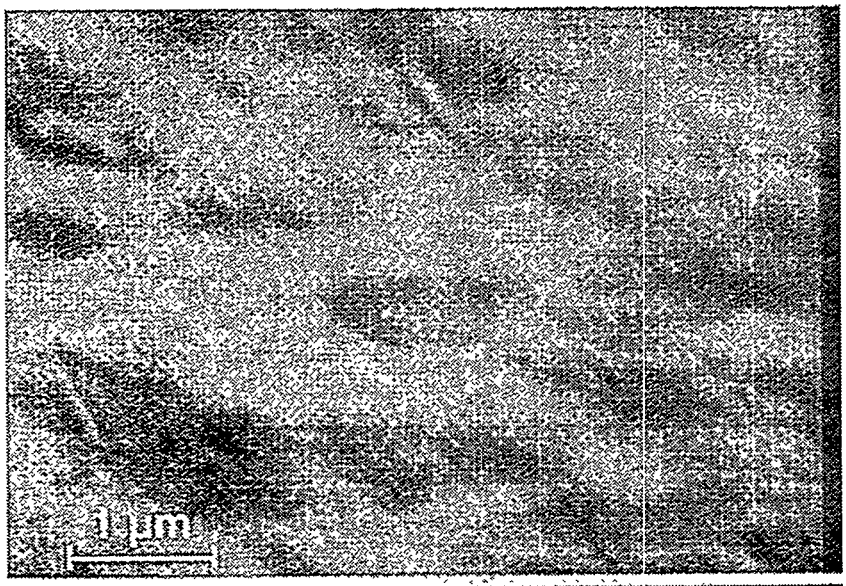

B

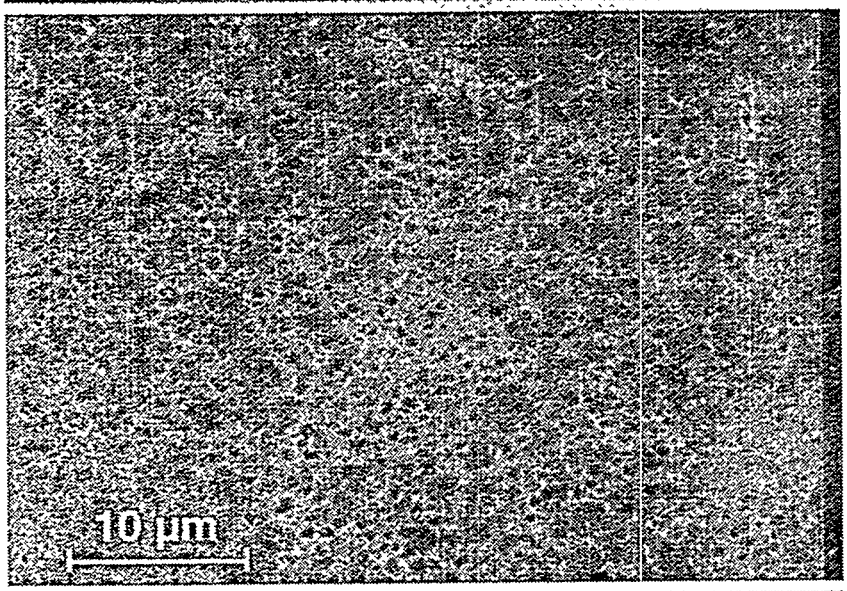

C

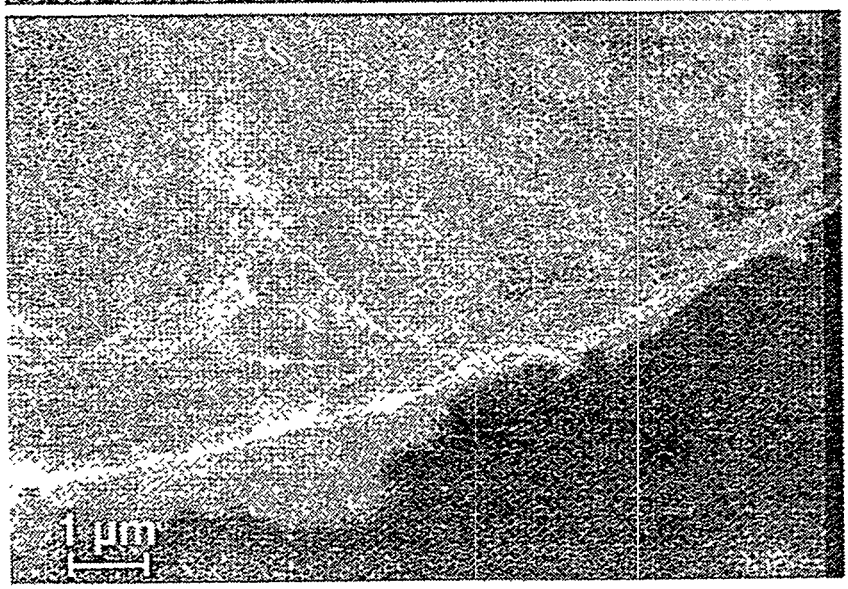

FIGURE 1

PRESENTATIONS

B.R. Mattes, "The Current Status of Polyaniline as a Gas Separation Membrane", A.V. Topchev Institute of Petrochemical Synthesis, Moscow, Russia Sept. 1994.

B.R. Mattes, Conjugated Polymers Modified by Chemical Treatments to Improve Gas Permeability, Kurcatov Institute, Moscow, Russia, Sept. 1994

J.P. Pellegrino and B.R. Mattes, "Polyaniline for Gas Separations: Sorption Measurements and Mechanistic Insights", Gordon Reserach Conference on Separation and Purification, New London, NH, Aug 1994

D. Belanger, J. Davey, F. Uribe and S. Gottesfeld " Electrochemical Capacitors Based on Conducting Polymer Active Materials", Abstract N0. 503, The Electrochemical Society Meeting in Miami Beach, Florida, October 1994

J.P. Ferraris, X. Ren and D.J. Guerrero, "A polythiophene-based anion exchange polymer that exhibits self-n-doping", Abstract N0. 506, The Electrochemical Society Meeting in Miami Beach, Florida, October 1994

J.P. Ferraris and X. Ren, "Solvent swelling-induced enhancement of the ionic conductivity of poly{3-(4-fluorophenyl) thiophene} films", Abstract N0. 507, The Electrochemical Society Meeting in Miami Beach, Florida, October 1994

INDUSTRIAL INPUT AND TECHNOLOGY TRANSFER

Electrochemical Capacitors

(1) This was the 2nd year of a CRADA agreement between LANL and Evans Finding Co., Rhode Island, on the development of electrochemical capacitors based on the conducting polymer active materials demonstrated at LANL. Interactions with Evens during this year continued to focus on effective transfer from cell development (LANL) to model, sealed device fabrication (Evans). Towards the end of this year, electrodes of polyaniline active material electrodeposited on titanium foils have been completed as the first element of the LANL technology to be transferred to Evans Co.. Evans Co. is about to fabricate the first sealed tri-cell ultracapacitor stack with these electrodes.

(2) Significant interest in Type III ultracapacitors has been expressed during this year by several industries in the electronics sector. We have started an interaction with Motorola, aimed at exploring the possible use of these capacitors in power systems for communications.

Conducting Polymer Membranes for Gas Separation

(1) A non-disclosure agreement between LANL and Praxair was signed late last year. Praxair is a subsidiary of Linde involved with commercial scale production of nitrogen. Praxair has evaluated our recent results on optimized doping for enhanced selectivity in conducting polymer membranes for O_2/N_2 separation, and will be testing conducting polymer membranes provided by LANL for evaluation in applications to air separations. It is hoped that, following this evaluation and the development of effective

asymmetric membranes at LANL, Praxair will become an active industrial partner in our gas separation project.

(2) As "spin-off" from this AIM effort, a collaborative research program on gas separation has been established with two Russian institutes. The Russian activity is devoted to another type of conjugated polymer membrane system.

PATENTS:

Metallization of Electronic Insulators-- S. Gottesfeld and F. Uribe, US Patent No 5,368,717 issued 1994.

Electrochemical Supercapacitors - A. J. Rudge, J. P. Ferraris and S. Gottesfeld, Revised Version submitted to US Patent Office, Sept., 1994

HIGHLIGHTS

1. We have demonstrated this year a new method for the fabrication of asymmetric membranes of polyaniline. Such membranes posses a thin, dense skin (~ 0.1 μm) on top of a thicker porous layer (~ 40 μm) -- a structure which enables an increase of gas permeability through the membrane by more than two orders of magnitude as compared with the state-of-the-art membranes made of the same conducting polymer material. Good mechanical stability of the membrane is rendered by high molecular weight polyaniline starting material prepared by a novel synthetic approach which was also developed this year. A respectable selectivity in O_2/N_2 separation has been demonstrated in the as-prepared asymmetric membrane, promising good combinations of high selectivity and permeability in optimally doped asymmetric membranes of this type. This is a significant step towards implementation of these conducting polymer membranes in industrial gas separation processes.

2. We ran during this year first tests of complete Type III ultracapacitors. The cells were based on a pair of electrodes loaded each with PFPT active material, placed in capacitor configuration in a cell with an appropriate electrolyte. PFPT is a p- and n-dopable material of high charge capacity developed earlier in this project. The tests this year went an important step further in obtaining an estimate for the energy and power densities that can be expected from the complete device based on the PFPT material, taking into account the weight of the active material plus all other components of the building block of the capacitor. The tests demonstrated an energy density for the complete device (excluding casing) of 10 W/kg and power density (calculated for 10 sec discharge) of 3.6 kW/kg of the device (excluding casing). These numbers are significantly higher than those demonstrated to date for carbon based ultracapacitors.

3. We were awarded this year a US patent on our earlier work in this AIM program, devoted to the application of conducting polymer films for metallization processes. The US patent, " Metallization of Electronic Insulators" (No 5,368,717) was awarded to S. Gottesfeld and F. Uribe.

PROJECT INVESTIGATORS

NAME	ACTIVITIES	FTE
Gottesfeld	Principal Investigator	0.15
Mattes*	Gas Separation	1.00
UT subcon.**	Conducting Polymers For electrochemical capacitors	0.50
Pellegrino***	Polyaniline/gas interactions	0.50
Derouin	Technical Assistance, Fabrication	0.15
Davey	Conducting Polymers for electrochemical capacitors	0.30

*Postdoc **John Ferraris + Ph.D students *** Sabbatical Visitor

Magnetic Field Processing of Inorganic Polymers

D. C. Kunerth
E. S. Peterson

Idaho National Engineering Laboratory
P. O. Box 1625
Idaho Falls, Idaho 83415-2209

INTRODUCTION

The purpose of this project is to investigate, understand, and demonstrate the use of magnetic field processing (MFP) to modify the properties of inorganic-based polymers and to develop the basic technical knowledge required for industrial implementation. Polyphosphazene membranes for chemical separation applications are being emphasized by this project. Previous work demonstrated that magnetic fields, appropriately applied during processing, can be used to beneficially modify membrane morphology. Figure 1 illustrates the modification in morphology that can be achieved. MFP membranes have significantly increased flux capabilities while maintaining the same chemical selectivity as the unprocessed membranes.

TECHNICAL PROGRESS FY-1994

Summary

FY-1994 efforts demonstrated the ability to fabricate and implement magnetically-processed polyphosphazene membranes in geometries suitable for industrial applications. The approach used is a tube-in-shell membrane module in which membranes are fabricated on the inner surface of tubular ceramic substrates surrounded by an external shell. Functionally, permeate from the feed stream on the inside of the tube migrates through the membrane and porous

ceramic substrate to the interior of the shell where it is transported to a collection point. A number of tube-in-shell membrane modules were fabricated and tested for their gas/gas and liquid/liquid separation characteristics.

CRADA activities between the INEL and ChromatoChem, Inc., Missoula MT, demonstrated that mating MFP membranes with ChromatoChem's current ion exchange technology provides a single system that can extract both heavy metal ions and trace organics from a feed stream.

1. Design, Fabricate, and Characterize Permanent Magnetic Yoke

Previous work demonstrated that DC magnetic fields generated by permanent magnets can be used to successfully process polyphosphazene membranes. Based upon these results, a permanent magnet system was designed and fabricated for casting membranes in ceramic tubes (10 mm dia. x 254 mm long).

2. Magnetically Process Membranes and Perform Separations

Membranes were cast in ceramic tubes and chemical separations performed in the tube-in-shell modules. Initial testing involved unprocessed membranes to develop baseline separation data. Both gas and liquid separations are to be evaluated. Liquid separations evaluated thus far are metal/organic from water and halocarbon from water. This work is an integral part of the CRADA with ChromatoChem, Inc. in which their metal ion separation technology is being evaluated and combined with the magnetically-processed membrane technology for high flux rate trace organic separations.

3. Membrane Performance

Membranes cast in ceramic tubes with and without magnetic field processing were evaluated for the separation of CO_2 from CH_4. A brief summary of the results is presented in Table 1. The results follow the same trends observed before: the magnetically-processed membranes have increased fluxes with separation factors similar to those of unprocessed membranes. This demonstrates the ability to fabricate improved membranes with geometries suitable for industry. Separation tests for H_2S from CH_4 are in progress.

The ChromatoChem CRADA work continued with the setup of test fixtures containing new column material. Trace metal ion/organic separations testing using this column material combined with polyphosphazene membranes was performed. An article discussing the technical work associated with the CRADA effort has been submitted to The Materials Society (TMS) for publication. The title is "Selective Separations of Trace Metals and Organics from Water" by E. S. Peterson, K. R. Arehart, D. C. Kunerth, M. L. Stone, and R. F. Hammen. This paper will be presented at the 124th TMS Annual Meeting, Las Vegas, Nevada, February 1995. A second paper covering additional magnetic field processing work is planned.

PUBLICATIONS

1. R. C. Boehm, "MNDO Model Structure for Poly(diphenoxyphosphazene) Derived from Cluster of Several Related Phosphazenes," Journal of Physical Chemistry, 1993, 97, pp. 13877-13886.

2. E. S. Peterson, K. R. Arehart, D. C. Kunerth, M. L. Stone, and R. F. Hammen, "Selective Separations of Trace Metals and Organics from Water," Proceedings of the 124th TMS Annual Meeting, Las Vegas, Nevada, February 1995.

PRESENTATIONS

AIM Annual Program Review, June 1995
124th TMS Annual Meeting, Las Vegas, Nevada, February 1995

HONORS AND AWARDS

None

PATENTS/DISCLOSURES

None

LICENSES

None

INDUSTRIAL INPUT AND TECHNOLOGY TRANSFER

ATOCHEM NA, King of Prussia, PA supplied some of the polyphosphazene materials used in the experiments. Triton Systems, Boston, MA is custom-manufacturing polyphosphazene materials. The CRADA between the INEL and ChromatoChem, Missoula, MT is being used to jointly develop a chemical separation system having extended capabilities.

COST SHARING

The ChromatoChem CRADA involves a 25% work-in-kind cost share.

ESTIMATED ENERGY SAVINGS

Improvement of polymer properties through the use of magnetic processing has potential to achieve significant energy savings. For example, if membranes having superior properties could be fabricated, their industrial implementation would become feasible, and energy would be saved. A recent DOE study (DOE/NBM-80027730) states that an annual energy savings of over 1 quad (equivalent to 170 million barrels of oil) could be achieved if membrane separations were fully utilized in only one application, liquid-to-vapor separations.

HIGHLIGHTS

The efforts of FY-1994 demonstrated that magnetically-processed membranes having extended capabilities can be fabricated and implemented in a geometry that is suitable for industry.

Table 1. Polyphosphazene Membrane Gas Separation Tests (CO_2 from CH_4)						
Temperature (°C)	30		50		70	
	CO_2	CH_4	CO_2	CH_4	CO_2	CH_4
Permeability (Barrers)						
Magnetic Processing	1.18	0.26	3.04	0.99	5.10	2.39
Conventional	0.53	0.13	1.25	0.40	2.46	1.15
Separation Factor (α)						
Magnetic Processing	4.50		2.98		2.06	
Conventional	4.22		3.11		2.10	
Fluxes ($1/m^2$-hr)						
Magnetic Processing	1.02		1.13		1.30	
Conventional	0.79		0.90		1.18	

a.

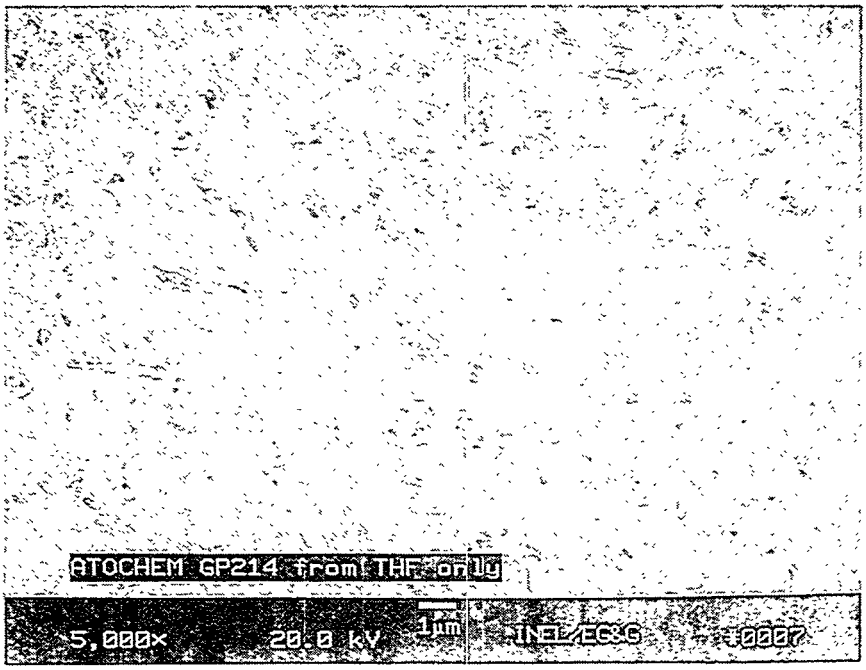

b.

Figure 1.

a. Polyphosphazene Membrane; 0 Tesla

b. Polyphosphazene Membrane; 1 Tesla

Polymerization and Processing of Organic Polymers in a Magnetic Field

Elliot P. Douglas
Polymers and Coatings Group
MST-7, E549
Los Alamos National Laboratory
Los Alamos, NM 87544

Introduction

The use of magnetic fields to affect the structure and properties of polymeric materials remains an area of great promise. Liquid crystalline polymers have been actively studied over the past 20 years for use in high performance structural applications. In particular, highly oriented fibers can exhibit remarkable increases in strength to weight performance compared to conventional materials. For example, the fibers marketed by DuPont under the tradename Kevlar are 20 times stronger than steel on an equivalent weight basis. However, larger bulk parts do not exhibit the same increases in strength due to a lack of orientation of the polymer molecules. Magnetic field processing of polymers remains an attractive solution to this problem.

Previous work under this program has clearly demonstrated that magnetic field processing has a beneficial affect on polymers. It was shown for example that drying a solution of cellulose in a magnetic field results in orientation and substantial improvements in mechanical properties. It was also demonstrated that larger graphitic filaments can be oriented in a magnetic field, demonstrating the feasibility of using magnetic fields to create advanced composites.

With this background, attention is now being focused on the use of magnetic fields to process liquid crystalline polymers. These materials are of commercial interest for use in high strength light weight applications such as automobile components. By undertaking a detailed analysis of the affect of magnetic fields on the structure and properties of liquid crystal polymers, we will be able to demonstrate the feasibility of using magnetic field processing to create the next generation of high performance materials.

Technical Progress

Summary

An extensive survey of the literature has been conducted on the use of magnetic fields to orient liquid crystalline materials. In general, it has been shown that liquid crystals can be oriented in a field, although the degree of orientation and the field strength required depend on factors such as viscosity, phase behavior, and chemical structure of the materials. Surprisingly, there has been little discussion of the resulting properties. Only two studies outside of our work have examined the mechanical properties of materials subjected to a magnetic field. Thus, the relationships among magnetic field processing, structure, and resulting properties remains an area open for investigation.

In February, 1994, a CRADA was executed with an industrial partner. The purpose of this CRADA is to investigate magnetic processing of liquid crystal polymers. Magnetic processing holds promise as a means of modifying the structure and properties of these materials through enhanced ordering of the individual molecules and liquid crystalline domains. Preliminary experiments conducted in low power magnetic fields have shown the feasibility of using magnetic fields to achieve orientation.

As part of our work we are utilizing a new variable field 20 Tesla superconducting magnet at the National High Magnetic Field Laboratory (NHMFL) at Los Alamos National Laboratory. Because of the use of liquid helium to cool superconducting magnets, great care must be taken not to overheat the magnet. Thus, we have designed and constructed a special high temperature probe (see Figure 1) which allows us to process materials in the magnet at elevated temperatures.

Milestones

1.0 Literature Search

An extensive review of the literature has revealed a body of work on the affect of magnetic fields on orientation of liquid crystalline materials. Orientation has been measured using x-ray scattering,[1] infrared spectroscopy,[2] nuclear magnetic resonance,[3] electron paramagnetic resonance,[4] light scattering,[5] and electron microscopy.[6] Materials examined

have included liquid crystal polymers,[2-4] polyribonucleotides[5] and metal-containing liquid crystals.[7]

In general, it has been found that magnetic fields can orient liquid crystals, although the amount of orientation depends on field strength, viscosity, phase behavior, and chemical structure. For example, low molecular weight liquid crystals are more easily oriented than polymeric liquid crystals due to their lower viscosity.[8] Also, one study found that nematic and smectic polyesters could be oriented in a magnetic field, while cholesteric polyesters could not.[9] Orientation in these systems is believed to occur due to two factors.[10] The first is the inherent anisotropy of diamagnetic susceptibility of rod-shaped molecules. The second is the tendency of liquid crystals to align even in the absence of a field; thus, application of even a small field can perturb the system enough to cause substantial alignment.

Despite the evidence that magnetic fields orient liquid crystal materials, there has been virtually no work on how that orientation affects properties. Several studies have shown that processing a liquid crystal polymer in a magnetic field results in an anisotropic coefficient of thermal expansion.[1,11] Two studies have measured mechanical properties of magnetically processed polymers. In one case there was little or no property improvement in polyethylene subjected to a magnetic field.[12] This is because polyethylene is not liquid crystalline and thus can not easily be oriented. In the other case substantial improvements were seen in the properties of an epoxy polymer that was processed in the presence of a magnetic field.[13] However, in both of these studies only one field strength was used and there was no measure of the orientation.

After reviewing the literature, it is apparent that the need still exists for a comprehensive study on the relationships between magnetic field strength, orientation, and properties of various liquid crystalline materials. We plan on providing that information in this program through a complete study of the affect of various processing conditions on properties and structure of liquid crystalline polymers. This information will allow us to optimize processing conditions to provide the maximum enhancement in a material's properties through the use of magnetic fields.

2.0 Industrial Collaboration

As part of our program on magnetic processing of polymers, a CRADA was executed with an industrial partner. The purpose of this CRADA is to investigate magnetic field processing of liquid crystalline polymers. Compared to conventional processing techniques such as injection molding or extrusion, magnetic field processing has the advantages of acting on the bulk of the sample, as well as providing a high amount of control over the structure through the use of different field strengths and processing times within the field.

The potential benefits of this CRADA to the U.S. are significant. Several U.S. companies supply structural materials to industries ranging from construction to automotive. Successful application of our technology to manufacturing processes will result in a new class of high strength, light weight structural materials.

3.0 Magnetic Processing in Low Power Fields

The liquid crystalline polymers have been exposed to a 1.2 T magnetic field while they were processed. We have constructed a special mold for use in this magnet. The mold consists of two steel plates, one of which contains a cavity for casting rectangular samples. The plates are held together with a series of screws. The desired temperature is maintained with heater cartridges controlled by a PID controller, and both the temperature and the magnetic field strength are monitored with probes placed inside the steel plates close to the sample.

Figures 2 and 3 give representative x-ray diffraction patterns for a liquid crystalline polymer. Figure 2 is the material processed with no magnetic field; the isotropic scattering pattern indicates that there is no orientation. Figure 3 shows the x-ray diffraction for the material processed in a 1.2 T field; the increased intensity in one direction over the others indicates that there is some level of orientation. However, measurements of the coefficient of thermal expansion (CTE) indicate no change upon application of the field. We note that significant orientation would be expected to result in a decreased CTE parallel to the orientation direction and an increased CTE perpendicular to the orientation direction. Higher field strengths will be necessary in order to achieve greater orientation and measurable changes in the CTE. Milestone 4.0 below describes our preparations for the use of higher field strengths.

In order to determine the effect of orientation on mechanical properties, we have prepared a series of samples in the 1.2 T field. These samples have been provided to the industrial partner for mechanical testing; test results are pending. Measurements will be made both parallel and perpendicular to the field direction in order to determine any anisotropy of properties that results from the orientation.

4.0 High temperature probe for 20 T superconducting magnet.

As part of our study, we are utilizing the National High Magnetic Field Laboratory (NHMFL) which is partially located at Los Alamos National Laboratory. As part of its facility at Los Alamos, the NHMFL has acquired a variable field 20 Tesla superconducting magnet. The use of this magnet will provide the higher field strengths needed to obtain substantial orientation in the processed materials.

The 20 T magnet available at the NHMFL consists of two main components, the magnet and the cryostat. The magnet itself consists of four concentric solenoids. The outer solenoid is wound from NbTi, while the inner three are wound from Nb_3Sn. The magnet itself is approximately two feet high, 15 inches in diameter, and has a bore diameter of 52 millimeters between the poles of the magnet. The field is varied simply by varying the current into the solenoids. In this way fields of up to 20 Tesla can be obtained. The field generated is very homogenous. Over an axial distance of 4 centimeters the field strength varies by only 1%.

In order for the superconducting solenoids to operate, they must be cooled to liquid helium temperatures. The cryostat provides insulation by immersing the magnet in liquid helium. Additional insulation is provided by a liquid nitrogen cooled outer shield. The cryostat vessel is approximately eight feet high and three feet in diameter, and completely surrounds the magnet. Samples are introduced into the bore of the magnet through a port at the top of the cryostat.

Processing of polymers typically takes place at temperatures up to 300° C. In order to process polymers in the superconducting magnet at these temperatures, great care must be taken to insulate the magnet from the sample area. If the insulation is not sufficient, the liquid helium coolant will boil off, resulting in a violent release of energy from the magnet.

In order to provide the necessary insulation, we have designed and constructed a special high temperature probe. A schematic diagram of this probe is shown in Figure 1. The main part of the probe consists of four concentric steel tubes that are sealed at both the top and bottom. At the top (the left side of Figure 1) are four vacuum manifolds which allow the spaces between the cylinders to be evacuated, providing the insulation. The sample is loaded into a mold that can be resistively heated (not shown in Figure 1), and attached to the end of a rod (also not shown in Figure 1). The rod is placed into the center of the probe, and the entire assembly is lowered into the magnet.

We have completed construction of this probe and begun operational testing. Initial tests indicate that the design is robust enough to provide the necessary vacuum. Additional tests will be performed to test the effectiveness of the insulation before it is used at high field strengths.

5.0 Kinetics of Orientation

An important factor in understanding orientation in a magnetic field is knowing how the molecules orient as a function of time. This can be important for designing processing schemes, as it may not be necessary to have a magnetic field present for the entire processing cycle. There are several ways that the kinetics can be measured. Conceptually, the simplest method is to process the materials only partially at a certain field strength, and then measure the orientation for samples that have been processed for different amounts of time. We plan to perform these experiments. More direct information can be obtained using solid-state NMR. In these experiments, the molecule is oriented in the magnetic field of the NMR, and the orientation can be followed as a function of time by taking NMR spectra during the orientation process. However, in order to perform these experiments one needs special deuterium labeled derivatives of the molecules of interest. The deuterated precursors needed can be difficult to obtain, and we have begun efforts to obtain these precursors in preparation of synthesizing the appropriate molecules.

References

(1) Barclay, G.G.; McNamee, S.G.; Ober, C.K.; Papathomas, K.I.; Wang, D.W. *J. Poly. Sci.: Part A: Poly. Chem.*, **30**, 1845 (1992)
(2) Zhao, Y. and Lei, H. *Macromolecules*, **25**, 4043 (1992)
(3) Moore, J.S. and Stupp, S. I. *Macromolecules*, **20**, 282 (1987)
(4) Lembicz, F. *Polymer*, **32**, 2898 (1991)
(5) Iizuka, E. and Kondo, Y. *Mol. Cryst. Liq. Cryst.*, **51**, 285 (1979)
(6) Hudson, S.D. and Thomas, E.L. *Poly. Prep.* **31**(1), 379 (1990)
(7) Maret, G. and Blumstein, A. *Mol. Cryst. Liq. Cryst.*, **88**, 295 (1982)
(8) Martins, A.F.; Ferreira, J.B.; Volino, F.; Blumstein, A.; Blumstein, R.B. *Macromolecules*, **16**, 279 (1983)
(9) Yamagisha, A.; Takeuchi, T.; Higashi, T.; Date, M. *J. Phys. Soc. Japan*, **58**, 2280 (1989)
(10) Barclay, G.G.; Ober, C.K.; Papathomas, K.I.; Wang, D.W. *Macromolecules*, **25**, 2947 (1992)
(11) Gray, M.E. and Harrison, I.R. *J. Appl. Poly. Sci.*, **28**, 3603 (1983)
(12) Gerzeski, R.H. *36th Int. SAMPE Symp.*, 1368 (1991)

MILESTONES DURING FY94

Construction of high temperature probe for 20 Tesla superconducting magnet.

This milestone was completed in September, 1994, with initial tests of the probe.

PUBLICATIONS

None

PRESENTATIONS

None

PATENTS/DISCLOSURES

None

LICENSES

None

INDUSTRIAL INPUT and TECHNOLOGY TRANSFER

Current work on this program is being done under the auspices of a CRADA, signed in February, 1994. The industrial partner is supplying the materials for magnetic field processing and test data on the effectiveness of the magnetic field processing.

COST SHARING

The industrial partner's contribution to the CRADA was $300K in in-kind funding over the period from February through September, 1994.

ESTIMATED ENERGY SAVINGS

This project has the potential for energy savings through the introduction of processing techniques to create high strength, light weight structural materials. Additional energy savings could result from the use of self-reinforcing liquid crystalline polymers in manufacturing processes. Liquid crystalline polymers do not require the use of reinforcements or fillers, resulting in less wear on manufacturing equipment, elimination of compounding as a processing step, and more efficient recycling of materials.

HIGHLIGHTS

CONSTRUCTION OF HIGH TEMPERATURE PROBE FOR 20 TESLA SUPERCONDUCTING MAGNET

A new probe for processing of polymers at temperatures up to 300° C inside a liquid helium cooled superconducting magnet has been constructed. This probe results in a 500° C temperature gradient across a distance of 0.5 inches. Initial tests indicate that this probe can be used to process polymers at field strengths up to 18 Tesla.

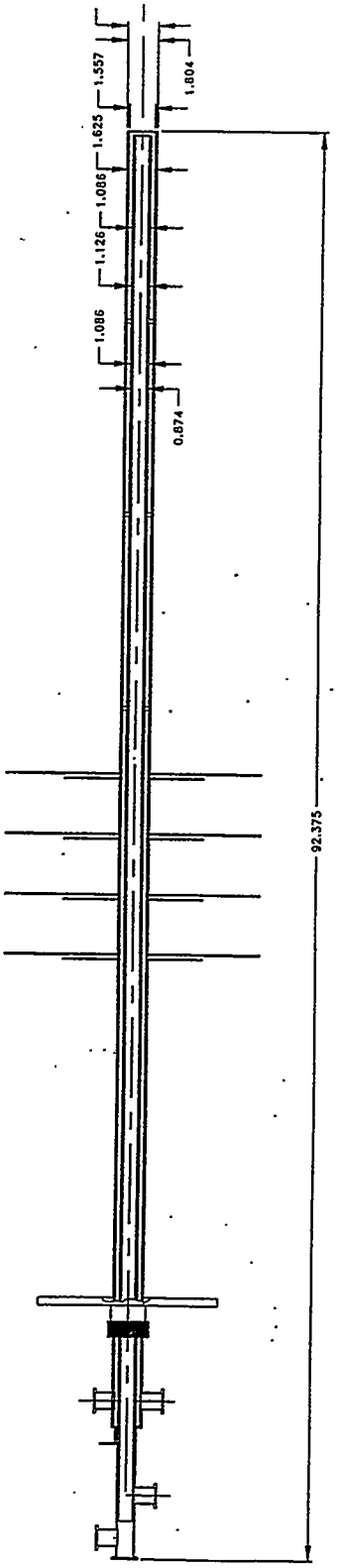

Figure 1: Schematic diagram of high temperature probe for 20 T superconducting magnet.

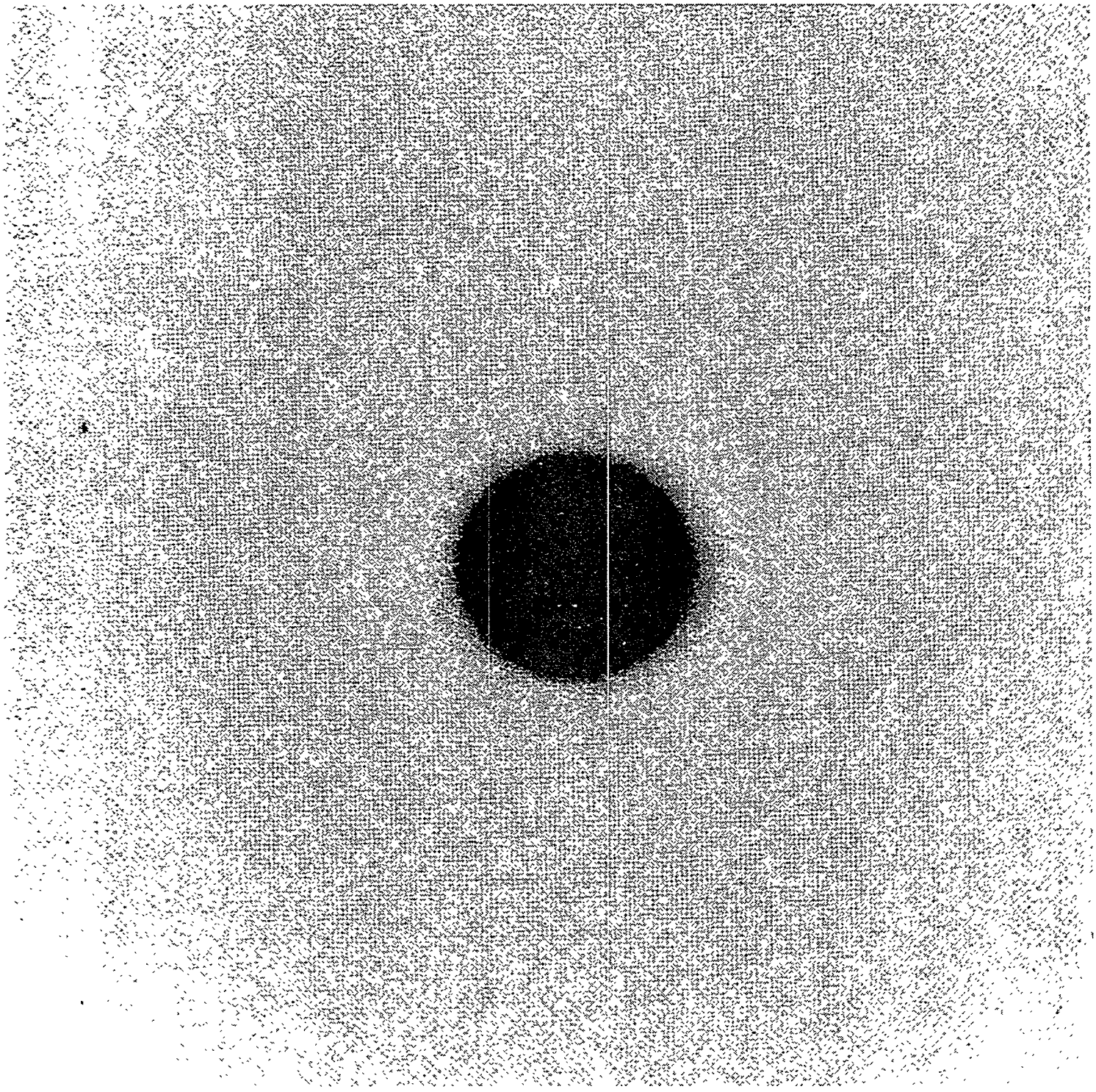

Figure 2: X-ray diffraction pattern for liquid crystal polymer processed with no magnetic field.

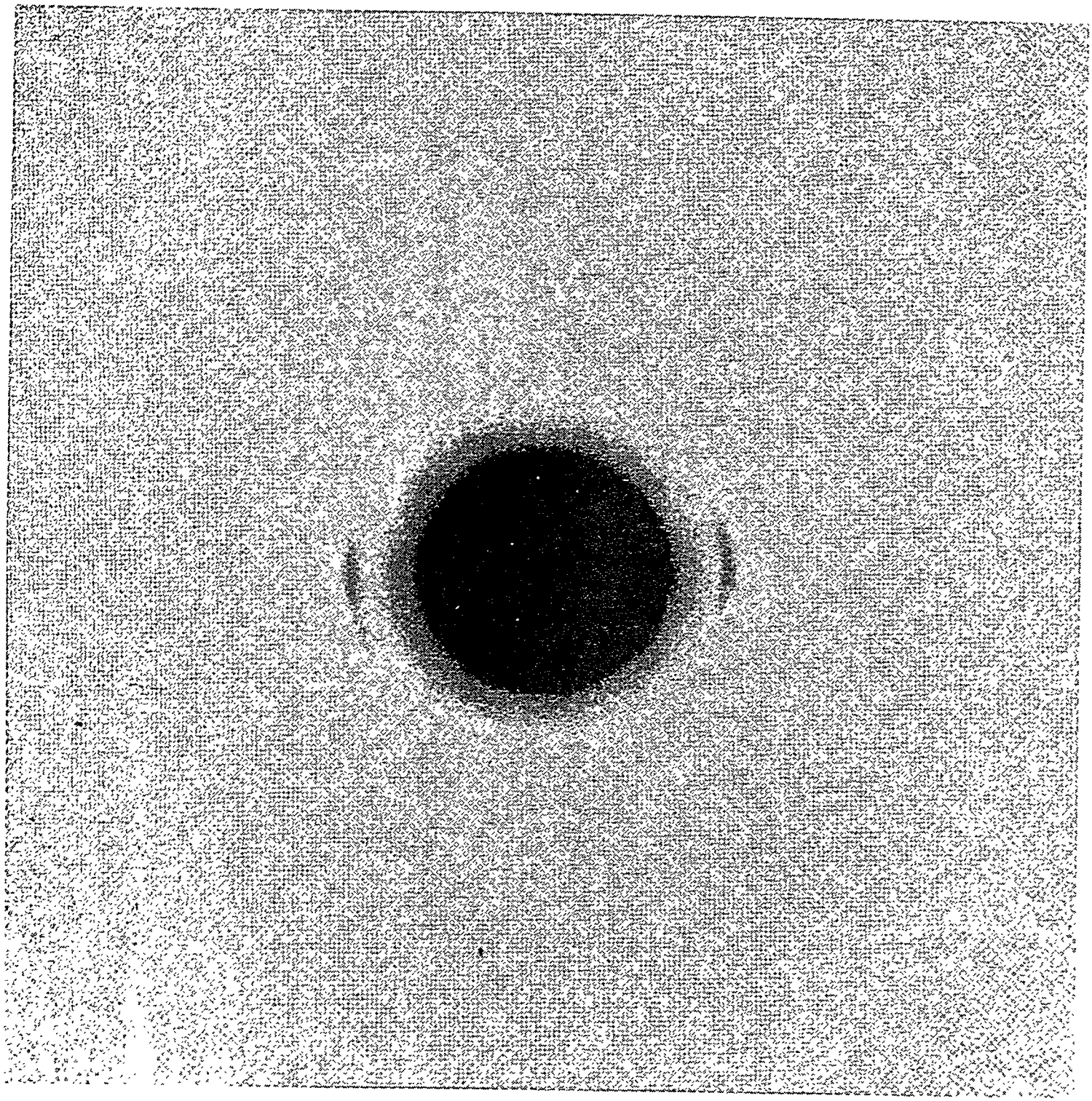

Figure 3: X-ray diffraction pattern for liquid crystal polymer processed in a 1.2 Tesla magnetic field.

NEW MATERIALS AND PROCESSES

ADVANCED MICROWAVE PROCESSING CONCEPTS

R. J. Lauf, A. D. McMillan, and F. L. Paulauskas

Metals and Ceramics Division
Oak Ridge National Laboratory
Oak Ridge, Tennessee 37831-6087

INTRODUCTION

The purpose of this work is to explore the feasibility of several advanced microwave processing concepts to develop new energy-efficient materials and processes. The project includes two tasks: (1) commercialization of the variable-frequency microwave furnace; and (2) microwave curing of polymer composites.

The variable frequency microwave furnace, whose initial conception and design was funded by the AIC Materials Program, will allow us, for the first time, to conduct microwave processing studies over a wide frequency range. This novel design uses a high-power traveling wave tube (TWT) originally developed for electronic warfare. By using this microwave source, one can not only select individual microwave frequencies for particular experiments, but also achieve uniform power densities over a large area by the superposition of many different frequencies.

Microwave curing of thermoset resins will be studied because it holds the potential of in-situ curing of continuous-fiber composites for strong, lightweight components. Microwave heating can shorten curing times, provided issues of scaleup, uniformity, and thermal management can be adequately addressed.

TECHNICAL PROGRESS

Microwave Furnace Development

In collaboration with our industrial partner, Lambda Technologies, Inc., we have conducted detailed experiments to characterize the power distribution in our "benchtop" variable frequency furnace. Thermal paper was used to accurately map the power density within the cavity over various frequency ranges. We characterized in detail the time-averaged power density function within the furnace cavity for different frequency ranges. These experimental results validated model calculations performed at Lambda.

Lambda is now actively commercializing the VFMF. A unit was delivered to New Jersey Institute of Technology in January 1994 and additional units are under

construction. Lambda is continuing in-house R&D activities on diamond film growth and polymer curing under SBIR grants.

Lambda's product line was officially launched at the Materials Research Society Spring Meeting in San Francisco, CA, in April 1994.

Polymer Curing

Epoxy resin, cast into disks up to 6 inches diameter and cured at a either a fixed frequency, or with insufficient frequency sweeping, tended to cure nonuniformly. It appeared that thermal runaway initiated in areas of high power density and then propagated to cover most of the specimen. In contrast, samples cured with adequate frequency sweeping were uniformly cured and showed no evidence of overheating, even when the sweep rate was fairly slow. Workers at Lambda have further scaled up the process, demonstrating uniform curing of resin plates up to 500 g.

Lambda has also reported on their collaborative work with a EniChem America to uniformly heat and post-cure large plates of isocyanate/epoxy PMC materials, and results are very encouraging.

Milestones

None this reporting period

PUBLICATIONS

Journals

1. R. J. Lauf, D. W. Bible, A. C. Johnson, and C. A. Everleigh, "2 to 18 GHz Broadband Microwave Heating Systems," Microwave Journal, November, 1993.

Other Publications

1. A. D. Surrett, R. J. Lauf, and F. L. Paulauskas, "Microwave Processing of Thermosetting Prepreg Laminates", 29th Microwave Power Symposium Proceedings, pp. 95-98, International Microwave Power Institute.
2. A. C. Johnson, R. J. Lauf, and A. D. Surrett, " Effect of Bandwidth on Uniformity of Energy Distribution in a Multi-Mode Cavity," MRS Symp. Proc. 247, Microwave Processing of Materials IV, pp. 453-8, 1994.

3. A. C. Johnson, R. J. Lauf, and A. D. Surrett, "Effect of Bandwidth on Uniformity of Energy Distribution in a Multimode Cavity," 29th Microwave Power Symposium Proceedings, pp. 160-163, International Microwave Power Institute.
4. A. D. Surrett, R. J. Lauf, F. L. Paulauskas, and A. C. Johnson, "Polymer Curing Using Variable Frequency Microwave Processing," MRS Symp. Proc. 247, Microwave Processing of Materials IV, pp. 691-6, 1994.

PRESENTATIONS

1. A. D. Surrett, R. J. Lauf, and F. L. Paulauskas, "Microwave Processing of Thermosetting Prepreg Laminates," presented at International Microwave Power Institute, Chicago, Illinois, July 25-27, 1993.
2. A. C. Johnson, R. J. Lauf, and A. D. Surrett, "Effect of Bandwidth on Uniformity of Energy Distribution in a Multimode Cavity," presented at International Microwave Power Institute, Chicago, Illinois, July 25-27, 1993.
3. A. C. Johnson, R. J. Lauf, and A. D. Surrett, " Effect of Bandwidth on Uniformity of Energy Distribution in a Multi-Mode Cavity," presented at the MRS Symposium, Microwave Processing of Materials IV, April 4-8, San Francisco, CA, 1994.
4. A. D. Surrett, R. J. Lauf, F. L. Paulauskas, and A. C. Johnson, "Polymer Curing Using Variable Frequency Microwave Processing," presented at the MRS Symposium, Microwave Processing of Materials IV, April 4-8, San Francisco, CA, 1994.

HONORS AND AWARDS

1. Plant Engineering Magazine 1993 Product of the Year finalist (sponsored by Cahners Publishing Company) for "Variable Frequency Microwave Furnace," November 18, 1993.

PATENTS/DISCLOSURES

1. R. J. Lauf, D. W. Bible, and F. L. Paulauskas, "Method for Curing Polymers", US Patent Application filed March 31, 1994.
2. D. W. Bible and R. J. Lauf, U.S. Patent 5,321,222, "Variable Frequency Microwave Furnace System," issued June 1994.

3. R. J. Lauf, A. D. Surrett, and A. J. Moorhead, "Method for Joining Carbon-Carbon Composites to Metals," ESID 1592-X, US Patent Application in preparation.
4. R. J. Lauf, A. D. Surrett, and A. C. Johnson, "Improved Microwave Tube," ESID 1581-X, US Patent Application in preparation.
5. R. J. Lauf, A. D. Surrett, C. A. Everleigh, and A. C. Johnson, "Improved Microwave and RF Load," ESID 1582-X, US Patent Application in preparation.

LICENSES

1. Lambda Technologies, Inc. (successor company to Microwave Laboratories, Inc.) has licensed the Variable Frequency Microwave Furnace covered by US Patent 5,321,222 and additional patents pending.

BIOMIMETIC THIN FILM SYNTHESIS

G. L. Graff, A. A. Campbell, N. R. Gordon, K. L. Simmons, P. C. Rieke, G. L. McVay, and B. C. Bunker

Introduction

The purpose of this program is to develop a new process for forming thin film coatings and to demonstrate that the biomimetic thin film technology developed at PNL is useful for industrial applications. In the biomimetic process, mineral deposition from aqueous solution is controlled by organic functional groups attached to the underlying substrate surface. The coatings process is simple, benign, inexpensive, energy efficient, and particularly suited for temperature sensitive substrate materials (such as polymers). In addition, biomimetic thin films can be deposited uniformly on complex shaped and porous substrates providing a unique capability over more traditional line-of-sight methods.

Technical Progress

I. *Tin Oxide Films*

Surface modification schemes for acetal and polystyrene have been developed, and crystalline SnO_2 films were successfully deposited on the plastics. Complex shaped components can be coated uniformly, and the coatings are typically 1 micron in thickness. One problem with the original deposition solution was the extremely low pH (pH=0-1). Solution conditions have been modified and tin oxide films have been deposited at pH=5-7. Achieving more benign deposition conditions satisfied a major program objective.

In soak tests performed to date, the coating did not completely stop permeation of fuel into the coated component (weight gain after several months). Film growth studies conducted on silicon substrates have further determined that the deposition rate for the dense SnO_2 films is extremely slow (5-10 angstroms/hr). This could be a serious limitation for the coatings effort.

As a potential alternative to tin oxide coatings, we identified a commercial supplier of chemically robust, conformal parylene coatings (Union Carbide). Parylenes are insoluble in all organic solvents up to 150°C. Sample parylene coatings were obtained on several complex shaped fuel pump components, and the coated parts were provided to AC Rochester for evaluation.

II. *Composite HDPE/Al Fuel Tank*

Significant progress has been made in the development of impermeable high density polyethylene (HDPE) fuel tanks. The basic design is to incorporate aluminum metal as a permeation barrier within the polymer. Investigations have been completed on both continuous sheet Al sandwiched between HDPE layers, and high aspect ratio Al flakes incorporated directly into the polymer. The continuous sheet composite has superior permeation resistance, while the flake composite has improved formability. Evaluation of the composite materials is now underway at AC Rochester. To evaluate blow molding properties, 50 pounds of HDPE/Al flake material

(containing 50 wt% Al) were pelletized and sent to AC. This material will be used in an attempt to blow mold a small plastic reservoir (windshield washer reservoir). Also, circular samples (3" diameter) of continuous sheet and Al flake composites were provided to John Giacchina (AC Rochester) for permeation studies in GM's test facilities. These samples will be subjected to alcohol containing fuels for several months to evaluate the barrier properties of each composite material. Finally, large sheets (2 X 2 feet) of sheet and flake composite materials were provided to GM to evaluate the material's performance when used in a stamping process. Initially, John will attempt to form an air cleaner housing using the HDPE/Al materials.

III. *Calcium Phosphate Films*

Calcium phosphate films are desirable for producing bioactive coatings on metals used in bone and dental implants. The quality (phase) of the deposited coatings and the deposition rates have been improved dramatically over the past year. The thermal decomposition of urea was used to increase film deposition rates by an order of magnitude, requiring only minutes to deposit several microns of coating. A license option agreement has been signed with Health Technologies Corporation, Dallas, TX, and a three year, ER-LTT collaborative research project for $600K has been negotiated. Final decisions on the license agreement and the collaborative research will be made in Feb. 1995.

IV. *Zirconium Oxide Films*

Stabilized ZrO_2 films have widespread application as gas sensors and are the material of choice for high temperature protective coatings on superalloys used in turbine applications. Research conducted during FY94 led to the successful biomimetic deposition of ZrO_2 precursor films on silicon and polystyrene substrates at 70°C. These precursor films could be fully converted to dense, polycrystalline ZrO_2 (tetragonal and monoclinic phase) at 400°C. Work is now underway to incorporate Y_2O_3 into the zirconia films to produce the robust, stabilized phase.

Milestones

I. *Composite Fuel Tank*

Samples of HDPE/Al sheet and flake composite materials have been synthesized and supplied to AC Rochester for chemical testing and evaluation in existing forming operations (blow molding and stamping).

II. *Complexing Agents*

Chemical complexing agents were identified that facilitated the deposition of SnO_2 films between pH=5 and pH=6 rather than the previous deposition conditions of pH=0.5. Deposition kinetics remain extremely sluggish after numerous attempts to improve the rates. Preliminary soak tests in alcohol fuels determined that the tin oxide coating was not completely impermeable to chemical attack.

III. *Electroless plating*

Test performed by John Giacchina determined that electroless plating was not an acceptable coatings option for the polymeric fuel pump components. We then worked to identify a highly durable, conformal coating (parylene) produced commercially by Union Carbide. Parylene coatings were successfully applied to acetal fuel pump components, and the coated parts were supplied to AC Rochester for evaluation.

Publications

1. L Song*, MJ Pattillo, GL Graff, AA Campbell and BC Bunker, *Heterogeneous Nucleation of Calcium Oxalate on Native Oxide Surfaces,* MRS Fall Proceedings, in press (1994).

2. BC Bunker*, PC Rieke, BJ Tarasevich, AA Campbell, GE Fryxell, GL Graff, L Song, J Liu, JW Virden and GL McVay, *Ceramic Thin Film Formation on Functionalized Interfaces Through Biomimetic Processing,* Science, **264**, 48-55 (1994).

3. AA Campbell*, BC Bunker, GE Fryxell, GL Graff, GJ Miller and DL Wheeler, *Surface Induced Mineralization: A New Method for Producing Bioactive Coatings for Orthopedic Implants,* in final preparation for submittal to **Nature.**

4. BC Bunker* and GL Graff*, *Aqueous Biomimetic Synthesis of Ceramic Thin Films,* **Materials Technology,** Feb. 1994.

Presentations

1. GL Graff*, MJ Pattillo, BJ Tarasevich and BC Bunker, *Deposition of Textured, Magnetic Iron Oxide Thin Films on Polymeric Substrates,* MRS Spring Meeting (1994).

2. GL Graff*, *Low Temperature Deposition of Dense Tin Oxide Thin Films on Polymeric Substrates,* MRS Spring Meeting (1994).

3. GL Graff*, *Deposition of Textured, Iron Oxyhydroxide Thin Films on Polymeric Substrates,* ACerS Annual Meeting (1994).

4. GL Graff*, *Low Temperature Deposition of Dense Tin Oxide Thin Films on Polymeric Substrates,* ACerS Annual Meeting (1994).

5. AA Campbell*, GL Graff, *Low Temperature Solution Deposition of Calcium Phosphate Coatings for Orthopedic Implants,* ACers Annual Meeting (1994).

6. J Liu*, GL Graff, MJ Pattillo, PC Rieke, L Song, BJ Tarasevich, JW Virden and BC Bunker, *Study of Nucleation and Growth of Thin Films on Functionalized Surfaces,* ACerS Annual Meeting (1994).

7. J Liu*, JW Virden, GL Graff, HJ Heinisch, RE Williford and RH Jones, *Aggregation and Consolidation of Colloidal Suspensions of Fine Ceramic Particles,* ACerS Annual Meeting (1994).

8. PC Rieke*, GE Fryxell, AA Campbell, GL Graff, BC Bunker, L Song, R Wiacek and J Liu, *Tailoring the Surface Energies of Self Assembled Monolayers to Control the Heterogeneous Nucleation of Minerals,* **invited talk,** MRS Fall Meeting (1994).

9. BC Bunker*, PC Rieke, BJ Tarasevich, AA Campbell, GE Fryxell, GL Graff, L Song, J Liu and JW Virden, *Surface Induced Mineralization of Ceramic Thin Films,* **invited talk,** Annual Biomedical Engineers Society Meeting, Tempe, AZ (1994),

10. AA Campbell*, GL Graff, GJ Miller and DL Wheeler, *Surface Induced Deposition of Calcium Phosphate Coatings for Orthopedic Implants,* Surfaces in Biomaterials '94, Scottsdale, AZ (1994).

Patents/Disclosures 2

Licenses 1 license option with Health Technologies Corporation

Industrial Input and Technology Transfer

Continued interactions with John Giacchina at AC Rochester have resulted in development of novel composite materials for potential use in fuel tanks and coatings for fuel pump components. To date, sample materials have been supplied to AC for performance evaluation.

PNL received over 300 inquiries concerning potential applications of biomimetic coatings in FY94. These contact resulted in (1) signing a license option agreement with Health Technologies Corporation (HTC), (2) a joint research contract with HTC calling for $600K from DOE with matching funds from HTC, (3) a private contract involving four research thrusts (the first is currently funded at $50K), and (4) submittal of joint industry/PNL proposals with LexaLite Corporation and Armstrong World Industries.

MATERIALS R&D — STUDENT INTERNSHIPS

R. B. Thompson, D. C. Jiles and L. S. Chumbley

Metallurgy and Ceramics Division
Ames Laboratory
Iowa State University
Ames, Iowa 50011

INTRODUCTION

This program has as an objective the conduct of programmatic research for the Advanced Industrial Concepts Materials Program while training minority graduate students in the process.

Well-known demographics indicate that minorities will constitute an increasing fraction of our future work force. Consequently, efforts have been initiated to increase the fraction of minorities and women who choose technical career paths. Included are a wide ranging set of programs beginning with pre-school education, progressing through efforts to retain students in technical paths in grades K-12 and undergraduate education, and ending with encouraging graduate education. The Materials R&D — Student Internships is a unique approach in the latter category. Here, we have focused on a particular area of applied materials research, the Advanced Industrial Concepts Materials Program. Our goal, then, is to educate minority graduate students in the context of this program. The Ames Laboratory was selected as a site for this pilot project since it is a DOE national laboratory, located on the campus of a major research university, which includes in its research interests programs with a strong technological flavor. Many of the Laboratory staff hold shared faculty appointments.

More specifically, the pattern through which a student will pass involves a sequence of steps progressing through recruitment, project selection, research, mentoring, and graduation. Recruiting is being accomplished by nationally advertising "AICD Materials Technology Fellowships for Minorities." We feel that it is essential to offer at least one such fellowship each year to maintain continued visibility on minority campuses and to establish effective working relationships with appropriate personnel. Other factors which we believe to be essential to the success of the project include offering each student a variety of project opportunities — active choice in project selection will greatly increase the student's

motivation and likelihood of success — and continued mentoring throughout the program. The projects offered to the students are consistent with the guidelines of the AIM program.

TECHNICAL PROGRESS — FY 1994

Summary

During FY 1994, the first minority fellow, Ms. Patricia Pulvirenti, continued with her third year of course work and research. She has now completed all of the courses required for the Ph.D. degree, but has not yet passed the Ph.D. preliminary examination. Ms. Pulvirenti has presented early research results at a conference and has participated in an international science exchange, spending the Summary of 1994 at the Institute of Elettrotechnico Nazionale Galileo Ferraris, in Turin, Italy. Her work is concerned with the dynamic magnetostrictive response of Terfenol-D, a highly magnetostrictive material. The second student, Ms. LaVonne Carson, completed her second full year of studies. Her work concerns the preparation of nanocrystalline materials and deposition of Cr layers using an inductively-coupled RF plasma. Each student is enrolled in the Materials Science and Engineering Department of Iowa State University. Technical progress on these projects is summarized below.

1. Development of Magnetostrictive Materials with Enhanced Energy Transfer Efficiency for Transducers and Actuators.

One of the factors limiting the high frequency response of magnetostrictive materials is the energy loss associated with both hysteresis and the eddy currents induced in the material by the time varying magnetic field. Ms. Pulvirenti has continued her studies of the time dependent magnetostrictive response of $Tb_{0.27}$ $DY_{0.73}Fe_{1.9}$ (Terfenol-D). The energy conversion in this material is less than 50% and her objective is to investigate possible improvements which could improve this efficiency and also extend the range of frequencies over which the material can be used. Potential applications include sensor and transducer applications, particularly adaptive vibration control.

It is the conductivity of the material which significantly reduces the magnetic field penetration (i.e. the permeance), and hence the strain at frequencies above 500 Hz. Possible solutions to reducing the conductivity are: (i) Surface modification by diffusion of aluminum into Terfenol, (ii) Alloying of aluminum, boron, silicon with Terfenol. Progress in each of these areas is discussed below.

(i) Surface Modification

A cylindrical sample of Terfenol was submerged in molten aluminum using a specially designed sample holder that allowed the sample to be removed before solidification of the aluminum. This left a layer of aluminum on the surface, 0.7 mm thick after six hours at 660°C. EDS scan showed little penetration of the aluminum into the bulk.

A series of anneals was then undertaken to promote diffusion of the aluminum into the bulk. The sample exhibited no improvement in magnetostriction at higher frequencies after the first anneal. There was an indication that the layer of pure aluminum hindered penetration of the magnetic field (Al has a higher conductivity than Terfenol alone). The amount of pure aluminum on the surface was found to have decreased to 0.3 mm after a second anneal. EDS also revealed that the transition layer increased. This suggests an increase in the skin depth, a possible indication that the permeability was improved. However, an EDS scan showed that Al did not diffuse more than 1.3 mm into the bulk, less than desired. An unfortunate by-product of this processing sequence was the fact that the sample became very brittle.

It is encouraging, however, that the pure Al layer decreased after the second anneal, and that perhaps better annealing conditions (i.e., vacuum) would produce a less brittle sample. This sample is currently being studied for its gyromagnetic remanence (GRM) properties by Alan Stephenson at the University of Newcastle in the UK. The underlying principle is that the sample is rotated in an alternating magnetic field causing the magnetic moments to flip back and forth and resulting in a remanent field. This remanent field increases with increasing magnetic field. It is hoped that the sample could be characterized in this way so as to provide further insight into the magnetization on a different scale.

(ii) Alloying of Terfenol with Al, B, Si

As an alternate processing route to obtain bulk alloying, nine samples of Terfenol with various alloying additions were made by the drop cast method. By alloying elements from group IIIA and IVA, it may be possible to provide scattering sites for the conduction electrons (since the impurity atoms will sit on interstitial sites) and thereby increase the resistivity. If this can be

achieved, the conductivity of the Terfenol samples may be reduced. Samples were made with 1%, 2%, and 3% Al, 1%, 2%, and 3% Si, and 1% and 2% B. These samples are currently being examined at the University of Hull. Complex permeability measurements will begin on these samples upon their return.

2. Exchange with Instituto Elettrotecnico Nazionale Galileo Ferraris (IENGF).

As part of a summer exchange, Ms. Pulvirenti performed experiments on three amorphous alloys of iron, cobalt and boron to test the predictions of the Preisach model of hysteresis, developed at the IENGF. Particular attention was placed on obtaining data to guide modification of this model to better apply to dynamic phenomena, in which losses increase with frequency.

The samples on which the experiments were performed were amorphous ribbons of $(Fe_{(1-x)}Co_x)_{85}B_{15}$, where x was 0, .21, and .64. Each sample was examined using a wattmeter designed and constructed at IENGF. Measurements were taken at frequencies ranging from .5 Hz to 20 kHz, and at magnetic inductions ranging from .25T to 1.2T. Using a digital feedback technique, the loss was measured at each frequency and induction. As expected, losses were greatest for high frequencies and high inductions. In addition, the loss-frequency relationship predicted by the Preisach model was apparent.

A second type of experiment was done where, in addition to the major hysteresis loop, minor loops were also measured. The information contained in the minor loops was then used to calculate the Preisach distribution, a three-dimensional probability function which is used to calculate the magnetic response. The distribution was calculated using a computer program written by Vittorio Basso of IENGF. Having obtained the Preisach distribution, certain parameters, representing physical characteristics of the particular samples were determined.

Based on this work, the Preisach model will be considered as an alternative theory in interpreting our measurements of the response of Terfenol-D.

3. Process of Nanocrystalline Materials Using an Inductive-Coupled RF-Plasma.

Previous studies have shown that reducing the grain size of a material to the order of a few nanometers can result in enhanced mechanical properties. As a result, nanocrystalline processing of large

quantities of material is of industrial significance. In this study conducted by Ms. Carson, the technique presently used to generate nanocrystalline materials involves the use of an inductively coupled plasma (ICP) as a heat source. The material, in powder form, is fed into an ICP torch where it is completely vaporized into its elemental constituents. Upon exiting the torch, the atomic species condense onto a cooled plate as nanocrystalline material. The material is then collected and analyzed using energy dispersive spectroscopy (EDS) and a scanning and transmission electron microscope (SEM, TEM). While this process may possess great potential to improve the properties of materials, there are limitations on the amount of material that can be generated at a given time.

In the previous year's work, the Cr_3Si, Ti_5Si_3, and $MoSi_2$ compounds were examined. Nanocrystalline material of Ti_5Si_3 and Cr_3Si was produced using a RF-ICP. However, when $MoSi_2$ powder was passed through the plasma very different results were obtained. X-ray scans showed that the material was a mixture of the molybdenum rich silicon compounds Mo_5Si_3 and Mo_3Si, with a few peaks being indexed as MoO_2 or MoO_3, and pure silicon. Since atomic emission spectroscopy showed that all the materials were totally vaporized in the plasma plume, incomplete vaporization was ruled out as a possible explanation of the differences. Since $MoSi_2$ is a line compound, additional line compounds were processed in FY 94 to see if nanocrystalline material could be obtained from line compounds in other systems.

A list of the additional compounds examined in FY 94 includes Cr_5Si_3, $CrSi_2$, $TiSi_2$, and Mo_5Si_3. These materials were chosen because of their high melting temperatures and the fact that they melt congruently. They were also selected because they are a mixture of line compounds and compounds that exist over a compositional range. The phase diagrams for all alloy systems studied are shown in Figure 1.

In the chromium - silicon system, Cr_5Si_3 and $CrSi_2$ were examined. Both compounds exist over a compositional range with the $CrSi_2$ existing over a very narrow range. Figure 2 shows the XRD result comparing the as-received material to the resultant material collected from the substrate following the plasma run of the Cr_5Si_3 and $CrSi_2$ compounds. It appears that in each case nanocrystalline material has been formed. Comparing the peaks suggests that this material has the same stoichiometry as the starting material.

Figure 3 shows the results of the $TiSi_2$, which was run in addition to the previously examined Ti_5Si_3. Ti_5Si_3 exists over a compositional range and has been shown to form nanocrystalline material upon condensing from the plasma onto the substrate. $TiSi_2$ on the other hand is strictly a line compound. As the x-ray results indicate, while it condenses out of the plasma in nanocrystalline form, it is not of the original stoichiometry.

The Mo_5Si_3 compound, which exists over a compositional range, was processed and examined. The XRD results are presented in Figure 4. From the scan, it initially appears that the material collected from the substrate is a mixture of several phases. However, if the most intense peaks (corresponding to Mo) are stripped from the scan, the remaining material is seen to be nanocrystalline Mo_5Si_3. This is in contrast to the processed $MoSi_2$ compound mentioned above, which is a line compound and did not form in the correct stoichiometry as nanocrystalline material.

These results show that the ease with which a material recombines to form nanocrystalline material may be related to two main factors, namely, the compositional range over which a compound exists and the difference in physical properties of the elemental constituents. If one examines the known physical and thermodynamic properties of the compounds used in this study, it can be seen that the melting points of the compounds are quite similar, although the boiling points are as yet unknown. The boiling points of the individual elements on the other hand can provide some idea of the possible vapor pressures of these constituents as the powders begin to vaporize in the plasma. The boiling points of Cr and Ti are quite similar but are slightly higher than that of Si. Presumably, Si will preferentially boil from the surface of the powder first, followed closely by Ti and Cr. Since the atoms then are all in close proximity to one another when complete vaporization occurs, recombination back into powder of the correct stoichiometric ratio (now in nanocrystalline form) is possible. This would be especially favorable if the compound existed over a slight compositional range, less favorable if dealing with a line compound. Thus, $TiSi_2$ would have a more difficult time forming that Ti_5Si_3, as seen experimentally.

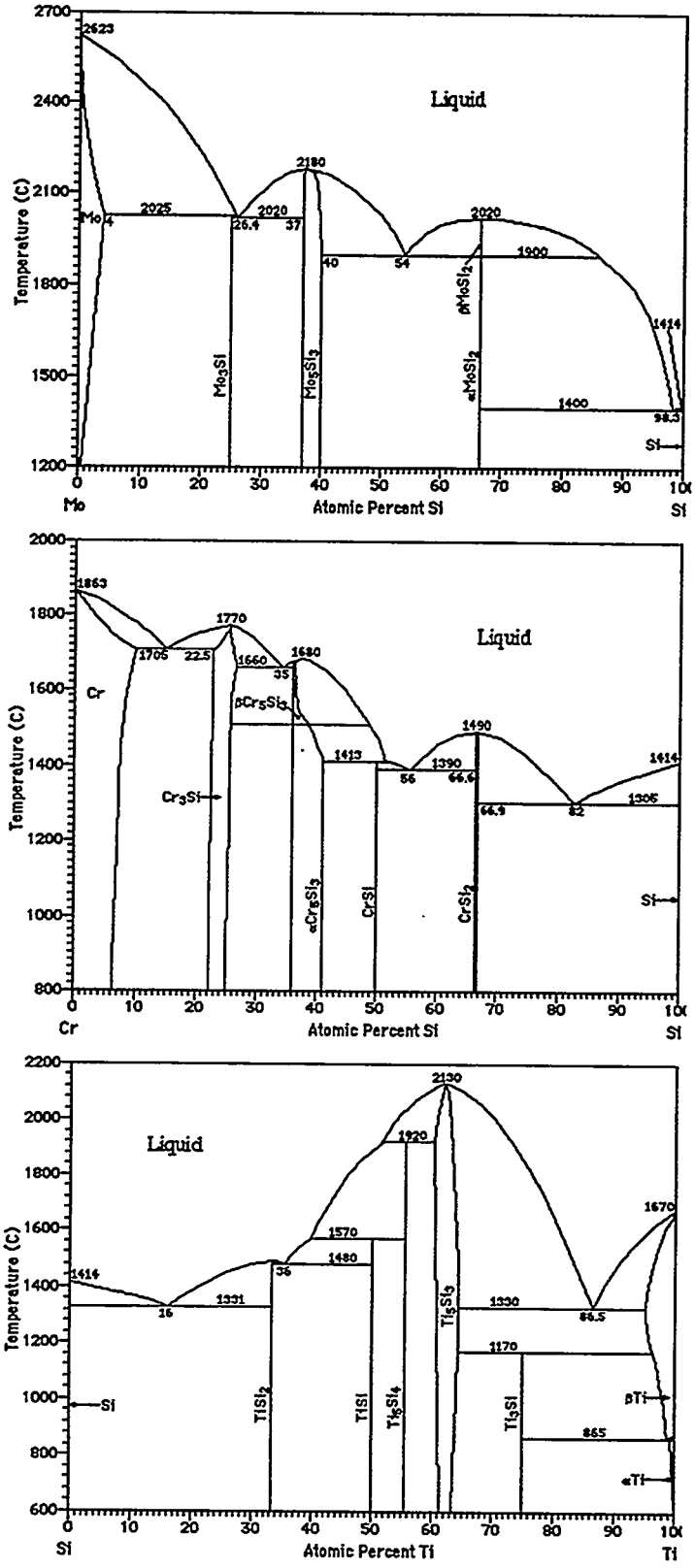

Figure 1. Phase diagrams of systems studied.

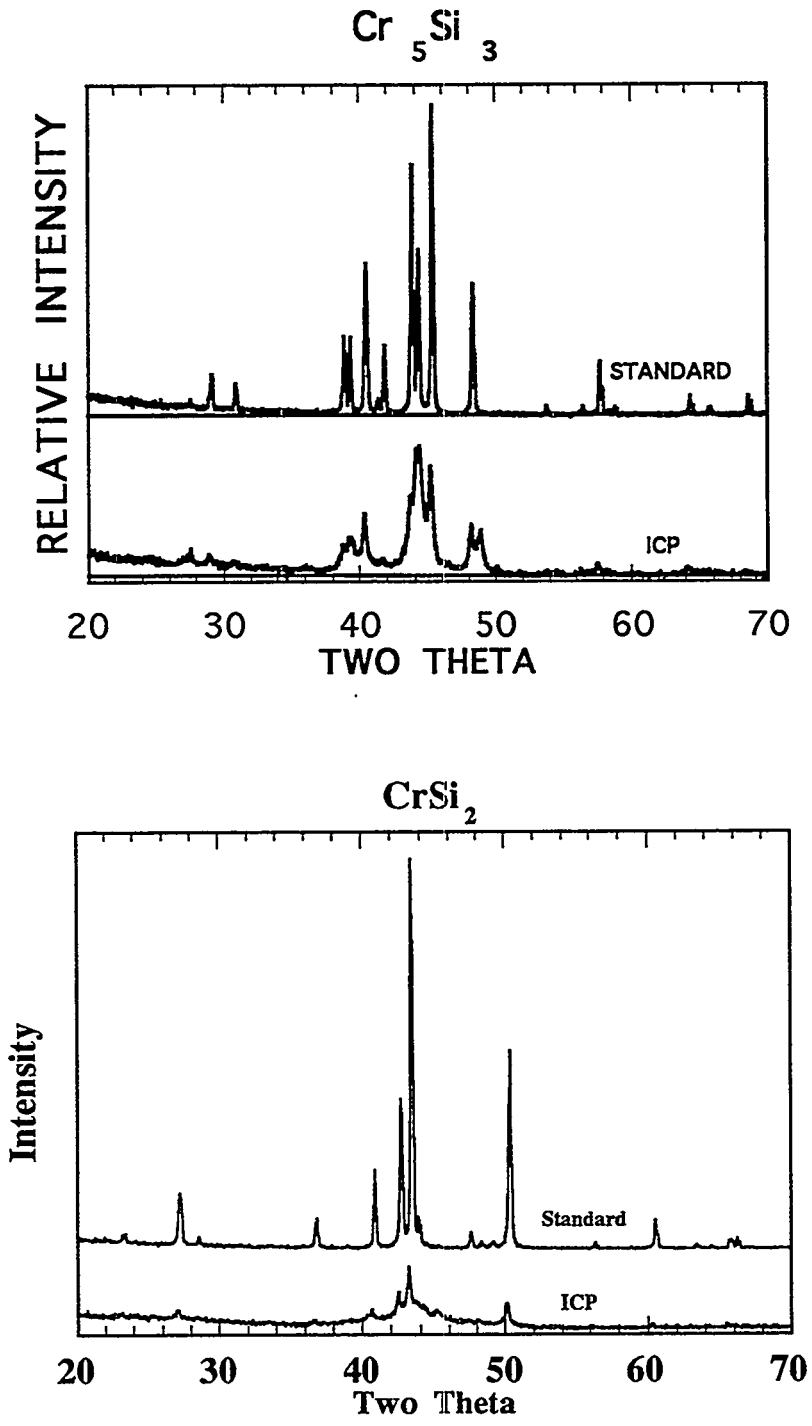

Figure 2. X-ray scans from Cr-Si compounds.

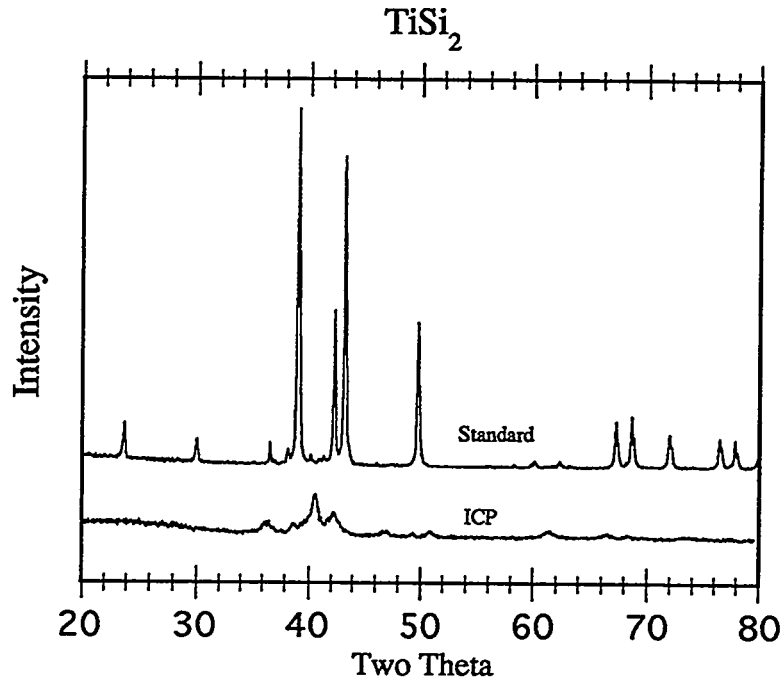

Figure 3. X-ray scan of Ti-Si compound.

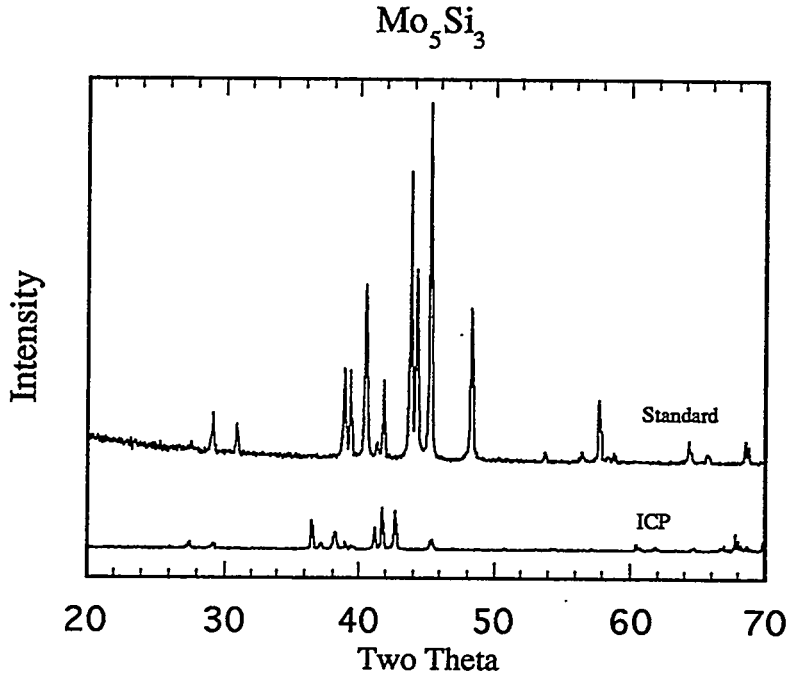

Figure 4. X-ray scan of Mo-Si compound.

For the molybdenum silicide compounds, the Mo is expected to have a vapor pressure which is quite low compared to that for Si. This may cause Si atoms to vaporize quickly from the introduced powder while the Mo is slightly delayed. This results in separation of the constituents in the axial direction as the $MoSi_2$ and Mo_5Si_3 powders pass through the ICP. Due to the large difference in density between Mo and Si, the swirling of the Ar gases present in the torch may cause a centrifugal separation to occur, producing a region near the center of the exiting plasma plume which is rich in Mo while the outer areas are Si rich. Upon exiting the torch the close proximity of Si to Mo needed for effective recombination into the original compound is absent Thus, even though the compound might exists over a compositional range, such as Mo_5Si_3, the separation of the constituents results in less nanocrystalline material being formed.

In order to understand exactly when different constituents begin to recombine in the plasma plume to form compounds, future work will focus on acquiring and installing a monochromator system that will allow profile studies of the plasma plume to be conducted. The goal of these studies will be to determine exactly what compounds and/or elemental species exist in the plasma plume as a function of distance from the exit point of the torch.

4. Deposition of Cr Using an Inductively-Coupled RF-Plasma.

A new thrust involving the plasma unit also has been initiated. Presently, the most widely used method of obtaining a thin layer of hard Cr on a part for wear applications is Cr-plating, involving the use of chemical baths. While quick, easy, and very cheap, this method also results in the production of large amounts of hazardous solutions that must be disposed. The cost of disposing these chemicals is increasingly dramatically, and efforts are underway to find alternative Cr plating techniques.

Initial attempts at using the plasma torch to deposit a layer of Cr on a substrate appear encouraging, though the results are very preliminary. In this effort, Ar gas is passed over Cr hexacarbonyl, which vaporizes and is carried into the plasma stream. The high temperatures of the plasma decompose the carbonyl, releasing Cr atoms which may then deposit onto a provided substrate. The micrograph below shows an SEM view of one such coating obtained on a Ta substrate. Unfortunately, these initial coatings are high in oxygen, as indicated by auger spectroscopy, and may be

Cr-oxides rather than Cr. However, the results appear promising enough that additional funding has been obtained from the Environmental Protection Agency. Presently, a statistical design of experiments analysis is being carried out to determine what are the best parameters for obtaining a good coating. Future plans include depositing layers in a controlled atmosphere chamber to reduce oxygen content, and using Cr powder, rather than Cr hexacarbonyl, as a feed material.

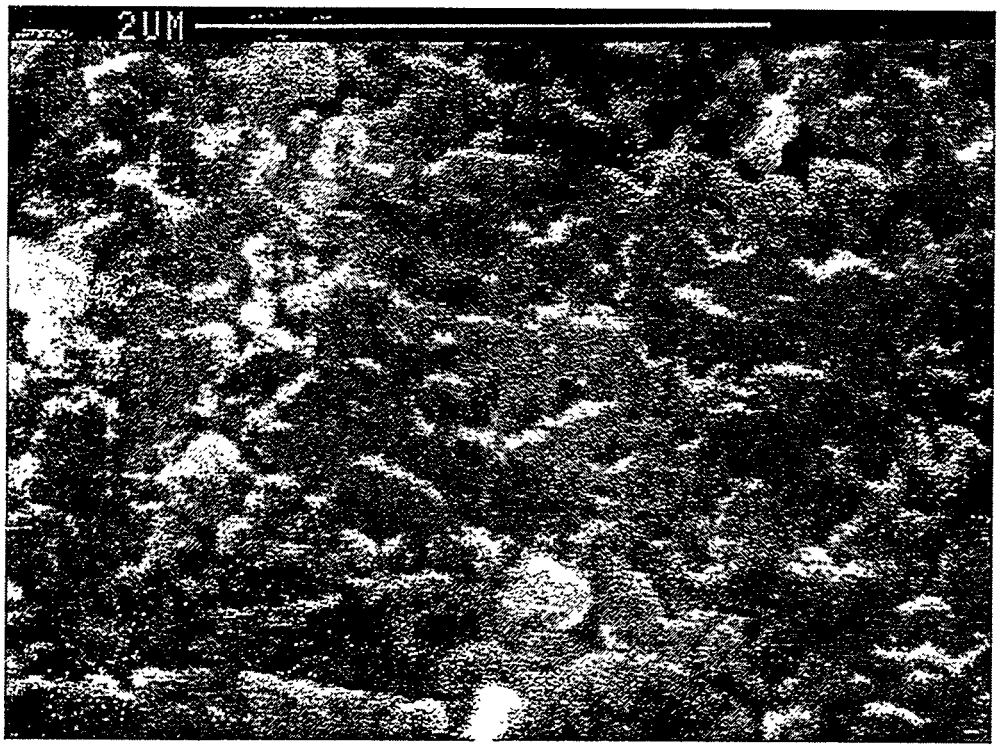

Figure 5. SEM micrograph of deposited coating.

MILESTONES DURING FY 1993

Milestones included continuing the work of our first and second student while adding a third student to the program. Milestones one and two were met, as described herein. The third student was not added due to uncertainties in budget prospects.

PUBLICATIONS

None yet directly involving students. Publications in closely related fields by principal investigators available on request.

PRESENTATIONS

1. L. S. Chumbley, K. L. Pauwels, H. Mahmood, L. Carson, "Plasma-Induced Dissociation of Intermetallic Silicides Powders to from Nanocrystalline Materials," poster presented at Conference on Nanophase Materials, Davos, Switzerland, March 1994.

2. T. W. Ellis, L. S. Chumbley, T. Lograsso, L. Carson, "Deposition of Cr using an RF-Plasma," informal presentation at Advanced Techniques for Replacing Chromium: An Information Exchange, a workshop sponsored by the Environmnetal Protection Agency, October 12-13, 1994, Johnstown, PA.

3. P. Pulvirenti, "Application of the Preisach Model to Hysteresis Loss Measurements of Amorphous Fe-Co-B Alloys," Magnetics Seminar Series, Iowa State University, November 9, 1994.

HONORS AND AWARDS, PATENTS/DISCLOSURES, LICENSES

None

INDUSTRIAL INPUT and TECHNOLOGY TRANSFER

There have been several inquiries about the use of Terfenol-D industrial applications based on both BES and AIM sponsored work. As a result of this, we have been successful in securing a cooperative research and development agreement (CRADA) with General Motors Corporation for the use of this material as a torque sensor.

Both John Deere, Inc. and Eaton, Inc. are interested in the Cr plating aspects of plasma processing and have contributed substrates and technical information as to the quality and thickness of desirable coatings.

COST SHARING

There is no direct industrial cost sharing on this project. However, NATO has provided a grant for a collaborative work with the United Kingdom, including $4K for the first stage and $5.8K for the second stage. The title of the grant is "Magnetostriction in Tb-Dy-Fe alloys: Measurement and modeling of properties." The objective of the grant is to enable us to use the facilities at the University of Hull, United Kingdom, for measurement of the frequency dependent properties of this alloy, particularly the permeability and magnetostriction.

Cost sharing by General Motors on the torque sensor CRADA is $67.4K.

The EPA has agreed to fund exploratory work in the use of the RF plasma for Cr plating for one year, with a possible renewal for second and third years pending the initial results. Both John Deere, Inc. and Eaton, Inc. have agreed to contribute substrates and perform standard industry tests as cost-share items in that program.

ESTIMATED ENERGY SAVINGS

This is difficult to calculate at this time. For example, for the Terfenol-D devices, it is reasonable to suppose that a 10% reduction in conductivity is achieved with the doping procedures used in the latest material. This would result in a 9% improvement in the eddy current losses under a constant voltage. However, the main issue here is not so much whether the direct energy losses can be improved for such small devices (which do not consume an excessive amount of power), but whether the frequency range of operation can be significantly enhanced, which would enable much larger, indirect energy gains on various industrial applications. We are now awaiting results from the University of Hull on the performance of nine doped specimens of Terfenol.

Presently, the disposal of solutions containing the Cr+6 ion must be carefully handled, packaged, and shipped to a licensed disposal point. A new method of CR deposition would result in energy savings by eliminating the need for such shipments. (R&D performed at Oak Ridge National Laboratory (ORNL) under DOE-EE-AIM Program support.)

HIGHLIGHTS

The highly magnetostrictive material Terfenol, with a range of compositions of the interstitials Al, Si and B, has been produced. The magnetoelastic properties have been modeled using numerical techniques, and the hysteretic properties have been modeled based on the Preisach model in an exchange with IENGF.

An inductively-coupled RF plasma system was used to study the formation of a variety of nanocrystalline materials, chosen to clarify our understanding of which compounds can or cannot be formed in this way. The results indicated that the ease with which materials recombine in the plasma to form nanocrystalline material appear to be related to two main factors: the compositional range over which the compound exists and the difference in physical properties of its elemental constituents.

Promising preliminary results have been obtained regarding the use of the plasma torch to deposit a layer of Cr on a substrate. Interested because of promise to reduce the use of chemical baths and the associated hazards of disposition, the EPA has provided additional support.

MICROWAVE JOINING OF SiC

R. Silberglitt and I. Ahmad

FM Technologies, Inc.
10529-B Braddock Road
Fairfax, VA 22032

W. M. Black, R. F. Cozzens, H. S. Sa'adaldin, T. H. Shan and Y. L. Tian

George Mason University
4400 University Drive
Fairfax, VA 22030

J. D. Katz

Los Alamos National Laboratory
Post Office Box 1663 Mail Stop G771
Los Alamos, NM 87545

INTRODUCTION

The purpose of this work is to optimize the properties of SiC-SiC joints made using microwave energy. The current focus is on optimization of time-temperature profiles, production of SiC from chemical precursors, and design of new applicators for joining of long tubes.

TECHNICAL PROGRESS FY 1994

Summary

In order to investigate the effect of joining temperature, tubes of reaction bonded silicon carbide (RBSC) were joined at four different temperatures from 1420°C to 1565°C. These specimens were sent to Los Alamos National Laboratory for evaluation. An automatic feedback control system was also used to heat SiC rods to temperatures between 1200°C and 1500°C in predetermined programmed cycles.

Direct comparisons were made of polycarbosilane (PCS) pyrolysis to form SiC using microwave and conventional heating. The pyrolysis temperature in both cases was 1400°C. Microwave heating showed a clear advantage both in heating rate (5 times faster) and in the crystallinity of the final product. Published data show that to achieve the sharpness of the X-ray

peaks observed for the PCS cured with microwave heating at 1400°C, conventional heating to 1700°C is necessary.

A new single mode applicator was designed and fabricated, composed of two double mitered H-plane waveguide corners (bends). This double mitered bend cavity was used to heat SiC rods and tubes, and provided a more rapid heating rate and higher specimen temperatures than could be achieved with the conventional rectangular cavity. The effect was greater for larger specimens. This cavity was used to join SiC rods at a joining temperature of 1455°C. The joined specimens were sent to Los Alamos National Laboratory for evaluation.

Milestones

1. Optimization of time-temperature profile.

Tubes of reaction bonded silicon carbide (RBSC) with a diameter of 3.49 cm (1.375 in) and a wall thickness of 0.476 cm (0.1875 in) were obtained from Golden Technologies, Inc., the Coors company responsible for advanced ceramics research. Specimens for joining experiments were prepared by cutting sections from these tubes 2.54 cm (1 in) in length. These tube sections were then polished to 5-10 μm surface finish. These specimens were placed in the 6 kW multimode microwave applicator inside a hybrid heating enclosure which was insulated on all sides with alumina blankets and boards. Pressure was applied with a load transmitted via a tube inserted through a 2.54 cm (1 in) diameter opening in the top of the insulation. The weight of the load was approximately 10.5 kg (23 lb), which provided a joining pressure of 0.23 MPa (32.8 psi). Specimens were joined at four different temperatures: 1420°C, 1465°C, 1515°C and 1565°C. In each case, the joining temperature was achieved in 35-45 minutes using up to 3.5 kW of microwave input power, with about 500 Watts of reflected power. The specimens were held at the joining temperature for 30 minutes, with the temperature during this time manually controlled to within 15°C. Microwave power was reduced to about 2 kW to maintain the joining temperature. The joined specimens were sent to Los Alamos National Laboratory for evaluation.

An automatic feedback control system was designed and connected to the TE_{103} single mode cavity. The primary control variable is microwave power level, which is adjusted based upon measurement of the surface temperature of the specimen with a two-color optical pyrometer. The control system development is funded under a grant to George Mason

University from the National Science Foundation Division of Design and Manufacturing. Current work is aimed at allowing computer control of the iris and plunger, in addition to the temperature feedback loop. SiC rods 0.952 cm (0.375 in) in diameter were heated to temperatures between 1200°C and 1500°C in predetermined programmed cycles using this control system. The data are shown in Figure 1, demonstrating control to within about 10°C.

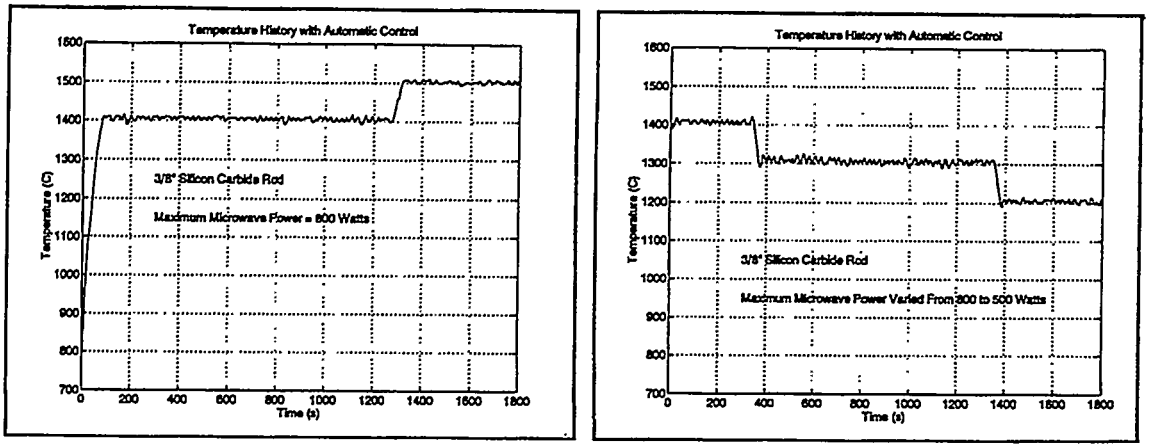

Figure 1: SiC Heating and Cooling Cycles Using Automated Feedback Control System

2. Formation of SiC from chemical precursors

SiC was produced in prior work from polycarbosilane (PCS) precursors using both conventional and microwave heating , but direct comparisons were difficult because the microwave decomposition was performed at 1500°C, while the conventional heating was performed at 1200°C, the maximum temperature of an available muffle furnace. During this contract period, we were provided access to a research grade graphitic furnace at the U.S. Naval Research Laboratory, which is capable of heating to 2500°C. This allowed direct comparison of PCS pyrolysis using microwave and conventional heating, with a pyrolysis temperature in both cases of 1400°C. PCS was Dow Corning X9-6348 with an average molecular weight of 1400. The microwave heating was performed in a fused silica crucible inside an alumina insulator, which was placed inside the TE_{103} single mode rectangular cavity at the maximum electric field position of the empty cavity.

For these experiments, the TE_{103} single mode applicator was modified to allow operation under controlled environment. A pressure window (Varian MA1360) was attached at the entry port of the applicator, which will allow a maximum gas pressure of 45 psi and a maximum

standing wave ratio of 1.15. The cavity end, the moving plunger and the two holes for temperature measurement were sealed with O-rings. A pair of ultra-torr fittings were connected to the cut-off tubes on the narrow side of the waveguide. The inner diameter (ID) of the fitting can be varied from 0.635 cm (0.25 in) to 1.905 cm (0.75 in) by introducing a set of adapters to match the size of the specimens. Gas flows in and out of the applicator through two fittings located at the front and back sides of the waveguide, respectively. Using this modified cavity, a gas mixture of 95% N_2 and 5% H_2 was flushed through prior to heating of the PCS to 1400°C for curing.

Infrared (IR) spectra of the PCS cured by both conventional and microwave heating showed a strong SiC absorption band centered at 800 cm^{-1}. However, the microwave heating showed a clear advantage both in heating rate (5 times faster) and in the crystallinity of the final product. Figure 2 is a comparison of heating profiles and Figure 3 is a comparison of X-ray spectra. *Published data [G. D. Soraru, F. Babonneau, J. D. Mackenzie, J. Mater. Sci. 25, 3889 (1990)] show that to achieve the sharpness of the X-ray peaks observed for the PCS cured with microwave heating at 1400°C, conventional heating to 1700°C is necessary.*

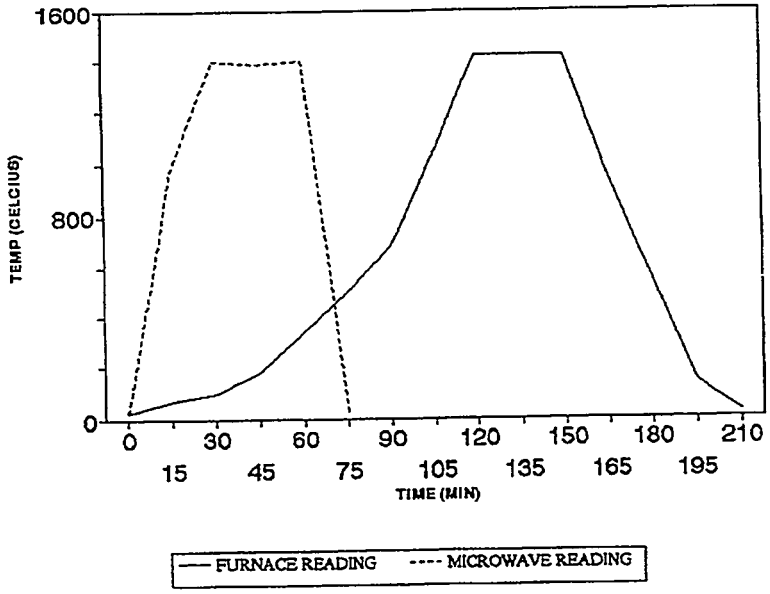

Figure 2: Temperature Profiles for Microwave and Conventional Pyrolysis of PCS

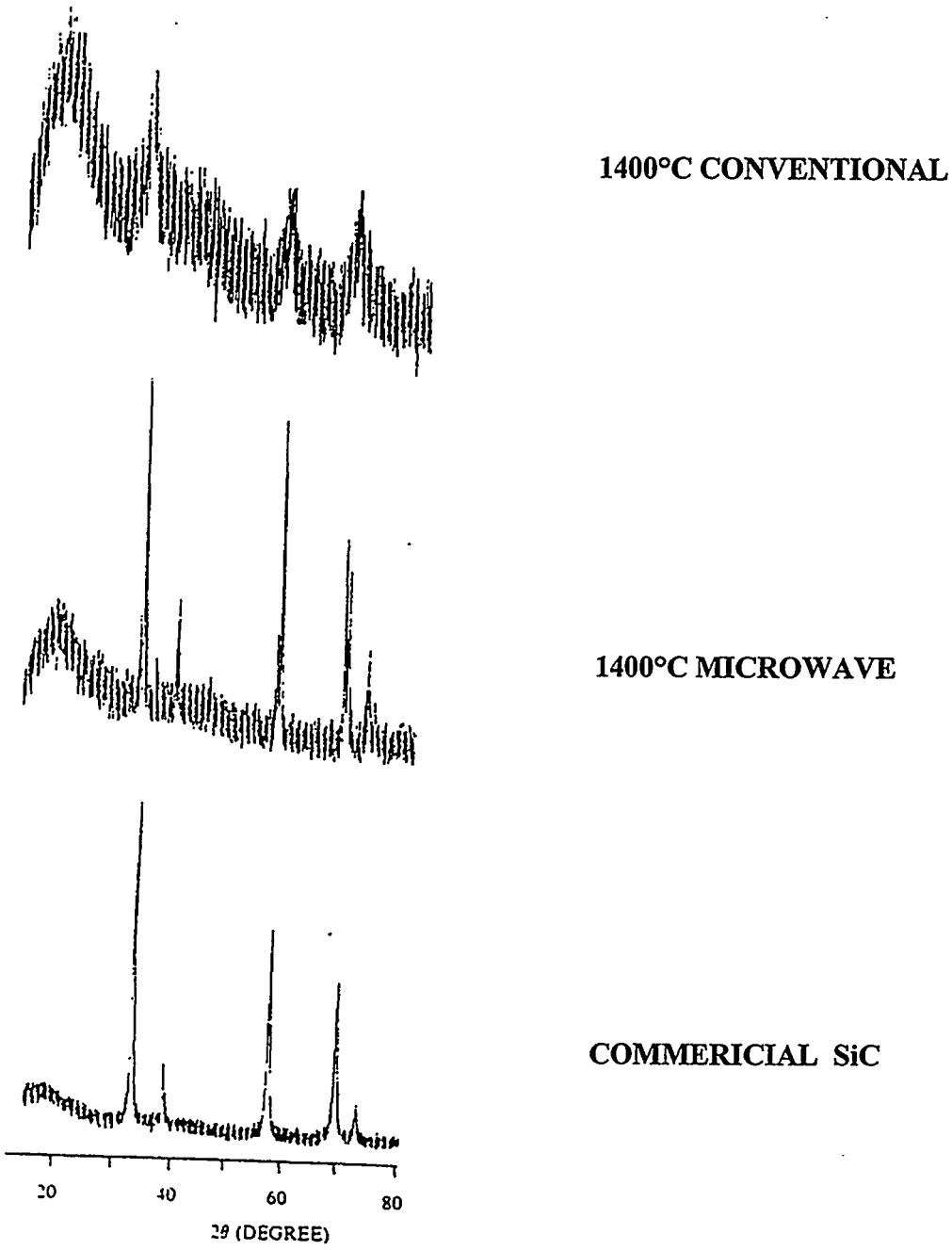

Figure 3: X-Ray Data for Microwave and Conventional PCS Pyrolysis Product

3. Development of new microwave applicators for long specimens

A new single mode applicator was designed and fabricated, composed of two double mitered H-plane waveguide corners (bends). Figure 4 is a schematic of this applicator. Its advantages over the single mitered bend applicator developed previously are the increased length of the heating zone and the ease with which the sample can be oriented vertically, to allow external compression. This cavity is excited in the TE_{104} mode or a higher order 10n mode, depending upon the length of the adjustable short arm. In order to compare this new applicator with a rectangular cavity of the same waveguide size, three different ceramic specimens were heated. The specimens were a sintered silicon carbide rod with diameter d = 0.95 cm (0.375 in) and length l = 7 cm (2.76 in), a RBSC rod with d = 1.5 cm (0.59 in) and l = 6.5 cm (2.56 in), and a RBSC tube with outer diameter (OD) of 1.5 cm (0.59 in), wall thickness of 0.2 cm (0.079 in) and l = 19 cm (7.48 in). The rod specimens were placed inside a block of alumina insulation and the long tube passed through the insulation. Temperature was monitored with a two-color optical pyrometer through a hole in the insulation. In all three cases, the double mitered bend cavity provided a more rapid heating rate and higher specimen temperatures than could be achieved with the rectangular cavity. The effect was greater for the larger specimens. Figure 5 shows the heating data for the RBSC tube, which was heated to almost 1400°C with 1.1 kW of input power, as compared to less than 1200°C in the rectangular cavity with the same input power.

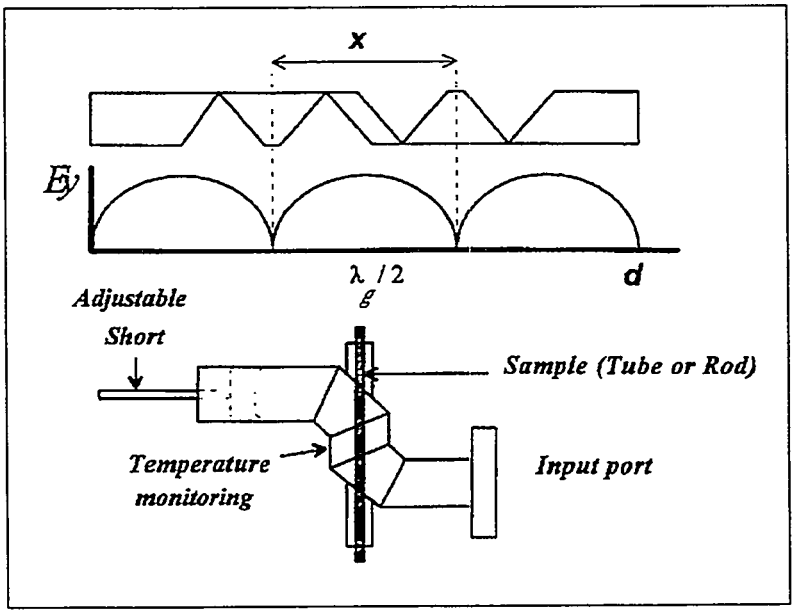

Figure 4: Schematic of Double Mitered Bend Cavity

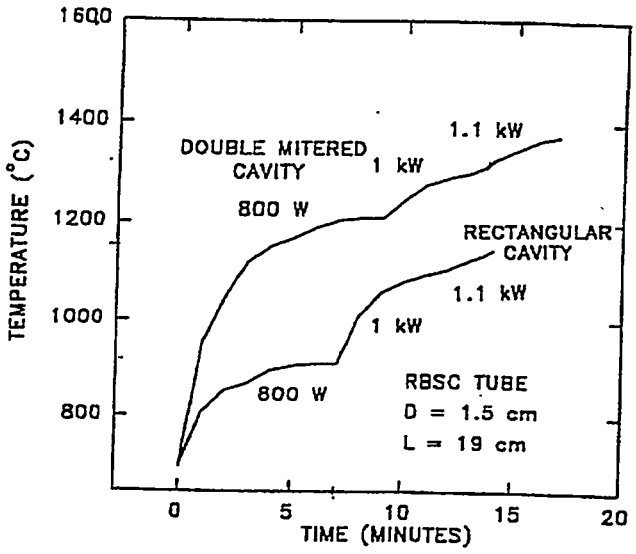

Figure 5: Heating Profiles for Rectangular and Double Mitered Bend Cavities

The double mitered bend single mode cavity was used to join two RBSC rods. The rods were 1.9 cm (0.75 in) and 1.5 cm (0.59 in) in diameter. The lengths of the rods were 5 cm (1.97 in) and 6 cm (2.36 in), respectively. The cavity and the orientation of the specimens was as indicated in Figure 4. The rods were inserted into a block of alumina insulation and placed along the axis of the cavity, which was oriented vertically to allow pressure to be applied with an external hydraulic press. Two alumina push rods 0.9 cm in diameter and 7.8 cm long were used to apply the pressure to the top and bottom specimens. Temperature was monitored through a hole in the cavity wall at the position indicated in Figure 4, using the optical pyrometer. The specimens were brought to a joining temperature of 1455°C in approximately 40 minutes by gradually increasing the input microwave power to a maximum value of 1550 Watts. The input power was then held at this value to maintain the joining temperature for 12 minutes. The reflected power during this time was 50 Watts. Figure 6 is a photograph of the joined specimens, which were sent to Los Alamos National Laboratory for evaluation.

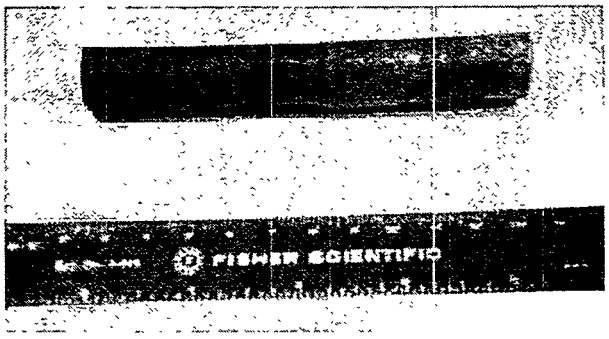

Figure 6: RBSC Rods Joined Using Double Mitered Bend Cavity

PUBLICATIONS

1. T.H.A. Shan, R. Cozzens, Y.L. Tian, and I. Ahmad, "Microwave Curing of Silicon Carbide Ceramics from a Polycarbosilane Precursor," *MRS Symposium Proceedings, Microwave Processing of Materials IV,* **347**, 729-734 (1994).
2. H.S. Sa'adaldin, W.M. Black, I. Ahmad, Y.L. Tian, and R. Silberglitt, "Alternative Cavity Designs for Microwave Joining of Long Ceramic Tubes," *MRS Symposium Proceedings, Microwave Processing of Materials IV,* **347**, 649-654 (1994).

PRESENTATIONS

1. R. Silberglitt, "Microwave Joining of Silicon Carbide," presented at the Advanced Industrial Materials (AIM) Review Meeting, Los Alamos, NM, June 3, 1994.
2. R. Silberglitt, "Microwave Sintering and Joining of Ceramics," presented as part of the short course on Microwave Technology in Chemistry and Ceramics, International Microwave Power Institute (IMPI) Annual Microwave Symposium, Chicago, IL, July 24, 1994.

INDUSTRIAL INPUT AND TECHNOLOGY TRANSFER

Golden Technologies, Inc., the Coors company responsible for ceramics R&D, has provided materials and joining requirements for radiant burner tube assemblies. Technology transfer plans include fabrication and scale-up of tube assemblies, and testing by the user industry under simulated service conditions.

COST SHARING

The Virginia Center for Innovative Technology has co-funded this project through a grant of $48.2K to George Mason University. GMU has absorbed $20.2K in overhead charges associated with this CIT grant and contributed $5.6K in graduate student tuition. The total state and university contribution to this project for FY 1994 was $74K.

HIGHLIGHTS

Microwave pyrolysis of polycarbosilane to form SiC was shown to be 5 times faster than conventional heating and to provide a product with excellent crystallinity at a lower pyrolysis temperature. A double mitered bend cavity was shown to provide more rapid heating to higher temperatures of SiC rods and tubes and was used to join SiC rods.

MICROWAVE PROCESSING OF CERAMIC OXIDE FILAMENTS

G. J. Vogt and J.D. Katz

Los Alamos National Laboratory
P.O. Box 1663
Los Alamos, New Mexico 87545

INTRODUCTION

The objective of the microwave filament processing project is to develop microwave techniques at 2.45 GHz to manufacture continuous ceramic oxide filaments. Microwave processing uses the volumetric absorption of microwave power in oxide filament tows to drive off process solvents, to burn out organic binders, and to sinter the dried fibers to produce flexible, high-strength ceramic filaments. The technical goal is to advance filament processing technology by microwave heating more rapidly with less energy and at a lower cost than conventional processing, but with the same quality as conventional processing. The manufacturing goal is to collaborate with the 3M Company, a US manufacturer of ceramic oxide filaments, to evaluate the technology using a prototype filament system and to transfer the microwave technology to the 3M Company.

TECHNOLOGY TRANSFER

A Cooperative Research and Development Agreement (CRADA), entitled "Microwave Processing of Continuous Oxide Ceramic Filaments," was conducted with the 3M Company, a manufacturer of continuous ceramic oxide fibers. The agreement was signed on October 22, 1993. This agreement will be the direct means of transferring this microwave technology to 3M. In this first year, our activities focused on the controlled sintering of a prototype ceramic oxide filament. The samples of prefired test tows were provided by 3M for microwave processing at Los Alamos. The 3M company will play a critical role in the technology development by supplying the needed expertise in sol-gel filament preparation and characterization.

The three-year program will develop microwave techniques for the drying, burnout, and sintering of a proprietary prototype filament. The potential energy and economic advantages of microwave processing will be evaluated through direct comparison with conventional thermal processing.

TECHNICAL PROGRESS

Summary

Significant progress was made toward controllable microwave sintering of a 3M proprietary ceramic oxide filament tow. We have successfully demonstrated that microwave heating can be started without breaking the continuous filaments. Also, we have shown that a microwave heated zone on the continuous filaments can be sustained and propagated along the moving filament tow. The prefired tows used in the project were thermally dried and prefired at 3M without the final sintering step. Measurement of the high-temperature dielectric constants was performed for the different 3M tows by Dr. Wayne Tinga at the University of Alberta. Development of the microwave sintering technology has proceeded successfully with only one major technical issue yet to be solved. That issue is the technical problem of controlling the filament temperature at the desired sintering temperature.

New Microwave Processing Laboratory

The microwave filament processing laboratory was moved during May from the Sigma Complex to the new Material Science Laboratory (MSL). The filament processing program has profited greatly from this new state-of-the-art facility, which presents a significant enhancement of our microwave processing capabilities. The laboratory move has given us the opportunity to redesign the microwave filament laboratory to accommodate the new instrumentation available in the MSL. The new instruments and capabilities include:

1. Microwave power sensors with the greater resolution needed for our work at low microwave power levels (<100W).

2. Computer data acquisition with LabView software.

3. A new Traveling Wave Tube (TWT) microwave source, covering a frequency range of 2.5-18 Ghz, with a broad band range available for controlling filament sintering with the large changes in fiber dielectric properties and cavity parameters.

4. An industrial CO_2 heating laser for preheating low-loss oxide filament in the microwave cavity.

Milestones

1. Demonstrate controlled microwave sintering of the prototype filament tows with resulting mechanical properties as good as, or better than, those obtained by conventional thermal sintering. This task for FY 1994 is the first-year goal of the filament processing CRADA. The goal is to develop a commercially viable microwave technique and cavity, operating at 2.45 GHz, to sinter the proprietary filament tows that have been conventionally dried and prefired. Microwave heating of the prototype fibers must be done in a controllable manner to achieve sintering and to retain the submicron-sized microstructure without overheating. Microwave heating experience with commercial aluminosilicate, alumina, and silicon carbide filament tows has served as an excellent starting point for the CRADA work.

Microwave Sintering of 3M Prototype Tows. Microwave heating behavior was characterized for conventionally processed and prefired filament tows. The prefired tows were thermally dried and prefired at 3M, leaving the final sintering step to be completed with microwave processing.

We have successfully demonstrated the ignition of microwave heating and the propagation of a heated zone along the length of a moving filament tow. Successful microwave processing requires that microwave heating be started without breaking the continuous filament, allowing the continuous tow to be pulled through the microwave cavity.

An essential feature for processing continuous tows is the ability to maintain a stationary heating zone, stationary relative to the microwave cavity, on the moving filament tow.

That is, the heating zone must propagate along the moving tow in the direction opposite to the tow motion. We can successfully confine a propagating heating zone in the microwave cavity for the prefired and fully-processed filament tows. A proper balance between pull speed and cavity power must be struck to maintain the heated zone within the microwave cavity. Under insufficient power, the heated zone will simply travel out of the cavity without any propagation. In general, a faster pull speed through the cavity will require more microwave power to sustain a propagating heating zone.

Only one technical hurdle remains to be solved to make microwave sintering viable for filament manufacturing. The filament temperature during sintering must be controlled in the desired temperature range to produce flexible, strong filaments.

Numerical Modeling of Microwave Heating. To aid our understanding of the burst heating in aluminosilicate and other ceramic tows, a time-dependent finite-difference model of microwave heating was developed for qualitative comparison with experiments. The model assumed a smooth time-dependent decrease in the dielectric loss factor for the filament tow while being heated to temperatures above the mullite phase transition temperature (~1250°C). The heat burst behavior was readily reproduced in the qualitative model using an exponential temperature-dependence for the dielectric loss of the amorphous filament tow. The burst-heating behavior in a Nextel 550 tow is depicted in Figure 1a from experimental temperature measurements taken with an Accufiber optical fiber thermometer. A numerical simulation of burst heating on a stationary filament tow in a TE_{103} cavity is presented in Figure 1b. The stationary tow was heated at constant power with irregular step increases in power, indicated by the sudden rise in temperature. The temperature changes in the first 140 seconds of the experiment are due to hybrid heating with a carbon coating. The carbon is completely removed after the first temperature spike at 140 seconds into the experiment.

The 1-D model included an estimated temperature-dependent dielectric loss function, adjusted to produce the same degree of mullite formation as in the experimental case. The total fraction of mullite formed (~40%) was estimated by x-ray diffraction analysis. The model gives

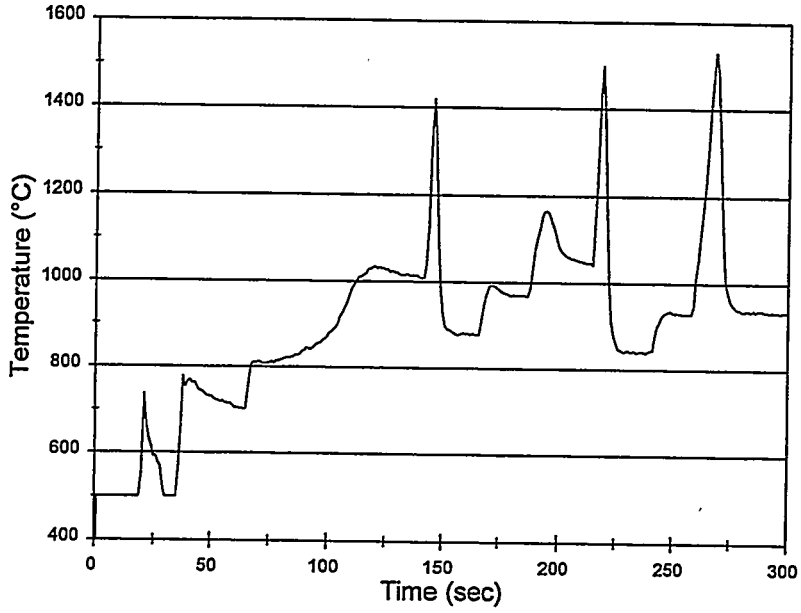

Figure 1a. Burst heating in a stationary Nextel 550 tow in a TE_{103} cavity. The microwave power was increased by step amounts, indicated by a sudden temperature rise.

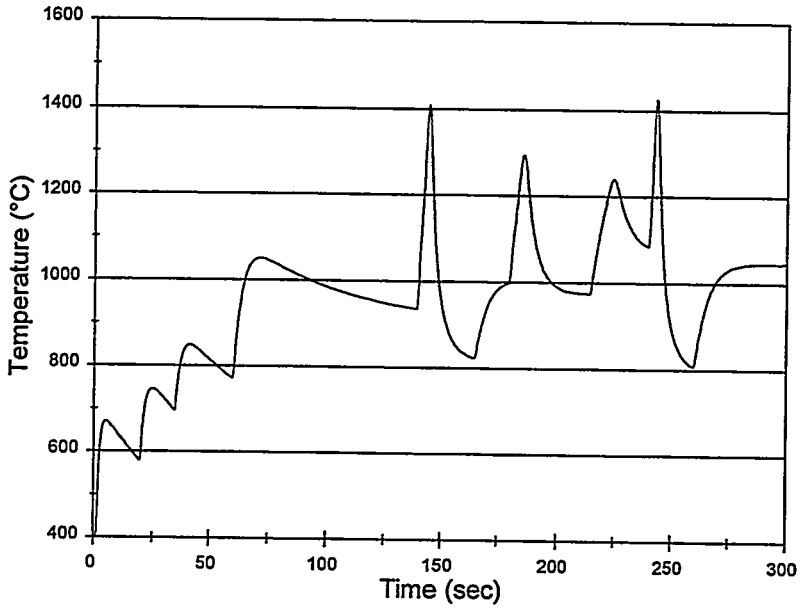

Figure 1b. Numerical simulation of the burst heating observed in a stationary Nextel 550 tow. Step increases in microwave power are indicated by a sudden temperature rise.

excellent qualitative agreement with the experimental observations. Major features of the tow heating behavior are reproduced by the simulation in Figure 1b, including temperature spikes, simple temperature step rises, and drops in the baseline temperature after a temperature spike. A quantitative model is not possible at this time due to lack of measured materials properties, including tow emissivity, dielectric constants, thermal conductivity, and mullite formation kinetics.

Numerical simulation for the microwave heating behavior of the ZAY filaments is not available at this time due to the lack of an adequate computer code capable of computing the coupled heat tranfer and electromagnetic interaction problems.

Dielectric Properties. The dielectric properties of the 3M prototype filament tows were measured by Dr. Wayne Tinga at the University of Alberta in Edmonton, Canada. Dr. Tinga has developed a novel high temperature dielectrometer to simultaneously heat and measure the dielectric properties of ceramic oxides. The dielectrometer design is well suited for characterizing filament samples, as this type of material cools too rapidly for reliable testing by the conventional cavity perturbation technique. Data on the high-temperature dielectric properties are needed to understand microwave heating, to properly design microwave processing schemes, and to develop realistic numerical models of the microwave heating.

Tow Temperature Measurements. Routine temperature measurements of a moving filament tow are not easily made in a microwave cavity due to the presence of the electromagnetic field and to the small diameter of the heated tow. However, the Accufiber optical fiber thermometry (OFT) system has readily provided the reliable temperature measurements that we need to control filament heating. A sapphire OFT sensor can be precisely positioned to view the filament tow within the microwave cavity, perpendicular to the applied microwave electric field without significantly affecting the cavity resonance.

During the past three months, we have, however, found a significant flaw in the OFT system while measuring temperatures with the dual-wavelength mode. The dual-wavelength mode is the preferred method to measure temperature in microwave filament processing. In the dual-

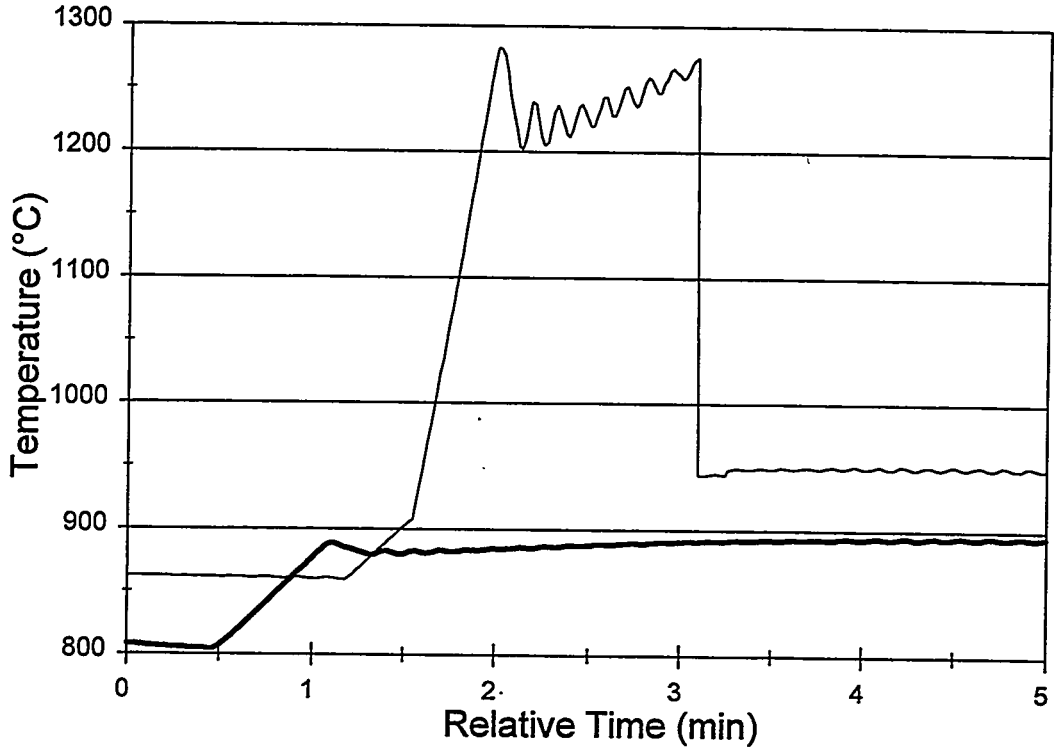

Figure 2. Temperature measurement by the optical fiber thermometer (OFT) in the dual wavelength mode (light line) during heat up from 860°C to 960°C. OFT measured temperature is typically high and remains high until OFT unit is cycled through single wavelength mode back to the dual wavelength mode. Temperature measurement in the single wavelength mode (dark line) is shown for a heatup from 800°C to 900°C.

wavelength mode, the OFT system lapses into a critical malfunction when trying to track rapid temperature changes greater than 100°C/min. The OFT system overestimates the temperature and then typically hangs up at a false reading that is much higher than the actual temperature. This malfunction is depicted in Figure 2 where the temperature of rapidly heated furnace is used to simulate filament heating. According to Luxtron Accufiber, the OFT defect resides in the system hardware and software. Fortunately, Accufiber believes that we can solve the system flaw with hardware and software modifications. The modifications will be completed and tested in FY95.

Active Process Control. Active, rapid feedback control is needed for practical microwave processing of continuous ceramic oxide filaments. Feedback control is required to maintain a well-tuned match between the microwave source and cavity where the heated filaments strongly interact with the cavity electromagnetic field. Also, active feedback control will be necessary to regulate the process temperature where the dielectric properties of the filaments change rapidly with temperature.

A traveling wave tube (TWT) amplifier has the essential characteristics to provide a much broader process control environment than is possible using a Magnetron oscillator. The Magnetron is an rf oscillator as well as an amplifier. Subtle changes in the Magnetron operating characteristics (e.g., power, VSWR match, and pulse structure) change the resonant cavity response and output frequency. By comparison, the TWT is exclusively an amplifier. Since the rf source is independent of the tube, changes in the operating parameters of the beam do not affect the beam bunching. As such, the power level can be adjusted over 40 dB (4 decades) without a power-related frequency shift.

The external oscillator configuration required by the TWT provides a highly versatile process control platform. By comparing a rf signal from the cavity to a reference signal from the amplifier, phase information can be used in a negative feedback loop to allow the oscillator to track the cavity frequency as it shifts due to the changing dielectric constant in the material being heated. By sampling the field level in the cavity with a detector, amplitude control can be done to maintain a consistent electric field level in the cavity, which is important for understanding and controlling the filament heating and temperature. Other control options are available to handle materials that tend to run away thermally, because their loss tangent rises dramatically above a critical temperature. One method is to tune the phase-lock circuit for a very narrow response, so when the material starts to run away, the material's dielectric shift will take the cavity out of range of the phase-lock loop and the cavity's electric fields will drop quickly. Another approach would be to measure the infra-red light emission and use that to attenuate the drive to the TWT to lower the power level.

Tests have shown that our rf oscillator/TWT does phase-lock favorably. The test bed included a copper TE_{103} cavity that was similar to the existing stainless steel cavity used in the magnetron system. Experiments with lossy silicon carbide ceramic tows have successfully demonstrated rapid feedback control over the cavity resonant frequency. An advanced copper cavity was designed and fabricated to implement the field measurement probe and light emission sensor, as well as the OFT sensor and video camera. This cavity will be used as a development bed for the heating control schemes described above.

PUBLICATIONS

1. G.J. Vogt, W.P. Unruh, and R.H. Plovnick, "Microwave Sintering of Continuous Zirconia Ceramic Fibers," in proceedings of Symposium O: Microwave Processing of Materials IV, MRS 1994 Spring Meeting on April 4-8, 1994, in San Francisco, California.

2. G.J. Vogt, W.P. Unruh, and J.R. Thomas, Jr., "Experimental Observations on Thermal Spikes in Microwave Processing of Ceramic Oxide Fibers," in proceedings of Symposium O: Microwave Processing of Materials IV, MRS 1994 Spring Meeting on April 4-8, 1994, in San Francisco, California.

3. J.R. Thomas, Jr., W.P. Unruh, and G.J. Vogt, "Mathematical Model of Thermal Spikes in Microwave Heating of Oxide Ceramic Fibers," in proceedings of Symposium O: Microwave Processing of Materials IV, MRS 1994 Spring Meeting on April 4-8, 1994, in San Francisco, California.

PRESENTATIONS

1. G.J. Vogt, W.P. Unruh, and R.H. Plovnick, "Microwave Sintering of Continuous Zirconia Ceramic Fibers," poster presentation to the Symposium O: Microwave Processing of Materials IV, MRS 1994 Spring Meeting on April 4-8, 1994, in San Francisco, California.

2. G.J. Vogt, W.P. Unruh, and J.R. Thomas, Jr., "Experimental Observations on Thermal Spikes in Microwave Processing of Ceramic Oxide Fibers," oral presentation to the Symposium O: Microwave Processing of Materials IV, MRS 1994 Spring Meeting on April 4-8, 1994, in San Francisco, California.
3. J.R. Thomas, Jr., W.P. Unruh, and G.J. Vogt, "Mathematical Model of Thermal Spikes in Microwave Heating of Oxide Ceramic Fibers," poster presentation to the Symposium O: Microwave Processing of Materials IV, MRS 1994 Spring Meeting on April 4-8, 1994, in San Francisco, California.
4. G.J. Vogt, J.D. Katz, B. Rusnak, and J.R. Thomas, Jr., "Microwave Processing of Ceramic Oxide Filaments," presented at the DOE/Advanced Industrial Concepts Materials Program, Annual Information and Review Meeting, Los Alamos, New Mexico, June 1-3, 1994.
5. G.J. Vogt, J.D. Katz, B. Rusnak, and J.R. Thomas, Jr., "Microwave Processing of Ceramic Oxide Filaments," poster presented at the MST Division Review, Los Alamos, New Mexico, June 23-24, 1994.

HONORS AND AWARDS

None.

PATENTS/DISCLOSURES

None.

LICENSES

None.

INDUSTRIAL INPUT AND TECHNOLOGY TRANSFER

We have negotiated a CRADA with the 3M Company for the microwave processing of continuous ceramic oxide filaments. The CRADA was signed by Los Alamos and the 3M

Company in October, 1993. The project is sponsored by the Advanced Industrial Materials Program, DOE-EERE.

COST SHARING

The Microwave Filament Processing program has benefitted greatly from the use of the state-of-the-art instrumentation available in the new microwave processing laboratory in the Material Science Laboratory.

HIGHLIGHTS

1. A CRADA on "Microwave Processing of Continuous Oxide Ceramic Filaments" was signed with the 3M Company. This three-year program started this year with work on microwave sintering of prototype filaments.

2. Important steps were demonstrated for controlled microwave sintering of the protoype filament tows. Microwave heating can be initiated without breaking the continuous filament tow or stopping the process. A microwave-driven heating zone can be maintained and propagated along continuous filaments moving through the microwave cavity.

3. The high temperature dielectric properties of the prototype filaments were measured in a novel self-heating dielectrometer for temperatures up to 1000°C. The fibrous material cools rapidly to near room temperature within several seconds due to a large surface area-to-volume ratio. This rapidly cooling material, which could not be tested by the conventional cavity perturbation techniques, can now be characterized by measuring its complex dielectric constant.

ADVANCED INDUSTRIAL MATERIALS PROGRAM

LIST OF INVESTIGATORS PARTICIPATING IN PROJECT

Project: Microwave Processing of Ceramic Oxide Filaments, G.J. Vogt

Reporting Period: Annual, FY 1994

Person Providing Information: Gerald J. Vogt

Name	Type of Position	Planned Time on Project (days/week)	Changes from Planned on Project 1st Qtr	2nd Qtr	3rd Qtr	Entire Year
G.J. Vogt	Principal Investigator	2-3	nc	nc	nc	nc
J.D. Katz	Permanent Staff	0-1	nc	nc	nc	nc
F.D. Gac	Permanent Staff	0	nc	nc	nc	nc
B. Rusnak	Permanent Staff	1	nc	nc	nc	nc
J.R. Thomas, Jr.	Visiting Staff	1	nc	nc	nc	0

SELECTIVE INORGANIC THIN FILMS

Mark L. F. Phillips, Lori A. Weisenbach, Mark T. Anderson,
Teresa V. Bohuszewicz, C. S. Ashley, and C. J. Brinker
Department 1846, Sandia National Laboratories
Albuquerque, NM 87185

D. S. Ballantine, Jr.
Departmentt of Chemistry
Northern Illinois University
DeKalb, IL 60115

S. S. Yee and K. S. Johnston
Department of Electrical Engineering
University of Washington
Seattle, WA 98195

INTRODUCTION

This project is developing inorganic thin films as membranes for gas separation applications, and as discriminating coatings for liquid-phase chemical sensors. Our goal is to synthesize these coatings with tailored porosity and surface chemistry on porous substrates and on acoustic and optical sensors. Molecular sieve films offer the possibility of performing separations involving hydrogen, air, and natural gas constituents at elevated temperatures with very high separation factors. We are focusing on improving permeability and molecular sieve properties of crystalline zeolitic membranes made by hydrothermally reacting layered multicomponent sol-gel films deposited on mesoporous substrates. We also used acoustic plate mode (APM) oscillator and surface plasmon resonance (SPR) sensor elements as substrates for sol-gel films, and have both used these modified sensors to determine physical properties of the films and have determined the sensitivity and selectivity of these sensors to aqueous chemical species.

TECHNICAL PROGRESS

Summary

Molecular Sieve Films: A goal of this project is to develop a class of molecular sieve membranes for light gas separation applications. These membranes are ideally composed of continuous, highly ordered, polycrystalline thin films of a zeolitic phase deposited on a porous substrate, such as a γ–Al_2O_3 gas filter. The membranes must be made thin and leak-free in order to achieve high permselectivities. We have demonstrated synthesis of microporous composite films by nucleating and crystallizing zeolitic phases from amorphous aluminosilicate films made via sol-gel routes. The films are then heated to calcine the zeolite and densify the matrix. This technique yields a "bricks and mortar" composite film that should combine the molecular sieve properties of zeolite phase

with the physical durability of the glassy host phase. A Technical Advance describing this process was filed.

To demonstrate that these films are useful for light gas separation or as catalytic membranes, we must measure their permeability to light gases (e.g., CH_4, N_2, O_2, CO_2). This requires depositing the films on a porous support, such as a mesoporous γ-Al_2O_3 tube or disk. This has been achieved by coating the amorphous nutrient onto the porous substrate, then crystallizing the nutrient.

Sensor Coatings: The project continued to evaluate coated APM oscillators in order to measure the chemical selectivities of sol-gel films, and also developed a method for using SPR to measure important physical properties of films such as refractive index, porosity, and thickness. Sol-gel sensor coatings were found to enhance refractive index sensitivity of SPR over a broader dynamic range. Improvements in sensitivity were also obtained with new sensing geometries; two Technical Advances describing these were filed.

Milestones

1. Synthesis of composite microporous films on porous supports:

The goal of this project element is to produce supported membranes with a high density (percent coverage) of very thin (< 1 μm thick) crystals of a desirable zeolite phase, surrounded by a continuous nonporous glassy phase. This is achieved by depositing multiple layers of sol-gel coatings onto a substrate that is either nonporous (e.g., a Si wafer) or mesoporous (e.g., a gas filter or membrane), allowing the film to nucleate in a humid atmosphere, crystallizing the film in steam, then heating the film to calcine the zeolite and densify the residual sol-gel film to a glass. The nutrient silica and alumina are contained within the sol-gel film, which ideally limits crystal thickness to approximately that of the initial film. Nucleation requires the presence of a template cation, which can be incorporated into the film structure or be present in the vapor phase. Synthesis of composite zeolitic membranes is made challenging by the daunting number of reaction parameters that control the quality of the films. These include, but may not be limited to, nucleation time, reaction time, nucleation temperature, reaction temperature, pH (or Na/Al ratio), concentration of mineralizer (such as F^-), substrate pore diameter, order of film layer deposition, age of sol before deposition, age of film before crystallization, and coating method (spin vs. dip).

The first successful composite films were made by spin-coating bilayer sol-gel films consisting of sodium and aluminosilicate alkoxides onto a Si wafer and exposing them to a humid atmosphere at elevated temperature. Once crystallized, the films were calcined and densified by heating to 500 °C in air. This process yields a continuous film consisting of very thin (<0.5 μm) zeolite crystals within a glassy matrix. X-ray diffraction data from these crystals are consistent with faujasite (Zeolite X). These films contained no macroscopic holes or cracks even after heat treatment, and are an order of magnitude thinner than any zeolite films reported in the literature (Figure 1). They are also more thermally robust, since the thermal expansion coefficients of

noncomposite films are generally different from their supports, causing the films to crack or peel upon calcination. A Technical Advance describing the composite films and routes to their synthesis was filed in September 1994.

Dip-coating the wafers with the same sols did not yield films that could be crystallized by this process. It appears that this is due to diffusion of Na ions into the aluminosilicate layer, which may inhibit nucleation by decreasing the Na concentration at the layer interface. It is thus likely that the method initially used for coating Si wafers is not directly applicable to γ-Al_2O_3 tubular membranes, since these must be dip-coated rather than spin-coated. The film microstructure obtained via spin coating, with its high shear rate and exposure to ambient humidity, is different than that of dip-coated films, which form in dry conditions at lower shear. This difference in microstructure may influence the nucleation rate.

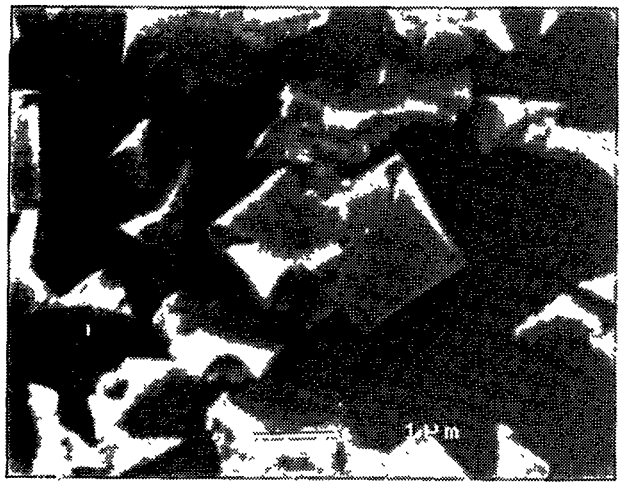

Figure 1a: SEM micrograph of zeolite crystals grown from a multilayer sol-gel film deposited on a Si wafer support.

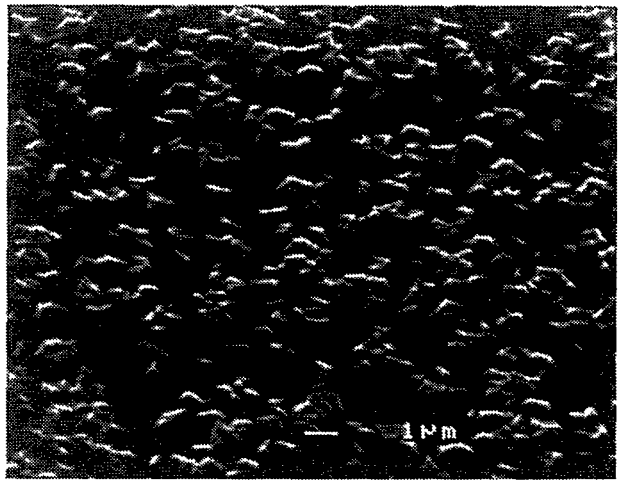

Figure 1b: SEM micrograph of densified film surface, tilted 50°. Note that crystal thickness (ca. 0.5 μm) is nearly that of the sol-gel film.

In an effort to adapt the spin-coat process to making supported membranes we studied the prospect of using Anodiscs®, flat porous alumina wafers that are available in a variety of pore sizes, as substrates for composite films. These can be spin-coated with nutrient, but SEM data indicate that even with pore sizes as small as 20 nm, capillary forces draw the liquid nutrient into the wafer, creating pinholes in the film. In addition, the discs warp upon heating or oxygen plasma treatment, which are necessary to densify the amorphous matrix and calcine the zeolite crystals. Anodiscs are therefore unsuitable for film deposition via sol-gel routes.

Since dip-coating appears to be the only option for depositing the films onto membranes, we began a set of experiments that identified and studied reaction parameters that influence quality

of dip-coated films. We found that exposing the films to increased temperature and humidity prior to crystallization appears to cause nucleation, and dip-coated films thus treated will crystallize under conditions where no crystals would otherwise form. On the other hand, previously viable films that had been aged at ambient temperature and humidity for at least one month failed to crystallize. Aging the sol-gel stock solutions increases their viscosity and produces lower-quality films. The presence of fluoride ion (which can be introduced to the reaction atmosphere from the Teflon liners of the autoclaves) is essential to formation of crystals within the nutrient sol-gel film. It appears that the presence of fluoride is necessary during crystallite growth period (>100 °C treatment), but not during the nucleation period (50 °C). This is consistent with the notion that fluoride acts as a mineralizer rather than as a template.

The data obtained from these experiments allowed us to improve dip coating technique and reaction conditions to the point where thin, continuous films containing zeolite crystals were obtained on a mesoporous γ–Al_2O_3 (U.S. Filter) membrane support. We used several techniques to attempt to identify the zeolitic phase deposited on the membrane tube, including thin film X-ray diffraction and scanning electron microscopy with energy-dispersive spectroscopy. Data were consistent with the zeolite phase LTN, a cubic, small-pore zeolite with a Na:Al:Si ratio of 1:1:1. This phase may be desirable for separating hydrogen from larger molecules such as methane and ethylene.

Permeability data are essential to determine if the membranes are truly continuous (leak-free), and to ensure that the zeolite crystals are free to allow gas flow from the surface to the support without obstruction from residual sol-gel material. Prior to measuring permeabilities of zeolitic films on gas membranes, SAW-BET analysis was carried out on reacted and calcined films deposited on quartz SAW (surface acoustic wave) devices. The absorption isotherm obtained from this analysis indicated that although the film had cracked, it also may be microporous. Permeation measurements of gas membranes coated with reacted, calcined zeolite films indicated that flow through the membranes is Knudsen-limited, as are the uncoated tubes (Figure 2). (Knudsen diffusion refers to separation based on molecular mean free path, which is related to the molecular weights of the diffusing species.) Though the gas flux through the membrane had decreased, indicating at least partial membrane coverage by the film, SEM results showed that the films were cracked or delaminated, due to poor surface adhesion.

A possible explanation for film cracking is condensation of water in the pores of the alumina tube, which can attack the sodium isopropoxide layer adjacent to the membrane. Subsequent films prepared in tubes wrapped with Teflon tape were far more robust, with one film reducing gas flux by a factor of 27, suggesting a continuous or near-continuous film. By improving the calcination/densification technique selectivities characteristic of surface selective adsorption have been measured, indicating that the effective membrane pore size has been reduced

without loss of permeability. This indicates that films on porous supports can be made leak-tight, and once the matrix is further densified, molecular sieving behavior should become apparent.

Future plans: We will continue to test reaction parameters that can affect film nucleation and crystallization such as nucleation time and temperature, film thickness, coating technique and fluoride concentration. We will also resume using organic templates to nucleate the films, and develop improved densification methods with the goal of eliminating porosity in the residual sol-gel matrix of the crystallized film.

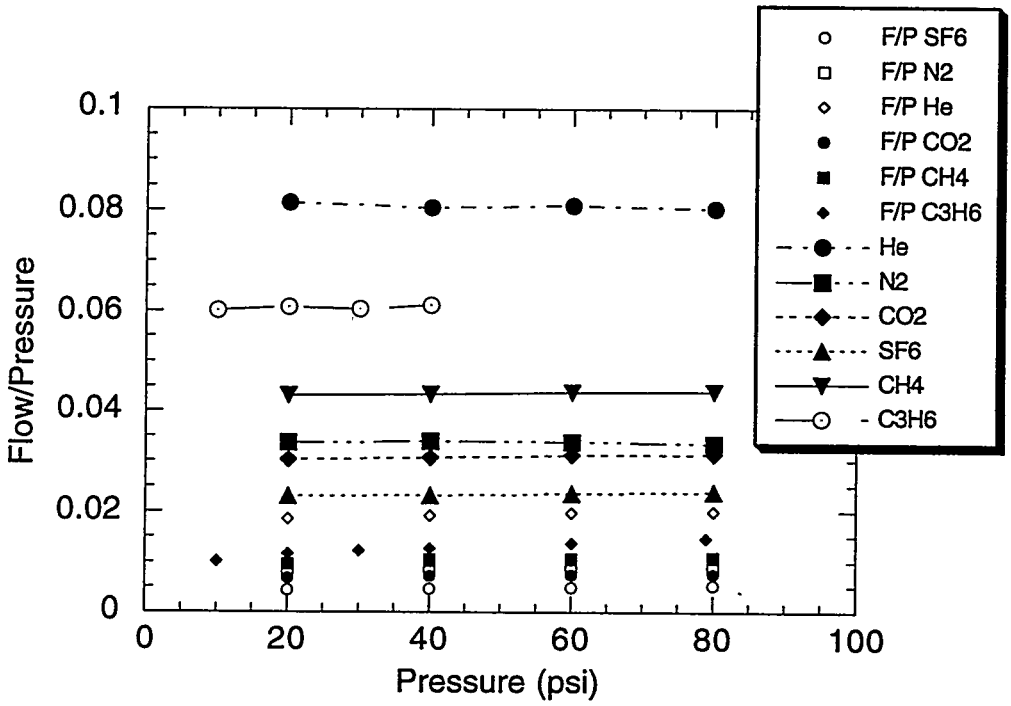

Figure 2: Permeation results for a γ–Al_2O_3 membrane (U.S. Filter), before and after coating with a sol-gel derived zeolite film. Unconnected points are flow/pressure values for the membrane before coating, and connected points correspond to flow rates of the coated membrane. The separation factors for both the coated and uncoated membrane are Knudsen-limited.

Impact: The petroleum and natural gas refining industries would significantly benefit from high permeability molecular sieve films capable of separating light, fixed gases, particularly if the membranes can be used at high temperatures. With sufficiently high permeability and low unit area cost, energy savings of several quad/yr could be achieved.[1] We believe that with appropriate stabilization, such as dealumination or rare earth exchange, composite zeolite membranes such as those we are developing can be made stable up to 1000 °C.

2. Synthesize zeolitic membranes from supported clay films:

Both nature and the detergent industry have known for some time that it is possible to convert clays into zeolites via treatment with aqueous alkali. Bhushan Karle, a University of New Mexico graduate student, has been working with Mark Phillips and Jeff Brinker to develop methods for synthesizing zeolite films from clays, and for measuring permeabilities of the resulting composites. Linde Type A zeolite, which is a very useful molecular sieve due to its interconncented pore structure and variable pore size, can be made from kaolin by conversion to metakaolinite followed by treatment with aqueous sodium hydroxide.[2] In the most elementary process, kaolinite is dry-pressed or slip-cast into discs, then sintered to yield amorphous metakaolinite. These discs can then be partially converted to Zeolite A (Figures 3a and 3b) by hydrothermal treatment in alkaline conditions (pH $\approx$ 13). The average pore size of the clay discs was determined to be approximately 15 nm, so the discs themselves are in principle sufficiently permeable to act as the porous film support. However, we have found it advantageous to make supports by sintering pellets made from isostatically pressed α–Al_2O_3. These supports are coated with kaolinite by slip-casting; the pellets are then heated to convert the kaolinite film to metakaolinite. We have constructed an apparatus for measuring gas permeabilities through underivatized and zeolite-coated metakaolinite-alumina discs. We have found that permeability of the alumina pellets decreases by two to three orders of magnitude upon coating with kaolinite. Once the clay film is converted to Zeolite A, however, gas separation factors reveal a significant contribution from viscous flow, indicating that large holes are still present in the membrane.

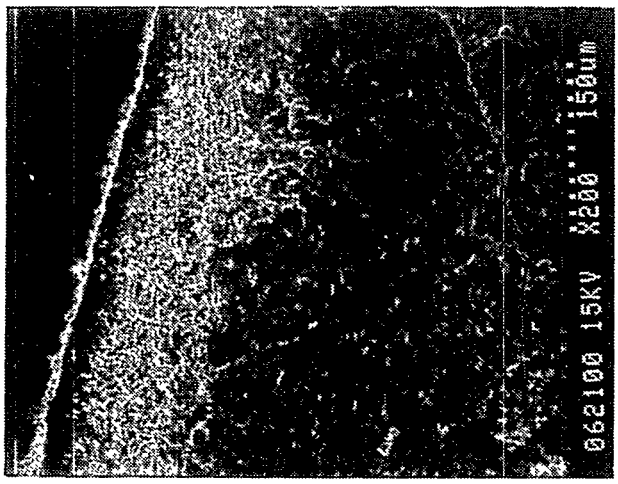

Figure 3a: Zeolite A film (left) grown into a metakaolinite disk. Film is ca. 150 μm thick.

Figure 3b: Zeolite A crystals grown from meta-kaolinite. Crystals are 3-5 μm across.

3. Measurement of apparent selectivities of APM device coatings:

Last year's report discussed the relationship between aqueous metal ion concentrations and frequency response in quartz acoustic plate mode (APM) devices coated with sol-gel films. In general, results were consistent with a pore conductivity model in which overlap of the ionic double layer within the pores results in enhanced conductivity, and thus an increased acoustoelectric response. This AE response dominates any affects attributable to mass-loading in the sol-gel film; sensitivity to changes in mass loading is essential to operating these devices as ion sensors. Follow-up studies were performed to clarify the role of the porous coating in the frequency response behavior. Specifically, the effects of pH and ionic radius were determined, and the AE response sensitivities of the different APM modes were studied.

It is postulated that changing solution pH may alter device response by changing the number of cation- or anion-exchangeable sites within the sol-gel film. In general, frequency shifts correlated with the specific conductance of the solutions at pH values between 2 and 10, and thus ionic selectivity was not imparted to the films by pH control. Similarly, the device response was sensitive to the charge on the analyte ions, but rather than being influenced by hydrated radius, the response also correlated with specific conductance. However, attempts to determine the variation of AE response sensitivity with the device oscillation mode indicate that AE sensitivity is frequency dependent, and that the device may be tunable for enhanced mass sensitivity and diminished acoustoelectric response.

It is expected that zeolitic films will improve sensitivity vs. the sol-gel coatings through increased porosity, and may increase chemical specificity through enhanced selectivity for metal ions of different size and charge.

4. Film characterization using surface plasmon resonance: The goals of this project are to use surface plasmon resonance (SPR) as a technique for measuring physical properties of porous thin films, such as thickness, refractive index, and porosity; and to use sol-gel films to modify the response of SPR devices to improve their sensitivity and selectivity as liquid phase sensors. A surface plasmon wave is a charge density wave that propagates along the interface between a metal (such as Ag or Au) and a dielectric (such as air or water). In a SPR sensor, the metal is deposited as a film upon a glass substrate, such as a fiber optic cable. When light propagating through the glass is totally internally reflected from the surface supporting the metal film, the evanescent electric field associated with the beam couples with an allowed surface plasmon wavevector in the film, resulting in a resonance. The allowed wavevectors, and thus the spectrum of transmitted light, are determined by the thickness and refractive index of the dielectric surrounding the metal film.

The sensitivity and specificity of the probe can be improved by depositing a sol-gel derived film onto the metal film. A high-index film improves the sensitivity of the probe to small changes of refractive index in low-index media. A film that is chemically specific to solution species of

interest (e.g. metal ions) will change its index reversibly upon sorption and desorption of the species. During the reporting period we have developed a technique for simultaneously determining wavelength dispersive refractive index and thickness of films using SPR measurements alone. If refractive index has been determined independently (e.g., via ellipsometry), it is possible to measure percent porosity of a film if the pores are filled with a fluid of known index, such as water. We have also determined that it is possible to optimize the sensitivity of a SPR sensor to a particular range of liquid refractive indices by coating it with a sol-gel film of the appropriate thickness or index. If several sensors are simultaneously used with films of different thicknesses or indices, a sensor array can be constructed that will be sensitive over a wide range of refractive indices.

In addition to using sol-gel films to tailor effective refractive index, improvements in SPR sensitivity were obtained by modifying the geometry of the sensor head; two Technical Advances have been filed. We are currently investigating the performance of chemically derivatized sol-gel films as discriminating elements that will render SPR devices sensitive to chemical changes in aqueous solution, such as metal ion concentration or the presence of biological agents.

Impact: If appropriately derivatized films for SPR sensors can be developed, this technique will have a significant impact on the markets for real-time industrial process monitoring and biomedical sensing.

References:

1. D. E. Fain, *MRS Bulletin* April 1994, p. 40.

2. L. V. C. Rees and S. Chandrasekhar, *Zeolites* **1993**, 524.

PUBLICATIONS

1. A. A. Russell, D. H. Doughty, D. S. Ballantine Jr., and R. Hart, "Frequency and Attenuation Response of Acoustic Plate Mode Devices Coated with Porous Oxide Films", *Analytical Chemistry* **1994**, *66(19),* 3108-16.

2. K. S. Johnston, R. C. Jorgenson, S. S. Yee, and A. A. Russell, "Characterization of Porous Sol-gel Films on Fiber Optic SPR Sensors", *Proc. SPIE* **1994**, *2068,* 87-93.

3. S. K. Karlsen, K. S. Johnston, R. C. Jorgensen, and S. S. Yee, "Simultaneous Determination of Refractive Index and Absorbance Spectra of Chemical Samples Using Surface Plasmon Resonance", *Applied Optics,* submitted 7/94, in press.

PRESENTATIONS

1. L. A. Weisenbach, M. T. Anderson, and M. L. F. Phillips, Nucleation and growth of zeolites from amorphous films, American Ceramics Society (NM Section), Albuquerque, NM, Oct. 1993.

2. L. A. Weisenbach, M. T. Anderson, and M. L. F. Phillips, "Nucleation and Growth of Zeolite Membranes", Materials Research Society, San Francisco, CA, April 1994.

3. M. L. F. Phillips, L. A. Weisenbach, M. T. Anderson, C. S. Ashley, T. V. Bohuszewicz, and C. J. Brinker, "Selective Inorganic Thin Films", Advanced Industrial Concepts Annual Review Meeting, Los Alamos, NM, June 1994.

4. R. C. Jorgensen, K. S. Johnston, M. N. Mar, S. K. Karlsen, and S. S. Yee, "Surface Plasmon Resonance Fiber Optic Sensor Long Term Stability and Robustness Studies", Europtrode Conference, Florence, Italy, April 1994.

5. R. C. Jorgensen, K. S. Johnston, and S. S. Yee, "In-line SPR Fiber Optic Sensors and Systems for Industrial Process Monitoring", IFPAC Conference, Houston, TX, January 1994.

HONORS AND AWARDS: None during this reporting period.

PATENTS/DISCLOSURES

1. U. S. Patent #5,224,972, "Coatings with Controlled Porosity and Chemical Properties", G. C. Frye, C. J. Brinker, D. H. Doughty, T. Bein, and K. Moller, July 6, 1993.

2. Technical Advance SNL S-82,323, SD-5518, "Thin Film Zeolitic Membranes Grown from Amorphous Precursor Films", L. A. Weisenbach, M. L. F. Phillips, and M. T. Anderson, Sept. 1994.

3. Technical Advance UW 05-94-80, "Planar Substrate Surface Plasmon Resonance Sensing Head", K. S. Johnston, S. K. Karlsen, R. C. Jorgensen, and S. S. Yee, May 1994.

4. Technical Advance UW 01-64-06, "Surface Plasmon Resonance Based Dispersion Sensor", S. K. Karlsen, K. S. Johnston, R. C. Jorgensen, and S. S. Yee, Jan. 1994.

LICENSES: None during this reporting period.

INDUSTRIAL INPUT AND TECHNOLOGY TRANSFER

Golden Technologies, Inc., has agreed to provide mesoporous tubular gas filters, which we will use as supports for our zeolitic films. They have also agreed to measure permselectivities of the resulting supported membrane at elevated temperatures (up to 600 °C).

COST SHARING: None during this reporting period.

HIGHLIGHTS: Composite films consisting of zeolite crystals embedded in an amorphous sol-gel matrix was synthesized by hydrothermally crystallizing supported multilayer sol-gel films. These films are continuous, thermally robust (to at least 500 °C), and thinner than previously reported thin films by an order of magnitude. These films can be deposited on porous substrates and operated as gas membranes. Zeolite membranes were also made from clay films supported on porous alumina.

Surface plasmon resonance (SPR) was used to measure refractive index, thickness, and porosity of sol-gel films deposited on metal film sensors. Derivatization of the sensing element with sol-gel films and improvements in SPR sensing geometry yielded significant improvements in sensitivity of the system to changes in refractive index.

SILICON CARBIDE POWDER SYNTHESIS

Greg Glatzmaier and Rasit Koc
Buildings and Energy Systems Division
National Renewable Energy Laboratory
Golden, Colorado 80401

Jack Sibold
Golden Technologies Company, Inc.
Golden, Colorado 80401

(Contribution unavailable due to protected CRADA information)

INTERNAL DISTRIBUTION

1-2. Central Research Library
3. Document Reference Section
4-5. Laboratory Records Department
6. Laboratory Records, ORNL RC
7. ORNL Patent Section
8-10. M&C Records Office
11. D. J. Alexander
12. K. B. Alexander
13. L. F. Allard
14. P. Angelini
15. B. R. Appleton
16. R. L. Beatty
17. P. F. Becher
18. T. M. Besmann
19. P. J. Blau
21. E. E. Bloom
22. R. A. Bradley
23. C. R. Brinkman
24. T. D. Burchell
25. W. H. Butler
26. N. C. Cole
27. K. M. Cooley
28. R. H. Cooper, Jr.
29. W. R. Corwin
30. D. F. Craig
31. S. A. David
32. C. E. DeVore
33. R. B. Dinwiddie, Jr.
34. J. R. DiStefano
35. D. S. Easton
36. M. K. Ferber
37. A. T. Fisher
38. E. L. Fuller, Jr.
39. E. P. George
40. B. G. Gieseke
41. G. M. Goodwin
42. H. W. Hayden, Jr.
43. L. L. Horton
44. J. A. Horton, Jr.
45. C. R. Hubbard
46. M. A. Janney
47. D. R. Johnson
48. R. R. Judkins
49. M. A. Karnitz
50. J. R. Keiser
51. E. A. Kenik
52. H. D. Kimrey, Jr.
53. D. M. Kroeger
54. R. J. Lauf
55. E. Lee
56. C. T. Liu
57. R. A. Lowden
58. G. M. Ludtka
59. L. K. Mansur
60. P. J. Maziasz
61. D. J. McGuire
62. R. A. McKee
63. K. L. More
64. R. K. Nanstad
65. T. A. Nolan
66. A. E. Pasto
67. K. P. Plucknett
68. J. B. Roberto
69. M. L. Santella
70. A. C. Schaffhauser
71. J. H. Schneibel
72. V. K. Sikka
73. P. S. Sklad
74. C. J. Sparks
75. S. Spooner
76. R. W. Swindeman
77. T. N. Tiegs
78. S. Viswanathan
79. J. M. Vitek
80. X. L. Wang
81. C. S. Yust
82. T. Zacharia
83. H. W. Foglesong (Consultant)
84. E. L. Menger (Consultant)
85. J. G. Simon (Consultant)
86. K. E. Spear (Consultant)

EXTERNAL DISTRIBUTION

87. **Advanced Refractory Technologies, Incorporated**, 699 Hertel Avenue, Buffalo, NY 14207

Keith A. Blakely

88-89. **Alfred University**, Center for Advanced Ceramic Technology, Alfred, NY 14802

Richard M. Spriggs
Harrie J. Stevens

90. **Allegheny Ludlum Steel Corporation**, Research Center, Alabama & Pacific Avenue, Brackenridge, PA 15014

Gerald L. Houze, Jr.

91. **Allied-Signal Aerospace Company**, Garrett Ceramic Components Division, 19800 S. Van Ness Avenue, Torrance, CA 90509

Maxine L. Savitz

92. **Allied-Signal, Incorporated**, Ceramics Program, P.O. Box 1021R, Morristown, NJ 07960

Clifford P. Ballard

93-94. **Alloy Engineering and Casting Company**, 1700 West Washington Street, Champaign, IL 61821

Barry L. Fritz
James R. Lytle

95. **Aluminum Company of America**, Government Marketing, 1615 "M" Street, NW, Washington, DC 20036

Pam Patrick

96. **Andritz Sprout Bauer**, Sherman Street, Muncy, PA 17756

Ronald L. Musselman

97. **Argonne National Laboratory**, 9700 South Cass Avenue, Argonne, IL 60439

William A. Ellingson

98. **Army Materials Technology Laboratory**, Watertown, MA 37919

Robert N. Katz

99. **Army Research Office**, P.O. Box 12211, Research Triangle Park, NC 27709

Andrew C. Crowson

100. **Babcock & Wilcox**, 1562 Beeson Street, Alliance, OH 44601-2196

Todd Johnson

101-102. **Babcock & Wilcox**, 20 S. Van Buren Avenue, P.O. Box 351, Barberton, OH 44203-0351

John Clement
J. William Smith

103-109. **Battelle Pacific Northwest Laboratories**, Department of Materials Science, P.O. Box 999, Richland, WA 99352

Bruce C. Bunker, K2-45
A. A. Campbell, K2-44
N. R. Gordon, K2-44
Gordon L. Graff, K2-57
Gary L. McVay, K2-45
Larry R. Pederson, K2-44
Peter C. Rieke, K2-44

110. **Bethlehem Steel Corporation**, Homer Research Laboratories, Bethlehem, PA 18016

Charles R. Beechan

111. **Bethlehem Steel Corporation**, P.O. Box 248, Chesterton, IN 46304

Anthony Simola

112-113. **Black & Decker, Incorporated**, 701 East Joppa Road, TW 460, Towson, MD 21286

Nick Achterberg
Stephen R. Crosby

114-116. **Boeing Aerospace**, Material Lobby, Renton, WA 98124-2499

K. Y. Blohowiak, Building 7-20, Mail Stop 73-09
Thomas S. Luhman, Building 7-20, Mail Stop 73-09
M. S. Strasik, Building 7-20, Mail Stop 73-09

117-118. **Bowater, Inc.**, 5020 Highway 11, South, Calhoun, TN 37309

John E. Griffey
LeRoy Hershey

119. **Carpenter Technology Corporation**, 92 Burning Tree Lane, Reading, PA 19607

Robert L. Caton

120-121. **Carpenter Technology Corporation**, 101 West Bern Street, P.O. Box 14662, Reading, PA 19612-4662

Bradford A. Dulmaine
Nicholas Fiore

122. **Caterpillar, Incorporated**, Engineering and Research Materials, Technical Center, Building E, P.O. Box 1875, Peoria, IL 61656-1875

Michael H. Haselkorn

123. **Ceracon,** 1101 North Market Street, Suite 9, Sacramento, CA 95834

Henry S. Meeks

124. **Ceradyne, Incorporated,** 3169 Redhill Avenue, Costa Mesa, CA 92626

Joel P. Moskowitz

125-127. **Ceramatec, Incorporated,** 2425 South 900 West, Salt Lake City, UT 84119

Raymond Cutler
Ronald S. Gordon
David W. Richerson

128-129. **Corning Corporation,** Sullivan Park FR-02-5, Corning, NY 14831

Thomas P. DeAngelis
Frank E. Murphy, Jr.

130-132. **Cummins Engine Company, Incorporated,** P.O. Box 3005, Columbus, IN 47202-3005

Michael C. Brands, Mail Code 50165
Magan J. Patel, Mail Code 50183
James W. Patten, Mail Code 50183

133. **Delta M Corporation,** 525 Warehouse Road, Oak Ridge, TN 37830

Reginald W. McCulloch

134-135. **Dow Chemical Company, Incorporated,** 1776 Building, Midland, MI 48674

David A. Dalman
Richard D. Varjian

136. **Dynamet Technology, Incorporated,** 8 "A" Street, Burlington, MA 01803

Walter Bergler

137. **Eaton Corporation,** Corporate Research & Development, Milwaukee, Center, 4201 North 27th Street, Milwaukee, WI 53216

John W. Kroll

138. **Eaton Corporation,** 4010 North 27th Street, Milwaukee, WI 53216

Henry Kunsmann

139-140. **Electric Power Research Institute,** Nuclear Plant Corrosion Control, 3412 Hillview Avenue, Palo Alto, CA 94303

Ben Banerjee
Mohamad M. Behravesh

141. **Electric Power Research Institute,** 2000 L Street, Suite 805, Washington, DC 20036

W. Eugene Eckhart

142. **Energetics, Incorporated**, 7164 Gateway Drive, Columbia, MD 21046

Aziz Azimi

143. **EXXON R&D Labs**, P.O. Box 2226, Baton Rouge, LA 70821

R. C. Schucker

144-145. **FM Technologies, Incorporated**, Patriot Square, 10529-B Braddock Road, Fairfax, VA , 22032

I. Ahmad
Richard S. Silberglitt

146. **Ford Motor Company**, 35500 Plymouth Road, Box 13, Lovonia, MI 48150

Mark G. Shapona

147-151. **Ford Motor Company**, P.O. Box 2053, Dearborn, MI 48121-2053

John E. Allison, Mail Drop 3182
William E. Dowling, Jr., Room S2065
Norman A. Gjostein, Mail Drop 2247/SRL
Gorton M. Greene
Kenneth Hass, Room S3028

152. **Ford Motor Company**, P.O. Box 1899, Room 354, Dearborn, MI 48121

Vello Arrak

153. **Foster Wheeler Development Corporation**, 12 Peach Tree Hill Road, Livingston, NJ 07039

Jeffrey L. Blough

154. **Georgia-Pacific Corporation**, 133 Peachtree Street, NE, Atlanta, GA 30303

Karl T. Morency

155. **General Electric Company**, Research & Development, Met Building, Room 263, P.O. Box 8, Schenectady, NY 12301

Alan I. Taub

156-157. **General Electric Company**, One Newmann Way, Cincinnati, OH 45215

Ram Darolia, Mail Drop M-89
James Williams, Mail Drop H-85

158. **General Motors Corporation**, 1660 L Street N.W., Suite 400, Washington, DC 20036

Bo Campbell

159-162. **General Motors Corporation**, AC Rochester, 1300 North Dort Highway, Flint, MI 48556

R. F. Beckmeyer
Lawrence A. Carol
W. LaBarge
Carl E. Miller

163-169. **General Motors Corporation**, 30500 Mound Road, Warren, MI 48090-9055

M. S. Rashid
Edward F. Ryntz
James G. Schroth
Michael M. Shea
Susan Smyth
Charles S. Tuesday
Peter Vernia

170-173. **General Motors Corporation**, Saginaw Division, 3900 Holland Road, Saginaw, MI, 48601-9494

Steven L. Avery
Randy P. Bal
Jerry D. Jablonski
Charles R. Martin

174. **General Motors Powertrain Division**, 895 Joslyn Road, Pontiac, MI 48340-2920

Robert Wiltse

175-178. **General Motors Powertrain Division**, 1629 North Washington Avenue, Saginaw, MI, 48605-5073

Ron Cafferty
Paul N. Crepeau
Mark E. Hoover
Dennis Meyers

179. **General Motors Tech Center**, Composite Section Manufacturing Building, A/MD-24, 30300 Mound Road, Warren, MI 48090-9040

I. E. Poston

180-184. **George Mason University**, 4400 University Drive, Fairfax, VA 22030

W. M. Black
R. F. Cozzens
H. S. Sa'adaldin
T. H. Shan
T. L. Tian

185-190. **Georgia Institute of Technology**, School of Materials Engineering, 778 Atlantic Drive, Atlanta, GA 30332-0245

Steve Antolovich
W. Brent Carter
Joe K. Cochran, Jr.
S. Lee
Thomas L. Starr
S. R. Stock

191. **Georgia-Pacific Corp.**, 133 Peachtree Street, N.E., Atlanta, GA 30303

Karl T. Morency

192-194. **Golden Technologies Company, Incorporated**, Research & Development, 17750 West 32nd Avenue, Golden, CO 80401

Rick Kleiner
Dean Rulis
Jack Sibold

195. **T. M. Grace Company, Incorporated**, 2517 S. Harmon Street, Appleton, WI 54915

Thomas Grace

196. **Herty Foundation Development**, P.O. Box 7798, Savannah, GA 31418

James Anderson

197. **Hoskins Manufacturing Company**, 10776 Hall Road, Hamburg, MI 48139

Forrest Hall

198-200. **Hughes Research Laboratories**, 3011 Malibu Canyon Road, Malibu, CA 90265

Jesse Matossian
John McLendon
Robert Schumacher

201-204. **Idaho National Engineering Laboratory**, EG&G Idaho, P.O. Box 1625, Idaho Falls, ID 83415-2218

Elmer Fleischman
John E. Flinn
D. Kunerth
E. S. Peterson

205-209. **Institute of Paper Science & Technology, Inc.**, 500 10th Street, N.W., Atlanta, GA 30318

Jefferey A. Colwell
Maclin S. Hall
Robert H. Horton
Thomas McDonough
Dave Orloff

210-216. **Iowa State University**, Ames Laboratory, 126 Metals Development Building, Ames, IA 50011

L. Carson
L. S. Chumbley
D. C. Jiles
H. Mahmood
K. L. Pauwels
P. P. Pulvirenti
R. Bruce Thompson

217. **James River Corporation**, P.O. Box 2218, Richmond, VA 23217

Ronald Estridge

218. **John Hopkins University**, Center for Nondestructive Evaluation, Maryland Hall 107, Baltimore, MD 21218

Robert E. Green, Jr.

219-220. **Johnson Controls, Inc.**, 507 East Michigan Street, P.O. Box 423, Milwaukee, WI 53201

Carl F. Klein
Bryan L. McKinney

221. **Kaiser Aluminum & Chemical Corporation**, P.O. Box 870, Pleasanton, CA 94566

S. C. Carniglia

222-227. **Lawrence Berkeley Laboratory**, 1 Cyclotron Road, Mail Stop 90-2024, Berkeley, CA 94720

M. Ayers
W. Cao
Arlon J. Hunt
Robert Ritchie
P. Stevens
S. Zheng

228-231. **Lawrence Livermore National Laboratory**, P.O. Box 808, Livermore, CA 94550

M. Fluss, Mail Stop L-326
D. L. Haupt, Mail Stop L-326
John H. Kinney, Mail Stop L-356
Jeffery Wadsworth, Mail Stop L-353

232-252. **Los Alamos National Laboratory**, P.O. Box 1663, Los Alamos, NM 87545

P. G. Apen, D453
R. S. Barbero, E549
Hugh Casey, G770
R. G. Castro, G770
David E. Christiansen, C348
Robert P. Currier, G736
David J. Devlin, E549
Elliott P. Douglas, E549
N. E. Elliott, E549
Frank D. Gac, G771
Shimshon Gottesfeld, D429
P. J. Hay, B268
J. D. Katz, G771
R. LeSar, K765
John J. Petrovic, G771
A. Redondo, D429
Anthony D. Rollett, G770
B. Rusnak, H817
Donald G. Sandstrom, A140
J. R. Thomas, Jr., G755
Gerald J. Vogt, G771

253-254. **MTCI**, 5570 Sterrett Place, Suite 20, Columbia, MD 21044

Amal Mansour
Momtaz Mansour

255. **Metallamics, Inc.**, P.O. Box 1539, Traverse City, MI 49684

Robert R. McDonald, President

256. **National Aeronautics & Space Administration**, Materials & Structures Division, Code RM, 600 Independence Avenue, S.W., Washington, DC 20546

Samuel L. Venneri

257. **National Aeronautics & Space Administration**, Lewis Research Center, 21000 Brookpart Road, MS: 49-1, Cleveland, OH 44135

Joe Stevens

258. **National Forge Company**, Irvine, PA 16329

Ashok Khare

259-261. **National Institute of Standards and Technology (NIST)**, Gaithersburg, MD 20899

Edwin R. Fuller, Jr., Ceramics Division, Room, A256, Building 223
Richard E. Ricker, Depart. of Commerce, Materials Bldg., Room B254
Lyle Schwartz, Director

262-268. **National Renewable Energy Laboratory,** 1617 Cole Boulevard, Golden, CO 80401-3393

Helena L. Chum
Robert J. Evans
Gregory Glatzmaier
Steve Kelley
R. Joc
S. S. Shojaie
K. Tatsumoto

269-270. **National Science Foundation,** Metallurgy Section, 1800 "G" Street, N.W., Washington, DC 20550

Bruce A. MacDonald
Robert Reynik

271. **Naval Research Laboratory,** Building 43, Room 212, Code 6000, 4555 Overlook Avenue, SW, Washington, DC 20735-5341

Bhakta B. Rath

272. **North Carolina A&T State University,** Department of Mechanical Engineering, Greensboro, NC 27411

V. S. Avva

273-274. **North Carolina State University,** Department of Materials Science and Engineering, Box 7907, Raleigh, NC 27695-7907

Carl C. Koch
Nkadi Sukidi

275. **Norton Company,** Goddard Road, Northboro, MA 01532-1545

Normand D. Corbin

276. **Pask Research and Engineering,** Berkeley, California 94720

Antoni P. Tomsia

277-278. **Polytechnic University,** 333 Jay Street, Brooklyn, NY 11201

Giuliana C. Tesoro
Y. Wu

279-280. **Precision Castparts Corporation,** 4600 SE Harney Drive, Portland, OR 97206-0898

David A. Chang
Larry J. Watland

281. **Rapid Technologies, Incorporated,** P.O. Box 368, 170 Werz. Ind. Blvd., Newnan, GA 30264

Ed Dailey

282-283. **Rennsselaer Polytechnic Institute**, School of Engineering, Materials Engineering Department, 8th Street, Troy, NY 12180-3590

N. S. Stoloff

284. **Reynolds Metal Company**, P.O. Box 1200, Shefield, AL 35660

Nolan E. Richards

285-290. **Sandia National Laboratories**, Division 8361, P.O. Box 969, 7011 East Avenue, Livermore, CA 94551-0969

Mark D. Allendorf
T. M. Breunig
Donald R. Hardesty
M. C. Nichols
T. H. Osterheld
D. A. Outka

291-305. **Sandia National Laboratory**, 1515 Eubank, S.E., Albuquerque, NM 87185-5800

M. T. Anderson, Division 1846, Mail Stop 0607
C. S. Ashley
C. J. Brinker, Division 1846,Mail Stop 0607
Gary Carlson, Division 6211, Mail Stop 0710
Bob Eagan, Division 1800
Kevin G. Ewsuk, Division 1849, Mail Stop 0609
Gregory C. Frye, Division 1846
Kay Hays, Mail Stop 1709
Mark L. F. Phillips, Divison 1846, Mail Stop 0607
Steve J. Martin, Division 1163
Allen G. Sault, Division 6211
Dale W. Schaefer, Division 1810
R. D. Skocypec, Division 1513, Mail Stop 0835
Alan P. Sylwester, Division 6203, Mail Stop 0749
L. A. Weisenbach, Division 1846, Mail Stop 0607

306. **Sandia National Laboratory**, University of New Mexico, Advanced Materials Laboratory 1708, 1001 University Boulevard, SE, Suite 100, Albuquerque, NM 87106

Ronald E. Loehman

307. **Sandusky International**, 615 W. Market Street, Box 5012, Sandusky, OH 44871-8012

Charles W. Rainger

308. **TRW, Incorporated**, 23555 Euclid Avenue, Cleveland, OH 44117

A. L. Bement, Jr.

309. **Tennessee Technological University**, Center for Manufacturing Res. & Tech. Util. College of Engineering, P.O. Box 5014, Cookeville, TN 38505

Joseph T. Scardina

310-311. **The Carborundum Company**, P.O. Box 187, Keasbey, NJ 08832

Craig L. Dillman
Stanley Gursky

312. **The Carborundum Company**, P.O. Box 832, Niagara Falls, NY 14302

Monika O. Ten Eyck

313. **The Timken Company**, 1835 Dueber Avenue, S.W., Canton, OH 44706-2798

Robert L. Leibensperger

314-318. **The Pennsylvania State University**, Department of Materials Science and Engineering, Metals Science and Engineering Program, 221 Steidle Building, University Park, PA 16802

John Hellman
Paul R. Howell
George L. Messing
William A. Pratt
Richard E. Tressler

319-320. **The University of Tennessee**, Department of Materials Science & Engineering, Knoxville, TN 37996-2200

C. R. Brooks
Ben F. Oliver

321. **Thermo-Chem, Incorporated**, 5570 Sterrett Place, Suite 210, Columbia, MD 21044

David A. Scearce

322. **Thermo Electron Technologies**, 85 First Avenue, Waltham, MA 02254

Peter Reagan

323-324. **U.S. Air Force**, Wright Patterson AFB, Dayton, OH 45433-6533

Dennis M. Dimiduk, WRDC Material Laboratory
Allan Katz, AFWAL/MLLM Material Laboratory

325-343. **U.S. Department of Energy/Headquarters**, 1000 Independence Avenue, SW, Washington, DC 20585

Joseph E. DeWees, EE-233, 5F-043/FORS
Sidney Diamond, EE-34, 5G-064/FORS
Sarah Dillich, EE-232, 5F-059/FORS
Russell Eaton, III, EE-142, 6H-034/FORS
Marvin E. Gunn, Jr., EE-14, 6H-034/FORS
Douglas E. Kaempf, EE-234, 5F-043/FORS
Matthew J. McMonigle, EE-234, 5F-058/FORS
William A. Obenchain, EE-231, 5G-067/FORS
William P. Parks, Jr., EE-221, 5F-035/FORS
Marsha L. Quinn, EE-223, 6H-034/FORS
Scott L. Richlen, EE-221, 5F-035/FORS
Peter H. Salmon-Cox, EE-23, 5F-059/FORS
Robert B. Schulz, EE-34, 5F-064/FORS
Stanley F. Sobczynski, EE-231, 5F-059/FORS
Charles A. Sorrell, EE-232, 5F-059/FORS
Alan J. Streb, EE-20, 6B-052/FORS
Denise F. Swink, EE-20, 6B-052/FORS
Daniel E. Wiley, EE-233, 5F-059/FORS
Stanley M. Wolf, EM-542, 413/TREV

344-347. **U.S. Department of Energy**, 19901 Germantown Road, Germantown, MD 20585

James P. Carr, FE-72, 3035/270
Robert J. Gottschall, ER-131, J-322/GTN
Helen Kerch, ER-131, J-322/GTN
F. W. Wiffen, ER-533, G-258/GTN

348. **U.S. Department of Energy/Albuquerque**, P.O. Box 5400, Albuquerque, NM 87115

D. Morton

349. **U.S. Department of Energy/Oak Ridge**, Building 4500N, Mail Stop 6269, P.O. Box 2008, Oak Ridge, TN 37831-6269

E. E. Hoffman

350. **U.S. Department of Energy/Idaho**, 785 Dow Place, Idaho Falls, ID 83402

Joanne Malmo

351. **U.S. Department of the Interior Bureau of Mines**, 2401 "E" Street, NW, Washington, DC 20241

Garrett R. Hyde

352-353. **U.S. Department of the Interior Bureau of Mines**, Tuscaloosa Research Center, University of Alabama Campus, P.O. Box L, Tuscaloosa, AL 35486-9777

Sonya P. Holderfield
Johanna B. Salsman

354. **United Technologies Research Center**, East Hartford, CT 06108

Vincent C. Nardone

355. **University of Alabama**, Metal Casting Technology Center, P.O. Box 6374, Tuscaloosa, AL 35487

Thomas S. Piwonka

356-357. **University of Cincinnati**, Department of Materials Science & Engineering, 412B Rhodes Hall, Cincinnati, OH 45221-0012

J. A. Sekhar
Vijay K. Vasudevan

358-359. **University of Maine**, 5737 Jenness Hall, Orono, ME 04469-5737

Joseph Genco
Marquita Hill

360. **University of Missouri School of Mines & Met.**, Ceramic Engineering, 120 Fulton Hall, Rolla, MO 65401-0249

Robert E. Moore

361. **University of New Mexico**, Albuquerque, New Mexico 87106

William Fahrenholtz

362. **University of Pennsylvania**, Department of Mechanical Engineering, 111 Towne Building, 220 South 33rd Street, Philadelphia, PA 19104-6315

David Pope

363. **University of Utah**, Electrical Engineering Department, Salt Lake City, UT 84112

M. Iskander

364-366. **University of Wisconsin**, Department of Materials Science & Engineering, 1500 Johnson Drive, Madison, WI 53706

Marc A. Anderson
T. F. Kelly
Roger M. Rowell

367. **Vander Linden & Associates**, 5 Brassie Way, Littleton, CO 80123

Carl R. Vander Linden

368-369. **Virginia Polytechnic Institute and State University**, Department of Materials Engineering, Blacksburg, VA 24061

J. J. Brown
K. L. Reifsnider

370. **Westinghouse R&D**, 1310 Beulah Road, Pittsburgh, PA 15235

Garth Clarke

371. **Westvaco Corp.**, 11101 John Hopkins Road, Laurel, MD 20707-0000

W.B.A. Sharp

372. **Weyerhaeuser Paper Company**, Research and Development, WTC 2H22, Tacoma, WA 98477

Peter Gorog

373. **Worcester Polytechnic Institute**, Department of Mechanical Engineering, 100 Institute RJ, Worcester, MA 01609

Robert N. Katz

374. 9208 Burning Tree Road, Bethesda, MD 20817

Samuel Goldberg

375. 14390 W. 30th Avenue, Golden, CO 80401

David G. Wirth

376. **3M Industrial & Electronic Sector**, Research Laboratory, Building 201-4N-01, 3M Center, St Paul, MN 55144-1000

Ross H. Plovnick

377-386. **Department of Energy, Office of Scientific and Technical Information,** Office of Information Services, P.O. Box 62, Oak Ridge, TN 37831

For distribution by microfiche as shown in DOE/OSTI-4500, Distribution Category UC-310 [Industrial Programs (General)]